Many body effects in one-dimensional attractive Bose gases

HOLDAWAY, DAVID,IAN,HENRY

Many body effects in one-dimensional attractive Bose gases

David Ian Henry Holdaway

Abstract

In this thesis we investigate the properties of ultra-cold quantum gases in reduced dimension and the effects of harmonic confinement on soliton-like properties. We study regimes of agreement between mean-field and many-body theories the generation of entanglement between initially independent finite sized atomic systems.

Classical solitons are non-dispersing waves which occur in integrable systems, such as atomic Bose-Einstein condensates in one dimension. Bright and dark solitons are possible, which exist as peaks or dips in density. Quantum solitons are the bound-state solutions to a system satisfying quantum integrability, given via the Bethe Ansatz. Such integrability is broken by the introduction of harmonic confinement. We investigate the equivalence of the classical field and many-body solutions in the limit of large numbers of atoms and derive numerical and variational approaches to examine the ground state energy in harmonic confinement and the fidelity between a Hartree-product solution and a quantum soliton solution.

Soliton collisions produce no entanglement between either state and result only in an asymptotic position and phase shift, however external potentials break integrability and thus give the possibility of entangling solitons. We investigate the dynamical entanglement generation between two atomic dimers in harmonic confinement via exact diagonalisation in a basis of Harmonic oscillator functions, making use of the separability of the centre-of-mass component of the Hamiltonian. We show repulsive states show complex dynamics, but with an overall tendency towards states of larger invariant correlation entropy, whereas attractive states resist entanglement unless a phase matching condition is satisfied. This phase matching condition could in theory be used to generate states with highly non-Poissonian number superpositions in atomic systems with controlled number.

Many body effects in one-dimensional attractive Bose gases

David Ian Henry Holdaway

A thesis submitted in partial fulfilment
of the requirements for the degree of
Doctor of Philosophy

Department of Physics
Durham University

July 30, 2013

Contents

Page

Abstract **i**

Contents **ii**

List of Figures **vii**

List of Tables **viii**

Declaration **ix**

Acknowledgements **xi**

1 Introduction **1**
1.1 Motivations 1
1.1.1 Bose-Einstein condensation 1
1.1.2 Solitons 2
1.1.3 Motivating experiments and theory 4
1.2 Thesis layout 4
1.3 Summary of Publications arising from this work 5

I Background material **7**

2 Bose-Einstein condensation **8**
2.1 Harmonic oscillator potentials and ladder operators 8
2.1.1 The importance of Harmonic oscillator potentials . . . 8
2.1.2 Harmonic oscillator potentials in D dimensions 9
2.2 Interactions in a cold bose gas 13
2.2.1 A degenerate bose gas and the critical temperature . . 13
2.2.2 Scattering theory and the many-body problem 15
2.2.3 The contact scattering pseudo potential 19
2.2.4 Transformation to first quantisation 20
2.2.5 Scattering in strong transverse confinement 21
2.3 Derivation of the Gross Pitaevskii equation 23

2.3.1 The Onsager-Penrose condition and off-diagonal long range order . . . 23
2.3.2 The Hartree product state . . . 24
2.3.3 Decomposition of the field operator . . . 25
2.3.4 Condensate Collapse with attractive interactions . . . 27
2.4 Reduction of dynamics to 1D, regimes of different approximate models . . . 30
2.4.1 Full 1D: Wavefunction separable . . . 31
2.4.2 Quasi 1D . . . 33
2.5 Experimental realisation of BEC . . . 35
2.5.1 History and progress . . . 35
2.5.2 Techniques required to obtain a BEC in a dilute atomic gas . . . 36
2.5.3 Feshbach resonances . . . 38

3 Classical solitons and integrability 40
3.1 Classical integrability and conserved quantities . . . 40
3.1.1 Conditions for an integrable system . . . 40
3.1.2 Consequences of integrability . . . 41
3.2 Solutions in the nonlinear Schrödinger equation . . . 42
3.2.1 Bright soliton solution . . . 42
3.2.2 Solutions on a finite background . . . 42
3.2.3 Rescaling to dimensionless units . . . 43
3.2.4 Solitary wave solution to the non polynomial Schrödinger equation . . . 44
3.3 Multiple well-separated solitons in the 1D GPE . . . 45
3.3.1 General solutions for N_s solitons . . . 45
3.3.2 A collision between two solitons . . . 46
3.3.3 Importance of relative phase . . . 47
3.4 Integrability and soliton properties in systems of classical particles . . . 48
3.4.1 Two particles . . . 49
3.4.2 More than two particles . . . 50
3.4.3 Potentials giving classical integrability . . . 51
3.5 Quantum mechanics, wave particle duality, entanglement and measurement . . . 52
3.5.1 Wave particle duality . . . 52
3.5.2 Measurement . . . 54
3.5.3 Decoherence and the density matrix . . . 55
3.5.4 Entanglement . . . 56

4 Many body quantum physics in one spatial dimension 58
4.1 The Bethe ansatz and quantum integrability . . . 58
4.1.1 Quantum vs classical integrability and diffractionless scattering . . . 58

4.1.2 Two-body eigenstates of the contact interaction 61
4.1.3 The Bethe ansatz on the infinite line 63
4.1.4 The Bethe ansatz with periodic boundary conditions . 69
4.1.5 Attractive interactions with infinite periodic boundary conditions 70
4.1.6 Reduction to GPE results 72
4.2 Harmonic oscillator potentials and many body physics 76
4.2.1 Harmonic oscillator potentials for many non-interacting particles 76
4.2.2 Degeneracy of states in 1D many-body oscillators . . . 77
4.2.3 Creation and annihilation operators 79
4.2.4 Relation to ladder operators 80
4.2.5 A full set of ladder operators for the N particle system 82
4.2.6 The introduction of two body interactions 84

II Projects 88

5 A single quantum soliton in harmonic confinement 89
5.1 Preamble 89
5.2 Unit rescalings and key results 90
5.2.1 Known exact results 94
5.3 Perturbative and variational methods 96
5.3.1 Interaction dominated limit in a harmonic potential . . 96
5.3.2 Perturbation results 97
5.3.3 Variational minimization 98
5.4 Computational methods including a harmonic potential . . . 103
5.4.1 Overview 103
5.4.2 Computation procedure 103
5.4.3 Using different-width Hermite functions 104
5.4.4 Numerical ground states within the GPE approximation 105
5.5 Effects of harmonic confinement 106
5.5.1 Ground state energy 106
5.5.2 Universal behaviour 107
5.5.3 The classical soliton limit 108
5.6 Conclusions 112

6 Collisions with finite number systems 114
6.1 Introduction 114
6.1.1 Preamble 114
6.1.2 Motivating results and background 115
6.1.3 Chapter breakdown 117
6.2 System 118
6.2.1 Hamiltonian and unit rescaling 118

6.2.2 Initial condition . . . 118
6.3 Observables and measures of entanglement . . . 122
6.3.1 Left/right number . . . 122
6.3.2 von Neumann entropy and relaxation . . . 124
6.4 Analysis of the interacting system . . . 126
6.4.1 Left–right separation of the Hamiltonian . . . 126
6.4.2 Perturbative introduction of H_I . . . 127
6.5 Coherent state approximation in the strongly attractive regime 130
6.5.1 Generalised left-right separation . . . 130
6.5.2 Construction of oscillating quantum soliton states . . . 131
6.5.3 Predictions of oscillation amplitudes . . . 134
6.5.4 Possible Caveats of the model . . . 135
6.6 Mixing between different number configurations via time-dependent perturbation theory . . . 136
6.6.1 General setup . . . 136
6.6.2 Fourier approximation . . . 139
6.6.3 Instantaneous interaction approximation . . . 140
6.6.4 Amplitude bound to oscillations . . . 144
6.7 Possible experimental realisation of the four atom system . . . 145
6.7.1 Optical lattice scheme . . . 145
6.7.2 Experimental parameters . . . 147
6.8 Numerical method . . . 148
6.8.1 Basis set expansion . . . 148
6.8.2 Convergence testing . . . 149
6.9 Numerical results outside of the strongly attractive regime . . . 149
6.9.1 Preamble . . . 149
6.9.2 Left and right particle number dynamics . . . 150
6.9.3 Equilibration of energy into inter/intra-cluster excited states . . . 153
6.9.4 Relaxation to equilibrium . . . 156
6.10 Preliminary numerical results for the strongly attractive regime . . . 158
6.10.1 Preamble . . . 158
6.10.2 Left and right particle number dynamics . . . 159
6.10.3 Position of the transfer resonances . . . 162
6.11 Conclusions . . . 164

Outlook **168**

III Appendices 170

A Useful identities and integral results **171**
A.1 Special functions . . . 171
A.1.1 Exponential integrals and the Euler Gamma function . 171

A.1.2 Riemann Zeta function . . . 172
A.2 Identities involving Jacobi coordinates . . . 172
A.2.1 First identity . . . 172
A.2.2 Second identity . . . 173
A.3 Integral identities of Hermite and Laguerre polynomials . . . 174
A.3.1 Definition . . . 174
A.3.2 Identities and recursion relations . . . 175
A.3.3 Identities for width modifications . . . 175
A.3.4 Quadrature rules . . . 176

B Limiting cases of harmonically confined dimer state 178
B.1 Ground state energy for $H_{\mathrm{R}}(\xi_2)$ in the interaction dominated regime . . . 178
B.2 Energy difference between the ground and first exited state of the dimer state . . . 179

C The variational state 181
C.1 Preamble . . . 181
C.2 Normalization . . . 182
C.3 Kinetic and interaction energy . . . 184
C.4 Derivation of the first-order perturbation energy . . . 186
C.5 Energy correction to the Hartree product state . . . 190
C.6 Overlap of the relative components of the variational wavefunctions . . . 191

D Appendix to Chapter 6 192
D.1 Calculations for the number-to-the-right operator . . . 192
D.1.1 Analytically determined properties of $\hat{N}_R^2$ . . . 192
D.1.2 Numerical calculation of number variance . . . 194
D.1.3 Numerical calculation of restricted region expectation values . . . 194
D.2 Two cluster wavefunction evolution . . . 195
D.3 Energy bound for Hamiltonian variance . . . 196
D.3.1 Analytic calculations of ΔE . . . 197

References 199

List of Figures

Figure Page

2.1 Ground state widths and kurtosis 33

4.1 Ferriers diagram 79
4.2 Basis size reduction from projection. Published in [1] 85

5.1 First-order energy correction from confinement. Published in [1] 99
5.2 Wavefunction overlap with varying confinement. Published in [1]102
5.3 Energy increase from confinement. Published in [1] 108
5.4 Monte Carlo computed overlap between Hartree product soliton and quantum soliton. Published in [1] 110

6.1 Energy difference between cluster configurations. Published in [2] 130
6.2 Optical lattice diagram. Published in [2] 146
6.3 Convergence calculation. Published in [2] 150
6.4 Left/right number uncertainty after one collision and pseudo periodicity. Published in [2] 151
6.5 Left/right number uncertainty time evolution. Published in [2] 153
6.6 Right side expectation values, repulsive. Published in [2] . . . 154
6.7 Right side expectation values, attractive. Published in [2] . . . 155
6.8 Single body von Neumann entropy. Published in [2] 157
6.9 Pseudo period and number uncertainty, strongly attractive . . 159
6.10 Variation in initial transfer with separation 160
6.11 Strongly attractive number uncertainty 161
6.12 Fourier transform peaks 162
6.13 Right side expectation values, resonant 163

B.1 Ground and first excited state energy different in the dimer state 179

List of Tables

5.1 Table listing the parameters used in calculating the graph in Fig. 5.3 109

Declaration

I confirm that no part of the material offered has previously been submitted by myself for a degree in this or any other University. Where material has been generated through joint work, the work of others has been indicated.

David Ian Henry Holdaway
Durham, July 30, 2013

For my mother and father.

Acknowledgements

I would like to thank Tom Billam, Paul Halkyard and John Helm, and all the other people who have shared office 144d, for assistance in many mathematical and computational problems over the years, as well as a few less productive but enlightening political discussions! Also to Christoph Weiss for contributions and discussions on our publications, and Simon Cornish and his experimental group for discussions and their hard work and achievements. Finally of course, to Simon Gardiner, for supervision, discussions and dedicated editing over my PhD, and to Liz Wischhusen, for putting up with me while I was writing it!

Chapter 1

Introduction

1.1 Motivations

1.1.1 Bose-Einstein condensation

Bose-Einstein condensation (BEC) was originally theorised by Einstein in 1925, extending the theories of S. N. Bose [3], which were based on photon statistics, to particles of a finite mass via the introduction of a chemical potential, denoted μ, to the theory. The most general definition of a Bose-Einstein condensate is a system of particles with integer spin whose single-body density matrix has one large eigenvalue which is a finite fraction of the total number in the thermodynamic limit [4]. However, a more intuitive definition comes from the idea that the wavefunctions of the (identical) particles significantly overlap, hence they cannot be distinguished as individuals and behave as a single entity. To quantify this for a system with a number density n and thermal de-Broglie wavelength

$$\lambda_{\mathrm{dB}} = \sqrt{\frac{2\pi\hbar^2}{mk_BT}}\,, \tag{1.1}$$

one usually defines a measure called the phase space density

$$\mathrm{PSD} = \max(n)\lambda_{\mathrm{dB}}^3\,. \tag{1.2}$$

As this parameter tends to unity, the wavefunctions are around the size of the inter-atomic spacing and the quantum statistics become increasingly important. Condensation typically occurs when PSD $\gtrsim \zeta(3/2) \sim 2.6$ with $\zeta(x)$ the Riemann Zeta function (c.f. Sec. A.1.2); for liquid ^{4}He this condition is satisfied at temperatures of a few Kelvin[1]. However the high density of approximately 2×10^{22} atoms/cm^3 means the system is strongly interacting, leading to strong correlations between atomic positions effects and a condensate fraction lower than 10%, even as the temperature tends to absolute zero. This fraction is still sufficient to yield interesting properties like super-fluidity.

Dilute gases of Alkali atoms (number densities of the order of 10^{13} to 10^{15} atoms/cm^3) can satisfy weak interaction conditions[2] and tend to condensate fractions near 100% at sufficiently low temperatures. However condensation occurs at much lower temperatures, typically of the order of a few hundred nanoKelvin. These nearly pure condensates can often behave like a single nonlinear wavepacket or "super-atom" and respond in an identical way to external potentials. This wave can be made to interfere with itself like a single atom, but due to the large number of atoms present (typically 10^4 to 10^7) one can image entire momentum distributions without being as limited by shot noise. This classical picture sometimes breaks down and can miss interesting physics, a concept we explore within this thesis.

1.1.2 Solitons

What is a soliton?

Definitions of what exactly constitutes a soliton or a soliton supporting system differ somewhat between fields; a common definition [6] states that in order for a wave to be a soliton, it must

- be of permanent form (not undergoing dispersion),
- be localised within a region,

[1] At atmospheric pressure a phase transition is found to occur at around $T = 2.2K$ [5].

[2] Specifically that the number density times the cube of the s-wave scattering length is much smaller than unity.

- be able interact with other solitons, with the asymptotic outgoing form unchanged, except for a position and phase shift.

A notable point about the first two conditions is that they are properties obeyed by everyday solid objects, simply being in one distinct place at a given time and not changing its shape; these are however very interesting properties for a wave as any wave in a linear system will undergo dispersion, unless it is uniform throughout all space (which breaks condition two) or subject to some external potentials. The third condition is not a property of every day objects, even totally elastic collisions between several difference objects can change the outgoing momentum, and hence distinguishes what is so special about these wavepackets. We refer to solitons which are a peak/dip in density as bright/dark respectively.

Observation of solitons in nature

The first recorded observation of a bright soliton was by Scott Russell in August 1834. He observed a water wave in a shallow canal, created by a fast moving boat suddenly coming to a stop. Following it on horseback for a couple of miles, he noticed it maintained a constant velocity and shape as it propagated. After some time, the amplitude and velocity decayed slowly until he lost it in the winding canals. He originally referred to this phenomenon as a "wave of translation," the term soliton was coined afterwards. Mathematical models of shallow water waves use the Korteweg de Vries (KdV) equation [7] and have the following soliton solution[3]

$$h(x - x(0) - vt) = \frac{v}{2}\text{sech}^2\left[\frac{\sqrt{v}}{2}(x(0) - a - vt)\right] , \tag{1.3}$$

with v the velocity and h the height above the background level of the water. The $\text{sech}^2(x)$ (inverse $\cosh^2(x)$) profile is common for bright solitary waves.

Additionally signals between neurons have been predicted to be transmitted as solitons [8] and pulses of light can be transmitted as solitons in optical fibres with a focusing Kerr nonlinearity [9]. The focus of this work is around

[3]Up to unit rescalings to system dependent parameters.

solitons found in dilute gases of atoms, confined to one dimensional geometries.

1.1.3 Motivating experiments and theory

Interest in BEC solitons has increased in recent years thanks to experimental demonstrations of BEC in attractive gases (c.f. [10] and references herein). Attractive condensates exhibit a collapse phenomenon, which was observed by several groups [11–13]. Cornish et. al. later noticed localised remnants of the collapse which appeared to behave like solitons [14], forming a train that was stable for many collisions, despite containing too many atoms to have a stable local energy minimum. Trains of multiple solitons had been observed previously [15], but not directly following a collapse. Theoretical modelling of the multiple soliton system suggests a relative phase of π is required between neighbouring solitons to stabilise the system [16] and proposals have been made to generate solitons with controlled relative phase to test this [17]. Other research suggests solitons can exhibit Anderson localisation [18] and could be used to probe surface potentials [19].

In addition to these experiments, many-body calculations are possible for cold atoms in quasi one-dimensional geometries via the Bethe ansatz [20] and the system is often said to be quantum integrable and collisions between quantum solitons cannot transfer atoms. The interaction of solitons with narrow barriers can lead to coherent splitting [21] in the high kinetic energy regime, enhanced reflection and transmission [22, 23], or soliton barrier bound states [24] with attractive barriers. In the low energy regime there is the possibility of creating mesoscopic quantum superpositions [25, 26], and other beyond mean-field effects. Additionally, calculations suggest coherence between interacting solitons may be lost [27], leading to a fragmented system. Weak 3D effects also lead to broken integrability, allowing for inelastic scattering between solitons [28].

1.2 Thesis layout

This Thesis is organised as follows:

Chapter 2 discusses the onset of Bose-Einstein condensation and the derivation of the nonlinear wave equation describing the evolution, referred to as the Gross-Pitaevskii equation (GPE). We also include an explanation of dimensional reduction via harmonic confinement and a summary of experimental progress and techniques.
Chapter 3 introduces the concepts of classical integrability, and discusses soliton solutions to integrable systems and multiple soliton solutions to the one dimensional GPE.
Chapter 4 discusses many-body physics in one dimensional systems and the concept of quantum integrability and the Bethe ansatz. Additionally we derive a numerical method for calculations within a harmonic oscillator occupation number basis.
Chapter 5 includes calculations relating to a single soliton in harmonic confinement, discussing centre-of-mass separability and regimes of agreement between mean-field approximations and many-body results.
Chapter 6 investigates dynamics of collisions between two indistinguishable finite number systems, oscillating in a harmonic potential. This focuses on the generation of entanglement between each system and the trend to equilibrium at late times. We also discuss observed resonance effects, which are due to a phase matching.

1.3 Summary of Publications arising from this work

D. I. H. Holdaway, C. Weiss, and S. A. Gardiner, *Quantum theory of bright matter-wave solitons in harmonic confinement*, Phys. Rev. A **85**, 053618 (2012).

In this paper we investigated many-body quantum solutions to attractive bosons in harmonic confinement. We derive a variational method based on the Bethe Ansatz and a numerical method based on exact diagonalisation in a finite basis, making use of the separation of the Hamiltonian into two commuting parts. It is found that there is strong agreement between the centre-of-mass energy subtracted GPE solutions and true many-body grounds states

and high overlap between the Hartree product solution and the many-body cluster state with a localised centre-of-mass envelope.

D. I. H. Holdaway, C. Weiss, and S. A. Gardiner, *Collision dynamics and entanglement generation of two initially independent and indistinguishable boson pairs in one-dimensional harmonic confinement*, Phys. Rev. A **87**, 043632 (2013).

In this paper we investigated few-body collision dynamics between independent boson pairs, again in harmonic confinement. We investigate the rate of increases of invariant correlation entropy and number uncertainty between the two regions to the left and right of the trap centre. It is found that attractive systems resist entanglement forming between both sides unless resonance conditions are met.

Part I

Background material

Chapter 2

Bose-Einstein condensation, harmonic confinement and s-wave scattering

2.1 Harmonic oscillator potentials and ladder operators

2.1.1 The importance of Harmonic oscillator potentials

The harmonic potential $V(x) = kx^2/2 = m\omega^2 x^2/2$, is one the most widely utilised potentials in both classical and quantum physics. The prevalence in theoretical work is due in part to the fact that it is analytically solvable, but the physical importance is due to the properties of small oscillations about an equilibrium position $x_{\rm eq}$. This position can simply be rescaled out of any equation and so can be taken to be at zero without any loss of generality. We consider the Taylor expansion of the potential about $x = 0$:

$$V(x) = V(0) + V'(0)x + V''(0)\frac{x^2}{2} + \sum_{n=3}^{\infty} \frac{x^n V^{(n)'}(0)}{n!} \, . \tag{2.1}$$

Zeros of potentials are essentially arbitrary, hence we can set $V(0) = 0$. Gradients in potential energy give rise to forces (or spatial differences in rates of phase evolution for waves) which are real measurable effects. To be an equilibrium position, we require that the net force at that point is zero, i.e.

$$F(0) = -V'(0) = 0 \,, \tag{2.2}$$

so we can immediately ignore the first order derivative as well. There is however, no *ab initio* reason to assume the second derivative vanishes (although one can construct saddle-point potentials for which this is the case) and so for small enough displacements $V(x) \approx kx^2/2$ [with $k = V''(0)$] and thus $F(x) \approx -kx$. Within this small displacement approximation, we can easily solve Newtons equation $m\ddot{x} = -kx(t)$ for the displacement at a given time t

$$x(t) = x(0)\cos\left(\sqrt{\frac{k}{m}}t\right) + \dot{x}(0)\sqrt{\frac{m}{k}}\sin\left(\sqrt{\frac{k}{m}}t\right) \,. \tag{2.3}$$

The key point here being that oscillation occurs with a constant angular frequency $\omega = \sqrt{k/m}$ regardless of the initial condition. Additionally it is possible to solve all the eigenfunctions $\psi_n(x)$ for a quantum mechanical particle in a harmonic oscillator potential. These are given by

$$\psi_n(x) = \frac{\phi_n(x/a)}{\sqrt{a}} \tag{2.4}$$

with $a = \sqrt{\hbar/m\omega}$ the harmonic oscillator length and ϕ_n the Hermite functions

$$\phi_n(x) = \frac{H(x)}{\sqrt{n!2^n\sqrt{\pi}}}\mathrm{e}^{-x^2/2} \,. \tag{2.5}$$

Note that the Hermite polynomials $H(x)$ are defined in Eq. (A.12a). The energy eigenvalues $E_n = \hbar\omega(n + 1/2)$ are spaced linearly in units of $\hbar\omega$.

2.1.2 Harmonic oscillator potentials in D dimensions

If we consider a D dimensional harmonic oscillator system $V(\mathbf{r}) = m(\omega_1^2 r_1^2 + ...\omega_D^2 r_D^2)/2$ the dynamics can be split into many one dimensional equations.

Within classical mechanics, given an initial displacement and velocity in each direction, one simply has Eq. (2.3) for every dimension. Hence the problem is totally separable. This is not the case for, say, atoms in a 3D magnetic quadrupole potential: $V(x, y, z) = \mu \cdot \mathbf{B} = k\sqrt{x^2 + y^2 + k_2 z^2}$ [29].

Quantum mechanically we can again separate our Hamiltonian out into D commuting parts

$$\hat{H} = \hat{H}_1 + \hat{H}_2 + ... + \hat{H}_D \ , \tag{2.6}$$

$$\hat{H}_k = -\frac{\hbar^2}{2m}\frac{\partial^2}{\partial r_k^2} + \frac{m\omega_k^2 r_k^2}{2} \ , \tag{2.7}$$

where it can be seen that $[\hat{H}_k, \hat{H}_j] = 0$ if $j \neq k$ as they share no coordinates. Because of the commuting, we can construct eigenstates of the total Hamiltonian $\hat{H}$ through the individual Hamiltonians for each dimension. The eigenstates and eigenenergies are of the form:

$$\Psi_{n_1,..,n_D}(\mathbf{r}) = \phi_{n_1}(r_1)\phi_{n_2}(r_2)...\phi_{n_D}(r_D) \tag{2.8a}$$

$$E_{n_1,..,n_D} = \hbar\sum_{j=1}^{D}\omega_j(n_j + 1/2) \ , \tag{2.8b}$$

with $\phi_n(x)$ given by Eq. (2.5) with an appropriate harmonic oscillator length based on ω_j.

General ladder operators

Ladder operators are a useful tool for analysis of the quantum harmonic oscillator (QHO) system.[1] In general an operator $\hat{L}_-$ (with $\hat{L}_+ = (\hat{L}_-)^\dagger$), is a ladder operator to $\hat{O}$ if it satisfies

$$[\hat{O}, \hat{L}_\pm] = \pm c\hat{L}_\pm \ , \tag{2.9}$$

with c a constant that can be rescaled to unity by rescaling $\hat{O} \to \hat{O}/c$ without loss of generality, which we will assume from now on. Note that this structure implies that we can express $\hat{L}_+ = \hat{P} + i\hat{Q}$ where $\hat{P}$ and $\hat{Q}$ are symmetric operators [30]. When acting on any eigenstate of $\hat{O}$ with eigenvalue n we

[1] Additionally ladder operators are important for angular momentum algebra.

have the relation

$$\hat{O}\hat{L}_{\pm}|n\rangle = (\hat{L}_{\pm}\hat{O} + [\hat{O}, \hat{L}_{\pm}])|n\rangle = (n \pm 1)\hat{L}_{\pm}|n\rangle \ . \tag{2.10}$$

As such the eigenvalue is raised/lowered by unity. Additionally, we can see that $\hat{L}_{+}\hat{L}_{-}$ commutes with $\hat{O}$

$$\begin{aligned} \hat{O}\hat{L}_{+}\hat{L}_{-} &= ([\hat{O}, \hat{L}_{+}]\hat{L}_{-} + \hat{L}_{+}[\hat{O}, \hat{L}_{-}] + \hat{L}_{+}\hat{L}_{-})\hat{O} \\ &= \hat{L}_{+}\hat{L}_{-}\hat{O} \ . \end{aligned} \tag{2.11}$$

Ladder operator for the multidimensional harmonic oscillator

We specialise now to the QHO, defining the raising and lowering operators for dimension k, $\hat{a}_k^{\dagger}$ and $\hat{a}_k$, as [31]

$$\hat{a}_k = \sqrt{\frac{m\omega_k}{2\hbar}} \left(\hat{r}_k + \frac{i}{m\omega_k}\hat{p}_k \right) \ . \tag{2.12}$$

Here $\hat{p}$ is the momentum operator. These operators also satisfy the commutator relations

$$[\hat{a}_j, \hat{a}_k^{\dagger}] = \delta_{jk} \ , \tag{2.13}$$

which can be verified via $[\hat{r}_k, \hat{p}_j] = i\hbar\delta_{kj}$. We can now express the Hamiltonian as

$$\hat{H} = \hbar \sum_{k=1}^{D} \omega_k (\hat{a}_k^{\dagger}\hat{a}_k + 1/2) \ , \tag{2.14}$$

with each term in the sum corresponding to one of the Hamiltonians $\hat{H}_k$ in Eq. (2.7), with eigenstates which can be denoted as a tensor product of states $|n_1\rangle_1 ... |n_D\rangle_D$. Considering only one dimension,[2] we see that the state are non-degenerate and so the requirement that $\hat{a}^{\dagger}$ raises the eigenvalue by one [Eq. (2.10)] can be expressed as $\hat{a}^{\dagger}|n\rangle = f(n)|n+1\rangle$. We can determine

[2]Extending to many dimensions just involves noting that $\hat{a}_k|n_j\rangle_j = |n_j\rangle_j \hat{a}_k$ if $j \neq k$.

$f(n)$ by noting that via Eq. (2.13)

$$\langle n|\hat{a}\hat{a}^\dagger|n\rangle = 1 + \langle n|\hat{a}^\dagger\hat{a}|n\rangle \ , \tag{2.15}$$

which implies the important ladder property

$$\hat{a}^\dagger|n\rangle = \sqrt{n+1}|n+1\rangle \ . \tag{2.16a}$$

$$\hat{a}|n\rangle = \sqrt{n}|n\rangle \ . \tag{2.16b}$$

Using this it is possible to construct *all* the eigenstates from the ground state:

$$|n_1\rangle_1 ... |n_D\rangle_D = \frac{(\hat{a}_1^\dagger)^{n_1}}{\sqrt{n_1!}} ... \frac{(\hat{a}_D^\dagger)^{n_D}}{\sqrt{n_D!}}|0\rangle \ . \tag{2.17}$$

Degeneracy of states in symmetrical oscillators

In principle, if all the harmonic oscillator frequencies ω_k are different from one another by an irrational number then no degeneracy is present. However, if any ω_k/ω_j is close to a rational number then approximate degeneracies will need to be accounted for. We consider the simplest situation of $\omega_1 = \omega_2 = \ldots = \omega_D = \omega$, i.e. a spherical (or hyper-spherical in general) oscillator. The degeneracy g_n of states with energy $E_n = (n + D/2)\hbar\omega$ is given by the number of ways to construct the integer n from D non-negative integers (with repetition) [32], and is given by

$$g_n(D) = \binom{D+n-1}{n} = \frac{(D+n-1)!}{n!(D-1)!} \ , \tag{2.18}$$

noting the important physical cases of $D = 2$, $g_n = n + 1$ and $D = 3$, $g_n = (n + 1)(n + 2)/2$ with no degeneracies for $D = 1$. We note this is the same degeneracy as energy levels in a 1D many-body system with N distinguishable particles. The degeneracy for identical particles is discussed later in Sec. 4.2.2.

Summary

We introduced the harmonic oscillator potential and explained its importance within physics. We listed known results about Hamiltonian separability in multi-dimensional oscillators and introduced the ladder operators as tools to understand the system. Finally we noted the high degeneracies of symmetric oscillators, due to the linear spacing of the energy levels.

2.2 Interactions in a cold bose gas

2.2.1 A degenerate bose gas and the critical temperature

As we mentioned in Sec. 1.1.1, we can intuitively describe Bose-Einstein condensation (BEC) by comparing the thermal de-Broglie wavelength [Eq. (1.1)] with the average distance between the atoms, leading to a measure called the phase space density [Eq. (1.2)]. For PSD $\gtrsim 1$ the wavefunctions start to overlap. In a D dimensional system (reduced dimension is discussed in Sec. 2.2.5), with a number density n, this happens when[3]

$$k_B T < \max(n)^{2/D} 2\pi\hbar^2/m \; . \tag{2.19}$$

At this point bosonic spin statistics become important; a many-body wavefunction for N identical bosons must be symmetric with the interchange of any of the coordinates. The effect of this symmetry is to radically change the degeneracy of energy states. A system of N distinguishable particles will have an N-fold degenerate first excited state, with $N-1$ particles in the ground state and particle one, two, three,..., or N in the first excited state, whereas our bose gas only has one. This causes the deviation from the Maxwell-Boltzmann statistics that lead to a phase transition when PSD$\sim \zeta(3/2)$ [34].

This indistinguishably is somewhat counter intuitive but does occur in classical probability. If one asks "A couple has two children, at least one of which

[3]Equation (1.1) for the de-Broglie wavelength is also true for D dimensions, so long as the momentum dispersion relation is the same [33]

is male, what is the probability the other child is male?" the obvious answer appears to be 1/2 however it is in fact 1/3, because the information has only ruled out the possibility of having two girls, leaving the three equally likely outcomes: boy+boy, girl+boy and boy+girl (ordered by date of birth). As more information is available distinguishing the first and second born, such as the boy being born on a Tuesday (leading to a probability of 13/27 for two boys) the probability approaches 1/2.

We do not discuss the thermodynamics extensively here, but note that below some temperature T_c, referred to as the critical/condensation temperature in the literature, a Bose gas will have a macroscopic occupation of the ground state energy level. For a three dimensional Bose gas in a harmonic oscillator potential, we have to leading order in N,

$$T_c = \hbar\omega_{\text{av}}\zeta(3)^{-1/3}N^{1/3}\,, \tag{2.20}$$

with similar expressions for lower dimensional systems [35]. Again to leading order in N, the ground state occupation N_0 in a D dimensional harmonic oscillator in thermal equilibrium is found to be

$$N_0 \sim N[1-(T/T_c)^{\text{D}}]\,. \tag{2.21}$$

For this thesis we consider systems in which the temperature is considered to be low $T \ll T_c$ and as such can be considered to be zero, unless otherwise stated. At a many-body level this statement becomes somewhat ill defined, and so we say that there is no uncertainty in initial conditions and no coupling to any external systems beyond what is explicitly considered.

2.2.2 Scattering theory and the many-body problem

The many body problem in 3D

The most general 3D Hamiltonian describing a system of identical particles, in identical spin states, is given in second quantised form as

$$\hat{H} = \int d\mathbf{r}\, \hat{\Psi}^\dagger(\mathbf{r}) H_0(\mathbf{r}) \hat{\Psi}(\mathbf{r}) + \frac{1}{2} \iint d\mathbf{r} d\mathbf{r}'\, \hat{\Psi}^\dagger(\mathbf{r}') \hat{\Psi}^\dagger(\mathbf{r}) V(\mathbf{r}-\mathbf{r}') \hat{\Psi}(\mathbf{r}) \hat{\Psi}(\mathbf{r}') \tag{2.22}$$

$H_0(\mathbf{r}) = -\hbar^2\nabla^2/2m + V(\mathbf{r})$ contains the kinetic and external potential terms and $V(\mathbf{r}-\mathbf{r}')$ describes the interactions between the particles. In general this interaction potential can be very complicated. Taking a commonly used inter-atomic interaction potential (Van der Waals/Lennard-Jones) $V(r) = -C_6 r^{-6} + C_{12} r^{-12}$, where $r = |\mathbf{r}-\mathbf{r}'|$, this potential would support many bound states and considerably complicate the dynamics (even for a few atoms) and so must be simplified in order to deal with the many-body problem. It is possible to assign an effective range to any potential that falls asymptotically faster than $1/r$ [36], which has been calculated for an atomic potential [37]. However, for low momentum scattering we are interested in the classical turning point of the potential r_0 defined by $V(r_0) = 0$, after which point a relative wavefunction for two atoms with a relative momentum of zero must decay exponentially.

Solving the two body scattering problem in the zero momentum limit

First we wish to solve the two body scattering problem by finding solutions to the Schrödinger equation

$$\left(-\frac{\hbar^2\nabla^2}{m} + V(r) - E\right)\Psi(\mathbf{r}) = 0\,, \tag{2.23}$$

which is obtained by separating the centre-of-mass and relative wavefunctions of two identical particles. Here $\mathbf{r} = \mathbf{r}_1 - \mathbf{r}_2$ and the factor of two is missing from the kinetic energy as we are considering the reduced mass.

An incoming wave $\Psi_{\text{inc}}(\mathbf{r}) = \exp(ik \cdot z)$, with[4] $z = r\cos(\theta)$ and energy $E = \hbar^2 k^2/m$, has the asymptotic scattering wavefunction [34]

$$\Psi(\mathbf{r}) \to \mathrm{e}^{ikr\cos(\theta)} + \frac{\mathrm{e}^{ikr}}{r} f_k(\theta) \; . \tag{2.24}$$

This is valid for $r \gg r_0$ providing that $V(r)$ decreases faster than $1/r$ asymptotically. The function $f_k(\theta)$ is known as the scattering amplitude (with θ the angle between $\mathbf{r}$ and the axis of propagation of the incoming wave). This is related to the scattering cross section σ of two identical particles via

$$d\sigma = |f_k(\theta) \pm f_k(\pi - \theta)|^2 \sin(\theta) d\theta d\phi \; , \tag{2.25}$$

with the $+$ sign taken for Bosons and $0 \leq \theta \leq \pi/2$. For non-identical particles the $\pi - \theta$ term is missing and θ runs up to π. It is also known [38] that $f_k(\theta) \to -a_s$ with a_s a constant as $k \to 0$; as there is no angular dependence the angular momentum quantum number ℓ, is zero and this is a pure s-wave scattering solution. This result is intuitively obvious since, if there is no velocity, direction cannot be an important parameter after scattering.[5] Integrating Eq. (2.25) over the unit of solid angle of the upper half sphere then gives

$$\sigma(k = 0) = 8\pi a_s^2 \; , \tag{2.26}$$

or zero for fermions. Hence identical fermions do not interact via s-wave scattering.

The constant a_s is a highly important quantity called the s-wave scattering length. This quantity is also defined through the scattering phase shift, which can be extended to reduced dimensions [34]

$$\cot(\delta(k)) \to \begin{cases} -(ka_s)^{-1} & \text{In three dimensions} \\ \frac{2}{\pi}\log(ka_{\text{2D}}) & \text{In two dimensions} \\ ka_{\text{1D}} & \text{In one dimension} \; . \end{cases} \tag{2.27}$$

[4] Any direction of propagation can be rotated to the z axis.

[5] Alternatively, one can see that the classical turning point of the centrifugal barrier potential, $V_\ell \propto \ell(\ell+1)/r^2$, tends to infinity as the kinetic energy decreases, unless $\ell = 0$.

Bound state solutions in the scattering spectrum

We also note in passing the case of $E < 0$ solutions, i.e. bound states. These states exist in what are usually referred to as "open channels" in the scattering matrix. Considering again a low energy limit, where the $\ell = 0$ state dominates, we can express the asymptotic wavefunction of a bound state from scattering as

$$\Psi(\mathbf{r}) \to C\frac{\mathrm{e}^{-\kappa r}}{r} \,, \tag{2.28}$$

with κ defined by its relation to the energy $E = -\hbar^2\kappa^2/m$. If this energy is large, then for any $r \gg r_0$ (the asymptotic region), this wavefunction is already small and this bound state has little effect on the scattering length of the potential. However, if a bound state is present with a small energy, satisfying

$$|E| < \frac{\hbar^2}{m r_0^2} \,, \tag{2.29}$$

then the wavefunction will have a large penetration to the asymptotic region. If this is the case then one can identify $\kappa = k\cot(\delta_0)$ and so $\kappa \to -1/a_s$ and $f = 1/(\kappa + ik)$ in the $k \to 0$ limit [34]. The presence of a close-to-threshold bound state leads to a divergence in the scattering length of the form $a_s \sim \hbar/\sqrt{m|E|}$ and to the scattering cross section diverges as $\sigma \sim 1/(mE/\hbar^2 + k^2)$. This phenomenon is known as a Feshbach resonance [39].

Weak interactions in the uniform Bose gas

Interactions between atoms in a Bose gas will modify the ground state of a many-body system such that it is no longer uncorrelated. However, for weak repulsive interactions and large numbers of atoms, these correlations are likely to be minor, and can be added into the theory. For the case of a uniform Bose gas, free from external potentials, in a periodic box of volume V, we can expand $\hat{\Psi}(\mathbf{r})$ in Eq. (2.22) over momentum space

$$\hat{\Psi}(\mathbf{r}) = \sum_{\mathbf{p}} \frac{1}{\sqrt{V}} \hat{c}_{\mathbf{p}} e^{i\mathbf{p}\cdot\mathbf{r}/\hbar} \,. \tag{2.30}$$

In the limit $N_0 \to \infty$ we need only consider interactions between atoms in the zero momentum state; the matrix element $V_0 = \langle 0|\hat{V}|0\rangle$ can be computed

via the second Born approximation (see for example [40]) to be

$$V_0 = g_{3\mathrm{D}} + \frac{g_{3\mathrm{D}}^2}{V}\sum_{\mathbf{p}\neq 0}\frac{m}{\mathbf{p}^2} + \mathcal{O}(g_{3\mathrm{D}}^3)\,. \tag{2.31}$$

where we have introduced the interaction coupling parameter

$$g_{3\mathrm{D}} = \frac{4\pi\hbar^2 a_s}{m}\,. \tag{2.32}$$

If we take $1/N_0$ and na_s^3 to be small parameters and take $T = 0$, we can set $\hat{c}_0 = N_0$ (equivalent to ignoring the commutation relation with its complex conjugate) and derive expression for bulk properties in the condensate [34], including the pressure: $P = g_{3\mathrm{D}}n^2/2$ and sound velocity: $c = \sqrt{g_{3\mathrm{D}}n/m}$. Using the order $g_{3\mathrm{D}}^2$ approximations for V_0 in Eq. (2.31), Bogoliubov showed that the Hamiltonian could be put into the diagonalised form in terms of quasi particles, with energies [41]

$$\epsilon(p) = \sqrt{\frac{g_{3\mathrm{D}}np^2}{m} + \left(\frac{p^2}{2m}\right)^2}\,. \tag{2.33}$$

The final point we note on the weakly repulsive uniform gas is that if $|p| \ll mc$ (with c the sound velocity), then we have a phonon like relation $\epsilon(p) \sim pc$ and if $|p| \gg mc$ we have $\epsilon(p) \sim p^2/2m + ng_{3\mathrm{D}}$, a free particle like relation. This transition can be characterised by a momentum $p = \hbar/\xi$, at which the mean field interaction energy $ng_{3\mathrm{D}}$ and kinetic energy $p^2/2m$ are equal, with the length scale

$$\xi = \sqrt{\frac{\hbar^2}{2m|g_{3\mathrm{D}}|n}} = \frac{1}{\sqrt{2}}\frac{\hbar}{mc}\,, \tag{2.34}$$

often called the healing/correlation length. This is an important length, characterising scales on which the condensate can recover coherence after changes. It is essentially independent of the dimensions as the number density is rescaled by the same amount as the effective coupling parameter. It is also applicable in non-uniform condensates, where n can be taken as a peak or background density. Alternatively it is sometimes preferable to take a the local density in which case we refer to $\xi(\mathbf{r})$ as a local healing length. The background healing length determines the critical angular velocities for the

formation of vortices, and, up to a relativistic-like correction, the length of dark solitons [see Eq. (3.6)]. The peak healing length determines the condition for the Thomas-Fermi regime in repulsive condensates ($\nabla^2\sqrt{n} \ll \sqrt{n}/\xi(0)^2$ such that the quantum pressure can be neglected) and the bright soliton length [see Eq. (3.3)].

2.2.3 The contact scattering pseudo potential

In the dilute gas limit (satisfying $na_s^3 \ll 1$), scattering events between atoms will be dominated by 2-body events. At extremely low temperature these events will also be equivalent to $k \to 0$ limit. Therefore it is possible to replace the real interaction potential with one that gives the correct asymptotic scattering properties in the zero wavevector limit [42]. Denoting, $r = ||\mathbf{r}-\mathbf{r}'||$ the potential used is [6]

$$\begin{aligned} V(\mathbf{r}-\mathbf{r}') &= g_{3\mathrm{D}}\delta(\mathbf{r}-\mathbf{r}')\frac{\partial}{\partial r}r \\ &= g_{3\mathrm{D}}\frac{\delta(r)}{4\pi r^2}\frac{\partial}{\partial r}r \end{aligned} \tag{2.35}$$

where $g_{3\mathrm{D}}$ is the coupling parameter given in Eq. (2.32). This potential is often referred to as the Fermi-Huang pseudo potential. The $\frac{\partial}{\partial r}r$ term regularises any divergences of the wavefunction that are of the form $A(\mathbf{r}+\mathbf{r}')/r$, where $A(\mathbf{r})$ is a function that is non divergent. If $a_s > 0$, then this renormalized potential permits bound states between pairs of atoms with a reduced mass $\mu = m_1m_2/(m_1+m_2)$ of depth $E = -1/2\mu a_s^2$, even as the scattering cross section tends to zero. Several very deep molecular bound states usually exist for atomic scattering potentials, but a zero width potential can only support one. Interestingly recent work has shown this potential can be explicitly represented in Fourier space [43, 44]:

$$\delta(\mathbf{r})\frac{\partial}{\partial r}\left[r\exp(i\mathbf{r}\cdot\mathbf{k})\right] = \delta(\mathbf{r})\left[1-\frac{\delta(1/k)}{k}\right], \tag{2.36}$$

[6] This also requires that the effective range of the potential is much less than the average atomic separation, which is typically not the case for atoms such as Chromium, which posses strong dipolar interactions, scaling as r^{-3}.

hence the attractive component for $g_{3D} > 0$ applies if the occupation of states with $k \to \infty$ drop only as $1/k$.

If one ignores this regularisation term, an approach generally valid for a large number of atoms, we have $V(\mathbf{r} - \mathbf{r}') = g_{3D}\delta(\mathbf{r} - \mathbf{r}')$. This potential always has the same sign as g_{3D} and so positive (negative) a_s will mean repulsive (attractive) interactions between atoms. The Hamiltonian can now be simplified to

$$\hat{H} = \int d\mathbf{r}\, \hat{\Psi}^\dagger(\mathbf{r}) H_0(\mathbf{r}) \hat{\Psi}(\mathbf{r}) + \frac{g_{3D}}{2} \int d\mathbf{r}\, \hat{\Psi}^\dagger(\mathbf{r}) \hat{\Psi}^\dagger(\mathbf{r}) \hat{\Psi}(\mathbf{r}) \hat{\Psi}(\mathbf{r}) \,. \tag{2.37}$$

The removal of the regularisation does introduce some pathologies, such as the ultra-violet divergences in the anomalous average [45], which occurs in beyond mean-field treatments. Most relevant to this work is the lack of a global energy minimum at the mean field level if $a_s < 0$, which we will discuss in Sec. 2.3.4.

2.2.4 Transformation to first quantisation

We can transform our second quantised Hamiltonian into a first quantised Hamiltonian by considering its action on an arbitrary state ket in Fock space, defined via the vacuum state $|0\rangle$ and

$$|\psi\rangle = \sum_n \frac{a_n}{\sqrt{n!}} \int_{-\infty}^{\infty} \dots \int_{-\infty}^{\infty} \psi_n(\vec{\mathbf{r}}, t) \prod_{i=1}^{n} \hat{\Psi}^\dagger(\mathbf{r}_i) d\mathbf{r}_\mathrm{i} |0\rangle. \tag{2.38}$$

We use $\vec{x}$ to denote a set of particle coordinates $\{x_1, x_2, \dots, x_n\}$, in order to distinguish it from $\mathbf{r}$, which is used for vectors of spatial coordinates. Hence used together $\vec{\mathbf{r}} = \{\mathbf{r}_1, \dots, \mathbf{r}_n\}$ denotes a set of coordinates which are spatial vectors. This distinction is import for symmetrisation of many-body wavefunctions. The wave function and coefficients in Eq. (2.38) satisfy appropriate normalisation conditions

$$\Sigma_n |a_n|^2 = 1, \qquad \iint_{-\infty}^{\infty} |\psi_n(\vec{\mathbf{r}}, t)|^2 d\mathbf{r}_1 ... d\mathbf{r}_n = 1. \tag{2.39}$$

For most of our purposes however we will assume a definite number of atoms and hence $a_n = \delta_{N,n}$.

2.2.5 Scattering in strong transverse confinement

The Lieb–Liniger model of a 1D gas [20] with contact interactions $V(x_k - x_j) \propto \delta(x_k - x_j)$ is not immediately applicable to a three-dimensional state. In the presence of strong radial harmonic confinement, we can assume the radial degrees of freedom of all the atoms in the system are in the ground state of this external potential, as the interactions are too weak to change this. With this assumption, the radial degree of freedom of our many-body wavefunction is described by a product state $\Psi(\mathbf{r}_1, \ldots, \mathbf{r}_N) = \Psi(\vec{x}) \prod_k \phi_{0,0}(\rho_k)$ with $\rho_k = \sqrt{y_k^2 + z_k^2}$ and integrate the interaction terms (ignoring the regularisation) over the radial degrees of freedom. In the two body case this gives

$$\begin{aligned}
&\iint_{-\infty}^{\infty} dy_1 dy_2 dz_1 dz_2 \frac{\mathrm{e}^{-(y_1^2+z_1^2)/a_\perp^2}}{\pi a_\perp^2} \frac{\mathrm{e}^{-(y_2^2+z_2^2)/a_\perp^2}}{\pi a_\perp^2} g_{3\mathrm{D}} \delta(\mathbf{r}_1 - \mathbf{r}_2) \\
=& g_{3\mathrm{D}} \delta(x_1 - x_2) \int_{-\infty}^{\infty} dy_1 \int_{-\infty}^{\infty} dz_1 \frac{\mathrm{e}^{-(y_1^2+z_1^2)/a_\perp^2}}{\pi^2 a_\perp^4} \\
=& \frac{g_{3\mathrm{D}}}{2\pi a_\perp^2} \delta(x_1 - x_2) \,,
\end{aligned} \tag{2.40}$$

the many body case just includes $N(N-1)/2$ terms with an identical coefficient.

A more rigorous derivation by Olshanii [46] looks at the two-body scattering problem with the regularised contact potential in the presence of strong harmonic confinement, using the regularised interaction pseudo potential given by Eq. (2.36). This method assumes the incoming scattering states are in the ground state of a radial harmonic oscillator potential and have a relative kinetic energy which is less than the excitation energy to the first radially symmetric excited state ($2\hbar\omega_\perp$). This assumption means that outside of the range of the interaction potential (which is zero) the occupation of radial excited states by the outgoing scattering states must decay exponentially with the separation. Hence for an incoming scattering state of wavevector k_x the

outgoing scattering state is given asymptotically by

$$\Psi_{\text{asym}}(x,\rho) = \frac{\exp\left(-\rho^2/2a_\perp^2\right)}{\pi a_\perp}\left[\mathrm{e}^{ik_x x} + f_{\text{even}}\mathrm{e}^{ik_x|x|} + f_{\text{odd}}\text{sgn}(x)\mathrm{e}^{ik_x|x|}\right] , \tag{2.41}$$

with $f_{\text{odd}} = 0$ by Bose symmetry. Due to the continuity of the wavefunction, we can fix f_{even} by meshing the asymptotic expression [Eq. (2.41)] with boundary condition at the origin, set by $V(r)$ [Eq. (2.36)]. This leads to

$$f_{\text{even}} = -\frac{1}{1 + ik_x a_{1D} + \mathcal{O}(k_x a_\perp)^3} , \tag{2.42}$$

where we have introduced the 1D scattering length

$$a_{1D} = \frac{a_\perp}{a_s}\left(1 - \zeta(1/2)\frac{a_s}{a_\perp}\right) , \tag{2.43}$$

which satisfies Eq. (2.27). We note a_{1D} diverges as $a_s \to a_\perp/\zeta(1/2)$ and tends to a constant $a_{1D} \to -\zeta(1/2)$ as $|a_s| \to \infty$ (essentially shifting the position of Feshbach resonances). Intuitively this can be understood as being due to the coupling between the bound state of the scattering pseudo potential, with energy $\hbar^2/ma_s^2$, and the ground state of the trapping potential, with energy $\hbar\omega = \hbar^2/ma_\perp^2$.

The scattering amplitude [Eq. (2.42)] is known to be reproduced in the limit of $k_x \to 0$ by a contact pseudo-potential of the form [46]

$$V(x) = \frac{\hbar^2}{\mu a_{1D}}\delta(x) \sim \delta(x)\left[\frac{g_{3d}}{\pi a_\perp^2} + O\left(\frac{a_s}{a_\perp}\right)\right] , \tag{2.44}$$

which reduces to Eq. (2.40) if $|a_s| \ll a_\perp$.

Summary

We discussed the zero momentum limit of two-body scattering processes and how this lead to pure s-wave scattering, along with possible Feshbach resonances if a close-to-threshold bound state was present. We then noted how bulk properties of a uniform Bose gas could be derived at $T = 0$ and in the case of weak interactions, leading to the definition of the healing length as an important scale. Finally we introduced the interaction pseudo potential

to simplify the many-body Hamiltonian, and results for scattering in strong radial harmonic confinement.

2.3 Derivation of the Gross Pitaevskii equation

2.3.1 The Onsager-Penrose condition and off-diagonal long range order

In order to define Bose-Einstein condensation for systems that are interacting, we will need to generalise the notion of the macroscopically occupied lowest single particle eigenstate. For a weakly interacting condensate, we can consider any particles not in the ground state mode to be "non-condensate" atoms, often referred to as a quantum depletion. This criterion is less useful for more strongly interacting systems. For example, the ground state of repulsive atoms in a weak harmonic potential [$\max(n)g_{3\mathrm{D}} \gg \hbar\omega$] form a Thomas Fermi profile [34]. This density profile is much wider than the non-interacting ground state of the trap. Equally an attractive system will have a density profile which is much narrower than the ground state. In both cases one can show the occupation of the lowest mode of the harmonic oscillator is not significantly higher than any other, but both can be well described by a mean field approximation, indicating there is still macroscopic coherence. A more general criterion was devised in terms of the trace of the system's single body density matrix over all but one of the degrees of freedom [47]. This work lead to the general criterion in terms of the first order spatial correlation function [4]

$$g^{(1)}(\mathbf{r},\mathbf{r}') = \frac{\langle\hat{\Psi}(\mathbf{r})^\dagger\hat{\Psi}(\mathbf{r}')\rangle}{\sqrt{\langle\hat{\Psi}(\mathbf{r})^\dagger\hat{\Psi}(\mathbf{r})\rangle\langle\hat{\Psi}(\mathbf{r}')^\dagger\hat{\Psi}(\mathbf{r}')\rangle}} \to \frac{N_c}{N} \quad \text{as } |\mathbf{r}-\mathbf{r}'| \to \infty\ , \tag{2.45}$$

with N_c/N a finite fraction as $N \to \infty$, which is referred to as "off-diagonal long range order." This can also be expressed via eigenvalue decompositions of the single-body-density matrix (the top half of the fraction in Eq. (2.45))

$$\rho(\mathbf{r},\mathbf{r}',t) \equiv \langle\hat{\Psi}(\mathbf{r})^\dagger\hat{\Psi}(\mathbf{r}')\rangle = N_c\phi(\mathbf{r})^*\phi(\mathbf{r}') + \mathcal{O}(1/N)\ , \tag{2.46}$$

i.e. that it has one large eigenvalue with all others a small fraction of the total number of atoms. This forms the condition of validity for the GPE and the condensate number, where the maximally occupied state corresponds to the condensate wavefunction.

2.3.2 The Hartree product state

There are a number of possible way to derive the Gross-Pitaevskii equation (GPE) from Eq. (2.37). One method, most useful at $T = 0$, is to assume the many-body wavefunction is in Hartree product form, such that all atomic wavefunctions are exactly the same:

$$\psi_N(\mathbf{r}_1, ..., \mathbf{r}_N, t) = \prod_{j=1}^{N} \phi(\mathbf{r}_j, t) \ . \tag{2.47}$$

Such a wavefunction has many simple properties. The field operator takes the form $\hat{\Psi}(\mathbf{r}) = \hat{c}\phi(\mathbf{r})$ where $\hat{c}$ is an annihilation operator for a boson in that mode. The one body density matrix, defined in Eq. (2.46), simplifies to the form

$$\rho(\mathbf{r}, \mathbf{r}', t) = N\phi^*(\mathbf{r}, t)\phi(\mathbf{r}', t) \ , \tag{2.48}$$

and hence the density matrix of state ψ_N [Eq. (2.47)] has one large eigenvalue equal to N, the total number of atoms, and is thus totally condensed by the condition Eq. (2.46). Using this ansatz for the many-body wavefunction we can calculate the time evolution from the action functional derived from the Hamiltonian (2.37) and the wavefunction ψ_N:

$$S = N \int d\mathbf{r} \left\{ \phi^*(\mathbf{r}, t) \left[i\hbar \frac{\partial}{\partial t} - H_0(\mathbf{r}) \right] \phi(\mathbf{r}, t) - \frac{(N-1)g_{3\mathrm{D}}}{2} |\phi(\mathbf{r}, t)|^4 \right\} \ . \tag{2.49}$$

Extremising this action with respect to variations in $\phi^*(\mathbf{r}, t)$ then gives [48]

$$i\hbar \frac{\partial}{\partial t} \phi(\mathbf{r}, t) = H_0 \phi(\mathbf{r}, t) + g_{3\mathrm{D}}(N-1)|\phi(\mathbf{r}, t)|^2 \ . \tag{2.50}$$

The prefactor $(N-1)$ of the nonlinear term differs from that of the usual GPE found in the literature in which this factor is N. However, the validity

is only to order $1/\sqrt{N}$ and so this is not unexpected or inconsistent. In either case, the GPE tends to an exact description as $N \to \infty$ while $g_{1\mathrm{D}}N$ is held constant [49, 50]. The discrepancy is partly due to the way a Hartree product ansatz breaks the translational symmetry. If the centre-of-mass dynamics decouple from the interactions we can consider subtracting this energy from the Hamiltonian, which would reproduce the usual factor of N, which we show later in Sec. 5.2.

The Hartree-product method has the advantage of giving a tangible many-body wavefunction. It is found to work well at describing the physics of the system for systems with a high condensate fraction/weak correlation at zero temperature and can be extended to include occupation of multiple single particle wavefunctions via the multi-configuration time dependent Hartree method for Bosons (MCTDHFB) [51]. Without this extension, the theory is found to break down in the cases of high condensate depletion and in situations like double well potentials [52], where many body effects are present.

2.3.3 Decomposition of the field operator

Alternatively, we can consider the Heisenberg equation of motion for the field operator. As $\hat{\Psi}(\mathbf{r})$ is not explicitly time dependent, this can be written as

$$i\hbar\frac{d}{dt}\hat{\Psi}(\mathbf{r}) = [\hat{H}, \hat{\Psi}(\mathbf{r})] \,, \tag{2.51}$$

with the Hamiltonian (2.37). Using the bosonic commutation relation $[\hat{\Psi}^\dagger(\mathbf{r}), \hat{\Psi}(\mathbf{r}')] = \delta(\mathbf{r}-\mathbf{r}')$, we can simplify this equation to

$$i\hbar\frac{d}{dt}\hat{\Psi}(\mathbf{r}) = \left[H_0 + g_{3\mathrm{D}}\hat{\Psi}^\dagger(\mathbf{r})\hat{\Psi}(\mathbf{r})\right]\hat{\Psi}(\mathbf{r}) \,. \tag{2.52}$$

This is still a fully quantum mechanical equation, in order to simplify this to a classical field equation, (the GPE), we need to make an approximation. This is usually achieved by breaking the $U(1)$ symmetry, i.e. assuming our state has an indefinite number of atoms such that $\langle\hat{\Psi}\rangle = \sqrt{N_c} \neq 0$, with N_c the number of condensate atoms, and assuming all fluctuations about this

mean value are small [34]

$$\hat{\Psi}(\mathbf{r}) = \langle\hat{\Psi}(\mathbf{r})\rangle + (\hat{\Psi}(\mathbf{r}) - \langle\hat{\Psi}(\mathbf{r})\rangle) \equiv \sqrt{N_c}\Psi(\mathbf{r}) + \delta\hat{\psi}(\mathbf{r}) \ . \tag{2.53}$$

The operator $\delta\hat{\psi}(\mathbf{r})$ is assumed to have an expectation value of zero and we have taken $\Psi(\mathbf{r})$ to be normalised to unity. This is often called the Bogoliubov ansatz. Alternatively, one can also expand $\hat{\Psi}(\mathbf{r})$ into condensate and (small fluctuation) non condensate parts in a number conserving way [50]

$$\hat{\Psi}(\mathbf{r}) = \hat{c}\Psi^{(\mathrm{nc})}(\mathbf{r}) + \delta^{(\mathrm{nc})}\hat{\psi}(\mathbf{r}) \ . \tag{2.54}$$

Here $\hat{c}$ is an annihilation operator for a quantum in the condensate mode. This approaches assumes that there is one large eigenvalue $N_c \approx N \gg 1$ to the density matrix, with its eigenvalue relating to the population of the condensate atoms and corresponding eigenstate to the wavefunction.

Taking Eq. (2.52) to lowest order in either fluctuation operator results in the usual Gross Pitaevskii equation [53, 54] (GPE), valid to order $1/\sqrt{N_c}$:

$$i\hbar\frac{d}{dt}\Psi(\mathbf{r}) = \left[H_0 + N_c g_{3\mathrm{D}}|\Psi(\mathbf{r})|^2\right]\Psi(\mathbf{r}) \ . \tag{2.55}$$

This mean field equation is the workhorse of the majority of BEC physics. It is a type of nonlinear Schrödinger equation which is also used in other areas of physics such as nonlinear optics. In both the number conserving and symmetry breaking cases, the non-condensate dynamics are contained in the small fluctuation operator $\delta\hat{\psi}(\mathbf{r})$. Various expansions to higher orders in the fluctuation operator exist in both the number conserving [50] and symmetry breaking formalisms, allowing for the derivation of quantities like the sound velocity within the condensate, and the properties of collective excitations in a similar way to Sec. 2.2.2. However, $U(1)$ symmetry breaking expansions can show some non-physical pathologies in driven systems [55].

An important point about the GPE is that the time dependence of a stationary state (evolving only in phase) is governed by the chemical potential. In the symmetry breaking formulation, Eq. (2.53) implies that $\langle\hat{\Psi}(\mathbf{r})\rangle = \sqrt{N_c}\Psi(\mathbf{r})$,[7] this means that state with n particles is qualitatively

[7] Whereas for a number conserving derivation this expectation value would be identically

similar to a state with $n-1$ particles. This condition is satisfied for a Poissonian distribution of atom number, i.e. a coherent state

$$|N_c\rangle_\Psi = \exp\left(-\frac{|N_c|^2}{2}\right)\sum_{n=0}^{\infty}\frac{N_c^n}{\sqrt{n!}}|n\rangle \ , \tag{2.56a}$$

$$\hat{c}|N_c\rangle_\Psi = \sqrt{N_C}|N_c\rangle_\Psi \ . \tag{2.56b}$$

This would well describe a BEC coupled to an infinite thermal bath, with which it can exchange particles (grand canonical ensemble), resulting in an uncertainty in the number of condensate atoms. Assuming $N_c \gg 1$ we can treat the creation and annihilation operators as numbers, i.e. $\hat{c} \approx \sqrt{N_c}$, $\hat{c}^\dagger \approx \sqrt{N_c+1}$ and ignore any commutators. Averaging over states with time dependence of the form $e^{-iE(n)t/\hbar}$ then gives time dependence of the order parameter/single particle wavefunction of the GPE

$$\Psi(\mathbf{r},t) = \Psi(\mathbf{r})e^{-i\mu t/\hbar} \ , \tag{2.57}$$

where $\mu = E(N_C) - E(N_C-1)$ is the chemical potential of the system.

For what follows we will denote $N_C = N$ as we do not explicitly consider condensate depletion.

2.3.4 Condensate Collapse with attractive interactions

Lack of global energy minimum with the GPE model

Introducing attractive interactions also introduce new physics. Unlike their repulsive counterparts, attractive condensates are inherently unstable to collapse. With experimental considerations in mind, we consider the energy (with the Gross-Pitaevskii theory) of a condensate in a D dimensional symmetric harmonic trap (or in reality a cylindrical symmetric prolate trap with $3-D$ directions having extremely strong confinement compared to the other D, which we discuss in detail in 2.4) with an orbital $\Psi(\mathbf{r}) = L^{D/2}f(\mathbf{r}/L)$, with a variational length L and with $\mathbf{r}$ a radial coordinate for the appropri-

zero.

ate number of dimensions:

$$E = N \int d\mathbf{r} \left\{ L^{-D} f^*(\mathbf{r}/L) \left[-\frac{\hbar^2 \nabla^2}{2m} + \frac{m\omega^2 \mathbf{r}^2}{2} \right] f(\mathbf{r}/L) + L^{-2D} \frac{N g_{3\mathrm{D}}}{2} |f(\mathbf{r}/L)|^4 \right\}$$
$$= f_1 L^{-2} + f_2 L^2 + g_{3\mathrm{D}} f_3 L^{-D} \,. \tag{2.58}$$

Here all the function $f_k > 0$ are positive and $f_3 \propto N$, with values dependent on the definition of $f(\mathbf{r})$. For $D = 1$, we can differentiate Eq. (2.58) with respect to L and set the result equal to zero to find a finite value of L which minimises the energy, such as was considered in [56]. In the case of zero trapping ($f_2 = 0$) and $g_{3\mathrm{D}} < 0$, the minimising length scales inversely with the interaction strength: $L = 2f_1/|g_{3\mathrm{D}}|f_3$. In $D = 2$ an energy minimum exists[8], provided $f_1 + g_{3\mathrm{D}} f_3 > 0$, at $L = [f_2/(f_1 + g_{3\mathrm{D}} f_3)]^{1/4}$. However, it is clear that for $g_{3\mathrm{D}} < 0$ and $D = 3$, as $L \to 0$ the $g_{3\mathrm{D}} f_3 L^{-3}$ term dominates. As such we have $E \to -\infty$, and hence no finite width ground state.

In reality, below a certain L the GPE is not an adequate description of the system. Significant three-body effects leading to molecule formation and the repulsive components of the scattering potential begin to play a significant role. Arguments based around the GPE predict large ($N \gg 1$) attractive condensates will either disperse (without confinement) or undergo a phase transition to a solid or liquid phase [57]. This is hard to envisage in any realistic experimental scenario. What is usually observed is a collapse followed by expansion, possibly repeating several times, accompanied with jets of atoms [11–14].

Some theoretical work has been done to examine ways to make attractive condensates stable to collapse, such as introducing angular momentum [58, 59], and using Bose-Fermi mixtures with repulsive p-wave scattering [60].

Existence of local energy minima

Despite the lack of a finite global energy minimum in 3D, attractive condensates can exist in quasi-stable local energy minima, provided the number of atoms is below a critical value, which depends on a_s and external potentials. Within a harmonic confining potential, it is found that a stable

[8] Note that if $f_1 + g_{3\mathrm{D}} f_3 < 0$ then there is not even a local minimum.

local-minimum exists if

$$\Upsilon_{3\mathrm{D}} := \frac{N|a_s|}{(a_x a_y a_z)^{1/3}} < k_c \,, \tag{2.59}$$

with $a_x = \sqrt{\hbar/m\omega_x}$ the harmonic oscillator length in that direction and where k_c is a parameter depending on the trapping geometry; if $a_x = a_y = a_z$ we have $k_c \approx 0.5746$ [61] otherwise k_c is smaller than this value. A list of values has been calculated in [61] for radially symmetric traps. In Sec. 3.2.4 we show that this stability condition is relevant even when one of the trapping widths tends to zero. To match Eq. (2.59) up with this extreme 1D case we can take $a_y = a_z = \lambda a_x \equiv a_\perp$ and obtain

$$\Upsilon := \frac{N|a_s|}{a_\perp} < \lambda^{1/3} k_c \,, \tag{2.60}$$

and note this implies $k_c \sim \lambda^{-1/3} k_{1\mathrm{D}}$ as $\lambda \to 0$, with $k_{1\mathrm{D}} \lesssim 2/3$. We will refer to the left hand of Eq. (2.59), $\Upsilon_{3\mathrm{D}}$, as the "3D collapse parameter" and k_c as the "3D critical value", and their one-dimensional analogues in Eq. (2.60) as the collapse parameter and critical value, since these are more important for this work.

Summary

This section discussed off-diagonal long range order and a general criterion for Bose-Einstein condensation in terms of the single-body density matrix and its eigenvalues. Two derivations of the GPE were included, firstly using Hartree product ansatz for the many-body wavefunction and secondly expanding the field operator in terms of condensate and fluctuation components. Finally we investigated the lack of a global energy minimum in attractive condensates within the GPE model, and the importance of metastable local energy minima.

2.4 Reduction of dynamics to 1D, regimes of different approximate models

Dynamics in a particular dimension can be "frozen out" by confining them on length scales much smaller than the healing length [ξ in Eq. (2.34)]. In the case of cylindrically symmetric traps, the radial trapping strength can be increased in order to freeze out atomic dynamics in these directions; the wavefunction in these directions (for cold atoms) will essentially look like the ground state wavefunction of the trap. We noted in Sec. 2.1.1 that most potentials look harmonic near the minima, for example a Gaussian potential from a focused, red-detuned laser:

$$V(\rho) = V_0 \exp\left(-\frac{\rho^2}{L^2}\right) . \tag{2.61}$$

Taylor expansion of Eq. (2.61) up to second order: $V(\rho) = V_0(1-\rho^2/2L^2+..)$ means we can associate a harmonic oscillator frequency $\omega_\perp^2 = V_0/mL^2$ and length $a_\perp = \sqrt{\hbar/m\omega}$, so long as $L \gg a_\perp$.

With this as a justification, we specialise to the case where trapping in the radial directions can be considered harmonic, hence we take

$$V(\mathbf{r}) = V(x) + \frac{m\omega_\perp^2(y^2+z^2)}{2} , \tag{2.62}$$

with $V(x)$ potentially any axial potential. We consider two regimes, based on whether or not the nonlinear interaction is much smaller than the energy gap between the ground and first excited state of the radial potential, i.e. if the condition

$$\hbar\omega_r \gg N g_{3\mathrm{D}} \max(|\Psi(\mathbf{r})|^2) , \tag{2.63}$$

is satisfied. Expressed in terms of the peak healing length, this condition is $\xi \gg a_\perp$. The first regime relies on Eq. (2.63) being satisfied, the latter only requires $\xi \gtrsim a_\perp$. We noted when minimising Eq. (2.58) that the ground state width (and therefore peak density) for an attractive condensate with no trapping scaled inversely (linearly) with $Ng_{3\mathrm{D}}$, hence for Eq. (2.63) to be satisfied for an attractive ground state we require $\Upsilon \ll 1$.

2.4.1 Completely 1D: wavefunction fully separable into radial and axial components

Derivation of the 1D GPE

The simplest 1D reduction assumes the wavefunction is separable into an axial wavefunction [as we did for Eq. (2.40)], which contains all the dynamics of interest, and a radial component which is a ground state of the radial potential. This is assumption is valid when the condition (2.63) is satisfied. It is then possible to decompose the wavefunction as $\Psi(\mathbf{r}) = \psi(x)\phi(y,z)$ in much the same way as was used to derive Eq. (2.40), with

$$\phi(y,z) = (a_\perp^2\pi)^{-1/4}\exp\left(-\frac{y^2+z^2}{2a_\perp^2}\right) \tag{2.64}$$

where $a_\perp^2 = \hbar/(m\omega_\perp)$ is the radial harmonic oscillator length or zero point oscillation amplitude. It is then possible to integrate the GPE [Eq. (2.55)] over $dydz$ and obtain a 1D equation.

$$i\hbar\frac{\partial}{\partial t}\psi(x,t) = \left\{-\frac{\hbar^2}{2m}\frac{\partial^2}{\partial x^2} + V(x) + \hbar\omega_\perp[2a_sN|\psi(x,t)|^2+1]\right\}\psi(x,t) \tag{2.65}$$

To simplify Eq. (2.65), we can rescale the global phase evolution (equivalent to shifting the zero point energy) via $\psi(x,t) = \tilde{\psi}(x,t)\exp(-it\omega_\perp)$ to cancel the factor of $\hbar\omega_\perp$ and define a 1D coupling parameter as

$$g_{1\mathrm{D}} = 2\hbar\omega_\perp a_s\ . \tag{2.66}$$

In the case $V(x) = 0$, Eq. (2.65) then reduces to the nonlinear Schrödinger (NLSE):

$$i\hbar\frac{\partial}{\partial t}\tilde{\psi}(x,t) = -\frac{\hbar^2}{2m}\frac{\partial^2}{\partial x^2}\tilde{\psi}(x,t) + Ng_{1\mathrm{D}}|\tilde{\psi}(x,t)|^2\tilde{\psi}(x,t)\ . \tag{2.67}$$

1D ground states in harmonic confinement

It is experimentally relevant to consider $V(x) = m\omega_x^2 x^2/2$, and characterise the ground states of Eq. (2.65) for a given Ng_{1D} and ω_x. This is motivated both in understanding imaging data and optimising ramps (continuous modification) of the scattering length and axial trapping frequency to achieve adiabatic transition from a strongly trapped, repulsive condensate, to a weakly trapped, attractive condensate. We do not explicitly calculate adiabatic timescales here, but note that intuitively the best ramps should be those that minimise changes to the shape of the ground state.

We first note that ground state solutions exist in three limits, which we can express in terms of the healing length ξ [Eq. (2.34)] and the zero point harmonic oscillator length $a_x = \sqrt{\hbar/m\omega_x}$. The weak interacting limit, $\xi \gg a_x$, is solved by an ordinary Gaussian, $|\psi|^2 = \exp(-x^2/a_x^2)/a_x\pi^{1/2}$. The strongly interacting limit $\xi \ll a_x$ has two solutions; for $g_{1D} > 0$ we can neglect the kinetic energy term in Eq. (2.65), resulting in a Thomas-Fermi profile [34]

$$|\psi_{TF}|^2 = \frac{\max(2\mu - m\omega^2 x^2, 0)}{2Ng_{1D}}\,, \tag{2.68}$$

with $\mu = (9m\omega^2 N^2 g_{1D}^2/32)^{1/3}$ set by the normalisation. The standard deviation ($\sigma = \langle x^2 \rangle$) of this solutions scales as $(Ng_{1D}/m\omega^2)^{1/3}$. For $g_{1D} < 0$, the ground state will be far more narrow than a_x, and thus we can neglect the potential to get Eq. (2.67), the solution of which is a bright soliton, given later in Eq. (3.3). In both strongly interacting cases this approximation does not apply in the wings, where the local density (and thus local healing length) tends to zero, hence the asymptotic decay will always be Gaussian.

We numerically solve Eq. (2.65) for parameters relevant for the Durham ^{85}Rb experiment [62], using the numerical method outlined later in Sec. 5.4.4. Additionally to the standard deviation, we plot the excess kurtosis, $\gamma_2 = \langle x^4 \rangle/\sigma^2 - 3$ of the ground state functions in Fig. 2.1. The reason for considering the Kurtosis, is that it can be used to identify the type of ground state we see, as it is independent of the width. For the three extreme cases of the Thomas-Fermi profile, Gaussian and bright soliton we have $\gamma_2 = -6/7, 0, 6/5$ respectively; intermediate states will transition to these values slowly, as the

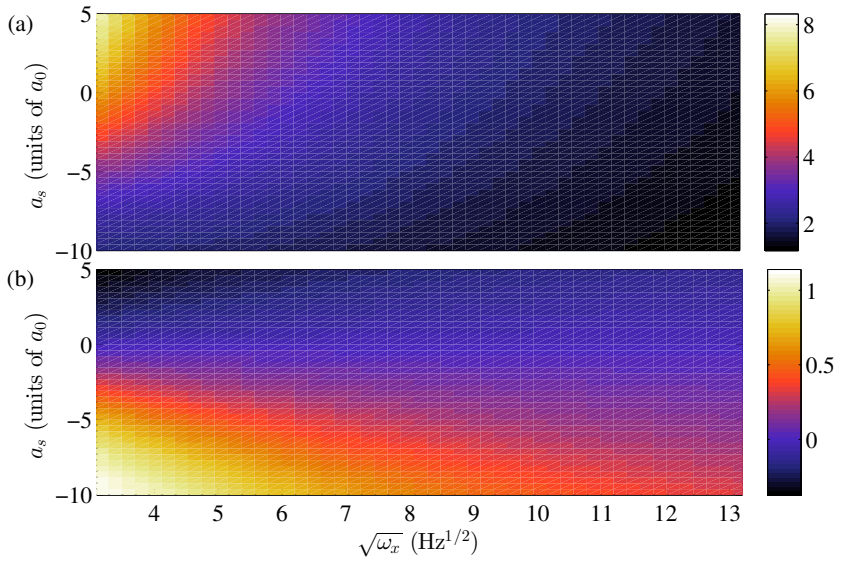

Figure 2.1: (a) Ground state widths (in μm), (b) Kurtosis, for a range of axial trapping frequency ω_x and scattering lengths, given in units of a_0, the Bohr radius. We plot the square root of ω_x to better demonstrate the behaviour at low values, ω_x runs from $2\pi \times 1.5$Hz to $2\pi \times 28$Hz. The other parameters used are $\omega_\perp = 2\pi \times \sqrt{28 \times 39}$Hz with 3000 atoms of ^{85}Rb.

ground state becomes more and more peaked with decreasing a_s.

The regime with both strong attractive interactions and axial trapping does not satisfy Eq. (2.63) and may in some cases correspond to systems with no local ground state. The values are still physically meaningful in that they are true if one takes $\omega_\perp \to \lambda\omega_\perp$ and $a_s \to a_s/\lambda$, which keeps $g_{1\mathrm{D}}$ the same but gives $\Upsilon_{3\mathrm{D}} \propto \lambda^{-2/3}$, which becomes small for λ sufficiently large, and hence 3D effects can be neglected. Strongly repulsively interacting 1D gases in harmonic confinement also have significant finite number and temperature effects which are beyond mean field theory [63].

2.4.2 Quasi 1D: radial component not independent of axial density

In the case where the energy change due to the nonlinearity is comparable to that of the radial trapping, the nonlinear effects will alter the wavefunction in the radial directions and so the axial and radial dynamics are no longer

separable. This is less extreme than the situation investigated in [46], in which the s-wave scattering length is comparable to the radial harmonic oscillator width, leading to confinement resonances when the regularisation term in Eq. (2.36) is included. As we will see for $a_s < 0$ having $|a_s| \sim a_\perp$ will inevitably result in a system which is unstable to collapse, and so this correction is largely irrelevant for the attractive system, unless N is 2 or 3 atoms.

A good approach to modelling this situation via mean field methods is given in [64], which modifies the harmonic oscillator width in Eq. (2.64) from $a_\perp$ into $\sigma^2(x,t)$, a function of the axial coordinate; $\sigma(x,t)$ is then treated it as a variational parameter. We then determined the time evolution by applying the principle of least action to the GPE action functional

$$S = \int dt \int_{-\infty}^{\infty} dxdydz \frac{\psi^*(x,t)}{2\pi\sigma^2} \exp\left[\frac{-(y^2+z^2)}{2\sigma^2}\right] \left\{ \frac{\omega_\perp^2(y^2+z^2)}{2} - i\hbar\frac{\partial}{\partial t} - \frac{\hbar^2}{2m}\nabla^2 + V(x) + \frac{g_{3\mathrm{D}}|\psi|^2}{2\pi\sigma^2} \exp\left[\frac{-(y^2+z^2)}{\sigma^2}\right] \right\} \exp\left[\frac{-(y^2+z^2)}{2\sigma^2}\right] \psi(x,t). \quad (2.69)$$

This approach makes three key assumptions:

- Slow axial variation: The radial degrees of freedom follow adiabatically the ground state of the combined potential of the radial harmonic oscillator potential and the nonlinearity for the current axial density.
- Smooth axial profile: The derivative of the variational width along the weakly confined direction $\partial\sigma(x)/\partial x$ is assumed to be negligible.
- Validity of the ansatz: The ground state of the combined potential in the radial degrees of freedom can be well described by a Gaussian profile.

The first and second assumptions rely on spatial (temporal) changes to $\psi(x,t)$ being small compared to $a_\perp$ $(1/\omega_\perp)$. These conditions can be violated by rapid changes to the axial density cased, for instance, by peaks and troughs due to an interference effect (e.g. after a collision with a barrier or other soliton), or by fast changes to $a_\perp$ or g_{3D}. The third assumption could be investigated numerically, but should generally be valid so long as the system is not too close to the collapse threshold.

The equation for the axial mean field wavefunction is known as the Non-polynomial Schrödinger equation (NPSE). It is also generally found to be in better agreement with full 3D numerical simulations of GPE dynamics than the usual 1D treatment [65]. The final equations obtained from minimising S with respect to variations in ψ^* and σ are:

$$i\hbar\frac{\partial}{\partial t}\psi(x,t) = \left[-\frac{\hbar^2}{2m}\frac{\partial^2}{\partial x^2} + \frac{g_{3\mathrm{D}}N}{2\pi}\frac{|\psi|^2}{\sigma^2} + \frac{\hbar\omega_\perp}{2}\left(\frac{\sigma^2}{a_\perp^2} + \frac{a_\perp^2}{\sigma^2}\right) + V(x)\right]\psi(x,t)\ . \tag{2.70a}$$

$$\sigma^2 = a_\perp^2\sqrt{1 + 2a_s N|\psi(x,t)|^2}\ . \tag{2.70b}$$

This equation features no rescaling of the chemical potential μ.

Summary

This section detailed the regimes of validity of effective 1D equations for condensates under strong radial confinement, noting the importance of the ratio of the healing length and radial width as the important parameter for separability. We also numerically investigated the widths of ground states for harmonically confined 1D condensates, using experimentally relevant parameters.

2.5 Experimental realisation of BEC

2.5.1 History and progress

The first attempts to create an atomic BEC were experiments with liquid ^{4}He in a dilution fridge [66]. Liquid ^{4}He, while a bosonic superfluid, strongly violates the diluteness condition $na_s^3 \ll 1$ resulting in only a small condensate fraction by the Onsager-Penrose definition, even as the temperature nears absolute zero [5]. However liquid ^{4}He still exhibits a critical temperature, below which it displays superfluid behaviour, showing no measurable viscosity and quantised vorticity [67].

The first confirmed experimental realization of BEC in dilute atomic gases

came in 1995 [68, 69], with considerable progress since. To date many atomic species have been successfully condensed [70, 71], which we split into subgroups: alkali metals [14, 68, 69, 72]: ^{7}Li, ^{23}Na, ^{39}K, ^{41}K, ^{85}Rb, ^{87}Rb, ^{133}Cs; effectively two electron atoms [73–75]: ^{40}Ca, ^{84,86,88}Sr, ^{170,174,176}Yb; strongly dipolar species [76–78]: ^{52}Cr, ^{164}Dy, ^{168}Er and finally spin polarised H and metastable ^{4}He [79].

Additionally temperatures of less than 500pK have been achieved [80, 81], with lifetimes of over a minute. More significantly for this work, it has been possible to tune the scattering length between hyperfine states of species with negative background ground scattering lengths, e.g. ^{85}Rb [14], ^{7}Li [15, 82] and ^{133}Cs [83, 84], to positive values, allowing them to be Bose condensed. After condensation is achieved the fields can be adjusted to return to $a_s < 0$ and create attractively interacting condensates. These condensates are unstable to collapse when held in confinement if they exceed a critical number of atoms, as discussed in 2.3.4.

Recent experiments have also been able to access reduced dimensional regimes, even going as far as to be able to manipulate the radial wavefunction with optimal control schemes, in order to place it in an excited state [85]. Additionally great progress has been made with lattice experiments [86], with the possibility to address single sites and observe quantum phase transitions.

2.5.2 Techniques required to obtain a BEC in a dilute atomic gas

Overview

A simplified process to form a condensate in a dilute atomic gas is carried out by loading the gas into a magneto optical trap (MOT) in an ultra-high vacuum, transferring the gas into a conservative potential and manipulating this potential to perform evaporative cooling until a desired temperature is achieved.[9] At this point the condensate can be manipulated as required; scattering lengths and external potentials can be modified via magnetic and

[9] Additional equipment/techniques may be required such as a Zeeman slower, multiple potentials for different stages of cooling (such as magnetic quadrupole potentials) and degenerate Raman side-band cooling [87].

electric fields or off resonant laser-light.

Electric and magnetic fields interacting with atoms

Atoms are by their nature quantum mechanical objects, especially in isolation. Alkali metal atoms can be treated like single electron atoms as the "core" electron wavefunction doesn't change significantly as the outer electron is excited. Therefore, we can consider a single-body Hamiltonian H_{atom} relating to this outer electron, with discrete eigenstates below a certain threshold. The addition of external electric and magnetic fields can be included via the dipole approximation [88]:

$$V = -\boldsymbol{\mu} \cdot \mathbf{F} \,, \tag{2.71}$$

with μ the magnetic (electric) dipole moment operator and $\mathbf{F}$ an external magnetic (electric) field. This operator V will couple different eigenstates of the atom as well as shifting their energies. Assuming the fields are weak, one can treat the system with perturbation theory to obtain energy level shifts, and mixing, of the eigenstates. For an electric field, the first order shift vanishes due to symmetry considerations[10], with a second order shift to the ground state of

$$E^{(2)} = -\frac{\alpha}{2}|\mathbf{F}|^2 \,. \tag{2.72}$$

Here we have introduced the polarisability α, the second order nature of this shift is due to the field imposing an orientation on the atoms. If the field $\mathbf{F}$ varies in space this will induce non-uniform potential which can be used for confinement. The mixing between states can also alter the scattering properties [39].

Light interacting with atoms can be described in the same way except that the electric and magnetic fields are time dependent and so V is time dependent. A time-averaged field will still produce a potential that can be used for confinement, creating harmonic or lattice potentials [86]. Inelastic photon scattering is significant if the light is near resonant with a transition, i.e. $\omega_{\text{laser}} \approx (E_n - E_0)/\hbar \equiv \omega_0$, which can be manipulated for cooling [88] but causes decoherence.

[10] Note that the energy levels shifts in magnetic fields do not vanish to first order.

Atom loss processes

Evaporative cooling is limited in efficiency by inelastic processes that cause a loss of atoms (which are not high in energy) from the system. Additionally such loss processes limit condensate lifetimes and can act as measurement like events. An ultracold gases in a conservative potential has three significant inelastic processes, resulting in the loss of atoms [29, 89]:

- Collisions with background gas (imperfect vacuums): rate $\propto N$.
- Collisions which change the hyperfine state of one or more atoms: rate $\propto N\langle n\rangle$.
- Collisions between atoms which form molecular states (via three-body processes [90]): rate $\propto N a_s^4 \langle n\rangle^2$.

These effects have different proportionality with the number density $\langle n\rangle$, assuming no significant correlation effects are present. The impact of loss processes is discussed further in Sec. 3.5.4.

2.5.3 Feshbach resonances

Feshbach resonances occur due to the existence of inter-atomic bound states, with an energy extremely close to the threshold for disassociation, as discussed in Sec. 2.2.2. These energy levels are generally tunable with external magnetic fields or laser fields, but optical Feshbach generally result in a large inelastic two body collision rate due to spontaneous emission [39], which makes them undesirable. Far from a resonance such changes are small, but in the vicinity of a magnetic feshbach resonance the s-wave scattering length behaves as [39]

$$a_s(B) = a_{\mathrm{bg}}\left(1 - \frac{\Delta}{B - B_0}\right) . \tag{2.73}$$

Here B is the magnetic field, a_{bg} is the background scattering length, Δ is the width of the resonance (both of which can be positive or negative) and B_0 is the centre of the resonance. Generally, for experimental purposes, wider resonances are preferred, because less precise control of the magnetic field is required. In theory these techniques can be used to achieve arbitrarily large

scattering lengths, but these typically result in larger two and three body inelastic losses.

Summary

This section reviewed some of the general progress in BEC experiments and covered the basic experimental procedures, including how atoms can be manipulated with external fields to modify inter-atomic interactions and the external potential. Additionally we briefly discussed the significant loss processes and their effect.

Chapter 3

Classical solitons and integrability

3.1 Classical integrability and conserved quantities

3.1.1 Conditions for an integrable system

The three conditions of 1.1.2 are good for getting a qualitative feel about what solitons are and where they are supported, but we require a more rigorous mathematical framework to describe them and predict where they occur. This leads to the notion of integrability. A Hamiltonian system is said to be integrable in the Liouville sense if there exists a maximal set of independent Poisson commuting invariants. For a $2N$ dimensional phase space, we have a set of N functions $f_1, \ldots, f_N$, with vanishing Poisson brackets with respect to one another: $\{f_k, f_j\} = 0$, and the Hamiltonian: $\{f_k, \mathcal{H}\} = 0$ [91]. Note the Poisson brackets are defined for a set of N generalised coordinates $\vec{q}, \vec{p}$ as

$$\{f, g\} = \sum_{k=1}^{N} \left(\frac{\partial f}{\partial q_k} \frac{\partial g}{\partial p_k} - \frac{\partial f}{\partial p_k} \frac{\partial g}{\partial q_k} \right) . \tag{3.1}$$

Integrability is an important concept as it determines if the behaviour of a system can be chaotic [92]; a two body planetary system is an integrable system (if the planets are treated as rigid bodies) and the dynamics can be solved exactly, whereas a three-body system is not integrable and is also chaotic [93]. Note that we can take f_1 to be the Hamiltonian $\mathcal{H}$ in all cases,

and so any $D = 2$ space is integrable if the Hamiltonian is time independent.

Integrability is often associated with solvability; analytic expressions can usually be found for integrable systems but it is not true to say that just because an analytic solution can be found a system is integrable. A good counter example is a particle in a 1D harmonic oscillator potential which is periodically kicked, instantaneously in time, with period τ:

$$\mathcal{H} = \frac{p^2}{2m} + \frac{m\omega^2 x^2}{2} + K\cos(kx)\sum_{n=-\infty}^{\infty}\delta(t - n\tau)\ . \tag{3.2}$$

Despite the fact it is possible to obtain an analytic solution for $x(t)$ [94], the system has no conserved quantities and hence is not integrable. The same is true for a periodically kicked rotor. Further more, the behaviour is chaotic, namely it satisfies the three criteria [95]:

- the system is sensitive to initial conditions,
- it is topologically mixing; and
- it has dense periodic orbits.

3.1.2 Consequences of integrability

Both the free GPE and the KdV have been shown to satisfy Liouville integrability [96]. One of the most interesting properties about solitons is that (in the absence of additional perturbations) any initial condition can be decomposed into soliton and radiation solutions via an inverse scattering transform [97]. Therefore, at asymptotically long times, the system will be described by a dispersed radiation component and isolated (and localised) solitons, given by analytic single soliton solutions which we examine in the next section. The radiation component is not analytically tractable, but will be of vanishing density if the system has no boundaries. This behaviour was shown numerically to be the case for the KdV system [98], with an initially smooth $\cos(\pi x)$ solution (and periodic boundary conditions) tending to a localised soliton train at long times. We examine the single soliton solutions to both these systems in the next section.

3.2 Solutions in the nonlinear Schrödinger equation

3.2.1 Bright soliton solution

If we have attractive interactions ($g_{1D} < 0$), the NLSE [Eq. (2.67)] has the bright soliton solution [6]

$$\psi(x,t) = \frac{1}{2\sqrt{\xi_s}}\text{sech}\left(\frac{x-x_0}{\xi_s}\right)e^{-i\mu t/\hbar}\,, \tag{3.3}$$

with

$$\xi_s = \frac{\hbar^2}{m|g_{1D}|N}\,, \quad \mu = -\frac{m|g_{1D}|^2N^2}{8\hbar^2}\,; \tag{3.4}$$

the initial position x_0 can be chosen arbitrarily due to the translation symmetry. The length factor ξ_s in Eq. (3.3) is called the soliton length; this length is also equal to the healing length at the peak of the soliton divided by $\sqrt{2}$. The time evolution of this state is simply a rotation of the global phase and is hence referred to as a stationary state, a nonlinear analogue to an eigenfunction. Exact solutions for stationary states also exist with box or periodic boundary conditions, given by Jacobi elliptic functions [99].

Unlike the bright soliton of the KdV [Eq. (1.3)], the GPE soliton does not exist on a finite background. Hence by Galilean invariance, we can express a soliton moving with velocity v as [100]

$$\psi(x,t) = \frac{1}{2\sqrt{\xi_s}}\text{sech}\left(\frac{x-x_0-vt}{2\xi_s}\right)\exp\left[\frac{i}{\hbar}\left(-\mu t + vxm - \frac{mv^2t}{2}\right)\right]\,. \tag{3.5}$$

Note that the phase evolution (and thus energy) is independent of the initial position x_0.

3.2.2 Solutions on a finite background

It is also physically relevant to consider excitations with a finite background number density n. These solutions cannot be normalised, and hence the GPE [Eq. 2.55] would need to be modified. This can be achieved by removing the

factor of N and taking the density (away from excitation we are considering) to be $|\psi(x)|^2 = n$.

Attractive condensates permit the spatially periodic Akhmediev breather[1] and time periodic Kuznetsov-Ma soliton as solutions [101, 102]. Interestingly when the period tends to infinity, both classes of solutions also tend to the so called Peregrine soliton, a highly focusing solution connected to rogue waves. Peregrine solitons have been observed in fibre optics [103].

Repulsive condensates ($g_{1D} > 0$) have a dark soliton solution. This is a density dip moving with velocity v along the uniform background and can be expressed as [104]

$$\psi(x - vt) = \sqrt{n}\left(i\frac{v}{c} + \sqrt{1 - \frac{v^2}{c^2}}\right)\tanh\left[\frac{x - vt}{\sqrt{2}\xi}\sqrt{1 - \frac{v^2}{c^2}}\right] , \tag{3.6}$$

with ξ the healing length [Eq. (2.34)] for a density n and $c = \sqrt{g_{1D}n/m}$ the sound velocity. These behave like quasi particles with negative mass, having a maximum energy of $E = 4\hbar cn/3$ when $v = 0$ and no energy as $v \to c$ where the solution in infinitely wide and has no amplitude.

3.2.3 Rescaling to dimensionless units

In order to simplify our equations, we rewrite Eq. (2.65) in terms of rescaled time and position coordinates and scaling out the constant factor of $\hbar\omega_\perp$. Assuming we are dealing with normalised solutions, we define our dimensionless time and position in soliton units as

$$\tilde{x} := \frac{m|g_{1D}|N}{\hbar^2}x = 2\Upsilon\frac{x}{a_\perp} , \qquad \tilde{t} := \frac{m|g_{1D}|^2N^2}{\hbar^3}t = 4\Upsilon^2\omega_\perp t , \tag{3.7}$$

with Υ the (1D) collapse parameter, defined in Eq. (2.60). We note that besides this factor these are just harmonic oscillator units in the radial degrees of freedom and the condition Eq. (2.63) is now $\Upsilon \ll 1$. Finally we define

$$\tilde{\psi}(\tilde{x}) = \frac{\hbar}{\sqrt{m|g_{1D}|N}}\psi(x) , \tag{3.8}$$

[1]Note that, confusingly, the NLSE from optics has time and space interchanged.

to be the wavefunction normalised with respect to $\tilde{x}$ (important for a non-linear problem). In these units, with $V(x) = m\omega_x^2 x^2/2$, the 1D GPE reduces to

$$i\frac{\partial}{\partial\tilde{t}}\tilde{\psi}(\tilde{x}) = -\frac{1}{2}\frac{\partial^2}{\partial\tilde{x}^2}\tilde{\psi}(\tilde{x}) + \frac{\hbar^3\omega_x^2\tilde{x}^2}{2mg_{1\mathrm{D}}^2N^2}\tilde{\psi}(\tilde{x}) + \mathrm{sgn}(g_{1\mathrm{D}})|\tilde{\psi}(\tilde{x})|^2\tilde{\psi}(\tilde{x})\ ; \tag{3.9}$$

which can be further simplified by collating the prefactor of $\tilde{x}^2$ into one term $\tilde{\omega^2}/2$. For convenience we drop the tildes when using these units.

3.2.4 Solitary wave solution to the non polynomial Schrödinger equation

Unlike the NLSE, the NPSE is not an integrable system, hence it does not permit true soliton solutions. However, it does have a localised solitary wave (a non dispersing localised) solution if the interactions are attractive. Considering the case $V(x) = 0$ and $a_s < 0$, we can rescale Eq. (2.70a) in soliton units [as defined in Eq. (3.7)]:

$$i\frac{\partial}{\partial t}\psi(x) = \left[-\frac{1}{2}\frac{\partial^2}{\partial x^2} + \frac{\frac{1}{4\Upsilon^2} - \frac{3}{2}|\psi(x)|^2}{\sqrt{1+4\Upsilon^2|\psi(x)|^2}}\right]\psi(x)\ , \tag{3.10}$$

leaving only the collapse parameter. Additionally, for $0 < \Upsilon < 2/3$ a bright-solitary wave solution can be obtained in implicit form [105]

$$\begin{aligned} x - vt =& \frac{2^{-1/2}}{\sqrt{1-\mu}}\mathrm{arctan}\left[\sqrt{\frac{\sqrt{1-2\Upsilon\psi(x)^2}-\mu}{1-\mu}}\right] \\ &- \frac{2^{-1/2}}{\sqrt{1+\mu}}\mathrm{arctanh}\left[\sqrt{\frac{\sqrt{1-2\Upsilon\psi(x)^2}-\mu}{1+\mu}}\right]\ . \end{aligned} \tag{3.11}$$

For $\Upsilon = N|a_s|/a_\perp > 2/3$ there is no stable solution and μ and σ are discontinuous, indicating this is the point at which the ground state is not stable and will collapse; this value is close to the value from full 3D numerical predictions of around $k_c = 0.675 \pm 0.005$ [from [106]] and experimental observations of the structure factor in this geometry. Note that to lowest order in Υ, Eq. (3.11) reproduces Eq. (3.5), so this parameter can be seen as

controlling the validity of a true 1D reduction for a ground state.

Summary

We investigated the bright soliton solution to the GPE, observing that the density formed a sech squared profile as was the case in the KdV soliton solution and introduced a dimensionless rescaling to make the NLSE parameter free. The implicit solution to the solitary wave solution to the NPSE was also given, noting the collapse parameter Υ can be considered a smallness parameter for the condition that 3D effects in the ground state can be neglected.

3.3 Multiple well-separated solitons in the 1D GPE

3.3.1 General solutions for N_s solitons

An important class of solutions for this work is the set of multiple soliton solutions. It is possible to analytically express a solution for a system with N_s solitons, with amplitudes A_j (summing to one half if we wish for the function to be normalised to unity), momentum per atom p_j,[2] initial positions x_{k0} and phases ϕ_{j0}, as the solution to a system of N_s coupled equations [9]

$$\psi(x,t) = \sum_{j=1}^{N_s} u_j(x,t) \tag{3.12a}$$

$$1 = \sum_{k=1}^{N_s} u_j(x,t) \frac{\gamma_j^{-1} + \gamma_k^*}{\lambda_j + \lambda_k^*} \quad \text{all } j\ . \tag{3.12b}$$

Here we have defined $\lambda_j = A_j + ip_j$ and $\gamma_j = \exp[\lambda_j(x - x_{j0}) + i\lambda_j^2 t/2 + i\phi_j]$. If each component is separated by many soliton lengths from all the others, we can obtain analytic expressions for each component:

$$u_j(x,t) = A_j \mathrm{sech}\left(A_j[x - x_j] + q_j\right) \exp\left[i\phi_j + i\Phi_j\right]\ , \tag{3.13}$$

[2] Or equivalently soliton velocity V_j as in these units $\hbar$ is effectively one.

where $x_j = x_{j0} + p_j t$ is the position and $\phi_j = \phi_{j0} + p_j x + t(A_j^2 - p_j^2)/2$ is the phase. The additional parameters that occur are Φ_j, the phase shifts and q_j, the collisional position shifts multiplied by the size A_j (hence the centre shift is q_j/A_j). These are not arbitrary and are fixed via

$$q_j + i\Phi_j = \sum_{k\neq j} \mathrm{sgn}(x_k - x_j) \ln\left(\frac{A_j + A_k + i[p_j - p_k]}{A_j - A_k + i[p_j - p_k]}\right), \tag{3.14}$$

for every $j = 1, .., N_s$. The function $\mathrm{sgn}(x_k - x_j)$ denotes a change of sign before and after collision, and the amplitude (phase) of the term in the logarithm determining the scattering position (phase) shift. When considering the quantum theory of this system we will see that Φ_j are the large N limits of scattering phase shifts between bound state strings (quantum solitons), in Eq. (4.27).

3.3.2 A collision between two solitons

A simple but important case is the situation with only two solitons. The two equations which then comprise Eq. (3.14) can be added together (noting that the prefactor will take opposite sign) to give

$$q_1 + q_2 + i(\Phi_1 + \Phi_2) = \mathrm{sgn}(x_2 - x_1) \ln\left(\frac{[p_1 - p_2] - i[A_1 + A_2]}{[p_1 - p_2] + i[A_1 + A_2]}\right). \tag{3.15}$$

Because q_k and Φ_k are real, and the term in the log is of unit magnitude, there is no real term on the right of Eq. (3.15), and hence $q_1 = -q_2$ (the position shifts per atom are equal). By subtracting $\Phi_1 + \Phi_2$ before the collision i.e. $t < (x_{10} - x_{20})/(p_2 - p_1)$ from the value after collision, the system has a total phase shift of

$$2|\Phi_1 + \Phi_2| = 4 \arctan\left(\frac{A_1 + A_2}{|p_1 - p_2|}\right), \tag{3.16}$$

modulo 2π. This is only relevant if there is some phase reference (e.g. additional solitons). A more important equation governs the relative quantities

$$q_1 - q_2 + i(\Phi_1 - \Phi_2) = \mathrm{sgn}(x_2 - x_1) \ln\left(\frac{[A_1 + A_2]^2 + [p_1 - p_2]^2}{i[A_1 - A_2] - [p_1 - p_2]^2}\right). \tag{3.17}$$

By separating into real and imaginary parts we can calculate the equations for the relative position and phase shifts:

$$\frac{q_1}{A_1} - \frac{q_2}{A_2} = \mathrm{sgn}(x_2 - x_1)\frac{A_2 - A_1}{2A_1A_2}\ln\left[\frac{(A_1 + A_2)^2 + (p_1 - p_2)^2}{(A_1 - A_2)^2 + (p_1 - p_2)^2}\right] , \quad (3.18a)$$

$$\Phi_1 - \Phi_2 = 2\mathrm{sgn}(x_2 - x_1)\arctan\left(\frac{A_1 - A_2}{p_1 - p_2}\right) , \quad (3.18b)$$

noting the shift is double that of the right hand side of the above equations as the values before and after are equal and opposite. Both of these relative shifts vanish if the two solitons are the same size (as the solitons both see the same extra potential and have the same mass) or if the relative velocity is large, as this results in a brief interaction time.

3.3.3 Importance of relative phase

It can be seen from Eq. (3.14), that the relative phase between two solitons, $\Phi_r = \phi_1(x_c) + \Phi_1 - \phi_2(x_c) - \Phi_2$ (colliding at some point x_c), has no effect on the asymptotic scattering. This property is important for deriving a particle model of solitons [100], effective at describing their locations at a given time. Despite this, relative phase does strongly effect the density *during* collisions; if $\Phi_r = 0$ the collisions will produce a density maximum at the centre, whereas $\Phi_r = \pi$ will produce a density minimum. High densities can cause the onset of collapse effects and radial excitation [17], and so systems with $\Phi_r = \pi$ between neighbouring solitons are generally predicted to be more stable. Relative phase is also important when external potentials are present, such as strongly peaked barriers [107].

It is noteworthy that Eq. (3.14) fails in the case that two solitons are of similar sizes and have near zero relative velocities. In this case it is found that the relative phase and position vary according to [9]

$$\frac{\partial^2}{\partial t^2}\Phi_r = 8\exp(-x_r)\sin(\Phi_r) \quad (3.19a)$$

$$\frac{\partial^2}{\partial t^2}x_r = -8\exp(-x_r)\cos(\Phi_r) , \quad (3.19b)$$

with exponentially decreasing interaction with the separation x_r. For certain

initial conditions, it is possible to obtain bound states with separations that oscillate about some value periodically. These soliton molecules, as they are often referred to in the literature [108], have no binding energy, which allows them to be broken easily.

Summary

This section quoted the inverse scattering result for a multiple soliton solution in the NLSE, along with the position and phase shifts that occur due to collisions. We noted that relative phase changes the density profile during collisions and introduces the possibility to form bound states. Such density changes are important when considering additional terms in the GPE which break integrability.

3.4 Integrability and soliton properties in systems of classical particles

Solitons are often said to behave like particles; as we noted earlier, out of the conditions (1.1.2), only the third condition (emerging unchanged from collisions besides a position and phase shift) is not automatically satisfied for a structureless particle. It is easier to think of an isolated bright soliton, such as those that occur with the attractive 1D GPE, to be particles rather than water waves or density dips in repulsive condensates. The latter can be thought of more as quasi-particles (likes holes in semi-conductors), a change of density over the uniform background which preserves its shape; in the former case this background is simply the vacuum state.

Classical particles have no phase property, hence all we require is particles to emerge asymptotically without their momenta/velocities changed, only their positions. If the particles are identical then we require the weaker condition that only a rearrangement of velocities is allowed, as this can still be mapped to position shifts on the original particles.

3.4.1 Two particles

The simplest example to satisfy 1.1.2 be would two structureless classical particles, heading directly towards another at non-relativistic speeds, free from external forces, but interacting with some conservative, effectively finite range potential $V(\mathbf{r}_1 - \mathbf{r}_2)$, such that $V(\mathbf{r}) \to 0$ if $|\mathbf{r}| > R$. This is equivalent to being confined to move in one dimension, which we will call x as the coordinates can always be rotated and translated such that the positions along the y and z axis are zero through all time. We can see that this system satisfies Liouville integrability as the energy $E = p_1^2/2m_1 + p_2^2/2m_2 + V(x_1 - x_2)$ and centre-of-mass momentum $p_c = p_1 + p_2$ must also be conserved which is $N = 2$ quantities as required. We can therefore look at the system in a frame moving with velocity $v = p_1/m_1 + p_2/m_2$ with respect to our original frame and consider p_c to be zero. This leaves only the relative momentum between the two $p_r = p_1 - p_2$ as a free parameter, which is fixed by the energy E (in this reference frame) via

$$\frac{p_r^2}{2\mu} = E - V(x_1 - x_2) \ , \tag{3.20}$$

with $\mu = m_1 m_2/(m_1 + m_2)$ the reduced mass. After the collision, when the particles are again separated by enough distance $|x_1 - x_2| > R$, the interaction is not felt and this relative momentum must be the same as it was initially, up to a factor of ± 1 depending on whether it was reflected or transmitted[3]. However, if we were to work out the full time evolution, p_r would have changed during the interaction time. Hence compared to the positions of the particles had they not been interacting, an attractive potential would put them slightly ahead and a repulsive potential slightly behind, leading to the position shift. If the two particles were identical, we can also not meaningfully say which one was which. The sign which occurred due to reflection is now meaningless and we can therefore state that the asymptotic velocity is unchanged.

We note that if $V(x) < 0$ for some x, it permits bound states, for which $\overline{p_r} = 0$ and $|p_r| < p_{\max}$. However, due to energy and momentum conservation of

[3]Transmission occurs if $V(x) < E$ for the whole range.

Eq. (3.20), if $V < 0$ then the relative momentum must increase to compensate and hence the two colliding particles cannot form a bound state unless they were in one at $t = 0$ and if they were, they can't possibly get out of it.

3.4.2 More than two particles

One might also consider adding a third particle to the system, noting the centre-of-mass momentum $\mathbf{p}_c = \mathbf{p}_1 + \mathbf{p}_2 + \mathbf{p}_3$ and energy E must still be conserved. If the third particle is not moving along the same axis as the other two it can collide skew and the problem becomes three dimensional. Any transfer of momentum off-axis instantly means asymptotic momentum is not conserved, leading to the first condition that the system must be effectively one dimensional (or, trivially, non interacting) with all three moving along the same axis. In one dimension we still require $N = 3$ invariants for integrability. Only two are apparent for a general potential and asymptotic relative momenta may not be conserved.

This is best demonstrated by the possibility to dynamically form bound-states. Assuming the centre-of-mass momentum to again be zero and that particles one and two end up in a bound state with energy E_{bound} such that $p_1 - p_2 = 0$,[4] we have from energy and momentum conservation

$$\begin{aligned} 0 &= p_1 + p_2 + p_3 \\ E - E_{\text{bound}} &= \frac{p_1^2}{2m_1} + \frac{p_2^2}{2m_2} + \frac{p_3^2}{2m_3} \,, \end{aligned} \tag{3.21}$$

and hence substituting in $p_3 = -p_1 - p_2 = -2p_1$ to the second line and rearranging gives

$$p_1 = \pm\sqrt{\frac{E - E_{\text{bound}}}{(4/m_3 + 1/m_1 + 1/m_2)}} \,, \tag{3.22}$$

and $p_3 = -2p_1$ to keep the new momentum zero. This of course leads to an asymptotic velocity shift compared with the starting values and hence these particles are no longer behaving like solitons.

[4] This is a simple choice for the bound state, more general choices would have $|p_1 - p_2| < p_{\max}$ and $p_1 - p_2$ time averaging to zero. But this assumption does not change the principle.

It therefore seems that in general the addition of a third particle breaks integrability of an interacting (1+1)D system, even when the particles are indistinguishable, due to these three-body interactions. However certain potentials which we discuss in the next section possess properties that mean they just so happen to permit such invariants and give asymptotic scattering properties that don't alter the incoming momenta, however these are special cases, not the general rule as was the case for $N = 2$. This should give some indication of why soliton properties imply particle like behaviour and why one dimension is so special for classical scattering. Later this concept is extended to quantum mechanical systems leading to the Bethe ansatz in Sec. 4.1.

3.4.3 Potentials giving classical integrability

It has been shown that N identical particles interacting with the potential

$$V(x) = -\frac{b^2 \wp(x/a|\omega,\omega')}{e_1 - e_3} + \text{const}\ , \tag{3.23}$$

i.e. a Calogero-Moser system [109], with $\wp$ Weierstrass's elliptic function,[5] satisfy Liouville integrability. Due to the conserved quantities, these potentials also preserve the asymptotic momenta of the particles [91]. The current form is however far too general; three important special cases are

$$V(x) = \begin{cases} \dfrac{g}{x^2} \\ \dfrac{g}{a^2 \sinh(x/a)^2} \\ \dfrac{g}{a^2 \sin(x/a)^2}\ , \end{cases} \tag{3.24}$$

with $g > 0$, these can all be related via lattice sums [91] and are totally impenetrable. We note that the potential $\tilde{V}(x) = -g\text{sech}^2(x/a)/(a^2)$, interesting in that it is reflectionless for certain g and is the nonlinear potential an atom would see interacting with a quantum soliton and a model potential for particle models of solitons [100], does *not* yield integrability for $N > 2$. This

[5] Here $e_1 = \wp(\omega|\omega,\omega')$ and $e_3 = \wp(\omega'|\omega,\omega')$ are the values at the half periods ω and ω'. If one is real and the other imaginary the values along x will be real.

is an interesting result in that it implies the particle model used in [100] does not constitute an integrable system for three or more identical sized solitons. However, a combination of two different types of particle, with the same mass, interacting between themselves via $V(x) = g/a^2 \sinh(x/a)^2$ and with the opposite type via $\tilde{V}(x) = -g\text{sech}^2(x/a)/(a^2)$ *does* result in an integrable system [91].

Summary

We introduced the concept of solitons behaving like particles, and the conditions for integrability in $1D$ *many-particle systems in the classical case. We show that, while a system of two identical particles is integrable and conserves momentum asymptotically, whereas a system of three or more is only integrable for certain interaction potentials.*

3.5 Quantum mechanics, wave particle duality, entanglement and measurement

3.5.1 Wave particle duality

One of the key concepts in quantum mechanics is the so called wave-particle duality, the idea that particles can behave as waves and vice versa. Within (non-relativistic) quantum mechanics, everything can be described by a wave-function (possibly with a very large number of degrees of freedom), with the dynamics described by the evolution in potentials via the Schrödinger equation

$$i\hbar\frac{\partial}{\partial t}|\psi(t)\rangle = \hat{H}|\psi(t)\rangle \ . \tag{3.25}$$

Here $|\psi(t)\rangle$ is the state of a quantum system at a time t with a Hamiltonian $\hat{H}$. For an initial condition $|\psi(0)\rangle$ the solution is

$$|\psi(t)\rangle = e^{-i\hat{H}t/\hbar}|\psi(0)\rangle \ , \tag{3.26}$$

although the solution of this equation is rarely simple to obtain, analytically or numerically, it is in principle a deterministic, linear wave equation [110]. This considers a system in isolation from, as it were, the rest of the universe. When extra pieces are added to the system (e.g. an observer) but not accounted for at a quantum mechanical level, the particle-like nature becomes apparent. In a classical mechanical sense, the most common particle-like property is a definite position and momentum and an absence of internal structure (or internal structure that doesn't affect the properties of interest). Within the theory of quantum mechanics, the former properties are not obtainable due to the position and momentum uncertainty relation $\Delta p \Delta x \geq \hbar/2$, but the idea of being structureless is a meaningful property which can be carried over. We will later see that this idea can be applied to solitons, where the internal structure cannot be altered as it is protected by integrability. Additionally if the values of position and momentum uncertainty can be considered small, typically if the mass is large, the particle like nature can be used completely. Combined with the idea of a measurement, where for simplicity we will say we can measure with arbitrary precision, one can take the idea of a particle in quantum mechanics to be a structureless object with some uncertainty in what a measurement will yield, with the probability being given by the particle's wavefunction in the Copenhagen interpretation of quantum mechanics.

Classical mechanics also includes a theory of waves in which everything is essentially deterministic. For example an electromagnetic wave of a single frequency can have a known electric and magnetic field at every point in space. Quantum mechanics states the energy of such a wave must be quantised in units of $\hbar\omega$. It is still however possible to have a state of arbitrary energy expectation value $E = \langle \hat{H} \rangle$, by taking a superposition of such states. The discrepancy comes again when the system is coupled externally to say, a perfect detector, which will find n energy packets of $\hbar\omega$ with n an integer. This is considered to be waves behaving as particles. The duality is also illustrated in Einstein's formula for fluctuations in black-body radiation [38]

$$\bar{\epsilon}^2 = \left(h\nu\rho + \frac{c^3\rho^2}{8\pi\nu^2} \right) d\nu \ , \tag{3.27}$$

where ν is the frequency. The former term is due to the particle like "shot noise" and the latter due to the wave like "speckle".

3.5.2 Measurement

Measurement has long been a difficult concept in quantum mechanics with a great deal of literature dedicated to it [110, 111]. Despite some of the conceptual difficulties, measurement theory is powerful enough to relate a great deal of information extracted from quantum mechanical systems to the internal processes. Theoretically one takes an observable, e.g. position, but in general any Hermitian operator $\hat{O}$ with a set of eigenstates $\hat{O}|n\rangle = \epsilon_n|n\rangle$, and interacts with a quantum system in order to obtain an outcome from the measurement [38]. If this measurement process is considered "perfect," performing the measurement on a state $|\psi\rangle = c_0|0\rangle + ...c_n|n\rangle + ..$ will project the state of the system into one of the eigenvalues of $\hat{O}$, with a probability of $|c_n|^2$. Hence this process will alter the quantum state of the system, unless it was originally an eigenstate of $\hat{O}$. Real measurements can be imprecise or destructive, which can also be accounted for within the theory [112]. Additionally measurements do not have to be performed by people, or by classical processes, they are simply anything interacting with the system that is not explicitly accounted for. Taking the example of a BEC in a vacuum chamber, blackbody radiation, thermal atoms, stray fields and inelastically scattered photons all constitute a measurement in this sense.

A contextually simple but illustrative experiment is the splitter of a single photon state with a 50-50 beam splitting in the path such that the reflected light would go to detector A and the transmitted to detector B. Repeating the process with many single-photon input states, separated in time, one would see approximately half the counts in detector A and the other half in detector B, with only statistical deviations, as one would expect for a classical light input. The number of coincidence counts in which A and B fire together (within the separation time of the input photons) is however suppressed compared to the classical expected value [113]; in fact for a perfect experiment, the number of coincidence counts would drop to zero.

3.5.3 Decoherence and the density matrix

Accepting that quantum mechanical systems will interact with their surroundings in a way that is intractable and also that we often do not know the exact quantum state of a many-body system, only bulk properties like temperature; means that we will require a statistical tool to analyse these systems. This leads to the density matrix formulation, in which we describe a system with a density[6] matrix [38]

$$\hat{\rho}(t) = \sum_k c_{jk} |\psi_j\rangle\langle\psi_k| \,, \tag{3.28}$$

and the von Neumann equation

$$\frac{\partial \hat{\rho}(t)}{\partial t} = -\frac{i}{\hbar}[\hat{\rho}(t), \hat{H}] \tag{3.29}$$

where $\hat{\rho}$ is Hermitian ($c_{jk} = c^*_{kj}$) and normalised such that $\mathrm{Tr}(\hat{\rho}) = 1$. If $\mathrm{Tr}(\hat{\rho}^2) = 1$, this operator is said to represent a "pure state" and this formulation is exactly the same as the Schrödinger formulation. However if $\mathrm{Tr}(\hat{\rho}^2) < 1$, the operator is said to represent a "mixed state" or statistical mixture.

This formalism can also include non Hermitian (loss/gain) processes and random processes by including these on the right hand side of Eq. (3.29), to make it a so called master equation. This is required to describe processes like laser cooling of an atomic gas, in which many intractable spontaneous (vacuum field stimulated) decay events from the excited to ground state occur; the density matrix is used to describe the state of an atom in the ensemble and give statistical agreement. Loss processes like this tend to have the effect of reducing the amplitude of the off-diagonal elements (coherences), so atoms will be less likely to be found in superposition of eigenstates than if the decay term was not present.

[6] Not to be confused with the single body density matrix [Eq. (2.46)].

3.5.4 Entanglement

Entanglement is manifest when the outcome of one measurement affects another. This typically leads to systems that are very sensitive to measurement effects and hence are often not stable. How entanglement is defined in general for many-body systems has been covered in detail (see for example [114] and references herein), but there are some subtleties for indistinguishable particles [115]. Non-entangled pure states can be expressed as an appropriately symmetrised tensor product of single particle states, if this is not possible the state can be considered entangled.

As a relevant example, we consider the ground state of N atoms confined to a 1D periodic box, which we assume is extremely wide, with contact interactions (discussed in detail in Sec. 4.1.4). The many-body wavefunction separates into a centre-of-mass wavefunction which is delocalised uniformly throughout the box and a relative component which holds all the information about pair correlations [$g^{(1)}(x, x')$ in Eq. (2.45)]. The non-interacting ground state will be a pure BEC and hence have $g^{(1)}(x, x') = 1$ and be described by a tensor product of N identical stages, and hence has no entanglement. A measurement of a single atomic position (by, say, scattering a single high frequency photon) gives no information about the position of the other $N-1$ atoms.

However, the stronger the interactions become, the stronger the pair correlations become and so the more information this one particle measurement carries about the position of the other $N-1$ atoms. Ultimately, in the strong interacting limit, we can say $g^{(1)}(x, x') \to \delta(x, x')$ for attractive bosons and $g^{(1)}(x, x') \sim |x - x'|$ as $x \to x'$ for repulsive bosons [116] (or non-interacting fermions). In this regime a measurement of a single atomic position, made with some uncertainty Δx, would fix the position of all the other atoms with roughly the same uncertainty. In the strongly attractive case, this would also localise the centre-of-mass position wavefunction to a width Δx (since all the atoms must be close together); noting that this wavefunction was totally delocalised before.

Typically the more atoms are present, the more likely measurement-like events will occur, for example the loss processes discussed in Sec. 2.5.2, which

makes it difficult to have such a delocalised state for large atom numbers and/or strong interactions. These loss processes have little effect on the Hartree-product states which have $g^{(1)}(x, x') = 1$, in the limit of large N, hence one expects such states to be more resilient to loss processes.

Summary

This section described the differences between the theories of classical and quantum mechanics when describing waves and particles, and the significance of measurement process. Basic measurement theory was introduced, along with processes which could be considered as measurements for our system. This leads on to the notion of decoherence and we introduced the density matrix as the usual statistical tool to deal with classical uncertainty in quantum systems. Finally we discussed entanglement, with relevance to quantum gases in 1D, including a discussion of pair correlations increase the impact of measurement like events on the system.

Chapter 4

Many body quantum physics in one spatial dimension

4.1 The Bethe ansatz and quantum integrability

4.1.1 Quantum vs classical integrability and diffraction-less scattering

Classical integrability was discussed earlier in section 3.1, along with its significance in terms of whether or not a system admits soliton solutions. The notion of classical integrability is well defined in terms of Poisson commuting invariants, and one could attempt to extend a similar notion to quantum integrability by exchanging the Poisson brackets for commutator brackets. This means for a system with N degrees of freedom that there exist N independent operators $\{\hat{L}_1, \ldots, \hat{L}_N\}$ satisfying $[\hat{L}_j, \hat{L}_k] = 0$ and $[\hat{H}, \hat{L}_k]$. This *can* be done but implies very little about the system [91], for example a set of 1D bosons with an elliptic interaction potential of Eq. (3.23) satisfies this condition, but no analytic solutions are known for the eigenstates. One therefore considers scattering without diffraction to be a condition of quantum integrability. Such systems are found to have eigenstates described by the Bethe ansatz, a set of plane waves which have a gradient discontinuity where coordinates in the many-body wavefunction meet. This is essentially a quantum

generalisation of the classical particle collisions considered in Sec. 1.1.2.

In order to describe this mathematically it is necessary to write the Hamiltonian for N particles with identical mass in one dimension, interacting with two body interactions only. In terms of 1D atomic position coordinates $\vec{x}$, we have

$$H(\vec{x}) = -\frac{\hbar^2}{2m}\sum_{k=1}^{N}\frac{\partial^2}{\partial x_k^2} + \sum_{k=2}^{N}\sum_{j=1}^{k-1}V(x_k - x_j) \tag{4.1}$$

which controls the time evolution of some many body wavefunction $\Psi(x_1, \ldots, x_N)$ which describes all the physical properties of the system. First we examine the simple case of $N = 1$; as there is no self interaction present all the eigenstates of the system are plane waves:

$$\psi(x_1)_{p_1} \propto \exp(i\frac{p_1}{\hbar}x_1) \tag{4.2}$$

with normalisation and quantisation of p, the momentum eigenvalue, determined by boundary conditions. This state also has energy eigenvalue $E = p^2/2m$. If another particle is added, the two will now interact with a potential $V(x_1 - x_2)$ (which must be symmetric). We note it is still possible to split the Hamiltonian into centre-of-mass and relative coordinates

$$\begin{aligned} H_{\mathrm{C}}(x_{\mathrm{C}}) &= -\frac{\hbar^2}{4m}\frac{\partial^2}{\partial x_{\mathrm{C}}^2}\ , \\ H_{\mathrm{r}}(x_{\mathrm{r}}) &= -\frac{\hbar^2}{m}\frac{\partial^2}{\partial x_{\mathrm{r}}^2} + V(x_{\mathrm{r}})\ , \end{aligned} \tag{4.3}$$

with $x_{\mathrm{C}} = (x_1 + x_2)/2$ and $x_{\mathrm{r}} = x_1 - x_2$, which commute with one another and thus share eigenstates. This is a very general property which we will later see applies to the N body case, even with the addition of harmonic confinement [see Eq. (4.83)]. Therefore the centre-of-mass momentum p_{C} is a good quantum number and must be preserved in a scattering event, along with the total energy. This means for an incoming scattering state

$$\langle x_1, x_2|\psi_S\rangle = \exp(i[p_1x_1 + p_2x_2]/\hbar) = \exp(i[p_{\mathrm{C}}x_{\mathrm{C}} + p_{\mathrm{r}}x_{\mathrm{r}}]/\hbar)\ , \tag{4.4}$$

a scattered wavefunction can only have a relative momentum p_{r} or $-p_{\mathrm{r}}$ as these are the only two possible values which obey both momentum and energy

conservation. If $V(x)$ is of finite range, or at least tends to zero faster than $1/|x|$ asymptotically, then for sufficiently large separations $|x_{\mathrm{r}}|$ our scattering state is

$$\Psi_{p_{\mathrm{C}},p_{\mathrm{r}}}(x_{\mathrm{C}},x_{\mathrm{r}},t) \propto \exp\left(i\frac{p_{\mathrm{C}}x_{\mathrm{C}}}{\hbar}\right)\left[\exp\left(i\frac{p_{\mathrm{r}}x_{\mathrm{r}}}{\hbar}\right) - \exp\left(-i\theta(p_{\mathrm{r}}) - i\frac{p_{\mathrm{r}}x_{\mathrm{r}}}{\hbar}\right)\right] . \tag{4.5}$$

The phase factor $\theta(p_{\mathrm{r}})$ would be zero for a non-interacting system. In quantum mechanics energy controls the rate of phase rotation in the wavefunction, hence travelling through a varying potential leads to a phase shift $\theta(p_{\mathrm{r}}) = -\theta(-p_{\mathrm{r}})$.

If more quanta are present (say N) it is not enough to simply have two conservation laws to set the asymptotic scattering wavefunction to have the same momenta as the incoming state. Non-diffraction is the condition that all the other possible scattering paths cancel out asymptotically leaving only those that rearrange the input momenta. If this is the case, one can see the phase shift from scattering the first particle through n of the others to cause a phase shift of $\exp[\sum_{k=2}^{n} -i\theta(p_1 - p_k)]$, as long as we are looking in a region where the interactions are weak.

So far we have ignored symmetry, however this is an important property which enforces the particle exchange symmetry $\Psi(x_1,\ldots,x_j,\ldots,x_k,\ldots,x_N) = \pm\Psi(x_1,\ldots,x_k,\ldots,x_j,\ldots,x_N)$ with $+$ corresponding to bosons and $-$ to fermions. This enforces an extra $N!$ constrains on the wavefunction, and can significantly effect two body scattering. For the rest of this section we will consider only bosons, as this is the focus of this work.

This leads to the question "what two-body potentials admit non-diffractive scattering?" and thus yield a system that is "integrable." This is the case if one has, for example, two body interactions given by Eq. (3.24) (but not the general elliptic potential) [91] or the contact potential

$$V(x_k - x_j) = g_{1D}\delta(x_k - x_j) . \tag{4.6}$$

We discussed in Sec. 2.2.5 how this potential is found to accurately describe interactions between cold bosonic atoms in one dimensional configurations. Additionally we need not worry about asymptotic scattering, as the potential

is zero range, which simplifies matters considerably. As a proof this potential obeys diffractionless scattering, we need to verify that states which are just sums of differently arranged incoming momenta are eigenstates to the Schrödinger equation, which we do in the following subsections.

For convenience we will rescale the position coordinates to $\tilde{x}_k = x_k\sqrt{m}/\hbar$ and $\tilde{g} = mg_{1D}/\hbar^2$, for the rest of this section but the tildes will be dropped for future convenience. This does not uniquely define a unit system but effectively coincides with harmonic units (codified as $\hbar = m = \omega_x = 1$) used in Chap. 6.

4.1.2 Two-body eigenstates of the contact interaction

In order to find the eigenstates of the two body problem with $V(x) = g\delta(x)$ in Eq. (4.3), our relative wavefunction $\psi(x_\mathrm{r})$ must satisfy $\psi(x_\mathrm{r}) = \psi(-x_\mathrm{r})$ by Bose symmetry, and from the kinetic part of the relative Hamiltonian in Eq. (4.3)

$$-\frac{\partial^2}{\partial x_\mathrm{r}^2}\psi(x_\mathrm{r}) = E_\mathrm{r}\psi(x_\mathrm{r}) \,, \tag{4.7}$$

when $x_\mathrm{r} \neq 0$. Ordinarily the only symmetric solutions to this equation are of the form $\cos(kx_\mathrm{r})$ (with $k = (p_1 - p_2)/2$ a relative momentum/wavenumber a real number), however, as we don't require this function to be a solution at zero we can additionally have $\sin(k|x_\mathrm{r}|)$ as a valid solution. Ignoring for now issues with the orthogonality of these solutions (which is only really a problem if the system is of finite extent, and thus doesn't affect this discussion) a state with relative energy $E_\mathrm{r} = k^2$ can be expressed in the form

$$\psi_k(x_\mathrm{r}) = \alpha\cos(kx_\mathrm{r}) + \beta\sin(k|x_\mathrm{r}|) \,, \tag{4.8}$$

with k taking in principle any real value, and α and β any complex values satisfying a normalisation convention. For general values of α and β, complex values of k are not possible as they would yield divergent solutions as $x_\mathrm{r} \to \infty$; however if we have $\beta = i\alpha$ our solution reduces to

$$\psi_k(x_\mathrm{r}) = \alpha\mathrm{e}^{ik|x_\mathrm{r}|} \,, \tag{4.9}$$

which tends to zero as $x_\mathrm{r} \to \infty$ if $\mathrm{imag}(k) > 0$ and so is also allowed, corresponding to a bound state. Periodic or hard-wall boundary conditions at some finite length L would modify this condition slightly, but this analysis is always valid in an $L \to \infty$ limit. The interaction term $g\delta(x_\mathrm{r})$ gives a boundary condition on the first derivative at $x_\mathrm{r} = 0$:

$$\lim_{\epsilon \to 0} \left[\frac{\partial}{\partial x_\mathrm{r}} \psi(x_\mathrm{r}) \right]_{-\epsilon}^{+\epsilon} = g\psi(0) \ . \tag{4.10}$$

Inserting our general form from Eq. (4.8) and taking the limit gives

$$-2k\beta = g\alpha \ , \tag{4.11}$$

which reduces our solution to

$$\psi_k(x_\mathrm{r}) = \alpha \left[\cos(kx_\mathrm{r}) - \frac{g}{2k} \sin(k|x_\mathrm{r}|) \right] \ . \tag{4.12}$$

Using the identity $\sin(x+y) = \sin(x)\cos(y) + \cos(x)\sin(y)$ we can simplify this to

$$\begin{aligned} \psi_k(x_\mathrm{r}) &= \frac{\alpha}{\sin(\theta)} \sin(k|x_\mathrm{r}| + \theta) \ , \\ \theta &= \arctan\left(-\frac{2k}{g} \right) \ , \end{aligned} \tag{4.13}$$

which includes the familiar interaction phase-shift term $\theta(k/g)$. Considering again the case $\beta = i\alpha$ this condition becomes

$$\begin{aligned} k &= -\frac{ig}{2} \\ \psi_\mathrm{bound}(x_\mathrm{r}) &\propto \alpha \mathrm{e}^{g|x_\mathrm{r}|/2} \ . \end{aligned} \tag{4.14}$$

Recalling that we require $\mathrm{imag}(k) \leq 0$, this condition can only be satisfied if $g < 0$ giving a bound state with relative energy $E_\mathrm{r} = -g^2/4$; for $g > 0$, no bound state exists.

4.1.3 The Bethe ansatz on the infinite line

We first consider the eigenstates of the system with free boundary conditions. Such a system is not usually considered in the literature due to the fact that there is no obvious way to take a constant density thermodynamic limit (although the limit $gN =$ constant is appropriate). In a repulsive gas, letting any boundary $L \to \infty$ with N finite just results in a low density limit that behaves as a non-interacting system. Periodic boundary conditions are therefore necessary for $g > 0$, which we discuss briefly in Sec. 4.1.4.

However, for $g < 0$, bound states lead to a highly non trivial finite number system [117]. As the system obeys diffractionless scattering, multiple scattering events can be described by a series of two body scattering events. Therefore, similar to the two body case, we can express all the eigenstates of the system as a symmetrised product of plane waves of (dimensionless) asymptotic [1] momentum/wavenumber λ_k (collectively referred to as $\vec{\lambda}$) in any region where $x_1 \neq x_2 \neq .. \neq x_N$. Since our state will possess bosonic symmetry we may as well simply consider the region $x_1 < x_2 < .. < x_N$, as other regions can be obtained by permuting one of the indices. Such a state is given by

$$\Psi(\vec{x}, \vec{\lambda}) = \mathcal{N} \sum_P A_P \exp\left(i \sum_{k=1}^{N} \lambda_{P(k)} x_k \right), \tag{4.15}$$

with P denoting the set of permutations of the set $\{1, 2, \ldots, N\}$, $\mathcal{N}$ a normalisation factor and we denote A_P as the "permutation coefficients" which ensure the function satisfies the $(N-1)$ boundary conditions where $x_j \to x_{j+1}$ (from below due to our region of choice) due to the delta function terms:

$$\left(\frac{\partial}{\partial x_j} - \frac{\partial}{\partial x_{j+1}} \right) \Psi|_{x_j \to x_{j+1}} = g\Psi|_{x_j = x_{j+1}} \, . \tag{4.16}$$

This boundary can be obtained by integrating the eigenvalue equation $H\Psi = E\Psi$ with respect to a variable $y = x_{j+1} - x_j$ over the infinitesimal range $(-\epsilon, +\epsilon)$ such as was considered in [117]. These boundaries are due to a

[1] These are momenta only in the sense of asymptotic scattering, and are therefore sometimes referred to as rapidities. They do constitute good quantum numbers for the system.

scattering event between the jth and $(j+1)$th elements which causes the state to acquire a phase of $\theta(\lambda(j+1)-\lambda(j),g)$ as given by Eq. (4.13). Adjacent element permutations are sufficient to generate every coefficient in the permutation group, as any permutation can be expressed in terms of pair-wise swaps of adjacent elements [91]. Hence we conclude from Eq. (4.16) that for a permutation P' swapping the jth and $j+1$th elements of P (with $x_j \neq x_{j+1}$), these permutation coefficients must satisfy

$$A_{P'} = \mathrm{e}^{i\theta(\lambda_{P(j+1)}-\lambda_{P(j)},g)} A_P \,, \tag{4.17}$$

$$= \frac{\lambda_{P(j+1)}-\lambda_{P(j)}+ig}{\lambda_{P(j+1)}-\lambda_{P(j)}-ig} A_P \,. \tag{4.18}$$

We note two things from Eq. (4.17); firstly that if $g=0$ this equation reduces to $A_P = A_{P'}$ as one would expect. Secondly, that if any $\lambda_k = \lambda_j$ with $j \neq k$, then we have $A_P = -A_{P'}$ despite the fact the rest of the wavefunction has not changed, meaning these two permutations will cancel each other out. This second point would lead to an exclusion principle regarding the relative momenta where it not for the fact that on the infinite line they are not quantised so one can have $|\lambda_j - \lambda_k|$ arbitrarily small, but with boundary conditions we will see this is the case.

Remarkably Eq. (4.17) completely determines A_P up to the identity permutation, which we can fix via the normalisation factor. A solution (not normalised) satisfying Eq. (4.17) is

$$A_P = \prod_{1\leq k<j\leq N} \sqrt{\frac{\lambda_{P(k)}-\lambda_{P(j)}+ig}{\lambda_{P(k)}-\lambda_{P(j)}-ig}} \,. \tag{4.19}$$

It is possible to verify Eq. (4.19) satisfies Eq. (4.17) by noting that switching the ℓth and $\ell+1$th elements of a permutation P will reorder terms, but only modify the one term in the product with $j=\ell+1$, $k=\ell$. By continuity it is possible to write an expression which is valid over all space (see for example [118]), however it is usually easier for calculations to simply consider the region $x_1 < x_2 < \ldots < x_N$ and include all the others by symmetry. The energy and centre-of-mass momentum eigenvalues can again by calculated by the asymptotic method (or equivalently by noting the kinetic energy

discontinuities cancel the interaction terms in the Hamiltonian exactly)

$$E = \frac{1}{2}\sum_k \lambda_k^2, \qquad p_c = \sum_k \lambda_k \ . \tag{4.20}$$

Additionally, it has been shown that these eigenfunctions make up a complete set [119].

Bound state string solutions

Attractive interactions ($g < 0$) allow the possibility of complex components in $\vec{\lambda}$, as they did in the two body case. One can assume the centre-of-mass momentum and energy eigenvalues remain real, and hence we must have $\mathrm{Im}(p_c) = \sum_k \mathrm{Im}(\lambda_k) = 0$ and $\mathrm{Im}(E) = \sum_k \mathrm{Re}(\lambda_k)\mathrm{Im}(\lambda_k) = 0$ as a condition. Additionally to these two conditions we must maintain the two body matrix scattering elements, given in Eq. (4.14) [recalling that $k = (p_1 - p_2)/2$], between particles in a bound state, implying that if the j and $j+1$th elements are in a bound state

$$\lambda_j - \lambda_{j+1} = i|g| \ . \tag{4.21}$$

Extending this to a bound state of n atoms we must have λ_j to λ_{j+n-1} all with the same real component and with the imaginary components spaced by $ig/2$. In general we can have any number $\eta \leq N$ of bound states present, each one characterised by the number of atoms N_α and real momentum per atom p_α. Hence we introduce the parametrisation for a bound state of N_α atoms

$$\lambda_\alpha^a = p_\alpha + i\frac{g}{2}(N_\alpha + 1 - 2a) \ , \tag{4.22}$$

with $\alpha = \{1, \ldots, \eta\}$ the string number, $a = \{1, \ldots, N_\alpha\}$ the position in the string, and the set $\{[p_1, N_1], \ldots, [p_\eta, N_\eta]\}$ corresponding to good quantum numbers for the system. To relate these labels back to the original index label j, we have α is the minimum number satisfying $\sum_{k=1}^{\alpha} N_k < j$, with N_k the size of the kth string, and $a = j - \sum_{k=1}^{\alpha} N_k$.

Reduced scattering matrix

The most important point to note about the presence of bound states is their effect on the permutation coefficients. Taking $P = I$ to be the identity permutation and P' to be the permutation switching λ_α^a with λ_α^{a+1}, the coefficient $A_{P'}$ is given by Eq. (4.19) to be

$$\begin{aligned} A_{P'} &= \frac{p_\alpha + i\frac{g}{2}(N_\alpha - 1 - 2a) - p_\alpha - i\frac{g}{2}(N_\alpha + 1 - 2a) + ig}{p_\alpha + i\frac{g}{2}(N_\alpha - 1 - 2a) - p_\alpha - i\frac{g}{2}(N_\alpha + 1 - 2a) - ig} A_I \\ &= 0/(-2ig) \ , \end{aligned} \tag{4.23}$$

i.e. we need not include in the wavefunction any permutations which switch any elements of the bound state strings. This implies that each of these bound state strings constitutes a structureless particle, and we should be able to derive the scattering phase shift from one string of size N_α and momentum per atom p_α and other of size N_β and momentum per atom p_α. Denoting $\tilde{P}$ a permutation which moves all the positions of string one to those of string two, we have

$$A_{\tilde{P}} = \mathrm{e}^{i\theta(N_\alpha, p_\alpha, N_\beta, p_\beta)} A_P \ . \tag{4.24}$$

This can be computed by applying Eq. (4.17) $N_\alpha N_\beta$ times. We denote for convenience the relative momentum per atom divided by the interaction strength

$$p_{\alpha,\beta} = \frac{p_\alpha - p_\beta}{g} \ , \tag{4.25}$$

and noting that

$$\lambda_\beta^b - \lambda_\alpha^a = p_{\alpha,\beta} + i\left(a - b + \frac{N_\beta - N_\alpha}{2}\right) \ , \tag{4.26}$$

we have a scattering matrix element $S(N_\alpha, N_\beta, p_{\alpha,\beta}) = \exp[i\theta(N_\alpha, p_\alpha, N_\beta, p_\beta)]$ of

$$\begin{aligned} S(N_\alpha, N_\beta, p_{\alpha,\beta}) &= \prod_{a=1}^{N_\alpha}\prod_{b=1}^{N_\beta}\left[\frac{p_{\alpha,\beta}+i\left(a-b+1+\frac{N_\beta-N_\alpha}{2}\right)}{p_{\alpha,\beta}+i\left(a-b-1+\frac{N_\beta-N_\alpha}{2}\right)}\right] \\ &= \left[\frac{p_{\alpha,\beta}+i\left(\frac{N_\beta-N_\alpha}{2}\right)}{p_{\alpha,\beta}-i\left(\frac{N_\beta-N_\alpha}{2}\right)}\right]\left[\frac{p_{\alpha,\beta}+i\left(\frac{N_\beta+N_\alpha}{2}\right)}{p_{\alpha,\beta}-i\left(\frac{N_\beta+N_\alpha}{2}\right)}\right] \\ &\quad\times\left[\prod_{j=1}^{N_\alpha-1}\frac{p_{\alpha,\beta}+i\left(\frac{N_\beta-N_\alpha}{2}+j\right)}{p_{\alpha,\beta}-i\left(\frac{N_\beta-N_\alpha}{2}+j\right)}\right]^2 . \end{aligned} \tag{4.27}$$

This matrix element is of unit absolute value, which reinforces the idea of these bound states as particles in their own right, with no accessible substructure through interactions under the Hamiltonian Eq. (4.1). External potentials and defects can potentially destroy this integrability and allow mixing between bound states.

Energy and momentum of strings

Our energy and centre-of-mass momentum are given as before. Expressed in the new quantum numbers we have

$$E = \sum_{\alpha=1}^{\eta} N_\alpha\left[\frac{p_\alpha^2}{2} - \frac{(N_\alpha^2-1)g^2}{24}\right], \quad p_c = \sum_{\alpha=1}^{\eta} N_\alpha p_\alpha \, . \tag{4.28}$$

The ground state of the system is the state with just one string, i.e.:

$$\begin{aligned} \lambda_j &= i\frac{g}{2}(N+1-2j) \, , \\ E_0 &= -\frac{g^2 N(N+1)(N-1)}{24} \, . \end{aligned} \tag{4.29}$$

In this case only the identity permutation coefficient remains finite and the wavefunction acquires the surprisingly simple form

$$\Psi(\vec{x}) = \mathcal{N}\prod_{1\le k<j\le N}\exp\left(\frac{g}{2}|x_j - x_k|\right) \, . \tag{4.30}$$

Excited states of the centre-of-mass are possible with continuous real momentum values, which can be scaled out via Galilean invariance; excitations breaking this bound state apart are however spaced with discrete spacings. For example the energy required to split one atom from this state, with a momentum relative to the centre-of-mass of the $N-1$ bound state of p_r, is

$$\begin{aligned}\Delta E &= \frac{p_r^2}{2} - \frac{g^2}{24}\left[N(N-1)(N-2) - (N+1)N(N-1)\right] \\ &= \frac{p_r^2}{2} + \frac{g^2 N(N-1)}{8} \, . \end{aligned} \tag{4.31}$$

Normalisation

On an infinite space, normalisation of plane wave states can become problematic. However we adopt the following general normalisation/orthogonality convention for many boson plane wave states in scattering theory

$$\begin{aligned}&\langle p'_M \sigma'_M, \ldots, p'_1 \sigma'_1 | p_1 \sigma_1, \ldots, p_N \sigma_N \rangle = \\ &\delta_{M,N} \sum_P \delta_\Gamma(p_1 - p'_{P(1)}) .... \delta_\Gamma(p_N - p'_{P(N)}) \, , \end{aligned} \tag{4.32}$$

with $\delta_{M,N}$ a Kronecker delta function and

$$\delta_\Gamma(p_k - p'_j) = 2\pi \delta_{\sigma_k, \sigma'_j} \delta(p_k - p'_j) \, . \tag{4.33}$$

In our case the parameters σ_k denote the number of atoms in a bound state as each bound state is treated like a unique, structureless particle of mass N_α. We denote a state with η bound states, each of size N_k with momentum per atom p_k, as $|p_1, N_1, \ldots, p_\eta, N_\eta\rangle$ and so we can express this orthogonality condition (taking as read that both states have η different particles) as

$$\begin{aligned}&\langle p'_1, N'_1, \ldots, p'_\eta, N'_\eta | p_1, N_1, \ldots, p_\eta, N_\eta \rangle = \\ &\prod_{\alpha=1}^{\eta} \sum_{\beta=1}^{\eta} \delta_{N_\alpha, N'_\beta} \frac{2\pi}{N_\alpha} \delta(p_\alpha - p'_\beta) \, , \end{aligned} \tag{4.34}$$

with the factor of N_α due to the fact we have chosen to use the momentum per atom of the bound states rather than the total momentum. For the case

of the ground state $\eta = 1$, Eq. (4.34) reduces to

$$\langle p', N|p, N\rangle = 2\pi\delta(N[p - p']) \ , \tag{4.35}$$

which is such that the Fourier transform of the wavefunction with respect to the centre-of-mass momentum eigenvalue $N \times p$, is normalised to unity.

4.1.4 The Bethe ansatz with periodic boundary conditions

If we take our system with the Hamiltonian Eq. (4.1) and place it in a periodic box of length L (such as would be imposed by a wide toroidal trapping potential [120]), it is now the case that one particle scattering off the other $N-1$ and making a full circle back to its initial condition must have accumulated no phase shift, else the periodicity $\Psi(x_1, \ldots, x_N) = \Psi(x_1 + L, x_2, \ldots, x_N)$ would be violated (true even for distinguishable particles). Identical particles have to satisfy the stronger constraint that permuting the two particles at either end of the ring must cause no change (a minus sign) to the wavefunction for Bosons (Fermions), i.e. $\Psi(x_1, \ldots, x_N) = \pm\Psi(x_2, \ldots, x_N, x_1 + L)$. Applying this condition to Eq. (4.15) gives

$$\begin{aligned} &\sum_P A_P \exp\left(i\sum_{j=1}^{N} x_j\lambda_{P(j)}\right) = \\ &\sum_P A_P \exp\left(i\sum_{j=2}^{N} x_j\lambda_{P(j-1)} + i(L + x_1)\lambda_{P(N)}\right) \ . \end{aligned} \tag{4.36}$$

We note such a change can be also be accomplished by $N-1$ pairwise swaps, and we will denote this permutation Q. Applying these permutations allows cancellation of the x dependence:

$$A_P = A_Q \exp\left(iL\lambda_{Q(N)}\right) \ , \tag{4.37}$$

noting $Q(N) = P(1)$. From Eq. (4.17) we can show that the two coefficients are related via

$$A_Q = A_P \prod_{\ell=1}^{N-1} -\frac{\lambda_{Q(N)} - \lambda_{Q(\ell)} + ig}{\lambda_{Q(N)} - \lambda_{Q(\ell)} - ig} \,, \tag{4.38}$$

and finally we choose $Q(N) = j$ to obtain the N Bethe ansatz equations for the allowed values of $\vec{\lambda}$

$$(-1)^{N-1} = \mathrm{e}^{i\lambda_j L} \prod_{k\neq j}^{N} \frac{\lambda_j - \lambda_k + ig}{\lambda_j - \lambda_k - ig}, \quad j = 1, \ldots, N \,. \tag{4.39}$$

This quantises $\vec{\lambda}$, and it is now meaningful that one cannot have two identical elements in this set. The normalisation factors for this system are also known by the Gaudin-Korepin formula [121]. The energy of the state is related to the scattering momenta, as it was in the free case.

These equations are necessary for the well studied case of repulsive bosons [20], the thermodynamics limit $N \to \infty$, $L \to \infty$ with constant density is known. The repulsive ground state is obtainable by comparisons with a Fermi sea, and excitations behaving in a similar way to holes. Extremely repulsive systems, satisfying $mg_{1\mathrm{D}}/\hbar^2 n \gg 1$, behave even more fermion-like, with the states described by symmetrised Slater determinants [116]. This has allowed for analytic work predicting correlation functions [122] and coherent states in harmonic confinement [123]. The regime for one-dimensionality to be valid has been investigated via extensions to the LL model [124] and the conditions for stability with attractive interactions [125].

However, as we mentioned before if $g < 0$ the behaviour of the ground state as $L \to \infty$ with N finite is non-trivial, giving rise to quantum solitons.

4.1.5 The Bethe ansatz with infinite size periodic boundary conditions and attractive interactions

Attractive interactions again allow the possibility of complex components in $\vec{\lambda}$ with periodic boundary conditions present, but additionally we require

that Eq. (4.39) must still be satisfied, i.e.

$$\mathrm{e}^{i\,\mathrm{Re}(\lambda_j)L}\mathrm{e}^{-\mathrm{Im}(\lambda_j)L} = \prod_{k\neq j}^{N} \frac{\lambda_j - \lambda_k + ig}{\lambda_j - \lambda_k - ig} \,. \tag{4.40}$$

Terms of order e^{-CL} with $C > 0$ will rapidly vanish as $L \to \infty$, implying at least one of the numerators on the RHS is exponentially small. Likewise for $C < 0$ this term will tend to infinity and at least one of the denominators on the RHS is exponentially small. This can be achieved by slightly modifying the string parametrisation to [126]

$$\lambda_\alpha^a = p_\alpha + i\frac{g}{2}(N_\alpha + 1 - 2a) + i\delta_\alpha^a \,, \tag{4.41}$$

with the labels α and a running over the same range as before and the (almost) good quantum numbers $\{p_1, N_1, \ldots, p_\eta, N_\eta\}$ characterising the state. The elements $\delta_\alpha^a \sim \mathrm{e}^{-|C|L}$ are referred to in the literature as string deviations and decrease exponentially with the ring length [126]. In the limit $L \to \infty$ these string deviations vanish, if the coefficients A_P are given by Eq. (4.19) the normalisation factor can be expressed as [118]

$$|\mathcal{N}_{\vec{\lambda}}|^{-2} = \frac{(|g|L)^\eta}{|g|^N N!} \prod_{\beta=1}^{\eta} N_\beta^2 \prod_{\alpha=1}^{\beta-1} \frac{p_{\alpha,\beta}^2 + \left(\frac{N_\alpha + N_\beta}{2}\right)^2}{p_{\alpha,\beta}^2 + \left(\frac{N_\alpha - N_\beta}{2}\right)^2} \,; \tag{4.42}$$

this expression[2] employs the convention that an empty product is equal to unity. By separating $p_{\alpha,\beta}$ into centre-of-mass and relative momentum, we can take states which are superpositions of these momentum values (either continuously or discretely) to construct soliton like states within a harmonic oscillator.

[2]The factor of $|g|^N N!$ is not present in the derivation of [118] due to a slightly different definition of the wavefunction.

4.1.6 Reduction to GPE results

Density about the centre of mass

It is of interest to know where and how these many-body results reduce to those of the GPE. The first known result is the number density (normalised to the atom number N) about the centre-of-mass position of the ground state (single string state) [127, 128]

$$\begin{aligned}\rho(x) &= \int dx_1 \dots dx_N |\Psi(\vec{x})|^2 \delta\left(\frac{1}{N}\sum_{k=1}^{N} x_k\right) \sum_{k=1}^{N} \delta\left(x - x_k\right) \\ &= N^2|g| \sum_{k=0}^{N-2} \left[\prod_{j=0}^{k} \frac{N-j-1}{N+j}\right] (-1)^k (k+1) \mathrm{e}^{Ng(k+1)|x|} \qquad (4.43)\end{aligned}$$

$$\tilde{\rho}(\tilde{x}) = N \sum_{k=0}^{N-2} \left[\prod_{j=0}^{k} \frac{N-j-1}{N+j}\right] (-1)^k (k+1) \mathrm{e}^{-(k+1)|\tilde{x}|} \qquad (4.44)$$

with $\Psi(\vec{x})$ given in Eq. (4.30) and $\tilde{x} = N|g|x$ and $\tilde{\rho}(\tilde{x})$ normalised w.r.t. $\tilde{x}$; note this rescaling is equivalent to soliton units ($\hbar = m = gN = 1$). This result isn't immediately obviously equivalent to the classical $N\mathrm{sech}^2(x/2)/4$ profile from a GPE soliton, however we note that for real x

$$\frac{1}{2}\mathrm{sech}\left(\frac{x}{2}\right) = \frac{e^{-|x/2|}}{1+e^{-|x|}} = e^{-|x/2|} \sum_{k=0}^{\infty} (-1)^k e^{-k|x|} \,, \qquad (4.45)$$

with the Taylor series converging absolutely everywhere except $x = 0$. Using this we can expand the classical soliton density as[3]

$$\rho^{\mathrm{sol}}(x) = \frac{N}{4}\mathrm{sech}^2\left(\frac{x}{2}\right) = N \sum_{k=0}^{\infty} (-1)^k (k+1) e^{-(k+1)|x|} \,, \qquad (4.46)$$

hence we can directly compare the density profiles of the many-body density about the centre-of-mass and the mean field prediction, dropping the tildes

[3]The result is obtained by taking the product of series and the identity $\sum_{k,j=0}^{\infty} f_{j+k} \equiv \sum_{K=0}^{\infty}\sum_{J=0}^{K} f_K = \sum_{K=0}^{\infty}(K+1)f_K$, where the reordering over $K = k+j$ and $J = k-j$ is permitted because the sum is absolutely convergent.

as all units are soliton units:

$$\frac{\rho^{\mathrm{sol}}(x)-\rho(x)}{N} = \sum_{k=0}^{\infty}\left[1-\prod_{j=0}^{k}\frac{N-j-1}{N+j}\right](-1)^k(k+1)\mathrm{e}^{-(k+1)|x|}$$
$$\sim \sum_{k=0}^{\infty}\left[\frac{1}{N}+\mathcal{O}\left(\frac{k}{N}\right)\right](-1)^k(k+1)\mathrm{e}^{-(k+1)|x|}\,. \qquad (4.47)$$

Because these deviations are of order $1/N$ for the lower order terms and higher order terms are exponentially suppressed anyway, these two densities can be said to be equal in the limit $N \to \infty$. This is however the density about the centre-of-mass, which for the cluster eigenstates is strictly delocalised over all space. This can be thought of purely as an uncertainty in the centre-of-mass position, however we show the fidelity of the many-body wavefunction with a Gaussian distribution of momentum and the Hartree product soliton state tends to a large value in Sec. 5.5.3.

Position and phase shifts from collisions

The second important result is the position and phase shift from a collision between two classical solitons as given in Eq. (3.14). This is again not immediately clear since the Bethe Ansatz eigenstates are totally delocalised states, and thus have total position uncertainty and also well defined number, and hence poorly defined phase. A superposition of single cluster states (ground states) with different centre-of-mass momentum would however be localised like a classical soliton. This principle has been used to study quantum solitons in optical fibres [117] by considering states which possess an uncertainty in the *total* (photon) number. We consider a slightly different situation, of a state which is an atomic coherent state [129], a superposition of *relative*

number and (dimensionless) relative momentum-per-atom

$$|\Psi\rangle_{2\,\mathrm{sol}} = \sum_{n=0}^{N} \sqrt{\binom{N}{n}} \cos^n(\vartheta/2) \sin^{N-n}(\vartheta/2) \mathrm{e}^{i(N-n)\phi} \iint dp_\mathrm{c} dp_\mathrm{rel}$$
$$f_n(p_\mathrm{c}) g(p_\mathrm{rel}) |n, p_\mathrm{c}/2 + p_\mathrm{rel}/2, N-n, p_\mathrm{c}/2 - p_\mathrm{rel}/2\rangle \tag{4.48}$$

$$f_n(p_\mathrm{c}) = \frac{\exp\left[-\frac{p_\mathrm{c}^2}{2\Delta p^2} - i x_0 p_\mathrm{c}(n - N/2)\right]}{\sqrt{\Delta p \sqrt{\pi}}} \tag{4.49}$$

$$g_n(p_\mathrm{rel}) = \frac{\exp\left[-\frac{(p_\mathrm{rel}-p_0)^2}{2\Delta p^2} - i x_0 N p_\mathrm{rel}/2\right]}{\sqrt{\Delta p \sqrt{\pi}}} \,. \tag{4.50}$$

Here if p_1 and p_2 are the momentum-per-atoms/velocities of either string then $p_\mathrm{rel} = p_1 - p_2$ and $p_\mathrm{c} = p_1 + p_2$. Before the collision the state has a soliton on the left of the centre with a number expectation value of $N\cos^2(\vartheta/2)$ and one to the right with a number expectation value of $N\sin^2(\vartheta/2)$, with a relative phase of ϕ between the two states. When viewed as separate objects, all possible number distributions between these solitons have equal mean velocities/momentum per atom; this implies each number configuration has a different mean centre-of-mass momentum $p_\mathrm{cm} = Np_\mathrm{c}/2 + (n - N/2)p_\mathrm{rel}$ (different from the setup we consider in Chap. 6 in harmonic confinement). If the states are well separated, before the collision only the identity permutation is significant, with all others decaying exponentially with the separation. After the collision and when the states are again well separated, there can be no number transfer (as bound state numbers are good quantum number), hence the number expectation values to the left and right will have reversed, so the permutation (for each n) which switches the positions $\mathcal{P} = [n+1, \ldots, N, 1, \ldots, n]$ will become significant. These permutations each have a different coefficient associated with them, the ratio of which is given by S in Eq. (4.27). This gives a scattering phase shift for each p_rel and n of

$$\begin{aligned}\theta(n, N-n, p_\mathrm{rel}) &= -i \log[S(n, N-n, p_\mathrm{rel})] \\ &= -2\sum_{j=0}^{n} (2 - \delta_{j,0} - \delta_{j,n}) \tan^{-1}\left(|g| \frac{N/2 - n + j}{p_\mathrm{rel}}\right). \end{aligned} \tag{4.51}$$

This is essentially a rescaling of the initial relative momentum and relative number distributions (the centre-of-mass properties remain the same).

Adapting the method of [117], we can Taylor expand θ to first order about the expected values of n and p_r

$$\theta(n, N-n, p_{\text{rel}}) \approx \theta(n_L, N-n_L, p_0)+(n-n_L)\frac{\partial}{\partial n}\theta|_{n_L,p_0}+(p_{\text{rel}}-p_0)\frac{\partial}{\partial p_{\text{rel}}}\theta|_{n_L,p_0} \ , \tag{4.52}$$

with $n_L = N\cos^2(\theta/2)$ the left number expectation value.

The momentum derivative gives a number weighted relative position shift, a rescale of x_0 by

$$\begin{aligned}\frac{1}{2N}\frac{\partial}{\partial p_{\text{rel}}}\theta|_{n_L,p_0} &= -\frac{1}{N}\sum_{j=0}^{n}(2-\delta_{j,0}-\delta_{j,n})\frac{|g|(N/2-n+j)}{p_{\text{rel}}^2+|g|^2(N/2-n+j)^2} \\ &\sim -\frac{1}{N|g|}\ln\left[\frac{N^2g^2+4p_{\text{rel}}^2}{|g|^2(N-2n)^2+4p_{\text{rel}}^2}\right] \ . \end{aligned} \tag{4.53}$$

The latter step is performed using the Euler-McLaurin formula to zeroth order. In order to compare this with Eq. (3.18a) (recalling that the shift is twice this value) we note firstly that Eq. (4.53) is equivalent to $q_1 - q_2$ so the $(A_1+A_2)/A_1A_2$ prefactor is not included and that $|g| = 1/N$ in soliton units and take $A_1 - A_2 = (N-2n_L)/2N$ and $p_1 - p_2 \to p_0$; this exactly reproduces Eq. (4.53), and so is the same up to high orders in the derivative expansion and truncation in the Euler-McLaurin formula.

The number derivative represents a shift in the relative phase between each soliton (a rescale of ϕ) due to the additional interaction; number is a discrete variable so we take the derivative to be the symmetric difference

$$\begin{aligned}\frac{\partial}{\partial n}\theta|_{n_L,p_0} &\sim \frac{1}{2}[\theta(n+1, N-n-1, p_0) - \theta(n-1, N-n+1, p_0)] \\ &= -\left[\tan^{-1}\left(|g|\frac{N-2n_L-2}{2p_0}\right) + 2\tan^{-1}\left(|g|\frac{N-2n_L}{2p_0}\right)\right. \\ &\quad \left. + \tan^{-1}\left(|g|\frac{N-2n_L+2}{2p_0}\right)\right] \ . \end{aligned} \tag{4.54}$$

Classically one expects no relative phase shift between solitons if they are the same size. Setting $n_L = N/2$ in Eq. (4.54) gives zero for $\frac{\partial}{\partial n}\theta|_{n_L,p_0}$ and this agrees with the classical case. If $n_L \neq N/2$ then a shift does occur.

Comparing with Eq. (3.18b) we have a difference of

$$|\delta\Phi_{\rm qm} - \delta\Phi_{\rm cls}| \sim \left[\tan^{-1}\left(|g|\frac{N-2n_L-2}{2p_0}\right) - 2\tan^{-1}\left(|g|\frac{N-2n_L}{2p_0}\right) + \tan^{-1}\left(|g|\frac{N-2n_L+2}{2p_0}\right)\right] , \tag{4.55}$$

which vanishes so long as either $|N-2n_L| \gg 1$ or $|(N-2n_L)g/p_0| \ll 1$, hence the quantum corrections only show for extremely slow collisions and low atom number.

Summary

We discussed the notion of quantum integrability in the sense of scattering without diffraction and the Bethe ansatz. We introduced the bound state string eigenstates to the attractive Lieb-Liniger equation, which describes cold Bose gases in 1D, including the scattering matrix elements of two strings. Additionally we investigated the effect of periodic boundary conditions, leading to the Bethe Ansatz equations. Finally we showed that the density about the centre of mass and position and phase shifts after collisions were the same for string solutions and a GPE solitons in the limit high N.

4.2 Harmonic oscillator potentials and many body physics

4.2.1 Harmonic oscillator potentials for many non-interacting particles

An interesting property of the harmonic oscillator potential is that having many quanta is in principle equivalent to having many dimensions. A Hamiltonian for N non-interacting particles can always be split into N commuting single particle Hamiltonians

$$\hat{H}(\mathbf{r}_1, \ldots, \mathbf{r}_N) = \hat{\mathcal{H}}(\mathbf{r}_1) + ... + \hat{\mathcal{H}}(\mathbf{r}_N) . \tag{4.56}$$

Likewise, each of the single particle Hamiltonians $\hat{\mathcal{H}}(\mathbf{r})$ can be separated into D commuting parts, where D is the number of spatial dimensions, and so it seems one must simply consider $N \times D$ one dimensional problems. One could therefore in principle define $N \times D$ ladder operators $\hat{a}_{j,k}$ (with $j = 1, \ldots, D$ and $k = 1, \ldots, N$) and derive the properties of the system this way. This is true if the particles are all distinguishable in some way. However if they are not then we are neglecting one of the most important symmetries in many-body physics, the bosonic or fermionic symmetry of the wavefunction:

$$\Psi(\ldots, \mathbf{r}_j, \ldots, \mathbf{r}_k, \ldots) = \pm\Psi(\ldots, \mathbf{r}_k, \ldots, \mathbf{r}_j, \ldots) \,, \tag{4.57}$$

with the $-$ sign occurring for particles with half integer spin (fermions). Considering for example Bosons, the state created by the action of a ladder operator for particle one on the ground state $a^\dagger_{1,1}|\text{ground}\rangle = |1\rangle_{1,1}|0\rangle_{1,2}\ldots|0\rangle_{N,D}$, does not satisfy bosonic symmetry and is not allowed. Similar properties are true for fermions but now the ground state is more complicated to express.

4.2.2 Degeneracy of states in 1D many-body oscillators

We now restrict ourselves to the $D = 1$ dimensional harmonic oscillator for simplicity. The imposition of permutational symmetry in the wavefunction changes the degeneracy of each energy level significantly. The degeneracy in this system has been investigated in, for example, [130–132] and references therein. For bosons, the degeneracy of the nth excited state with energy $E_n = (n+N/2)\hbar\omega$, is given by the number of ways to partition n using N non-negative integers *without* repetition. We will show later that this is equivalent to using only numbers less than or equal to N [133]. It is conventional to denote the ways to partition a number n in exactly ℓ numbers greater than or equal to a as $\Phi(n, \ell, a)$. We can split the partitions of n into partitions that use the number a at least once and those that do not, i.e. partitions which have a minimum of $a + 1$ or larger. There are no partitions satisfying $a > n$ and only one partition with $a = n$ (the number n) and therefore $\ell = 1$

or $a = n = \ell = 0$. These properties allow us to derive the recurrence relation:

$$\Phi(n,\ell,a) = \begin{cases} 0 & \text{if } a > n \text{ or } a = n \text{ and } \ell \neq 1 \\ 1 & \text{if } a = n \text{ and } \ell = 1 \\ \Phi(n,\ell,a+1) + \Phi(n-a,\ell-1,a) & \text{otherwise} \end{cases} \tag{4.58}$$

and $\Phi(0,0,0) = 1$. So the degeneracy of the nth excited state is thus

$$g_n = \Phi(n,\ell,0)\ . \tag{4.59}$$

Equally we could consider the degeneracy of fermionic states in a harmonic oscillator, which for a state of energy E_n (the energy of the nth bosonic excited state) would be the number of ways to partition n using N non-identical non-negative integers which we can denote $\tilde{\Phi}(n,\ell,a)$. This function can be split into distinct parts as before, and one obtains essentially the same recurrence relation as Eq. (4.58), except the first non-zero value for $\ell = N$ wouldn't occur until $n = 0 + 1 + 2 + ... + N - 1 = N(N-1)/2$ with $E = \hbar\omega N^2/2$ the fermionic ground state energy. This leads us to the remarkable conclusion that $\tilde{\Phi}(n + \ell(\ell-1)/2, \ell, a) = \Phi(n,\ell,a)$ and the fermionic degeneracy for the nth excited state *is exactly the same as for the bosonic case*, given in Eq. (4.59); the only difference being that the ground state energy is larger.

We also note that $\Phi(n,\ell,0)$ is equal to the number of ways to partition n using only numbers less than or equal to ℓ. Given ℓ numbers $\{a_1,\ldots,a_\ell\} \geq 1$, which partition n, ordered such that $a_1 \leq a_2 \leq \ldots \leq a_\ell$, then we can equally partition n with $b_1 = a_\ell - a_{\ell-1}$ ones and $b_2 = a_{\ell-1} - a_{\ell-2}$ twos etc, in a dual partition. This property can be easily shown visually via a Ferriers diagram such as Fig. 4.1. Naturally this dual partition has only numbers up to ℓ. This identity is also useful for understanding a many-body ladder operator treatment of the system. We therefore introduce the notation $p([a,b],n)$ being the number of ways to partition an integer n using only integers $a \leq z \leq b$. In order to compute these for a given b, we use the

recurrence relation

$$p([a,b],n) = \begin{cases} 0 & \text{if } a \geq \min(\mathrm{n},\mathrm{b}) \text{ and } n \neq 0 \\ 1 & \text{if } [a = n \text{ or } n = 0] \,\&\, a \leq b \\ p([a+1,b],n) + p([a,b],n-a) \text{ otherwise} , \end{cases} \tag{4.60}$$

derived via the same logic as before.

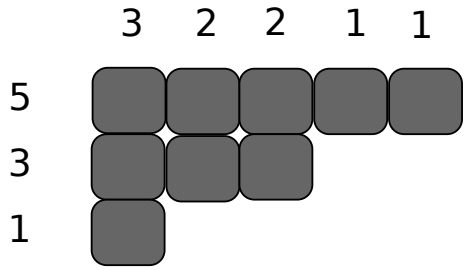

Figure 4.1: This diagram shows a visualisation of a partition of the number eight, this can be thought as a partition into the five integers $\{1,1,2,2,3\}$ along the top or the dual partition of three integers $\{5,2,1\}$ along the side.

4.2.3 Creation and annihilation operators

The most common way of dealing with indistinguishably is to change to an occupation number representation of the wavefunction

$$|\Psi\rangle = |n_0, n_1, n_2, \ldots, n_\infty\rangle \, , \tag{4.61}$$

with n_k denoting the number of quanta present in the kth oscillator state, which for bosons can be any integer (subject to the constraint that the total number is N) and for fermions must be either 0 or 1. This representation can be converted to a normalised wavefunction via the symmetrisation operator, which we define via its action on a many-body wavefunction or state ket:

$$\begin{aligned} \hat{S}_\pm[f(\vec{x})] &= \frac{1}{\sqrt{N!}} \sum_P (\pm)^{[P]} f(x_{P(1)}, \ldots, x_{P(N)}) \\ \hat{S}_\pm[|n_1\rangle_1, \ldots, |n_N\rangle_N] &= \frac{1}{\sqrt{N!}} \sum_P (\pm)^{[P]} |n_{P(1)}\rangle_1 \ldots |n_{P(N)}\rangle_N \, , \end{aligned} \tag{4.62}$$

with P the set of all permutations of $\{1, \ldots, N\}$, and the minus sign only for fermions where the number of pair-wise swaps to make the permutation P from the identity permutation is odd. This operator has the disadvantage of not preserving normalisation. On states which already satisfy the correct symmetry, it will add a factor of $\sqrt{N!}$ to the norm and on states which have the opposite permutational symmetry it will return zero. Only states which have no permutational symmetry have their norm preserved. We can use this to express our wavefunction as

$$\langle x_1, \ldots, x_N | n_0, n_1, n_2, ...n_\infty \rangle = \hat{S}_\pm \prod_k \frac{1}{\sqrt{n_k!}} \prod_{j=1}^{n_k} \phi_k[x_{n_0+\cdots+n_{k-1}+j}] \ , \quad (4.63)$$

with the factors of $1/\sqrt{n_k!}$ necessary to provide normalisation. We can now define creation and annihilation operators $\hat{c}_k^\dagger$ and $\hat{c}_k$ via

$$\hat{\Psi}(x) = \sum_{k=0}^{\infty} \phi_k(x) \hat{c}_k \ , \quad (4.64)$$

which satisfy

$$\hat{c}_k^\dagger | \ldots, n_k, \ldots \rangle = \sqrt{n_k + 1} | \ldots, n_k + 1, \ldots \rangle \quad (4.65)$$

$$\hat{c}_k | \ldots, n_k, \ldots \rangle = \sqrt{n_k} | \ldots, n_k - 1, \ldots \rangle \ . \quad (4.66)$$

These operators have the advantage of preserving the symmetry of the state, and we can use them to express the Hamiltonian as

$$\hat{H} = \hbar\omega \sum_{k=0}^{\infty} (k + 1/2) \hat{c}_k^\dagger \hat{c}_k \ . \quad (4.67)$$

4.2.4 Relation to ladder operators

Creation and annihilation operators[4] are however not simple to relate back to the original ladder operators of the Hamiltonian. However, to see that it is possible we transform to a coordinate system known as normalised Jacobi

[4]We note $\hat{c}_k^\dagger$ and $\hat{c}_k$ are also ladder operators to the Hamiltonian as they satisfy Eq. (2.9) (with $c \propto k$), however we are interested in Ladder operators which preserve total number.

coordinates [134]

$$\xi_1 \equiv \frac{1}{\sqrt{N}} \sum_{k=1}^{N} x_k \tag{4.68}$$

$$\xi_k \equiv \sqrt{\frac{k-1}{k}} \left[x_k - \frac{1}{k-1} \sum_{j=1}^{k-1} x_j \right] \quad \text{k>1} \ . \tag{4.69}$$

Using these coordinates we can express the 1st quantized Hamiltonian as

$$H(\xi_1, \ldots, \xi_N) = \sum_{k=1}^{N} \left(-\frac{\hbar^2}{2m} \frac{\partial^2}{\partial \xi_k^2} + \frac{m\omega^2 \xi_k^2}{2} \right) \ . \tag{4.70}$$

Via the identity Eq. (A.11), this is again in the form of N separable single coordinates commuting Hamiltonians with normal Harmonic oscillator eigenfunctions. We can then express eigenstates as being a product of these states, but again the total wavefunction must obey the correct permutational symmetries so we require the symmetrisation operator again:

$$\Psi(\xi_1, \ldots, \xi_N) \propto \hat{S}_{\pm} \left[\phi_{n_1}(\xi_1) \phi_{n_2}(\xi_2) ... \phi_{n_N}(\xi_N) \right] \ . \tag{4.71}$$

Taking the example of $N = 2$, we have $\xi_2 = (x_2 - x_1)/\sqrt{2}$ and symmetrisation demands that the eigenfunctions of the $k = 2$ component of the Hamiltonian (4.70) satisfy $\phi_k(\xi_2) = \pm\phi_k(\pm\xi_2)$. Hence only even (odd) functions are allowed for bosons (fermions). However, regardless of N, symmetry imposes no constraints to functions of the (scaled) centre-of-mass position coordinate ξ_1; any function of ξ_1 is unchanged by permutations of $x_1, \ldots, x_N$ and thus can simply be factors out of the symmetry operator, and can therefore take normal harmonic oscillator eigenfunctions. We can define a many-body ladder operator which raises the centre-of-mass mode state by one in terms of the single particle ladder operators via

$$\hat{A}_1^{\dagger} = \frac{1}{\sqrt{N}} \sum_{k=1}^{N} \hat{a}_k^{\dagger} \ . \tag{4.72}$$

The action of this operator on a Fock state with energy E creates a state which is a superposition of Fock states with energy $E + \hbar\omega$ [the degeneracy of the nth excited state is given in Eq. (4.59)]. We wish to express this operator

in terms of creation and annihilation operators. In the single particle case, $N = 1$, $\hat{A}_1^\dagger$ is just the ordinary ladder operator. Given that $\hat{A}_1^\dagger$ gives non-zero values on a one particle state and preserves number it must be expressible in the form

$$\hat{A}_1^\dagger = \sum_{\ell,k} C_{\ell,k} \hat{c}_\ell^\dagger \hat{c}_k \ , \tag{4.73}$$

with $C_{\ell,k}$ some coefficients. Because the energy is raised by one quantum, it is also clear that $C_{\ell,k} = \tilde{C}_k \delta_{\ell,k+1}$ must be only populated on the upper diagonal. Finally given $\hat{a}^\dagger|n\rangle = \sqrt{n+1}|n+1\rangle$, we have that

$$\hat{A}_1^\dagger = \frac{1}{\sqrt{N}} \sum_{k=0}^{N} \sqrt{k+1} \hat{c}_{k+1}^\dagger \hat{c}_k \ . \tag{4.74}$$

4.2.5 A full set of ladder operators for the N particle system

In principle one could define more many-body ladder operators. A set of N would be required for an N body system, based on the Jacobi coordinates

$$\hat{A}_k \propto \sqrt{\frac{m\omega}{2\hbar}} \left(\hat{\xi}_k + \frac{i}{m\omega} \hat{\Pi}_k \right) \ , \tag{4.75}$$

with $\hat{\Pi}_k$ the momentum in Jacobi coordinates. These operators increase/decrease the state they act on by one unit of $\hbar\omega$ and would be sufficient for systems of distinguishable particles, but for indistinguishable particles they must be symmetrised.

Taking the simple example of $N = 2$ and $\hat{A}_2$ we see that the symmetrisation operator simply takes $\xi_2 \to -\xi_2$ and $\hat{S}_+ \hat{A}_2 = 0$ and $\hat{S}_- \hat{A}_2 = 2\hat{A}_2$. Equally

$$\left(\hat{\xi}_2 + i \frac{\partial}{\partial \xi_2} \right)^2 = \hat{\xi}_2^2 - \frac{\partial^2}{\partial \xi_2^2} + i \left(1 + \xi_2 \frac{\partial}{\partial \xi_2} \right) \ , \tag{4.76}$$

is symmetric in ξ_2 and so $\hat{S}_+ (\hat{A}_2)^2 = 2(\hat{A}_2)^2$ and $\hat{S}_- (\hat{A}_2)^2 = 0$. Continuing this for higher powers we see that only operators $(\hat{A}_2)^{2n}$ with n an integer/half-odd-integer satisfy bosonic/fermionic symmetry, other states will

vanish after the symmetrisation operator is applied.

Each application of the independent (upwards) ladder operators (in any order) to the ground state gives a unique state, with an energy equal to the energy raising of each operator applied times the number of applications. Therefore, in order to give the correct degeneracy g_n, given by Eq. (4.59), which is equal to the number of ways to partition n using integers less than or equal to N, each operator for the nth mode in identical particles must have energy levels spaced by n. Therefore we define

$$\hat{\tilde{A}}_k = \left[\hat{A}_k\right]^k \tag{4.77}$$

as the ladder operators for identical particles, with symmetry dealt with later. We note that the bosonic/fermionic ground states $|\text{ground}\rangle^{(b/f)}$ are related via

$$|\text{ground}\rangle^{(f)} \propto \hat{S}_-\{\hat{A}_2[\hat{A}_3]^2...[\hat{A}_N]^{N-1}\}|\text{ground}\rangle^{(b)} \ . \tag{4.78}$$

Similar to the case of the $\hat{A}_1$, as given in Eq. (4.72), we can argue that we must be able to express any symmetrised $\hat{\tilde{A}}_k$ as

$$\hat{\tilde{A}}_k = \sum_{j_1,....,j_{2k}=0}^{\infty} C_{j_1,...,j_{2k}}\delta_{j_1+..+j_k+k,j_{k+1}+..+j_{2k}}\ \hat{c}^\dagger_{j_1}...\hat{c}^\dagger_{j_k}\hat{c}_{j_{k+1}}...\hat{c}_{j_{2k}} \ , \tag{4.79}$$

because the application to states with $N < k$ must be zero and it must lower (or raise for the conjugate) the energy of a state by $k\hbar\omega$. One could in principle derive a recursion relation for the constants, $C_{j_1,...,j_{2k}}$, based on the commutator relations $[\hat{\tilde{A}}^\dagger_j, \hat{\tilde{A}}_k] \propto \delta_{k,j}$ and fix them via the expectation value on the ground state: $\langle\text{ground}|\hat{\tilde{A}}_j\hat{\tilde{A}}^\dagger_j|\text{ground}\rangle$. This could be set to j or unity depending on what convention we wish to adopt; we take the latter for simplicity, i.e. each ladder quanta is considered to have an energy of $k\hbar\omega$.

With these operators from Eq. (4.79), we can define any possible bosonic eigenstate in the system as

$$|\Psi\rangle_{j_1,...,j_N} \propto \hat{S}_+\left\{\prod_{k=1}^{N}\frac{(\hat{\tilde{A}}^\dagger_k)^{j_k}}{j_k!}|\text{ground}\rangle^{(b)}\right\} \ , \tag{4.80}$$

with energy $E = \hbar\omega(N/2 + j_1 + 2j_2 + ... + Nj_N)$ and express the Hamiltonian as

$$\hat{H} = \hbar\omega \left[\frac{N}{2} + \sum_{k=1}^{N} k \hat{\tilde{A}}_k^\dagger \hat{\tilde{A}}_k \right] . \tag{4.81}$$

The fermionic states would be defined analogously.

4.2.6 The introduction of two body interactions

Centre-of-mass separability

The full N operator algebra of Sec. 4.2.5 has proven not to be particularly useful for computations in systems with two-body interactions, as one would need to consider all the N commutation relations $[\hat{\tilde{A}}_k^\dagger, \hat{H}_I]$ with the interaction Hamiltonian

$$\begin{aligned} \hat{H}_I &= \int dx \int dx' \hat{\Psi}^\dagger(x) \hat{\Psi}^\dagger(x') V(x - x') \hat{\Psi}(x') \hat{\Psi}(x) \\ &= \sum_{jk\ell n} V_{jk\ell n} \hat{c}_j^\dagger \hat{c}_k^\dagger \hat{c}_\ell \hat{c}_n \ , \end{aligned} \tag{4.82}$$

which is highly non-trivial. That is, with the expectation of the centre-of-mass (c.o.m.) mode creation operator, as we have that [135]

$$[\hat{A}_1^\dagger, \hat{H}_I] = 0 \tag{4.83}$$

for *any* two body interaction $V(x - x')$; we show explicitly the commutation with the c.o.m. and interaction Hamiltonians later in Sec. 5.2. We can therefore consider the action of the c.o.m. Hamiltonian, $\hat{H}_{\rm C} = \hat{A}^\dagger \hat{A}$ separately to that of the interaction and relative degrees of freedom, or equivalently construct eigenstates from each Hamiltonian separately. Additionally the two body problem can be solved analytically for a contact interaction, which we discuss in Sec. 5.2.1.

Projection to the zero centre-of-mass excitation basis

We wish to derive a matrix which projects the occupation number notation states into eigenstates of the centre of mass operator. This is achieved by

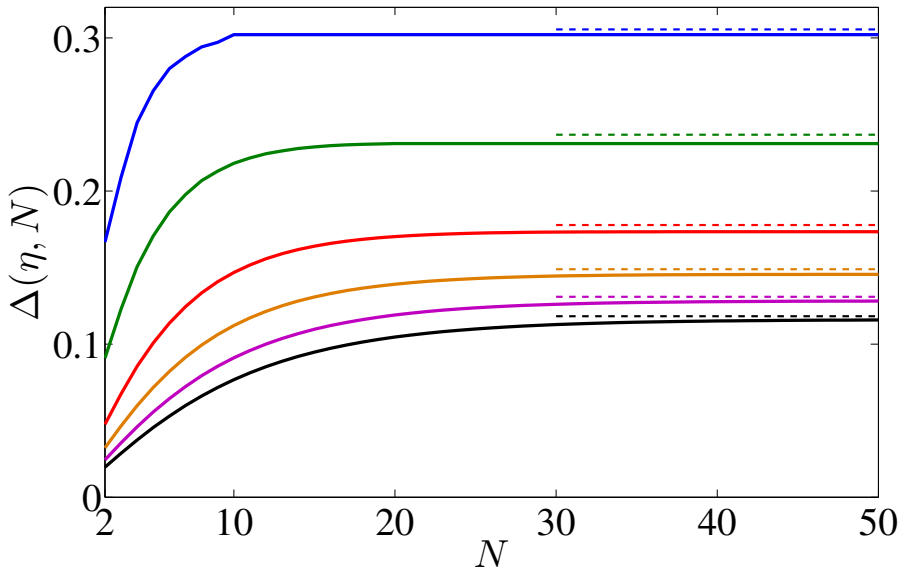

Figure 4.2: Reduced basis size divided by truncated basis size, given by Eq. (4.86), for different cut-off energies. Top to bottom lines are for cut-off energies $\eta = 10, 20, 40, 60, 80, 100$, dotted lines are the estimate of Eq. (4.89). Basis reduction is most significant for small N but Eq. (4.89) provides a good estimate of the reduction for large N.

diagonalising an occupation number basis in terms of

$$\hat{A}_1^\dagger \hat{A}_1 = \sum_{j,k=0}^{\infty} \sqrt{(j+1)(k+1)}\hat{c}_{k+1}^\dagger \hat{c}_k \hat{c}_j^\dagger \hat{c}_{j+1} \tag{4.84}$$

with $\hat{A}_1$ given by Eq. (4.72). This is a reasonably simple operation as $\hat{A}_1^\dagger \hat{A}_1$ only mixes states of the same energy and so is block diagonal. Each block can be diagonalised separately, considerably reducing the time taken; the blocks are also relatively sparse further simplifying the problem. The eigenvectors therefore form a new basis we call the "projected basis," and form a matrix which projects into this basis (which has the same eigenvalues as before). We know via Eq. (4.83) that $\hat{H}_I$ can only mix states to states with the same quanta of centre-of-mass excitation and so $\hat{H}_I$ is block diagonal in the projected basis. Additionally we need only consider states satisfying $\hat{A}|\psi\rangle = 0$ (zero c.o.m. excitation quanta), denoted the "reduced basis", in order to diagonalise a relative Hamiltonian, containing all the relative eigenstates; excited c.o.m. states could be added via the action of $\hat{A}^\dagger$ on these relative

eigenstates.

We use this property to simplify exact diagonalisation routines for systems of harmonically confined Bosons interacting with a Lieb-Linger type contact potential [Eq. (4.6)] in chapters 5 and 6. For the purpose of computation we impose a cut of excitation energy η (i.e. the maximum additional quanta of energy above the ground state, implicitly in units of $\hbar\omega$), with the basis truncated so that states with $E - E_0 > \eta$ are excluded. Note that this also implies a mode cut off: $N_k = 0$ if $k > \eta$. It is not generally possible within this method to impose any other mode cut off as higher modes are required to create the zero c.o.m. excitation states.

The full size of this truncated basis is given by the number of ways to partition all the integers up to η using integers between one and N, the number of states with zero c.o.m. excitation states can use only two to N. We define the ratio of these two basis sizes as:

$$\Delta(\eta, N) = \frac{\sum_{n=0}^{\eta} p([2, N], n)}{\sum_{n=0}^{\eta} p([1, N], \eta)} \,. \tag{4.85}$$

We can use Eq. (4.60) to write $p([2, N], \tilde{E}) = p([1, N], \tilde{E}) - p([1, N], \tilde{E} - 1)$. In the sum from 0 to η, all terms cancel apart from the one at the end point of the sum, $p([1, N], \eta)$. Hence the size of the reduced basis is the degeneracy of the ηth energy level in the occupation number basis, and we have

$$\Delta(\eta, N) = \frac{p([1, N], \eta)}{\sum_{n=0}^{\eta} p([1, N], n)} \,. \tag{4.86}$$

The basis reduction for $N = 2$ can be calculated by noting there are $\lfloor k/2 \rfloor + 1$ ways to partition k using 1 and 2 (the notation $\lfloor k \rfloor$ means round k down to the nearest integer), thus the reduced basis is $\lfloor \eta/2 \rfloor + 1$ in size, the number of states in the truncated occupation number basis is

$$\sum_{k=0}^{\eta} (\lfloor k/2 \rfloor + 1) = \begin{cases} 1 + \eta + \eta^2/4 & \text{if } \eta \text{ even} \\ 1 + \eta + (\eta^2 - 1)/4 & \text{if } \eta \text{ odd.} \end{cases} \tag{4.87}$$

To leading order the reduction $\Delta(\eta, N)$ goes as $2/\eta$. Such simple analytic expressions are not known for general N, however we have the following

expression by Ramanujan [133]

$$p([1, N \geq \eta], \eta) \sim \frac{1}{4\eta\sqrt{3}} \exp\left(\pi\sqrt{\frac{2\eta}{3}}\right) \text{ as } \eta \to \infty, \tag{4.88}$$

which can be used to get an asymptotic estimate of the basis reduction by replacing the sum in Eq. (4.86) with an integral, giving

$$\frac{p([1, N \geq \eta], \eta)}{\int_0^\eta p([1, N \geq \eta], \eta')d\eta'} \sim \frac{\pi}{\sqrt{6\eta}} - \frac{1}{\eta} + \mathcal{O}(\eta^{-3/2}) \, . \tag{4.89}$$

This will be our best estimate for the reduction achieved for large N, improving slower than the $\propto 1/\eta$ reduction for the $N = 2$ case. This asymptotic estimate is included in Fig. 4.2, along with the reduction for intermediate values of N.

Summary

This section described the importance of indistinguishably between particles in a harmonic oscillator, and how many identical particles is therefore not the same as many spatial dimensions or distinguishable particles; degeneracy of energy levels were calculated for the former case, the latter having been covered earlier. We derived a ladder operator formulation of the many-body harmonic oscillator, which was used to derive a centre-of-mass separated numerical method, which we later use to investigate systems with two-body interactions.

Part II

Projects

Chapter 5

A single quantum soliton in harmonic confinement

5.1 Preamble

This chapter focuses on the work relating to publication [1], with contributions made by C. Weiss and S.A. Gardiner. The paper investigates bright quantum-matter-wave solitons in the presence of harmonic confinement, beyond the Gross-Pitaevskii equation. The primary motivation behind this work is that almost all current experimental work with attractive BECs, and indeed most repulsive BECs, is done in the presence of harmonic confinement. Periodic waveguides [136] can be achieved to an extent, but suffer from large atom losses due to a "circle (or torus) of death" and considerable difficulty in combining with Feshbach control of atomic interactions and/or achieving a quasi 1D geometry. We look for regimes of agreement between exact many-body quantum theory and mean field approximations (specifically with a Hartree product ansatz for the many body wavefunction) within the Lieb-Liniger (LL) model. This lead to an unusual unit rescaling to keep the energy of a Hartree product state constant.

The key results from this work were the derivation of a first order energy correction to the internal energy of a quantum soliton, which is also used as the basis of a variational model, and also numerical calculations of the overlap between a product state and a centre-of-mass confined quantum soliton.

This chapter is organised as follows: Section 5.2 introduces the unit rescaling used to keep the mean field soliton length constant throughout the paper, and the known exact results in the absence of trapping (using the Lieb-Liniger model [20]) in these units. Also included is the separability of the many-body Hamiltonian and the existence of the Kohn mode, as well as the exact eigenstates for two interacting bosons in a harmonic potential. Section 5.3 derives a perturbative energy correction to the relative ground state energy due to the introduction of a harmonic trapping potential, along with a variational procedure to estimate the ground state in the limit of weak trapping. Section 5.4 introduces the numerical method used to perform calculations in the many-body system for varying 1D harmonic trapping potential, using a basis set of harmonic oscillator eigenstates, which are projected to a centre-of-mass excitation basis. Section 5.5 numerically investigates changes to the relative component (i.e. having excluded the centre of mass) of the ground state as the trapping potential is increased. These calculations are performed for different numbers of atoms and compared with predictions based on the GPE. Section 5.5.3 examines quantitatively the overlap between the mean field approximation of the ground state and the many-body solutions, along with finding a regime of agreement where the difference between the two models is small in every respect. Section 5.6 summarizes and comments on the results.

5.2 Unit rescalings and key results

Separation of the centre-of-mass coordinate x_{C} in first quantisation

We consider a 1D system of identical bosonic atoms with attractive ($g_{1\mathrm{D}} < 0$) contact interactions in an axial harmonic trapping potential. This system is described by the first quantised Hamiltonian

$$H(\vec{x}) = \frac{\hbar^2}{2m}\sum_{k=1}^{N}\left[-\frac{\partial^2}{\partial x_k^2} + \frac{m\omega_x^2 x^2}{2}\right] + g_{1\mathrm{D}}\sum_{k=2}^{N}\sum_{j=1}^{k-1}\delta(x_k - x_j)\ , \tag{5.1}$$

where $\vec{x}$ is a shorthand for the set of all N coordinates $\{x_1, x_2, \ldots, x_N\}$.

As the external potential is harmonic, the centre-of-mass dynamics separate and are independent of any two-body interactions. Consequently the centre-of-mass eigenstates are simple harmonic oscillator eigenstates or plane waves, respectively. In the former case this is referred to as the Kohn mode. This may be readily seen by expressing the first-quantized form of the Hamiltonian [Eq. (5.1)] in terms of the (unnormalised) Jacobi coordinates, i.e.,

$$x_{\mathrm{C}} = \frac{1}{N}\sum_{k=1}^{N} x_k, \tag{5.2}$$

together with

$$\xi_k \equiv x_k - \frac{1}{k-1}\sum_{j=1}^{k-1} x_j, \tag{5.3}$$

for $k \in \{2, 3, 4, \ldots, N\}$, which differ from Eq. (4.69) via a scaling factor. We choose these as these include the actual centre-of-mass position and not a version rescaled by $\sqrt{N}$. The Hamiltonian can then be phrased as $H = H_{\mathrm{C}} + H_{\mathrm{R}}$, where

$$H_{\mathrm{C}}(x_{\mathrm{C}}) = -\frac{\hbar^2}{2Nm}\frac{\partial^2}{\partial x_{\mathrm{C}}^2} + \frac{Nm\omega_x^2 x_{\mathrm{C}}^2}{2}, \tag{5.4}$$

$$\begin{aligned} H_{\mathrm{R}}(\vec{\xi}) = &\sum_{k=2}^{N}\left[-\frac{\hbar^2 k}{2m(k-1)}\frac{\partial^2}{\partial \xi_k^2} + \frac{(k-1)m\omega_x^2\xi_k^2}{2k}\right] - g_{1\mathrm{D}}\sum_{k=2}^{N}\delta\left(\xi_k + \sum_{\ell=2}^{k-1}\frac{\xi_\ell}{\ell}\right) \\ &- g_{1\mathrm{D}}\sum_{k=2}^{N}\sum_{j=2}^{k-1}\delta\left(\xi_k + \sum_{\ell=j+1}^{k-1}\frac{\xi_\ell}{\ell} - \frac{j-1}{j}\xi_j\right), \end{aligned} \tag{5.5}$$

$\vec{\xi}$ is a shorthand for $\{\xi_2, \xi_3, \xi_4, \ldots, \xi_N\}$, and we have used the identity $x_k - x_j = \xi_k + \sum_{\ell=j+1}^{k-1}\xi_\ell/\ell - [(j-1)/j]\xi_j$ (with $b > a$ and $\xi_1 \equiv x_{\mathrm{C}}$). In cases where the upper limit of a sum is less than its lower limit, the sum is taken $= 0$.

Centre of mass separated Hartree factorisation

Just as in the 3D case [Eq. (2.50)], minimising the Hamiltonian (5.1) with a Hartree wave-function $\psi_{\mathrm{H}}(\vec{x}) = \prod_{k=1}^{N}\phi(x_k)$ leads to a GPE with a rescaled nonlinear factor proportional to $N-1$. In this chapter we *choose to retain the proportionality to* $(N-1)$, as this way we cannot underestimate the relative

ground state energy compared to the true value.

If instead of taking $\phi(x)$ to minimise the action functional obtained from $\hat{H}$ we instead consider just minimising $H_{\mathrm{R}} = H - H_{\mathrm{C}}$, we will obtain a different equation to Eq. (2.50). This adds an extra term to S in Eq. (2.49) (allowing for the fact this is now in 1D) equal to

$$\begin{aligned} E_{\mathrm{cm}} &= \int dx_1 \ldots \int dx_N \left[\prod_{k=1}^{N} \phi^*(x_k)\right] \left[-\frac{\hbar^2}{2Nm}\frac{\partial^2}{\partial x_{\mathrm{C}}^2} + \frac{N\omega_x^2 x_{\mathrm{C}}^2}{2m}\right] \left[\prod_{k=1}^{N} \phi(x_k)\right] \\ &= \int dx_1 \ldots \int dx_N \left[\prod_{k=1}^{N} \phi^*(x_k)\right] \left\{\sum_{j=1}^{N} \left[-\frac{\hbar^2}{2Nm}\frac{\partial^2}{\partial x_k^2} + \frac{\omega_x^2 x_k^2}{2Nm}\right] \right. \\ &\quad \left. + 2\sum_{1\le j<k\le N} \left[-\frac{\hbar^2}{2Nm}\frac{\partial}{\partial x_k}\frac{\partial}{\partial x_j} + \frac{\omega_x^2 x_k x_j}{2Nm}\right]\right\} \left[\prod_{k=1}^{N} \phi(x_k)\right] . \end{aligned} \tag{5.6}$$

This expression consists of many identical integrals over different coordinates, hence we can simplify it to

$$\begin{aligned} E_{\mathrm{cm}} = \int dx \phi^*(x) \left[-\frac{\hbar^2}{2m}\frac{\partial^2}{\partial x^2} + \frac{\omega_x^2 x^2}{2m}\right] \phi(x) + (N-1) \iint dx dx' \\ \phi^*(x)\,\phi^*(x') \left[-\frac{\hbar^2}{2m}\frac{\partial}{\partial x}\frac{\partial}{\partial x'} + \frac{\omega_x^2 x x'}{2m}\right] \phi(x)\,\phi(x') \ , \end{aligned} \tag{5.7}$$

and if $\phi(x)$ is symmetric about $x = 0$ (or any point x_0 for the derivatives) then the cross terms vanish by symmetry; if this is the case and E_{cm} is simply equal to the energy of a single particle eigenstate. Minimising Eq. (2.49) after subtracting E_{cm} results in

$$i\hbar\frac{N}{N-1}\frac{\partial}{\partial t} = \left[-\frac{\hbar^2}{2m}\frac{\partial^2}{\partial x^2} + \frac{m\omega_x^2 x^2}{2} - Ng_{1\mathrm{D}}|\phi(x)|^2\right]\phi(x) \ , \tag{5.8}$$

note that (assuming $N \neq 1$) the extra factor on the left can be removed by rescaling to $\tilde{t} = Nt/(N-1)$ giving the usual GPE with nonlinearity scaled by N. It also tends to unity as $N \to \infty$.

This treatment would only really describe the wavefunction about the centre-of-mass position. In order to include the centre-of-mass behaviour in a con-

sistent way we need to consider a more complicated many-body wavefunction

$$\tilde{\psi}_{\mathrm{H}}(\vec{x},t) = \int dx_0 f(x_0,t) \prod_{k=1}^{N} \phi(x_k - x_0, t) \; , \tag{5.9}$$

i.e. a superposition of product states with different centre-of-mass positions, similar to what was considered in [127] for a free soliton. The function $\phi(x_k - x_0, t)$ would be determined by extremising the functional equation $S = \int d\vec{x}\psi^*(i\hbar\frac{\partial}{\partial t} - H_{\mathrm{R}})\psi$ with respect to variations in $\phi^*(x)$. $f(x_0,t)$ would be set by minimising $S = \int d\vec{x}\psi^*(i\hbar\frac{\partial}{\partial t} - H_{\mathrm{C}})\psi$, with respect to variations in $f^*(x_0,t)$. This might be an interesting approach to adding centre-of-mass dispersion into a mean-field theory (within free space or harmonic confinement), but we do not explore this further.

Rescaling to dimensionless form

It is convenient to rescale our description of the system in terms of an effective $\hbar = m = g_{1\mathrm{D}}(N-1) = 1$ unit system, which we will still refer to as soliton units for this chapter, but it is important to note they are different to Eq. (3.7). Space, time and energy scales are then given in units of $\hbar^2/mg_{1\mathrm{D}}(N-1)$ (the classical soliton length [56]), $\hbar^3/mg_{1\mathrm{D}}^2(N-1)^2$, and $mg_{1\mathrm{D}}^2(N-1)^2/\hbar^2$, respectively.

We work within this system of units for the rest of this chapter. The Hamiltonian [Eq. (5.1)] transforms to

$$H(\vec{x}) = \sum_{k=1}^{N}\left[-\frac{1}{2}\frac{\partial^2}{\partial x_k^2} + \frac{\gamma^2 x_k^2}{2}\right] - \frac{1}{N-1}\sum_{k=2}^{N}\sum_{j=1}^{k-1}\delta(x_k - x_j), \tag{5.10}$$

or in second quantisation

$$\hat{H} = \int dx \hat{\Psi}^\dagger(x)\left[-\frac{1}{2}\frac{\partial^2}{\partial x^2} + \frac{\gamma^2 x^2}{2} - \frac{\hat{\Psi}^\dagger(x)\hat{\Psi}(x)}{2(N-1)}\right]\hat{\Psi}(x) \; , \tag{5.11}$$

and the time-independent Hartree GPE [Eq. (2.50)] becomes

$$\mu\phi(x) = \left[-\frac{1}{2}\frac{\partial^2}{\partial x^2} + \frac{\gamma^2 x^2}{2} - |\phi(x)|^2\right]\phi(x). \tag{5.12}$$

We have introduced the dimensionless parameter γ, which is the square of the ratio of the classical soliton length to the harmonic oscillator length $\sqrt{\hbar/M\omega_x}$ [56], i.e.,

$$\gamma = \frac{\hbar^3\omega_x}{Mg_{1\mathrm{D}}^2(N-1)^2}. \tag{5.13}$$

Within our chosen system of units γ appears in the rescaled Hamiltonian and GPE as a dimensionless effective trap frequency. This also reveals γ to be the only free parameter in the GPE, which as a description of the system is effectively a classical field limit, and the particle number N appears as an additional free parameter in the fully quantal Hamiltonian. With this dimensionless rescaling, the normalized ground-state of H_{C} is exactly

$$\psi_{\mathrm{C}}(x_{\mathrm{C}}) = \left(\frac{N\gamma}{\pi}\right)^{1/4} \exp\left(-\frac{N\gamma x_{\mathrm{C}}^2}{2}\right), \tag{5.14}$$

with eigenenergy $= \gamma/2$.

5.2.1 Known exact results

Ground states in free space

In the case where there is no axial trapping potential, i.e., $\gamma = 0$, the GPE stationary state [Eq. (3.3)] and many-body ground state [Eq. (4.30)] are known. Within our unit system these are given by

$$\psi_{\mathrm{H}}(\vec{x}) = \frac{1}{2^N}\prod_{k=1}^{N} \operatorname{sech}\left(\frac{x_k - x_0}{2}\right) \tag{5.15}$$

and

$$\psi_{\mathrm{G}}(\vec{x}) = \sqrt{\frac{(N-1)!}{(N-1)^{N-1}}} \exp\left(-\sum_{k=2}^{N}\sum_{j=1}^{k-1}\frac{|x_k - x_j|}{2[N-1]}\right). \tag{5.16}$$

with the normalising factor calculated in Sec. C.2. As a result of not breaking the translation symmetry, the many-body state is localized in the sense that $\psi_{\mathrm{G}}(\vec{x}) \to 0$ as $|x_k - x_j| \to \infty$, for any $k \neq j$ and we recalled from Sec. 4.1.6 that the density about the centre-of-mass is the same as the Hartree solution as $N \to \infty$.

The energies $E_{\rm H}$ and $E_{\rm G}$ corresponding to the wave-functions $\psi_{\rm H}(\vec{x})$ and $\psi_{\rm G}(\vec{x})$ are given by

$$E_{\rm H} = -\frac{N}{24}, \tag{5.17}$$

$$E_{\rm G} = -\frac{N(N+1)}{24(N-1)} \equiv E_{\rm H} - \frac{N}{12(N-1)}. \tag{5.18}$$

As one would expect, the exact eigenenergy $E_{\rm G}$ is less than $E_{\rm H}$, and the difference in energy *per particle* $(E_{\rm H} - E_{\rm G})/N = 1/12(N-1)$ vanishes as $N \to \infty$.

Two interacting bosons in a harmonic potential

The case of two identical bosons in a harmonic potential with contact (δ-function) interactions is also exactly solvable [137, 138]. In this case the eigenfunctions of $H_{\rm R}(\xi_2)$, defined through $H_{\rm R}(\xi_2)\phi_n(\xi_2) = E_{{\rm R},n}\phi_n(\xi_2)$, are given by

$$\phi_n(\xi_2) = \mathcal{N}_n U(-\nu_n, 1/2, \gamma\xi_2^2/2)e^{-\gamma\xi_2^2/4}, \tag{5.19}$$

where $U(a,b,z)$ is the Tricomi confluent hypergeometric function [139], and $\mathcal{N}_n$ is a normalization constant. The ν_n are implicit solutions of

$$\frac{\Gamma(1/2-\nu_n)}{\Gamma(-\nu_n)} = \frac{1}{2\sqrt{2\gamma}}, \tag{5.20}$$

and set the eigenvalues of $H_{\rm R}(\xi_2)$ through

$$E_{{\rm R},n} = \left(2\nu_n + \frac{1}{2}\right)\gamma. \tag{5.21}$$

Attractive interactions must reduce $E_{\rm R,0}$ from the noninteracting case, so that $E_{\rm R,0} < \gamma/2 \Rightarrow \nu_0 < 0$. As outlined in Appendix B.1, it then follows that in the limit $\gamma \to 0$ (interaction dominated regime) $E_{\rm R,0} \to -1/4 + \mathcal{O}(\gamma^2)$. This is in agreement with the *total* ground state energy $E_{\rm G}$ for the case of two attractively interacting bosons in free space [Eq. (5.18)], as one would expect due to the centre-of-mass energy of the free space ground state being $= 0$. In the opposite limit of $\gamma^{-1} \to 0$ (trap dominated regime) harmonic-oscillator eigenvalues and eigenfunctions must result, i.e., $E_n \to$

$(2n + 1/2)\gamma$ and $U(-\nu_n, 1/2, \gamma\xi_2^2/2) \to H_{2n}(\sqrt{\gamma}\xi_2)/2^{2n}/\sqrt{2}$, where the H_{2n} are even Hermite polynomials [due to Bose symmetry $\phi_n(\xi_2) \equiv \phi_n(-\xi_2)$, i.e., eigenfunctions must be even].

5.3 Perturbative and variational methods

5.3.1 Interaction dominated limit in a harmonic potential

In the case where $\gamma \ll 1$, we may consider the effect of the trap to be dominated by the effect of the interactions, and therefore negligible in H_{R}. As there are no interactions present in H_{C}, the effect of the trap is in this case always significant, even in the interaction dominated regime.

We may therefore consider a limiting case Hamiltonian H_0, composed of H_{R} [Eq. (5.5)] with $\gamma = 0$, plus H_{C} [Eq. (5.4)]. Written in terms of conventional single-particle coordinates,

$$H_0(\vec{x}) = -\frac{1}{2}\sum_{k=1}^{N}\frac{\partial^2}{\partial x_k^2} + \frac{\gamma^2}{2N}\left(\sum_{k=1}^{N} x_k\right)^2 - \frac{1}{N-1}\sum_{k=2}^{N}\sum_{j=1}^{k-1}\delta(x_k - x_j), \quad (5.22)$$

and the correctly normalized ground state ψ_0 can be put together from Eq. (5.16) multiplied by Eq. (5.14), i.e., $\psi_0 \equiv \psi_{\mathrm{C}}\psi_{\mathrm{G}}$, with the sum of the corresponding eigenvalues determining the overall energy E_0. Hence, in terms of single-particle coordinates

$$\psi_0(\vec{x}) = \left(\frac{N\gamma}{\pi}\right)^{1/4} \exp\left(-\frac{\gamma}{2N}\left[\sum_{k=1}^{N} x_k\right]^2\right)\psi_{\mathrm{G}}(\vec{x}), \quad (5.23)$$

and, from Eq. (5.18) plus $\gamma/2$ (the harmonic oscillator zero-point energy),

$$E_0 = -\frac{N(N+1)}{24(N-1)} + \frac{\gamma}{2}. \quad (5.24)$$

This interaction dominated limit does not correspond to any physical system but is a useful starting point for perturbation theory.

5.3.2 Perturbation results

To proceed from the approximated Hamiltonian (5.22), we include the effect of the harmonic trap on the relative degrees of freedom via Rayleigh-Schrödinger perturbation theory. The full Hamiltonian (5.1) can be written as $H(\vec{x}) = H_0(\vec{x}) + \Delta H(\vec{x})$, with

$$\Delta H(\vec{x}) = \frac{\gamma^2}{2}\left[\sum_{k=1}^{N} x_k^2 - \frac{1}{N}\left(\sum_{k=1}^{N} x_k\right)^2\right] . \tag{5.25}$$

As $\Delta H(x) \propto \gamma^2$, we expect perturbation theory to yield particularly good results in the limit of small γ. For the first-order energy correction to the ground state,

$$\begin{aligned} E^{(1)} &= \langle\psi_0|\Delta\hat{H}|\psi_0\rangle \\ &= \int d\vec{x}\ \psi_0(\vec{x})^* \Delta H(\vec{x})\psi_0(\vec{x}) , \end{aligned} \tag{5.26}$$

which also serves as a definition of the bra-ket notation, we find (Appendix C.4):

$$E^{(1)} = \gamma^2 \frac{(N-1)^2}{N} \sum_{k=1}^{N-1} \frac{1}{k^2} . \tag{5.27}$$

The sum in Eq. (5.27) is simply the second Harmonic number, for which the asymptotic behaviour in the $N \gg 1$ limit is given by [140]

$$\sum_{k=1}^{N-1} \frac{1}{k^2} \sim \frac{\pi^2}{6} - \frac{1}{N-1} + \mathcal{O}\left([N-1]^{-2}\right) . \tag{5.28}$$

Thus, asymptotically the energy correction goes as

$$E^{(1)} \sim \gamma^2 \left[\frac{\pi^2}{6}N - \frac{\pi^2}{3} - 1 + \mathcal{O}\left(N^{-1}\right)\right] . \tag{5.29}$$

For large N, this coincides with the result obtained using the free space Hartree solution, given in Eq. (5.15), as an approximation for the ground

state (Appendix C.5)

$$E_{\mathrm{H}}^{(1)} = (N-1)\int_{-\infty}^{\infty} dx \frac{\mathrm{sech}(x/2)^2}{4}\frac{\gamma^2 x^2}{2}$$
$$= \gamma^2(N-1)\frac{\pi^2}{6}\,. \tag{5.30}$$

These results are displayed in Fig. 5.1; for small N there is a large difference between the result predicted by the Hartree product state [Eq. (5.30)] and the result predicted by the exact many-body ground state [Eq. (5.27)] of the approximate Hamiltonian (5.22). There is also a weak number dependence from the Harmonic series in Eq. (5.27). However as $N \gg 1$ both methods give the same energy correction per atom, $\pi^2\gamma^2/6$. For $N = 1000$ the relative difference $(E_{\mathrm{H}}^{(1)} - E^{(1)})/E^{(1)} \approx 0.0016$ is already small.

5.3.3 Variational minimization

In order to improve the value for the ground state energy beyond the first-order-perturbation-theory result (5.27), we introduce the following (normalized) variational ansatz

$$\psi_{\mathrm{var}}^{(\lambda)}(\vec{x}) \equiv \psi_{\mathrm{C}}(x_{\mathrm{C}})\mathcal{N}\lambda^{(N-1)/2}\exp\left(-\lambda\sum_{1\le k<j\le N}\frac{|x_k - x_j|}{2[N-1]}\right)\,, \tag{5.31}$$

with $\gamma > 0$ and the constant $\mathcal{N}$ the same as Eq. (5.16),

$$\mathcal{N} = \sqrt{\frac{(N-1)!}{(N-1)^{N-1}}}\,, \tag{5.32}$$

which is calculated in appendix C.2. With just $\mathcal{N}$ as a prefactor the equation would be normalized with respect to $\lambda\vec{x}$. Scaling this out along with $\gamma \to \gamma/\lambda^2$ to keep the centre of mass the same, gives the extra factor of $\lambda^{(N-1)/2}$. Since the centre-of-mass wave-function is unchanged, we will only have a correction to the relative energies. These are calculated in Appendices C.3 and C.4. The total energy for this wave-function is

$$\langle\psi_{\mathrm{var}}^{(\lambda)}|\hat{H}|\psi_{\mathrm{var}}^{(\lambda)}\rangle = \left(2\lambda - \lambda^2\right)E_{\mathrm{G}} + \frac{E^{(1)}}{\lambda^2} + \frac{\gamma^2}{2} \tag{5.33}$$

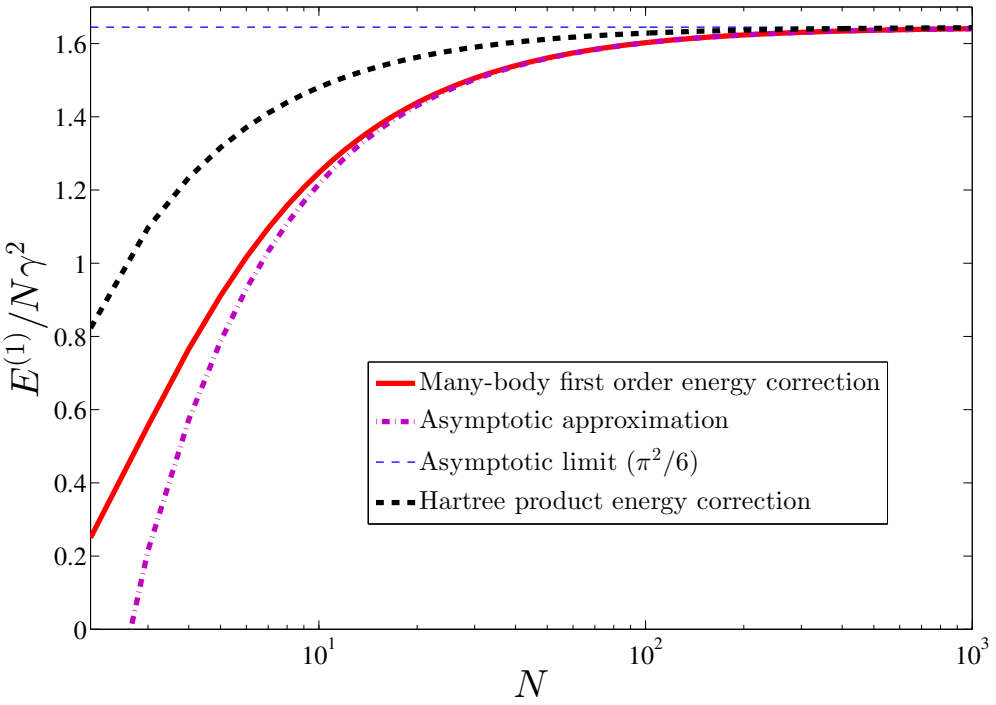

Figure 5.1: First-order energy correction per atom for a many-body quantum soliton with the centre-of-mass in the lowest eigenstate of a harmonic oscillator given in Eq. (5.23). The exact solution given in Eq. (5.27) and its expansion up to next-to-leading order, given in Eq. (5.29), begin to agree for $N \gtrapprox 10$ with the latter always underestimating the true value. Both curves approach the approximate result predicted by the Hartree approximation [Eq. (5.30)]. The relative difference between different predictions lies below 1% for $N \gtrapprox 165$.

for the expectation values of each section of the relative Hamiltonian, with E_{G} being the (negative) ground state energy of the free soliton in soliton units given in Eq. (5.18), and $E^{(1)}$ the first-order correction given by Eq. (5.27). In order to calculate the energy minimum, the derivative of Eq. (5.33) with respect to λ has to be zero:

$$(2-2\lambda)E_{\mathrm{G}} - \frac{2E^{(1)}}{\lambda^3} = 0\,, \tag{5.34}$$

which (for $\lambda \neq 0$) is equivalent to a 4th order polynomial in λ

$$\lambda^4 - \lambda^3 - \kappa = 0\,, \tag{5.35}$$

where the constant κ is defined as the ratio of the first-order correction to the absolute value of the ground state energy

$$\begin{aligned}\kappa &\equiv -\frac{E^{(1)}}{E_{\mathrm{G}}} \\ &= \gamma^2 \frac{24(N-1)^3}{(N+1)N^2} \sum_{j=1}^{N-1} \frac{1}{j^2} \, .\end{aligned} \tag{5.36}$$

For fixed N, $\kappa \propto \gamma^2$, the value of this prefactor is an increasing function of N with a minimum of $\kappa = 2\gamma^2$ at $N = 2$ with an asymptotic limit of [cf. Eq. (5.29)]:

$$\lim_{N\to\infty} \kappa = 4\pi^2\gamma^2 \, . \tag{5.37}$$

Thus, κ is small for $\gamma \ll 1$.

Equation (5.35) has four roots, only one of which is real and positive which we denote λ_0, corresponding to an energy minimum. This solution can be derived analytically [140] (cf. Ref. [56]); it is given by:

$$\lambda_0 \equiv \frac{1}{4}\left(1 + \sqrt{\Lambda} + \sqrt{3 - \Lambda + 2\Lambda^{-1/2}}\right) \, , \tag{5.38}$$

with

$$\Lambda = 1 + \frac{2\,(2/3)^{2/3}\left(-9\kappa + \sqrt{81\kappa^2 + 768\kappa^3}\right)^{2/3} - 16\,(2/3)^{1/3}\,\kappa}{\left(-9\kappa + \sqrt{81\kappa^2 + 768\kappa^3}\right)^{1/3}} \, . \tag{5.39}$$

This is the value used in all the figures; however it is enlightening to take a Taylor expansion of λ_0 about $\kappa = 0$, which yields

$$\lambda_0 = 1 + \kappa - 3\kappa^2 + O(\kappa^3). \tag{5.40}$$

Taking Eq. (5.40) to first order in κ and substituting back into Eq. (5.33) leads to the minimum in the energy of

$$E \simeq E_{\mathrm{G}} + \frac{\gamma^2}{2} + E^{(1)} + \frac{(E^{(1)})^2}{E_{\mathrm{G}}} + \mathcal{O}([E^{(1)}]^3/|E_{\mathrm{G}}|^2) \, , \tag{5.41}$$

valid in the limit $\kappa \ll 1$.

As the variational Ansatz (5.31) does not affect the centre-of-mass part of

the wave-function, the overlap between this variational Ansatz and the state Eq. (5.23) (i.e. the $\lambda = 1$ state) is an interesting physical quantity; its modulus squared is the fraction of the relative wave-function which is projected to the relative ground state if the trapping potential was turned off quasi-instantaneously (cf. [127]). The overlap is given by (see Appendix C.3):

$$\langle \psi_{\mathrm{var}}^{(\lambda_0)} | \psi_0 \rangle = \left(\frac{2}{\lambda_0^{1/2} + \lambda_0^{-1/2}} \right)^{N-1} . \tag{5.42}$$

In the absence of external confinement this overlap can be understood as follows: given a system initially in the ground state (a quantum soliton with a width $N\lambda$) and then instantaneously changing the scattering length (so the new ground state has a width which is wider/narrower) then Eq. (5.42) is the amount of the wavefunction projected to the new many-body ground state. This ground state occupation is not the same as the soliton amplitude discussed the next paragraph.

It has been shown at the mean field level that a GPE initial state $\phi(x) \propto \mathrm{sech}(x/2A^2)$, which is broader than ground state for $A > 1$, tends asymptotically to multiple solitons [141]. The number of solitons is found equal to the nearest integer to A, with a radiation component (dispersing as $t \to \infty$) of $[A - \mathrm{round}(A)]^2/A^2$.[1] The same situation was considered at beyond mean-field level using the MCTDHTB method [142], this work found that the state evolved to a fragmented system. Investigating this instantaneously modification using a full basis of LL eigenstates is a possibility for future research.

Using the approximation (5.40), the overlap (5.42) approximately is $[1 + \kappa^2/8 + \mathcal{O}(\kappa^3)]^{(1-N)}$ and we thus expect the overlap to vanish in the limit $N \to \infty$ for $\kappa > 0$. Rather than investigating the total wave-function overlap (5.42), the Nth root of Eq. (5.42), an effective single-particle overlap, is a more suitable value in the limit $N \gg 1$ as it tends to a constant as $N \to \infty$ and is related to comparing two GPE orbitals. Note that for two Hartree-product wave-functions, the effective single-particle overlap would be independent of N, but the Nth root of Eq. (5.42) still is N-dependent due to the N-dependence of λ_0 in Eq. (5.40).

[1] Note this implies there is no soliton if $A < 1/2$, i.e. the initial condition is too peaked.

Figure 5.2 (a) shows the overlap Eq. (5.42) as a function of γ for various particle numbers and the exact value of λ_0. As expected, the N-dependence is quite strong. Figure 5.2 (b) shows the Nth root of the overlap Eq. (5.42), i.e. the effective single-particle overlap. The effective single-particle overlap is larger than 0.99 for $\gamma \lesssim 0.15$ for all N, indicating that $\psi_0(\vec{x})$ from Eq. (5.23) is still a good description in this parameter regime and the trap has had little effect on the internal degrees of freedom. The limit $N \to \infty$ is nearly reached for particle numbers as low as $N = 100$ [note that in panel (a), the limit $N \to \infty$ would lie on the coordinate axes].

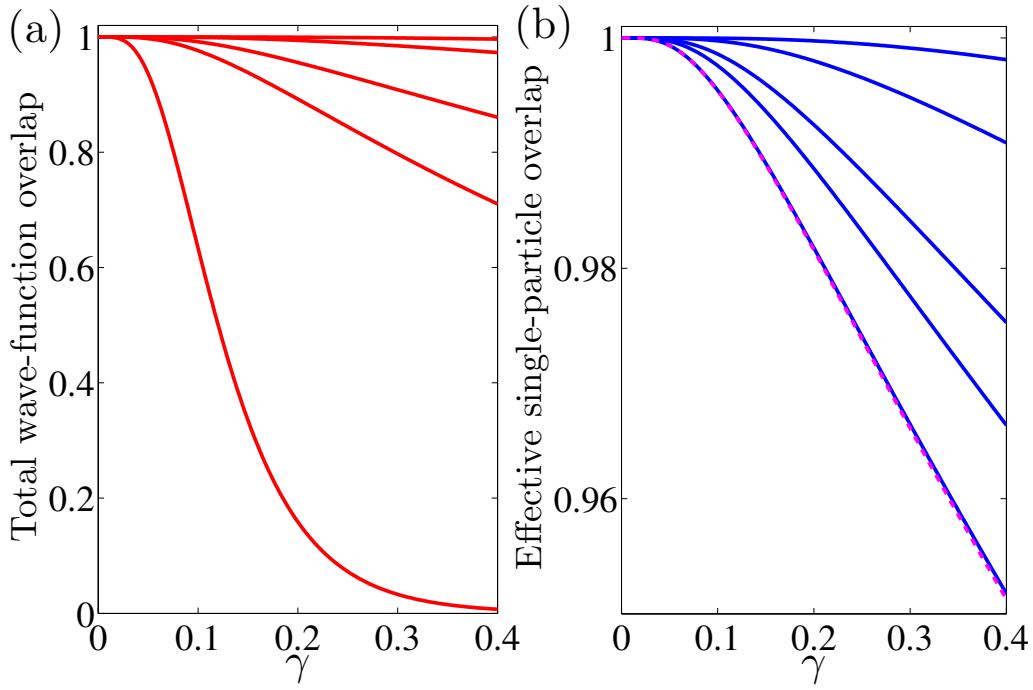

Figure 5.2: (a) Total wave-function overlap, given by Eq. (5.42), (b) effective single-particle overlap, given by the Nth root of Eq. (5.42), of the variationally obtained solutions for different rescaled trap frequencies γ with the free space ground state solution ($\gamma = 0$) with a Gaussian envelope for the centre of mass. Effective single-particle overlap is treated as the Nth root of the total overlap as for two different product states this is independent of number and equal to the overlap between the single-particle wave-functions. Bottom to top the solid lines on both graphs correspond to $N = 100, 10, 6, 3, 2$, the dashed line corresponds to the $N \to \infty$ limit of the variational many-body solution [using κ from Eq. (5.37)] and is very close to the $N = 100$ line.

5.4 Computational methods including a harmonic potential

5.4.1 Overview

While the focus of the previous section lies on the case of small γ, the numerical methods introduced in this section work well for $\gamma \gtrsim 0.16$, as the ground state becomes less strongly correlated. The importance of this value is commented on later in the results section.

5.4.2 Computation procedure

We expand the field operator over the set of Hermite functions

$$\sqrt{W}\varphi_k(Wx) = \sqrt{\frac{W}{k!2^k\pi^{1/2}}}H_k(Wx)\exp\left(-W^2x^2/2\right) \ , \tag{5.43}$$

where H_k are the Hermite polynomials, giving $\hat{\Psi}(x) = \sum_k \sqrt{W}\varphi_k(Wx)\hat{c}_k$ and W is a scaling factor, appearing as an inverse width. The Hamiltonian (5.11) in this basis can be split into three separate parts (c.f. A.3.3):

$$\hat{H}_{\mathrm{K}} = \frac{W^2}{4}\sum_k \left[(2k+1)\hat{c}_k^\dagger\hat{c}_k - \sqrt{(k+1)(k+2)}(\hat{c}_{k+2}^\dagger\hat{c}_k + \hat{c}_k^\dagger\hat{c}_{k+2})\right] \ , \tag{5.44}$$

the kinetic energy part of the Hamiltonian,

$$\hat{H}_{\mathrm{P}} = \frac{\gamma^2}{4W^2}\sum_k (2k+1)\left[\hat{c}_k^\dagger\hat{c}_k + \sqrt{(k+1)(k+2)}(\hat{c}_{k+2}^\dagger\hat{c}_k + \hat{c}_k^\dagger\hat{c}_{k+2})\right] \ , \tag{5.45}$$

the external potential energy part of the Hamiltonian, and

$$\hat{H}_{\mathrm{I}} = -\frac{W}{N-1}\sum_{k\ell mn} f_{k\ell mn}\hat{c}_k^\dagger\hat{c}_\ell^\dagger\hat{c}_m\hat{c}_n \ . \tag{5.46}$$

the interaction Hamiltonian. The factor of $f_{k\ell mn}$ is the integral of four Hermite functions (with W set to unity) over all space, i.e.

$$f_{jk\ell n} = \int dx\ \varphi_j^*(x)\varphi_k^*(x)\varphi_\ell(x)\varphi_n(x) \ . \tag{5.47}$$

This can be calculated exactly in terms of gamma functions $\Gamma(x)$ and a standard hypergeometric function ${}_3F_2$ evaluated at unity [143]

$$f_{jk\ell n} = \frac{1}{\sqrt{2}\pi^2}\sqrt{\frac{j!}{k!\ell!n!(j-n)!}}\Gamma([k+\ell-j+n+1]/2)\Gamma([k-\ell+j-n+1]/2) \\ \times\ \Gamma([-k+\ell+j-n+1]/2){}_3F_2([-n,(j-n+k-\ell+1)/2, \\ (j-n-k+\ell+1)/2];[1+j-n,(j-n-k-\ell+1)/2],1)\ , \quad (5.48)$$

although we have found it easier to evaluate via Gauss-Hermite Quadrature, as discussed in Sec.A.3.4. Without interactions, the ideal gas Hamiltonian is given by

$$\hat{H}_{\rm ideal} = \hat{H}_{\rm K} + \hat{H}_{\rm P}. \quad (5.49)$$

For $W = \sqrt{\gamma}$, the basis states are eigenstates of the non-interacting Hamiltonian. The total Hamiltonian can therefore be expressed as

$$\hat{H} = \gamma\sum_k\left(k+\frac{1}{2}\right)\hat{c}_k^\dagger\hat{c}_k - \frac{\sqrt{\gamma}}{2(N-1)}\sum_{jk\ell n} f_{jk\ell n}\hat{c}_j^\dagger\hat{c}_k^\dagger\hat{c}_\ell\hat{c}_n\ , \quad (5.50)$$

and we refer the ground state of this as $|\psi_{\rm g}(\gamma)\rangle$ and the ground state energy as

$$\langle\psi_{\rm g}(\gamma)|\hat{H}|\psi_{\rm g}(\gamma)\rangle = E_g(\gamma)\ . \quad (5.51)$$

In order to do computations we truncate the states to only include those with an energy [with respect to Eq. (5.49)] which lies below an energy cut-off $E_{\rm cut}$. This basis is then projected into a state with zero centre-of-mass excitation as detailed in Sec. 4.2.6, along with the considerable reduction to the basis size shown in Fig. 4.2, with no loss of accuracy.

5.4.3 Using different-width Hermite functions

Using functions with $W = \sqrt{\gamma}$, such that they are eigenstates of $\hat{H}_{\rm ideal}$, is not desirable in the $\gamma \to 0$ limit because the basis will consist of states much wider than the wave-function we are using them to construct. For an infinite basis, the ground state should be independent of the basis used to describe the system (in our case, it should be independent of the value of W). For

numerical calculations, the basis will be finite and thus some choices of W are better than others. In Sec. 5.5, we will calculate the ground state for $\gamma = 0$ in order to determine the optimal value for W to be used in the calculations.

For arbitrary W, the full Hamiltonian reads:

$$\hat{H} = \sum_k \frac{W^2 + \gamma^2 W^{-2}}{2}\left(k + \frac{1}{2}\right)\hat{c}_k^\dagger \hat{c}_k - \frac{W}{2(N-1)}\sum_{jk\ell n} f_{jk\ell n}\hat{c}_j^\dagger \hat{c}_k^\dagger \hat{c}_\ell \hat{c}_n + \sum_k \frac{\gamma^2 W^{-2} - W^2}{4}\sqrt{(k+1)(k+2)}(\hat{c}_{k+2}^\dagger \hat{c}_k + \hat{c}_k^\dagger \hat{c}_{k+2}) \,, \tag{5.52}$$

which includes extra mixing terms in the ideal gas Hamiltonian (5.49). This causes a fairly significant issue in that it is no longer possible to exactly separate centre-of-mass eigenstates in this basis, meaning the full basis would need to be used in order to achieve the centre-of-mass ground state, making exact diagonalisation too slow. The solution to this is therefore to reduce the basis in the same way as before, but accept that the centre-of-mass wave-function we end up with is given by

$$f_{\mathrm{C}}(x_{\mathrm{C}}) = \sqrt{\frac{W}{\pi^{1/2}}}\exp\left(-N\frac{W^2 x_{\mathrm{C}}^2}{2}\right) \,, \tag{5.53}$$

which is not an eigenstate and has energy $E_{\mathrm{C}} = (W^2 + \gamma^2 W^{-2})/4$ rather than the true $\gamma/2$. Thus we know the true ground state is the wave-function we obtained, multiplied by $\sqrt{\sqrt{\gamma}/W}\exp\left([\gamma - W^2]Nx_{\mathrm{C}}^2/2\right)$. This approach has the huge advantage that, if W is kept constant, the occupation of the basis states for the ground state should change very little as $\gamma \to 0$ where they will tend to the solutions on the infinite line.

5.4.4 Numerical ground states within the GPE approximation

Within the GPE approximation, we can obtain the ground state by solving Eq. (5.12) as the ground state is the only stationary state of the system. The method used here is to again expand over a finite basis set of Hermite

functions of arbitrary width scaling W

$$\phi(x) = \sum_{k=0}^{\eta} c_k \sqrt{W} \varphi_k(Wx) \,, \tag{5.54}$$

then to produce a set of $\eta + 1$ nonlinear equations in the coefficient set $\vec{c}$ (which will be real), by integrating Eq. (5.12) multiplied by $\varphi_k(x)$ over all space, for $k = \{0, \ldots, \eta\}$, giving

$$\begin{aligned} 0 = &- \mu c_k + \frac{W^2 + \gamma^2 W^{-2}}{2}(k + 1/2)c_k - \frac{W}{2(N-1)} \sum_{\ell,j,n=0}^{\eta} f_{jk\ell n} c_\ell^* c_j c_n \\ &+ \frac{\gamma^2 W^{-2} - W^2}{4} \left(\sqrt{(k+1)(k+2)} c_{k+2} + \sqrt{k(k-1)} c_{k-2} \right) \,. \end{aligned} \tag{5.55}$$

We also take an $(\eta+2)$th equation, relating to the normalization $\sum_k |c_k|^2 = 1$. Denoting the vector with an equation at each position as $\vec{F}(\vec{c})$, we wish to solve $\vec{F} = \vec{0}$. We use Newton's method (see, for example [135]) to iteratively solve for $\vec{c}$, via[2]

$$J(\vec{c}^{(n)}) \, (\vec{c}^{(n+1)} - \vec{c}^{(n)}) = \vec{F}(\vec{c}^{(n)}) \,, \tag{5.56}$$

where J is the $\eta+1$ by $\eta+2$ Jacobian matrix associated with $\vec{F}$. We perform this calculating with increased η until convergence is achieved.

5.5 Effects of harmonic confinement

5.5.1 Ground state energy

Using the methods from the previous two sections, we investigate the effect an external potential has on the relative component of the ground state $|\psi_{\rm g}\rangle(\gamma)$ [cf. Eq. (5.51)]. This is important to quantify how soliton-like the state is, along with what excitations can be expected if the state is released quasi-instantaneously from the potential. Such dynamics have already been considered using the GPE in [127].

Figure 5.3 shows $\Delta E/N$, the energy difference per atom between the numer-

[2] This stepwise process is repeated until the stepwise change in μ and $\vec{c}$ are smaller than 10^{-7}.

ically calculated ground state energy $E_{\rm g}(\gamma)$ and the ground state energy of the artificial Hamiltonian (5.22) given by Eq. (5.24), for a range of γ and N values. It is produced by calculating the ground state energy via the three numerical methods, namely exact diagonalisation in a basis of Hermite functions with either optimized widths for weak trapping (shown in table 5.1), or widths which are eigenstates of the non interacting problem, and variational minimization, for a range of γ and taking the smallest value. This is because, due to the variational principle, all of these techniques produce only values greater than or equal to the ground state energy, hence the method leading to the lowest value is the best estimate for this parameter set.

5.5.2 Universal behaviour

If we instead define[3] $\tilde{\gamma} = \gamma(N-1)^2/N^2$ and $\Delta\tilde{E} = \Delta E[(N-1)/N]$, a more universal behaviour is present in $\Delta\tilde{E}$, with little number dependence as shown in fig. 5.3 (b). This is essentially the rescaling to make the GPE obtained from the centre-of-mass separated Hartree factorisation [Eq. (5.8) in Sec. 5.2], independent of N and dimensionless. The fact this produces such clear agreement indicates this centre-of-mass separated factorisation gives much better agreement with the full many body case. The increased trapping makes the state more product like and hence less pair correlated, meaning it can be described better by the GPE.

To see this analytically, we note that for $\tilde{\gamma} \ll 1$, our variational result of Eq. (5.41) for the energy is applicable. ΔE is obtained by subtracting the factor of $E_G + \gamma^2/2$, then converting to our rescaled units we have

$$\frac{\Delta\tilde{E}}{N} \approx \tilde{\gamma}^2 \frac{N}{N-1}\sum_{k=1}^{N-1}\frac{1}{k^2} - \tilde{\gamma}^4 \frac{24N^3}{(N^2-1)(N-1)}\left[\sum_{k=1}^{N-1}\frac{1}{k^2}\right]^2 + \mathcal{O}(\tilde{\gamma}^6)\,. \quad (5.57)$$

The N dependent factor of order $\tilde{\gamma}^2$ (which is the rescaled first order energy correction) is 2 for $N = 2$ and decreases monotonically to $\pi^2/6 \approx 1.6$ as $N \to \infty$, hence for very small $\tilde{\gamma}$, the $N = 2$ line is largest, but the difference is very small. The order $\tilde{\gamma}^4$ term has negligible number dependence and so is

[3]Equivalent to using the normal soliton units [Eq. (3.7) in which $g_{1\rm D}N = 1$ and time is further rescaled by a factor of $1 - 1/N$.

unlikely effect the ordering of these lines within for the range of variational models validity. On the other end of the scale, as $\gamma \to \infty$ (the trap dominated system) we can neglect interactions in Eq. (5.11), giving a ground state of a product of Gaussians of width $1/\gamma$, subtracting the centre-of-mass energy gives $\Delta E \to \gamma(N-1)/2N + \mathcal{O}(\sqrt{\gamma})$ or, in our rescaled units, $\Delta\tilde{E} \to \tilde{\gamma}/2 + \mathcal{O}(\sqrt{\tilde{\gamma}})$ and so to leading order, the N dependence vanishes.

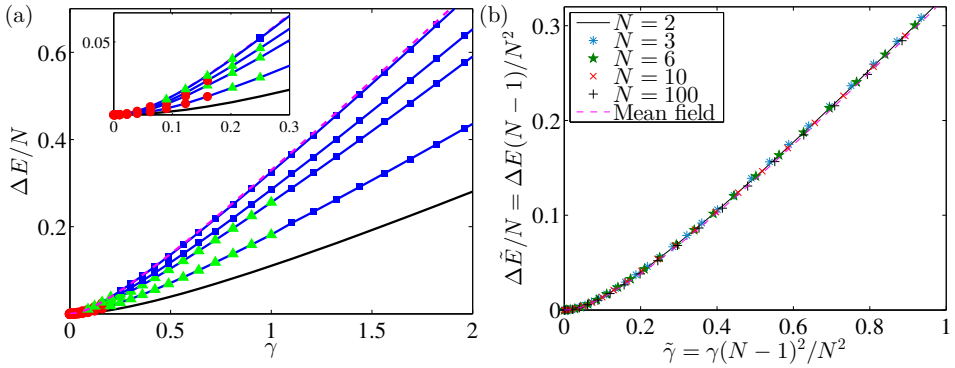

Figure 5.3: Difference between the ground state energy per atom and the energy of a free many body ground state with a Gaussian centre-of-mass profile, (a) is in terms of E_0/N [as defined in Eq. (5.24)] as a function of rescaled trapping strength γ and (b) with a rescaled $\tilde{\gamma} = \gamma(N-1)^2/N^2$ and $\Delta\tilde{E} = \Delta E(N-1)/N$. From bottom to top the lines on (a) are $N = 2, 3, 6, 10, 100$ and the dotted top line is the GPE prediction (which will agree with the many body results as $N \to \infty$) outlined in Sec. 5.4.4. The markers indicate a point on the line generated by different methods, (red) circles use the variational solution Eq. (5.33), (green) triangles use the fixed width basis sets to find the lowest eigenvalue of the Hamiltonian (5.52), cf. table 5.1. (Blue) squares are obtained using the basis of eigenstates of the non interacting Hamiltonian (5.49) to find the lowest eigenvalue of Eq. (5.50). The $N = 2$ line is plotted using the exact solution [Eq. (5.21)] detailed in Sec. 5.2.1 and the mean field line is obtained by the method explain in Sec. 5.4.4. The inset shows a zoom of the low γ section, demonstrating the initial quadratic dependence on γ. Figure (b) shows the universal behaviour present using rescaled units, this is the same data as in (a), however the numerical lowest eigenvalues are plotted as points to make them visible.

5.5.3 The classical soliton limit

As shown in Fig. 5.3, for low γ the variational ansatz (5.31) gives the best estimate for the ground state energy of all the methods used in this pa-

N	η	W	Reduced basis size
3	84	2	631
6	38	1	3009
10	28	0.5	2534
100	24	0.5	1575

Table 5.1: This table shows the parameters used in calculating the graph in Fig. 5.3, where N is atom number, η is the cut-off and W is the width taken for the fixed width calculations (coarsely chosen to minimize the ground-state energy at $\gamma = 0$). The reduced basis size is the number of states (with zero centre-of-mass excitation) used in the exact diagonalisation of the Hamiltonian. The bases are chosen to be a reasonable computational size, however the numerics are less reliable for small γ

per. For low enough γ, this variational ansatz is also very close to the product of the free many-particle solution with a Gaussian centre-of-mass wave-function (5.23) (see Fig. 5.2). In the limit of small γ, the integral

$$\mathcal{B} = \int_{-\infty}^{\infty} dx_1 \ldots \int_{-\infty}^{\infty} dx_N \; \psi_0(\vec{x})\psi_{\mathrm{H}}(\vec{x}) \tag{5.58}$$

can thus be used to investigate deviations of the Hartree-product wave-function (5.15) from the true many-particle ground state (which is well approximated by $\psi_0(\vec{x})$ for $\gamma \ll 1$). As was the case for Fig. 5.2, the effective single-particle overlap $\mathcal{B}^{1/N}$ will also be considered, as we are interested to see how well the wave-function is described by a product state, and when comparing two product states with different single-particle wave-functions, this quantity is independent of the atom number N.

In order to make an educated guess about what range of γ will give a large overlap, we look at the expectation value of the square of the centre-of-mass location over the Hartree-product wave-function (Appendix C.5):

$$\langle \psi_{\mathrm{H}} | x_{\mathrm{C}}^2 | \psi_{\mathrm{H}} \rangle = \frac{\pi^2}{3N} \; . \tag{5.59}$$

This value is identical to the variance of the centre of mass, as both the many body and Hartree states are centred about $x = 0$. A variance calculation can also be performed for Eq. (5.23), this is particularly simple as the centre of

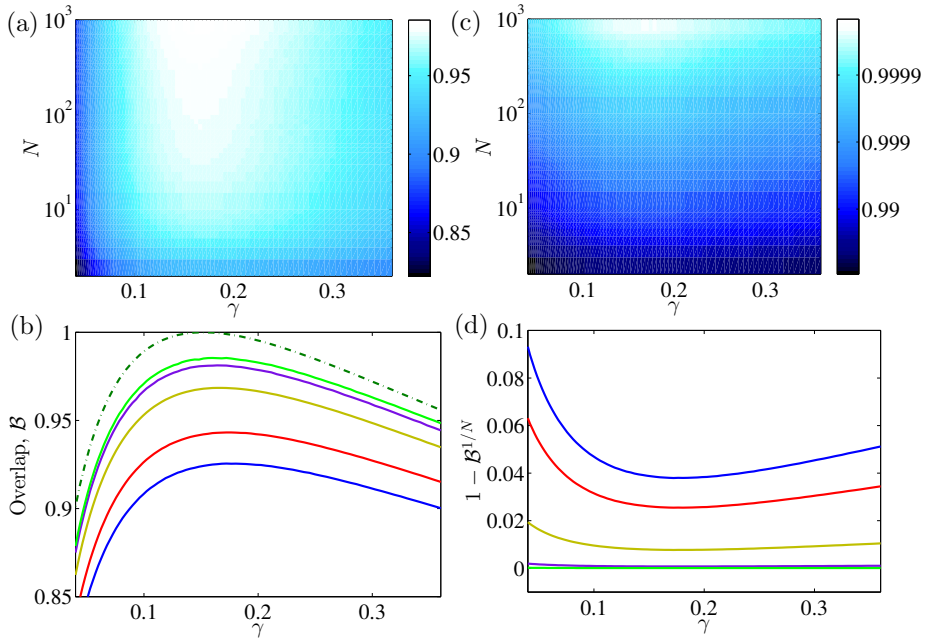

Figure 5.4: (a) 2D projection of overlap, $\mathcal{B}$ as defined in Eq. (5.58), between many-body free state with a Gaussian envelope (of width $\propto 1/\gamma$) given in Eq. (5.23) and the mean field soliton solution, given in Eq. (5.15), for a range of N and γ. (b) shows Horizontal slices through (a), and the dash-dotted line is the analytic estimate, based purely on centre-of-mass position uncertainty, given by Eq. (5.61). (c) shows effective single-particle overlap $\mathcal{B}^{1/N}$ and (d) shows the residuals $1-\mathcal{B}^{1/N}$ for given N values again via slices through (c). The solid lines in the lower figure (b) correspond to $N = 2, 3, 10, 100, 1000$ in that order from bottom to top, and this ordering is reversed for figure (d). As expected, the effective single-particle overlap plot (c) show a rapid convergence to unity as N increases. [(a) and (b)] suggest that most of the γ dependence in $\mathcal{B}$ is due to the effective "centre-of-mass width" of the Hartree-product solution, since the shape of each overlap curve is similar, besides a small offset, to the dash-dotted line. This indicates that a Hartree soliton is a very good approximation to the many body solution if the centre-of-mass wave-function is also localized.

mass is explicitly separate and is given by

$$\langle\psi_0|x_{\mathrm{C}}^2|\psi_0\rangle = \frac{1}{2\gamma N}\,. \tag{5.60}$$

As the Hartree-product state is uncorrelated, for a large enough N the distribution associated with the centre-of-mass location will therefore tend to a Gaussian (with variance of $\pi^2/3N$) via the central limit theorem. We therefore consider an effective centre-of-mass wave-function that is the square root

of this distribution, yielding the overlap integral

$$I(\gamma) = \int_{-\infty}^{\infty} dx_{\mathrm{C}} \left(\frac{3N^2\gamma}{2\pi^4}\right)^{1/4} \exp\left[-N\frac{(\gamma + 3/2\pi^2)x_{\mathrm{C}}^2}{2}\right]$$
$$= \frac{(24\pi^2\gamma)^{1/4}}{\sqrt{2\,\gamma\,\pi^2 + 3}}\,, \tag{5.61}$$

which reaches its maximum $I\left(\gamma_{\max}\right) = 1$ for

$$\gamma_{\max} = \frac{3}{2\pi^2} \simeq 0.15\,. \tag{5.62}$$

As the above analysis focuses on the centre-of-mass part of the wave-function, and thus Eq. (5.61) is likely to overestimate the overlap $\mathcal{B}$ as defined in Eq. (5.58), Eq. (5.61) also predicts a $\gamma \to 0$ behaviour of the form $I(\gamma) \sim c\gamma^{1/4}$ with c a constant. Figure 5.4 shows a numerical calculation of $\mathcal{B}$ for a range of γ and N, the integration is performed via Monte Carlo methods, i.e. weighted sampling using random variables with a $\mathrm{sech}(x/2)^2/4$ distribution (obtained via the ziggurat algorithm [144]) until a standard error of $< 10^{-4}$ is obtained.

It can be seen from Fig. 5.4 (a) and (b) that maximum overlap occurs just slightly above $\gamma = 0.16$ [close to the analytic estimate (5.62)] and improves as N increases. Based on our previous discussion of effective centre-of-mass width, the top value should relate to the overlap of the relative degrees of freedom, although this is not well defined. Graphs (c) and (d) show the Nth root of (a) and (b), effectively overlap at the level of single particles, which tends extremely rapidly to unity as N increases for any γ over the range shown.

A useful point that this high overlap implies is that the many-body state Eq. (5.23), is extremely well approximated by the Hartree product state if the centre-of-mass envelope squared is approximately the statistical distribution that would arise from taking the mean of the N independent probability distributions $|\phi|^2$ [with ϕ given in Eq. (3.3) setting $\xi \to \sqrt{2}$] associated to single atom positions in the product state. For this reason the Hartree product state would be expected to well approximate the ground state of the system, even at a many-body level, if the centre-of-mass envelope is local-

ized to the size of this distribution (i.e. $\gamma \approx 3/2\pi^2$) by the potential. The converse to this is also true, an initial condition that is given by Eq. (5.15) is well approximated by Eq. (5.23) with $\gamma \approx 3/2\pi^2$. This could be used to estimate centre-of-mass position uncertainty of a state, initially given by a Hartree product wave-function, as it evolves in time, using known results for the spreading of Gaussian wavepackets.

We also consider how these many-body effects would affect experimental observations. From a measurement the atomic density, one could use the mean of this signal to determine the centre-of-mass of the system. If the state of the system is well approximated by Eq. (5.23), the observed location would vary shot to shot with a probability distribution given by $|\psi_{\mathrm{cm}}(x_{\mathrm{C}})|^2 \propto \exp(-N\gamma x_{\mathrm{C}}^2)$ (combined with any experimental uncertainties associated with density measurement). For $\gamma < \gamma_{\mathrm{max}}$, this distribution would be wider than one would expect using the product approximation. Most notably if the centre-of-mass wave-function is wider than a classical soliton width $1/\sqrt{\gamma N} \gtrapprox 1$, this jumping effect would be most clearly visible. Non-zero temperature would further increase this effect, by introducing a statistical mixture of excited states of the centre of mass. As a purely mechanical analogy, one could think of taking a photo of a swinging pendulum at a random time, the shape always looks the same but its position appears random.

5.6 Conclusions

In this chapter, we studied a 1D system of identical Bosons with attractive contact interactions, a Lieb-Liniger(-McGuire) gas, in the presence of a harmonic trapping potential. We presented variational and numerical many-body calculations, in both cases making use of the separability of the centre-of-mass Hamiltonian to split the problem into relative and centre-of-mass degrees of freedom. We used a unit system such that the Hartree soliton length is set to unity ($\hbar = m = g(N-1) = 1$), leaving two parameters, the number of atoms, N, and $\sqrt{\gamma}$, the dimensionless ratio between the Hartree soliton and harmonic oscillator lengths.

Our key results are firstly that we have derived a first order energy correction

to the ground state of the relative degrees of freedom from the introduction of a harmonic oscillator potential [given in Eq. (5.27)], which is used in a variational minimization technique. This is proportional to γ^2 and the correction per atom tends to the mean field prediction from below, the relative difference is less than 1% for $N > 165$.

Secondly we have determined the validity range of γ of our many body-ansatz, consisting of the free many-body ground state with a Gaussian envelope as given in Eq. (5.23). Essentially as the trapped ground state deviates from this it becomes less "soliton like." We quantify this with the "effective single-particle overlap", given by the Nth root of the overlap between a variationally obtained ground state and our ansatz. For N large, this overlap is greater than 0.99 for $\gamma \lesssim 0.16$. Numerical calculations of energy in the strongly trapped region, $\gamma > 1$, indicate energies are still considerably lower than the non interacting case.

Thirdly we showed, via a numerical investigation of overlap between the free Hartree product solution and the free many-body ground state with a Gaussian envelope [given in Eq. (5.23)] describing the centre-of-mass wave-function, that the two wave-functions can have high agreement, even at a many-body level. This high overlap occurs when the modulus square of the envelope function matches the probability distribution, associated with the Hartree product, for the centre-of-mass position, which occurs when $\gamma \approx 0.16$.

In addition to these physical results, we outlined a numerical method for computing many body eigenstates, using a basis set of harmonic oscillator eigenstates, truncated at a particular energy. This is then projected into a subspace of states with the centre-of-mass wave-function in a specific state, as outlined in Sec. 4.2.6, allowing us to investigate the internal degrees of freedom separately.

Chapter 6

Collisions with finite number systems

6.1 Introduction

6.1.1 Preamble

This chapter focuses on the work relating to publication [2], entitled "Collision dynamics and entanglement generation of two initially independent and indistinguishable boson pairs in one-dimensional harmonic confinement", with contributions made by C. Weiss and S.A. Gardiner. Some results relating to strongly attractive interacting cases within the chapter are not yet published, due to lack of satisfactory convergence in the numerics, which we explain in the relevant sections. The paper [2] investigates finite number effects in collisions between two states of an initially well known number of identical bosons with contact interactions, oscillating in the presence of harmonic confinement. The primary motivation behind this work was to study soliton collisions in harmonic confinement and the resulting entanglement generation and non classical number statistics. However, investigations lead to the study of equilibration and characterisation of states at late times via measures such as the single-body von Neumann entropy, which proved interesting to study for repulsive systems in addition to attractive systems, demonstrating their qualitative difference in behaviour and entanglement generation.

We consider an initial condition which is an excited state constructed by taking two $N/2$ (interacting) atom ground states and placing them at an equal and opposite distance (denoted x_0) from the centre of a harmonic trap. This setup has two free parameters, the displacement and the ratio of interaction strength and harmonic oscillator length, we focus on varying the latter. The numerics focus on the case of $N = 4$; the simpler case of $N = 2$ has been covered elsewhere [138], but due to the large number of conservation laws present, a two body system has very constrained dynamics. In the non-interacting case, such a system would display periodic oscillations with a half harmonic-oscillator period (due to the left-right symmetry). With the addition of contact interactions between the bosons, collisions generate entanglement between each of the states and distribute energy into other modes of the oscillator. We study the system numerically via exact diagonalisation of the Hamiltonian within a finite basis set, as was the case in the previous chapter, investigating left/right number uncertainty as our primary measure of entanglement. Additionally we study the time-evolution and equilibration of the single-body von Neumann entropy for both the attractive and repulsive cases. We identify parameter regimes for which attractive interactions create behaviour qualitatively different from that of repulsive interactions, due to the presence of bound states (quantum solitons) and explain the processes behind this.

Our key results are that the single-body von Neumann entropy grows faster for repulsive systems than attractive systems with the same $|a_s|$, as does the relative number uncertainty (although small revivals are shown), indicating the attractive system resists entanglement. That is, except for certain attractive values that match resonance conditions, allowing for transfer to an entangled state (a superposition of $N - 1$ atoms left and 1 right and the reverse) to happen without cancellation. We also observe emergence of a pseudo period, which is approximately linear with the interaction strength.

6.1.2 Motivating results and background

Negative scattering lengths give interesting possibilities in double-well and lattice physics, both systems which are experimentally realisable with a small,

well known number of atoms. Repulsive interactions between atoms are known to give rise to the Mott insulator state [145], with a near-definite atom number per lattice site. If one has a definite number of atoms per site, there is effectively a total uncertainty in relative phase between lattice sites and thus no phase coherence. A measurement of relative phase should give totally random results and indeed this is what one finds when imaging the moment distribution of such a lattice, i.e no distinguishable interference patterns. Attractive interactions could in theory be used to squeeze number statistics the opposite way, such that the ground state would tend to a superposition of a quantum soliton (N atom bound state) delocalised over every lattice site. When only two sites are present, such a state is referred to as a NOON state [146], which is useful for non shot noise limited interferometry [147]. However, phase differences between the two sites have almost no energy cost making them degenerate and hence systems where the ground state is such a superposition are known to be extremely unstable if any coupling to the environment is present, typically replacing quantum uncertainty with statistical uncertainty. It is therefore preferable to create such states dynamically, for example by splitting a moving quantum soliton [148, 149].

Any closed quantum system with no decoherence effects will be described by a wavefunction that will evolve deterministically. As such, the wavefunction, at any point in time $|\psi(t)\rangle$, maps back to a unique $|\psi(0)\rangle$ with no uncertainty. Recent experiments have the potential to observe this deterministic behaviour in systems with a small number of cold atoms [150, 151], with dynamics that can be analytically calculated and with precise tuning available in the scattering length and confinement potentials. Strongly correlated effects and quantum superpositions are generally much easier to achieve in few-body systems. Despite this one can still envisage collective properties (such as expectation values of operators) of a time-dependent finite system tending to constant values when averaged over reasonable timescales, or relaxation of local operators, as shown in [152]. Non-integrable systems, upon coupling to another larger system, usually tend to an equilibrium configuration at long times, independent of the initial state of either system (except for the total energy); however recent theoretical observations have thrown doubt on this [153]. Additionally, when two coupled systems contain a sim-

ilar number of elements the situation is less clear still. Our system is non-integrable and contains two initially independent subsystems of the same size; hence, we are interested to what extent equilibration occurs or where it is resisted. Quantum systems, for example atoms populating sites in an optical lattice [154], are known to show partial revivals of the initial state in time, but are generally observed to show weaker revivals as time progresses in an apparent damping. We are interested in whether certain measures, specifically the number to the left and right of the trap centre and the single body von Neumann entropy, tend to constant values when averaged over sufficient timescales.

Entanglement between identical bosons is not as easy to define as that between distinguishable particles [114]. One can consider a bipartite partitioning [155] which can be into sets of lower and more highly excited states, or via states occupying separate regions of space — in our case the left and right of the centre-of-mass. We wish to observe the generation of entanglement between initially independent systems develop over time. In the absence of interactions, no real entanglement can be generated between the two subsystems (although our chosen measure is only meaningful when the subsystems are well separated). Additionally, with strong interactions the effect of the confinement may be diminished, and the integrability of the free system (see Sec. 4.1) may also affect entanglement generation, particularly in the attractive case where a new length scale is introduced which can be smaller than the confinement [1].

6.1.3 Chapter breakdown

The chapter is organized as follows: Section 6.2 introduces the one dimensional Hamiltonian and the unit rescaling to harmonic oscillator lengths, used throughout this chapter. Next, the initial condition is introduced, with specific cases of interest mentioned. Section 6.3 discusses observables and measures of entanglement that we will use to investigate the system, including the variation in the number to either side of the trap centre, and the single-body von Neumann entropy. Section 6.4 begins an analytic investigation of the system, focusing on the mechanisms by which interactions mod-

ify the dynamics of each displaced state and generate entanglement. This model is specialised to strong attractive interactions in Sec. 6.5. Section 6.6 investigates the number exchange processes predicted in Sec. 6.4 using time-dependent perturbation theory. Section 6.7 discusses a possible experimental realisation of the system, using ultracold atoms in an optical lattice, with parameters discussed for Caesium. Section 6.8 contains a brief description of the numerical method, based on exact diagonalisation. Section 6.9 presents numerically obtained results for the evolution of our observables and entanglement measures in the system. Section 6.11 summarizes and concludes.

6.2 System

6.2.1 Hamiltonian and unit rescaling

We again use the Hamiltonian (5.1), but rescale to harmonic oscillator units (codified as $\hbar = \omega_x = m = 1$), meaning that length is in units of $\sqrt{\hbar/m\omega_x}$, time in units of $1/\omega_x$, and energy in units of $\hbar\omega_x$; a harmonic oscillator period is then 2π. The Hamiltonian rescales to

$$H(\vec{x}) = \sum_{k=1}^{N}\left(-\frac{1}{2}\frac{\partial^2}{\partial x_k^2} + \frac{x_k^2}{2}\right) + g\sum_{k=2}^{N}\sum_{j=1}^{k-1}\delta(x_k - x_j)\ , \tag{6.1}$$

where $g = g_{1\mathrm{D}}\sqrt{M/\hbar^3\omega_x}$ is the new dimensionless coupling parameter, which quantifies the relative strength of interaction. This relates to the parameter γ [defined in Eq. (5.13)] through $\gamma = [g(N-1)]^{-2}$.

We again make use of the separation of the Hamiltonian into two commuting components as described in Sec. 5.2.

6.2.2 Initial condition

General N-body case

We consider a highly non-mean-field-like initial condition, taking two $N/2$-atom ground states (for a given g), equally and oppositely displaced from the trap centre by a distance x_0, and symmetrizing. The initial ($t = 0$)

wavefunction is then

$$\begin{aligned}\psi(\vec{x},0) =& \frac{B}{\sqrt{N!}}\sum_{\{\mathcal{P}\}} f^{(N/2)}(x_1 - x_0, .., x_{N/2} - x_0) \\ & \times f^{(N/2)}(x_{N/2+1} + x_0, ..., x_N + x_0)\ ,\end{aligned} \tag{6.2}$$

where $f^{(N/2)}(x_1, \ldots, x_{N/2})$ is the ground state for $N/2$ atoms (generally numerically determined) in the harmonic trap, $\{\mathcal{P}\}$ is the set of all permutations of $\vec{x}$, and B is a normalizing factor. Such an initial condition may be motivated by the idea of making two separate BECs and allowing them to collide within a harmonic trapping potential, or from rapidly modifying a Mott insulator state in an optical lattice (as we will discuss in Sec. 6.7). If the left and right components are well separated, i.e., the width of the atomic density distribution corresponding to $f^{(N/2)}$ is significantly less than x_0, then there is a well-defined number of $N/2$ atoms either side of the trap, and left- and right-atoms are distinct by virtue of their position. Furthermore, as the centre-of-mass dynamics are decoupled [1] and straightforward to determine, the dynamics experienced by an initial condition such as ψ can be readily extended to incorporate any initial condition for the centre of mass, e.g., in particular, an overall oscillation about the trap centre [100].

Conveniently, $\psi(\vec{x}, t)$ is in the ground state of the centre-of-mass component of $H(\vec{x})$. To show this, we use unnormalised Jacobi coordinates for a total of N identical particles, as defined in Eq. (5.3) and Eq. (5.2).

Now using the Jacobi coordinates for $N/2$ particles, and considering these $N/2$ particles in isolation, we can partition the $N/2$-particle ground state into centre-of-mass dependent and independent components: $f^{(N/2)}(x_1, \ldots, x_{N/2}) = \varphi(\xi_2, \ldots, \xi_{N/2})\, \mathrm{e}^{-N x_{\mathrm{C}(N/2)}^2/4}$. Substituting Eq. (A.5) into this expression, we can then define $\tilde{f}^{(N/2)}$ through

$$\begin{aligned}f^{(N/2)}(x_1, \ldots, x_{N/2}) =& \varphi(\xi_2, \ldots, \xi_{N/2})\, \mathrm{e}^{\sum_{k=2}^{N/2}[(k-1)/2k]\xi_k^2 - \sum_{k=1}^{N/2} x_k^2/2} \\ =& \tilde{f}^{(N/2)}(x_1, \ldots, x_{N/2})\, \mathrm{e}^{-\sum_{k=1}^{N/2} x_k^2/2},\end{aligned} \tag{6.3}$$

where $\tilde{f}^{(N/2)}$ (as it can also be written as a function of $\{\xi_2, \xi_3, \ldots, \xi_{N/2}\}$ only) is clearly independent of $x_{\mathrm{C}(N/2)}$.

If we now expand to a full set of N coordinates, $\tilde{f}^{(N/2)}(x_1,\ldots,x_{N/2})$ is also clearly independent of $x_{\mathrm{C}(N)}$, as is (by symmetry) $\tilde{f}^{(N/2)}(x_{N/2+1},\ldots,x_N)$. Noting further that displacement by x_0 will not affect that part of $f^{(N/2)}$ independent of the centre-of-mass coordinate, then for the identity permutation of $\psi(\vec{x})$

$$\begin{aligned} f^{(N/2)}(x_1-x_0,\ldots,x_{N/2}-x_0)f^{(N/2)}(x_{N/2+1}+x_0,\ldots,x_N+x_0) \\ = \tilde{f}^{(N/2)}(x_1,\ldots,x_{N/2})\tilde{f}^{(N/2)}(x_{N/2+1},\ldots,x_N) \\ \times \mathrm{e}^{-\sum_{k=1}^{N}x_k^2/2-x_0\left[\sum_{k=N/2+1}^{N}x_k-\sum_{k=1}^{N/2}x_k\right]-Nx_0^2/2}\,. \end{aligned} \tag{6.4}$$

By the identities Eq. (A.5) and Eq. (A.11), the exponential reduces to $\mathrm{e}^{-Nx_{\mathrm{C}(N)}^2/2}\mathrm{e}^{-N\left(\sum_{k=N/2+1}^{N}\xi_k/k-x_0^2/2\right)}$, that is a term proportional to the centre of mass ground state multiplied by a function of independent Jacobi coordinates. The identity permutation of ψ can thus be written as a product of the centre of mass ground state and a function of the other independent Jacobi coordinates. This separation from the centre of mass ground state occurs for every permutation of the coordinates x_k, and so we conclude that the centre-of-mass component of $\psi(\vec{x})$ is indeed in the ground state.

Taking a slightly different initial condition, when one combines ground states from two trapping potentials that are not equal to the final potential (with, e.g., tighter harmonic trapping), will introduce a breathing motion, which can still be considered separately from the remaining dynamics. It is also significant to note that the kind of initial condition we consider does not have a well defined relative phase between the left and right components [156]. If a relative number uncertainty between left and right were to develop then this would no longer be the case, and a meaningful relative phase could in principle be extracted.

Time evolution for the non-interacting case

If we take the case where $g = 0$, we can express the full time dependent wavefunction [which we label $\psi_0(\vec{x},t)$] analytically, as a symmetrized product

of two $N/2$-atom product states

$$\psi_0(\vec{x},t) = \frac{B_0}{\sqrt{N!}} \sum_{\{\mathcal{P}\}} \prod_{k=1}^{N/2} \phi(x_k, -x_0, t) \prod_{j=N/2+1}^{N} \phi(x_j, x_0, t) \; . \tag{6.5}$$

Here $\phi(x, \pm x_0, 0)$ is a Gaussian displaced by $\pm x_0$ from the trap centre, and [100, 157]

$$\begin{aligned} \phi(x, x_0, t) = \left(\frac{1}{\pi}\right)^{1/4} \exp\left(-\frac{[x - x_0\cos(t)]^2}{2}\right) \\ \times \exp(i[t/2 - x_0\cos(t)x + x_0\sin(2t)/4]) \; , \end{aligned} \tag{6.6}$$

corresponding to an expectation value of the energy per particle of $E = (x_0^2+1)/2$, and the normalisation constant $B_0 = 1 + \mathcal{O}(\mathrm{e}^{-2x_0^2})$.

Special case of four atoms

If $N = 4$, the $f^{(2)}$ appearing in Eq. (6.2) are known analytically [137, 138], and may, if $g < 0$, for sufficiently large g and x_0, be considered to be bound-state dimers, held within an overall harmonic trapping potential. The general form is given by

$$\begin{aligned} f^{(2)}(x_1, x_2) &= \mathcal{N} U\left(-\nu, 1/2, \frac{[x_1 - x_2]^2}{2}\right) \mathrm{e}^{-x_1^2/2}\, \mathrm{e}^{-x_2^2/2} \\ &= \mathcal{N} U(-\nu, 1/2, \xi_2^2/2)\, \mathrm{e}^{-\xi_2^2/4}\, \mathrm{e}^{-x_\mathrm{C}^2} \; , \end{aligned} \tag{6.7}$$

with U Tricomi's confluent hypergeometric function, $\mathcal{N}$ a normalisation constant, and ν the effective quantum number (equal to zero for $g = 0$), as determined by the transcendental equation $\Gamma(1/2 - \nu)/\Gamma(-\nu) = -g/2^{3/2}$. This state has an energy of $2\nu + 1$, where there is a contribution of $1/2$ due to the centre of mass. Equation (6.7) can then be inserted into the initial condition

$$\begin{aligned} \psi(x_1, x_2, x_3, x_4, 0) = &\frac{B}{\sqrt{4!}} \sum_{\{\mathcal{P}\}} f^{(2)}(x_1 - x_0, x_2 - x_0) \\ &\times f^{(2)}(x_3 + x_0, x_4 + x_0) \; , \end{aligned} \tag{6.8}$$

where $\{\mathcal{P}\}$ is the set of all 4! permutations of $\{x_1, x_2, x_3, x_4\}$. Note that, as $f^{(2)}(x_1, x_2) = f^{(2)}(x_2, x_1)$, the number of distinct permutations actually reduces to $4!/2!2! = 6$.

6.3 Observables and measures of entanglement

6.3.1 Left/right number

For our system, one useful measure to track the generation of entanglement is the variance in particle number to the left and right of the system's centre of mass (which we will generally consider to be fixed at the origin). The initial condition we consider has $N/2$ atoms to either side with essentially no possibility of, say, $N/2+1$ to the right and $N/2-1$ to the left (probabilities for measuring such unequal partitions decrease in a Gaussian manner with the initial separation). Hence the left- and right-particle-number-variance will initially be zero. As the left- and right-particles approach and collide, all number partitionings become possible, and so this measure is only informative when the particle density at the location of the centre of mass is small.

We define a number-to-the-right operator

$$\hat{N}_R = \int_0^\infty dx\, \hat{\Psi}^\dagger(x)\hat{\Psi}(x)\ , \tag{6.9}$$

[or in first quantisation $\sum_{k=1}^{N} \Theta(x_k)$, where Θ is the Heaviside step function]; imaging one side of the trap would correspond to a projective measurement into the eigenstates of this operator, as is discussed in Sec. 6.7. The expectation value of $\hat{N}_R$ is the mean number of particles on the right-hand-side. As the system is parity preserving, $\langle \hat{N}_R \rangle = N/2$ for all time for the initial conditions we consider.

The more informative number-to-the-right variance is

$$\Delta N_R = \langle \hat{N}_R^2 \rangle - \langle \hat{N}_R \rangle^2\ , \tag{6.10}$$

which, for our initial condition of two well-separated left and right compo-

nents of definite number, should be approximately zero. From Eq. (D.6), the variance for a product state $\psi(\vec{x}) = \prod_{k=1}^{N} \phi(x_k)$ [symmetric about the trap centre so that $\langle \hat{N}_R \rangle = N/2$] is

$$\Delta_P N_R = \langle \hat{N}_R \rangle (1 - \langle \hat{N}_R \rangle / N) = N/4 \,, \tag{6.11}$$

which evaluates to unity if $N = 4$ (this is however the same as a symmetric superposition of one and three atoms to the right/left). It can also be shown (Appendix D.1.1) that for the case of $N = 4$ and no interactions ($g = 0$) [given by Eq. (6.5)], this variance evolves as

$$\Delta_P N_R = 1 - \mathrm{erf}^2 \left[x_0 \cos(t) \right] + \mathcal{O}(\mathrm{e}^{-2x_0^2}) \,, \tag{6.12}$$

with erf the error function[1]. Hence, we have a function with period $T = \pi$, which is equal to unity when $t = (n+1/2)\pi$ and vanishingly small in x_0 when $t = n\pi$.

In general our wavefunction is not an eigenstate of $\hat{N}_R$, and contains components of different $\hat{N}_R$ eigenstates (for some given overall N, meaning that an additional specification of number-to-the-left operator eigenstates is not necessary). One can, however, calculate expectation values of operators defined over restricted regions of state space, specific to having exactly n (of N) atoms to the right of the trap centre. An expectation value for an operator $\hat{O}$ defined in this region is then

$$\langle \hat{O} \rangle_{n,N-n} = \frac{N! \int_0^\infty dx_1 \dots dx_n \int_{-\infty}^0 dx_{n+1} \dots dx_N \, \psi^*(\vec{x}) \, O(\vec{x}) \, \psi(\vec{x})}{n!(N-n)! P_{n,N-n}} \,, \tag{6.13}$$

with

$$P_{n,N-n} = \binom{N}{n} \int_0^\infty dx_1 \dots dx_n \int_{-\infty}^0 dx_{n+1} \dots dx_N \, |\psi(\vec{x})|^2 \tag{6.14}$$

the probability that a perfect measurement of $\hat{N}_R$ will find n of N atoms to the right (or equivalently $N - n$ to the left) of the trap centre. This is equivalent to taking the usual expectation value over a new (normalised)

[1] The error function satisfies $\mathrm{erf}(0) = 0$ and $\mathrm{erf}(\pm x) \to \pm[1 - \exp(-x^2)/(\sqrt{\pi} x)]$ as $x \to \infty$.

wavefunction $\psi_{n,N-n}(\vec{x})$ defined by

$$\psi_{n,N-n}(\vec{x}) = \frac{\psi(\vec{x}) \sum_{\mathcal{P}} \prod_{k=1}^{n} \Theta(x_k) \prod_{j=n+1}^{N} \Theta(-x_j)}{\sqrt{P_{n,N-n}}} \,, \tag{6.15}$$

where $\mathcal{P}$ is the set of all unique permutations, of which there are $N!/n!(N-n)!$, hence the factors in Eqs. (6.14) and (6.13). Each such wavefunction is an eigenstate of $\hat{N}_R$, with eigenvalue n. In principle one can partition the Hilbert space in such a way that it is the tensor product of a subspace describing only how many particles are to the left/right of the trap centre, and a subspace describing all other relevant properties of the system state. We may denote the set of eigenstates of $\hat{N}_R$ spanning this number subspace by $\{|N-n,n\rangle\}$, such that

$$\hat{N}_R|N-n,n\rangle = n|N-n,n\rangle \,. \tag{6.16}$$

Further, it is also useful to consider distance-to-the-right and distance-to-the-right-squared operators, i.e.,

$$\hat{X}_R^{(j)} = \int_0^\infty dx\, x^j \hat{\Psi}^\dagger(x)\hat{\Psi}(x) \tag{6.17}$$

[given by $\sum_{k=1}^{N} \Theta(x_k) x_k^j$ in first quantisation], for $j = 1, 2$. We denote the restricted (to having n of N atoms to the right of the trap centre) expectation values of the position-to-the-right operator

$$R_{n,N-n}(t) = \langle \hat{X}_R^{(1)} \rangle_{n,N-n} \,. \tag{6.18}$$

These trace particle like tracks, with widths around them described by

$$\sigma_{n,N-n}(t) = \sqrt{\langle \hat{X}_R^{(2)} \rangle_{n,N-n} - R_{n,N-n}^2(t)} \,. \tag{6.19}$$

6.3.2 von Neumann entropy and relaxation

Averaging over all individual particles results in the single-body density matrix

$$\rho(x,x',t) = \langle \hat{\Psi}^\dagger(x')\hat{\Psi}(x) \rangle \,, \tag{6.20}$$

which is normalised to the total particle number N [$\int dx\, \rho(x,x,t) = N$]. From this, single-body properties of the many-body system may be determined, specifically the von Neumann entropy, sometimes referred to as the Invariant Correlation Entropy (ICE) [158] as it is independent of the basis chosen, at least up to truncation errors. Equation (6.21) is simply the position-representation rendering of $S_{\mathrm{vN}} = -\operatorname{Tr}\{(\rho/N)\ln(\rho/N)\}$, where the single-body density matrix ρ may of course be expressed in terms of any sufficiently complete basis (numerically, we employ the orthonormal Hermite functions, and the trace becomes a sum of discrete diagonal matrix elements).

$$S_{\mathrm{vN}}(t) = -\int dx \left(\frac{\rho(x,x,t)}{N}\right) \ln\left(\frac{\rho(x,x,t)}{N}\right) . \tag{6.21}$$

Relaxation, in the sense of tending to states of higher entropy, is not thought to be present if the system is fully integrable. This is the case when $g = 0$, or if the trapping is removed and the eigenstates are given by the Bethe ansatz, discussed in Sec. 4.1. However, as the integrability is broken by the trapping, we expect some degree of thermalisation due to (previously forbidden) mixing between states. It is of interest to determine how such thermalisation timescales vary with the interaction strength and initial separations.

For a product state, ρ has a single non-zero eigenvalue of value N, meaning $S_{\mathrm{vN}} \to 0$ (this is equivalent to a Bose–Einstein condensate being exactly described by a Gross–Pitaevskii wavefunction). A larger value of S_{vN} indicates occupancy of multiple eigenstates of ρ, equivalent to population of non-condensate modes due to to thermal excitations, or to quantum or dynamical depletion [55, 159].

If the system equilibrates, S_{vN} will tend to a constant value. As our initial conditions result in repeated collisions at the trap centre, the value of S_{vN} shows distinct oscillations that decay only slowly. We therefore also consider a time average over an oscillator period

$$\bar{S}_{\mathrm{vN}}(t) = \frac{1}{2\pi}\int_{t}^{t+2\pi} dt'\, S_{\mathrm{vN}}(t') , \tag{6.22}$$

along with its variance

$$\Delta\bar{S}_{\mathrm{vN}}(t) = \frac{1}{2\pi}\int_{t}^{t+2\pi} dt' \left[S_{\mathrm{vN}}(t') - \bar{S}_{\mathrm{vN}}(t)\right]^2 \ . \tag{6.23}$$

If $S_{\mathrm{vN}}(t)$ tends to a constant value, this will be shown by a relaxation of $\bar{S}_{\mathrm{vN}}(t)$ to a constant value, and a relaxation of $\Delta\bar{S}_{\mathrm{vN}}(t)$ to 0, with the relaxation of $\bar{S}_{\mathrm{vN}}(t)$ tending to occur on a significantly faster time scale than that of $\Delta\bar{S}_{\mathrm{vN}}(t)$.

6.4 Analysis of the interacting system

6.4.1 Left–right separation of the Hamiltonian

As our initial condition consists of left and right components that are well separated and therefore distinguishable, we can initially treat the left and right components separately. As these left and right clusters only interact for a short-time during collisions in the centre (so long as they stay as distinct clusters), it makes sense to treat interactions between these clusters perturbatively at early times. We therefore split the Hamiltonian into three, restricting the coordinates to the region $x_1 \leq x_2 \leq x_3 \leq x_4$, which is sufficient due to Bose symmetry. The three components are

$$\begin{aligned}
H_L(x_1, x_2) &= \sum_{k=1}^{2}\left(-\frac{1}{2}\frac{\partial^2}{\partial x_k^2} + \frac{x_k^2}{2}\right) + g\delta(x_2 - x_1) \ , \\
H_R(x_3, x_4) &= \sum_{k=3}^{4}\left(-\frac{1}{2}\frac{\partial^2}{\partial x_k^2} + \frac{x_k^2}{2}\right) + g\delta(x_4 - x_3) \ , \\
H_I(x_2, x_3) &= g\left[\delta(x_3 - x_1) + \delta(x_3 - x_2) + \delta(x_1 - x_4) + \delta(x_2 - x_4)\right] \ .
\end{aligned} \tag{6.24}$$

Due to the zero width of the delta function, only adjacent interaction terms [$\delta(x_k - x_j)$ with $k - j = 1$] contribute to H_I (so only $\delta(x_3 - x_2)$ remains), as the other terms constitute a set of zero measure in the region we are considering. The condition $x_1 = x_2$ occurs infinitely more often than $x_1 = x_3$ as this necessarily also implies $x_2 = x_3$, and so is a set of lower dimensionality. As $[\hat{H}_L, \hat{H}_R] = 0$, if we neglect $\hat{H}_I$ our system can be described by a tensor

product of the left and right components as these components commute. Each Hamiltonian $\hat{H}_{L/R}$ can further be split into centre-of-mass $\hat{H}^{(\mathrm{C})}_{L/R}$ and relative $\hat{H}^{(\mathrm{R})}_{L/R}$ parts, generating the dynamics of the left and right centre-of-mass and relative coordinates [$x_{\mathrm{C}(L)} = (x_1 + x_2)/2$, $x_{\mathrm{C}(R)} = (x_3 + x_4)/2$, $x_{\mathrm{R}(L)} = x_2 - x_1$, and $x_{\mathrm{R}(R)} = x_4 - x_3$, respectively], which again mutually commute.

We consider the centre-of-mass wavefunction of an n atom cluster, which is a Gaussian displaced from the trap centre by some value X_n. Without the influence of $\hat{H}_I$ our system consists of two indistinguishable clusters (with internal degrees of freedom considered to be in the ground state) undergoing simple harmonic motion. The primary reason for separating the Hamiltonian in this way is that our initial condition is in the ground state of $\hat{H}^{(\mathrm{R})}_{L/R}$ and is a displaced ground state of $\hat{H}^{(\mathrm{C})}_{L/R}$, hence any change to these wavefunctions is an excitation of the system.

6.4.2 Perturbative introduction of H_I

Overview

We consider the effect of introducing the Hamiltonian H_I, from Eq. (6.24), to the system. We look at three notable effects: changes to the wavefunction describing the left/right separation of the clusters; changes to the internal degrees of freedom within the clusters to the left and right; and interactions transferring atoms from one side to the other, creating a symmetric superposition.

Inter-cluster wavefunction changes and pseudo-periodicity

The centre-of-mass wavefunctions of each side, described by $\hat{H}^{(\mathrm{C})}_L + \hat{H}^{(\mathrm{C})}_R$, can change, so long as the *global* centre-of-mass wavefunction remains constant. Such changes lead to entanglement between the left and right clusters. To see this we note initially that the two cluster wavefunction could be written as a product of left and right sides

$$\psi_0(x_{\mathrm{C}(L)}, x_{\mathrm{C}(R)}) \propto \mathrm{e}^{-[x_{\mathrm{C}(L)} - x_0]^2} \mathrm{e}^{-[x_{\mathrm{C}(R)} + x_0]^2} + \mathcal{T}_{\mathrm{perm}} \,, \tag{6.25}$$

with $\mathcal{T}_{\text{perm}}$ denoting the permutation of R and L. This can be written in such a way as to explicitly separate the global centre of mass:

$$\psi_0(x_{\mathrm{C}(L)}, x_{\mathrm{C}(R)}) = \mathrm{e}^{-[x_{\mathrm{C}(L)}+x_{\mathrm{C}(R)}]^2/2} \times \left\{ \mathrm{e}^{-[x_{\mathrm{C}(L)}-x_{\mathrm{C}(R)}-2x_0]^2/2} + \mathcal{T}_{\text{perm}} \right\} . \tag{6.26}$$

The first term describes the global centre-of-mass and is therefore fixed, the latter term, however, will be modified by interactions. Any such change (other than modifying x_0 or multiplying by $\exp(ip[x_{\mathrm{C}(L)} - x_{\mathrm{C}(R)}])$, which are simply shifts of the initial position and momentum, respectively) means that there will be terms involving products of the form $x_{\mathrm{C}(L)}x_{\mathrm{C}(R)}$, such that the wavefunction cannot be separated, indicating entanglement between the left and right sides. Such entanglement is notable in the context of solitons in free space, as integrability means collisions cannot create entanglement once the states are asymptotically separated, although higher order non-linearities can also lead to entanglement [160]. Additionally, during collisions with attractive (repulsive) interactions, each cluster will accelerate (decelerate), subsequently returning to near its initial velocity, leading to a pseudo-periodicity.

Intra-cluster wavefunction changes

The internal degrees of freedom described by $\hat{H}^{(\mathrm{R})}_{L/R}$ are initially in the ground state. Interactions during collisions will introduce excitations, with the energy transferring from the centre-of-mass energy of each cluster. By conservation of energy this must reduce the amplitude of the oscillation. Attractive interactions will suppress such excitations, as the energy separation between ground and first (even parity) exited state is greater than the harmonic oscillator level spacing, whereas for repulsive interactions this gap will be smaller, reaching a minimum of -1.85 at $g = 2.28$ [c.f. App. B.2]. Note that when highly excited modes of the relative degrees of freedom $x_{\mathrm{R}(L)}, x_{\mathrm{R}(R)}$ are populated, these will always have a significant occupation for both L and R. One expects a qualitative difference in behaviour between the attractive and repulsive cases to occur when the change between the first and second relative excited states differs by an amount of order unity in harmonic oscillator units $[\hbar\omega_x]$. For strongly attractive interactions, energies scale as $-g^2n(n^2-1)/24$

and so when $x_0 < |g|/\sqrt{6(N^2-1)}$ there is not enough energy to break the initial bound-state clusters, making the relative degrees of freedom effectively inaccessible.

Left/right atom transfer

Finally, the interactions can transfer an atom from one side to the other, mixing to a set of states with a symmetric superposition of three and one atoms at either side of the trap (and, ultimately, back from this to the original state). There cannot be significant transfer to a state where there is a cluster of four atoms in the ground state (apart from the centre-of-mass degree of freedom) on one side and zero on the other side, due to the invariance of the centre-of-mass wavefunction, unless the state has all four atoms directly at the trap centre. The state satisfying this condition is the ground state of the system, and so the only possible population is that at $t = 0$.

A feature that distinguishes this effect from intra-cluster excitations is the energy difference between the two configurations, denoted $\Delta E_{\text{int}} = E_{3,1} - E_{2,2}$. For $g < 0$ the ground state of a three atom relative Hamiltonian (that part of the Hamiltonian independent of the centre of mass) plus a single free atom is lower in energy than two sets of two atoms in their relative ground states. The opposite is true for $g > 0$, but the energy difference can only be of the order of the harmonic oscillator energy spacings, and so suppression is unlikely unless x_0 is small. The energy difference ΔE_{int} can take a variety of values when intra-cluster states are excited, but in the interest of studying transfer interactions, we look at the energy difference between two isolated ground states of $N = 2$ atoms and one $N = 3$ and one $N = 1$ atom ground states. This can be estimated analytically in three limits:

$$\Delta E_{\text{int}} \sim \begin{cases} g/\sqrt{2\pi} & \text{if } |g| \ll 1 \\ 1 & \text{if } g \gg 1 \\ -g^2/2 - 7/12g^2 & \text{if } g \ll -1, \end{cases} \tag{6.27}$$

the approximations used being overlapping non-interacting ground states, effective fermionisation [161] (Tonks gas) and bound state clusters [162] with

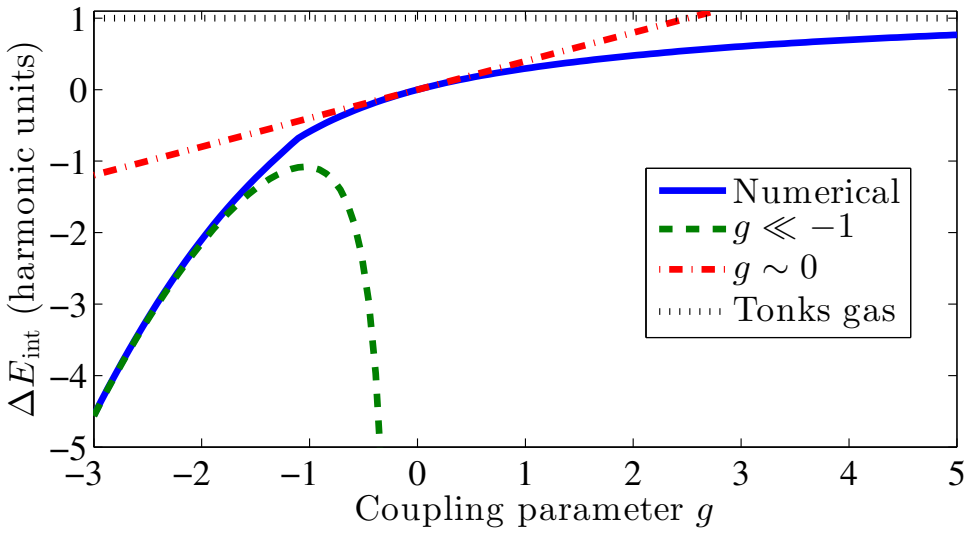

Figure 6.1: Energy difference $\Delta E_{\rm int} = E_{3,1} - E_{2,2}$ between two+two and three+one atom ground state clusters (in harmonic energy units $\hbar\omega$) as a function of the dimensionless coupling parameter g (quantifying the interaction strength). Analytic estimates from Eq. (6.27) are shown for comparison, with the Tonks gas being the $g \to \infty$ limit.

the first order energy correction from the trapping potential [Eq. (5.27)], respectively. Numerically determined values of $\Delta E_{\rm int}$ are shown in Fig. 6.1; this energy proves to be an important quantity in Sec. 6.6 (note that this does not include the energy from the momentum/displacement of the clusters). Viewed classically, this transfer interaction causes transfer to a state where the kinetic energy of the clusters was different from the original by an amount equal to $\Delta E_{\rm int}$, in order to conserve energy.

6.5 Coherent state approximation in the strongly attractive regime

6.5.1 Generalised left-right separation

The states formed by a transfer of atoms in the soliton like regime $|g| \gg 1$, $g < 0$ are a superposition of two separate n and $N - n$ body clusters, to

the left and right respectively. We are interested in how such states evolve in time and whether it is possible to predict quantities like the single body density and conditional position expectation values following a measurement of the number left and right of the centre. The suppression of intra-cluster excitation allows us to consider this situation analytically in a way simply not possible in the repulsive or weakly attractive cases, even for the case of general atom number.

The symmetrisation of the available states which can be mixed to be a transfer interaction is important only when the two clusters are not well separated. Assuming they are well separated, we can consider the evolution separately by splitting the N body Hamiltonian 6.1 in a way similar to Eq. (6.24), but more general. Within the region $x_1 \leq x_2 .. \leq x_N$ we have two separate n and $N-n$ body Hamiltonians $\hat{H}_L$ and $\hat{H}_R$, and an interaction term $\hat{H}_I$, in which we include only the term which contributes.

$$\begin{aligned}
\hat{H}_L(n) &= \sum_{k=1}^{n}\left(-\frac{1}{2}\frac{\partial^2}{\partial x_k^2}+\frac{x_k^2}{2}\right)+g\sum_{k=2}^{n}\delta(x_k-x_{k-1})\ , \\
\hat{H}_R(n) &= \sum_{k=n+1}^{N}\left(-\frac{1}{2}\frac{\partial^2}{\partial x_k^2}+\frac{x_k^2}{2}\right)+g\sum_{k=n+2}^{N}\delta(x_k-x_{k-1})\ , \\
\hat{H}_I(n) &= g\delta(x_{n+1}-x_n)\ .
\end{aligned} \tag{6.28}$$

As before we have $[\hat{H}_L(n), \hat{H}_R(n)] = 0$ and we can neglect $\hat{H}_I(n)$ if we are considering situations when the clusters are far from the trap centre. Each Hamiltonian $\hat{H}_L(n)$ can again be split into a centre of mass $\hat{H}^{(\mathrm{C})}_{L/R}$ and relative part $\hat{H}^{(\mathrm{r})}_{L/R}$ which again commute, (note for $n = 1$ there is only centre of mass). The centre-of-mass coordinate of the left side is $x_{\mathrm{C}} = (x_1 + \ldots + x_n)/n$ and so we have

$$\hat{H}^{(\mathrm{C})}_{L} = \frac{1}{2}\left(-\frac{1}{n}\frac{\partial^2}{\partial x_{\mathrm{C}}^2}+nx_{\mathrm{C}}^2\right)\ . \tag{6.29}$$

6.5.2 Construction of oscillating quantum soliton states

We assume the centre-of-mass wavefunction of an n atom cluster is that of a Gaussian displaced from the centre by X_n at $t = 0$. Such a state evolves

according to Eq. (6.6), up to scaling factors, and will have a combined kinetic and potential energy of $(nX_n^2+1)/2$. We must also have a right cluster of $N-n$ atoms, initially located at $-X_n n/(N-n)$, due to the constraint that the global centre-of-mass position expectation value is located at $x=0$. All possible wavefunctions that can evolve from a symmetric initial condition must also posses left-right symmetry, and so wavefunctions must be a *symmetrised* product of both sides. The details of combining this second cluster are shown in App. D.2.

For the relative degrees of freedom we will assume each side is in the *relative ground state* for n attractive atoms, with eigenenergies $\epsilon_n+\tilde{\epsilon}_n$ with the former relating to the interaction and kinetic energy and the latter to the potential energy, which we assume take the strongly interacting values [1]

$$\begin{aligned}\epsilon_n &\sim -g^2 n(n+1)(n-1)/24,\\ \tilde{\epsilon}_n &\sim \sum_{k=1}^{n-1} 1/k^2 g^2 n\ .\end{aligned} \tag{6.30}$$

For $n=2$ these values are correct to one percent when $g<-2.3$. Adding the left and right centre-of-mass energies $\langle \hat{H}_L^{(\mathrm{C})}\rangle + \langle \hat{H}_R^{(\mathrm{C})}\rangle$, the total energy of such a state is given by

$$\begin{aligned}E_{n,N-n} &= \epsilon_n + \epsilon_{N-n} + \tilde{\epsilon}_n + \tilde{\epsilon}_{N-n} + \frac{Nn}{N-n}X_n^2 + 1\\ &\sim -\frac{Ng^2}{24}\left[N^2 - 3n(N-n) - 1\right]\frac{Nn}{N-n}X_n^2 + 1\ .\end{aligned} \tag{6.31}$$

We define $|\psi_{n,N-n}(0)\rangle$ to be an n atom cluster to the left and an $N-n$ cluster to the right, displaced by X_n and $-X_n n/(N-n)$ respectively (with unit norm), such that our initial condition is $|\psi_{N/2,N/2}(0)\rangle$. When left and right are well separated, the time evolution is determined by the first two terms in Eq. (6.28)

$$|\psi_{n,N-n}(t)\rangle = \exp\left\{-i[\hat{H}_L(n)+\hat{H}_R(n)]t\right\}|\psi_{n,N-n}(0)\rangle\ . \tag{6.32}$$

Because of the symmetry of all states about the centre of the trap, we need

only consider symmetric states, hence we define

$$|\varphi_{n,N-n}(t)\rangle = \mathcal{N}_{n,N-n}(t)\left[|\psi_{n,N-n}(t)\rangle + |\psi_{N-n,n}(t)\rangle\right] , \tag{6.33}$$

with the normalisation term

$$\left[\mathcal{N}_{n,N-n}(t)\right]^{-2} = \left[\langle\psi_{n,N-n}(t)| + \langle\psi_{N-n,n}(t)|\right]\left[|\psi_{n,N-n}(t)\rangle + |\psi_{N-n,n}(t)\rangle\right] . \tag{6.34}$$

If we assume the bound states in the relative degrees of freedom are sufficiently like the Bethe ansatz cluster states, that states with a different pair of bound states are orthogonal, and so if $n' \neq n$ and $n' \neq N$ then $\langle\psi_{N-n,n}(t)|\psi_{N-n',n'}(t)\rangle = 0$ and $\mathcal{N}_{n,N-n}(t) \to 1/\sqrt{2}$.

Introducing back interactions, each $H_I(n)$ from Eq. (6.28) can mix different $|\varphi_{n,N-n}(t)\rangle$. It will also affect the relative position between the two sides (by populating inter-cluster excited states). We temporarily neglect this effect for the purpose of this analysis, but note it will introduce a greater uncertainty in positions at late time. Within this set of approximations, we can express any possible wavefunction the system can take as

$$|\psi(t)\rangle \simeq \sum_{n=1}^{N/2} c_{n,N-n}(t)|\varphi_{n,N-n}(t)\rangle . \tag{6.35}$$

The single cluster state is assumed to be negligible due to reasons of energy and centre-of-mass momentum conservation. The coefficients $c_{n,N-n}$ are those considered in Sec. 6.6.3 for the strongly attractive perturbation theory. In the case of our four atom system, these approximations give us the simple wavefunction

$$|\psi(t)\rangle \simeq c_{2,2}(t)|\varphi_{2,2}(t)\rangle + c_{1,3}|\varphi_{1,3}(t)\rangle , \tag{6.36}$$

with the initial condition that $c_{2,2}(0) = 1$. To zeroth order in H_I the dimers would simply oscillate perfectly with a period of π, this is in principle obtained in the limit the initial separation tends to infinity, or trivially when $g \to 0$. The mixing between the $N/2, N/2$ and $n, N-n\ +\ N-n, n$ states can be seen as being due to the coupling between the Bethe ansatz eigen-

states due to the harmonic trapping, or from the $H_I(n)$ in our coherent state model. The rate of transfer should depend on this coupling, which we use as a parameter in Sec. 6.6, but both coupling terms are hard to calculate directly.

6.5.3 Predictions of oscillation amplitudes

If we assume our state remains of the form Eq. (6.35), we can make analytic predictions of X_n, the maximum displacements of the oscillating clusters in $|\varphi_{n,N-n}(t)\rangle$, by assuming they have the same energy as $|\varphi_{N/2,N/2}(t)\rangle$. This condition $E_{N/2,N/2} = E_{n,N-n}$ with E defined in Eq. (6.31), implies

$$\begin{aligned} &Nx_0^2 + 2\epsilon(N/2) + 2\tilde{\epsilon}(N/2) + 1 = \\ &\frac{Nn}{N-n}X_n^2 + 1 + \epsilon(n) + \epsilon(N-n) + \tilde{\epsilon}(n) + \tilde{\epsilon}(N-n)\ , \end{aligned} \tag{6.37}$$

with x_0 the initial position of the $N/2$ clusters. Within the strongly interacting regime, one can neglect contributions of order $1/g^2$ and simplify this expression to

$$X_n^2 = \frac{N-n}{n}\left\{x_0^2 + \frac{g^2}{8}\left[\frac{N^2}{4} - n(N-n)\right]\right\}\ , \tag{6.38}$$

To estimate the uncertainty in these values due to the possibility of collisions mixing to states with a different energy, we can derive bounds based on the Hamiltonian variance. These bounds should be considered weak and subject to all the prior assumptions in Sec.6.5. As our Hamiltonian is time independent, the variance of its expectation value

$$\Delta E \equiv \sqrt{\langle \hat{H}^2\rangle - \langle \hat{H}\rangle^2}\ , \tag{6.39}$$

is constant. This is because the time evolution operator $U(t) = \exp(-i\hat{H}t/\hbar)$ [with $|\psi(t)\rangle = U(t)|\psi(0)\rangle$] commutes with $\hat{H}^\nu$ ($\nu = 1, 2, 3, \ldots$), hence we have: $\langle\psi(t)|\hat{H}^\nu|\psi(t)\rangle = \langle\psi(0)|\hat{H}^\nu|\psi(0)\rangle$ for and positive integer ν. This remains true if one shifts $\hat{H}$ by a constant offset value. We consider only the $N = 4$ case as this is used in the numerics.

In the limit $x_0 \gg 1$, we can treat each side separately to get an analytic expression (c.f. appendix D.3.1)

$$\Delta E \to 2x_0 \ . \tag{6.40}$$

When the two states in our model have negligible overlap, one can derive the bound on the energy difference (appendix D.3)

$$|E_{2,2} - E_{3,1}| \leq \frac{\Delta E}{\sqrt{p(1-p)}} \ , \tag{6.41}$$

with $p = |c_{2,2}|^2$. This bound tends to infinity as p tends to 1 or 0, but this would imply there is no occupation of one of the states anyway, so this is physical. This modifies Eq. (6.38) to an inequality, in the strongly interacting limit we have

$$\left(\frac{g^2}{8} + x_0^2 - \frac{\Delta E}{2\sqrt{p(1-p)}}\right) \leq \frac{X_1^2}{3} \leq \left(\frac{g^2}{8} + x_0^2 + \frac{\Delta E}{2\sqrt{p(1-p)}}\right) \ . \tag{6.42}$$

This allows for additional discretion in the particles kinetic energy and thus maximum position reached after each collision. The upper bound is stricter than the lower, as we have neglected mixing to more excited states.

6.5.4 Possible Caveats of the model

We have so far ignored the possibility of mixing to states made up of more than two clusters, e.g. one bound state and two free particles. For the case of $N = 4$, the possible energies of such states are much larger than the 2,2 or 1,3 geometries in the limit of strong interactions

$$\begin{aligned} E_{2,1,1}(X_{1,1}, X_{1,2}, X_2) &= \left(-\frac{g^2}{4} + \frac{3}{2} + x_2^2 + \frac{X_{1,1}^2 + X_{1,2}^2}{2}\right) \\ E_{1,1,1,1}(X_{1,1}, X_{1,2}, X_{1,3}, X_{1,4}) &= \left(2 + \sum_{k=1}^{4} \frac{X_{1,k}^2}{2}\right) \ . \end{aligned} \tag{6.43}$$

These states are energetically accessible if the initial kinetic energy is larger than the interaction energy, hence initial conditions satisfying $g^2 + 1/2 > 4X_2^2$ should immediately see a suppressed mixing into these states. This is however

not the case if $N > 4$, even with $N = 6$ the $\{4, 1, 1\}$ state still has lower internal energy than the $\{3, 3\}$ state. However, we still expect approximate conservation of the momentum variance over a collision, provided that the internal length scales are much smaller than a harmonic oscillator length (i.e. the collision is similar to one in free space). This would mean only weak mixing could occur to states that have all the particles sitting at the trap centre with no momentum. That said, the values of the outer positions are much less constrained; the centre-of-mass condition implies only that the sum of all the maximum positions vanishes, i.e. $\sum_{k,n} nX_{n,k} = 0$. This allows for a wide variation in trajectories with no obvious preferences between them. These states are very difficult to include in the model, however the effect would likely be similar to that of increased relative position uncertainty between the clusters.

In addition to this, so far we have assumed the shape of the centre-of-mass wavefunction of each particle to be the ground state of the corresponding centre-of-mass Hamiltonian. If this was allowed to vary there would be freedom to transfer kinetic energy goes into exciting this mode. This increases the separation uncertainty between the states until the process of a collision is more or less continuously happening to some extent. In addition to this, if the clusters go "out of sync" because the pseudo periodicity effect is different for each n, the model is no longer valid.

6.6 Mixing between different number configurations via time-dependent perturbation theory

6.6.1 General setup

We now investigate the atom transfer effect outlined in Sec. 6.4.2, predicted to be most significant for $g < 0$. We can write our wavefunction at any point in time as

$$|\psi(t)\rangle = c_{2,2}(t)|\varphi_{2,2}(t)\rangle + c_{1,3}(t)|\varphi_{1,3}(t)\rangle + c_{0,4}(t)|\varphi_{0,4}(t)\rangle \ , \tag{6.44}$$

with $|\varphi_{n,N-n}(t)\rangle$ normalised wavefunctions that are superpositions of states with n and $N-n$ atoms to the left and vice versa, and $\{c_{n,N-n}\}$ a set of complex constants, the modulus squares of which are the probabilities to find n or $N-n$ atoms on either side. In order to qualitatively predict the incremental changes to $\{c_{n,N-n}(t)\}$ from before to after a collision, we use time dependent perturbation theory. We are interested in the states away from the collision and so we ignore the $c_{0,4}(t)$ component and look at the variation in $c_{2,2}(t)$ and $c_{1,3}(t)$.

In general $|\varphi_{n,N-n}(t)\rangle$ will be a set of states, made up of many different components which are continually mixed even when the states are not in collision; we treat these kets as being simply one time dependent state and assume the centre-of-mass motion of each $n, N-n$ atom cluster in $|\psi_{3,1}(t)\rangle$ undergoes harmonic oscillation and is periodic in time with period $T=\pi$. Formally we therefore say $|\varphi_{n,N-n}(t)\rangle$ are the same as those given in Eq. (6.33),[2] with the time evolution of the states $|\psi_{n,N-n}(t)\rangle$ determined by Eq. (6.32). This assumes that any internal relative excitations (in the sense of Sec. 6.4.2) in all $|\varphi_{n,N-n}(t)\rangle$ are small compared to the ground state. This approximation is expected to work better for $g<0$, for reasons outlined in Sec. 6.4.2, and at short-times. In the strongly attractive regime, the states will have no intra-cluster excitations. However within this treatment we are still neglecting inter-cluster excitations, which will try to address later by including a pseudo period.

Our wavefunction

$$|\psi(t)\rangle \simeq c_{2,2}(t)|\varphi_{2,2}(t)\rangle + c_{1,3}(t)|\varphi_{1,3}(t)\rangle \ , \tag{6.45}$$

must solve the Schrödinger equation

$$i\frac{d}{dt}|\psi(t)\rangle = [(\hat{H}_L + \hat{H}_R) + \hat{H}_I]|\psi(t)\rangle \ . \tag{6.46}$$

Taking the Hamiltonian on the fundamental region $x_1 \leq x_2 \leq x_3 \leq x_4$, and

[2] Although these are now general n body ground states and not quantum solitons.

noting the time dependence of Eq. (6.32), this implies

$$\begin{aligned} & i\left[\dot{c}_{2,2}(t)|\varphi_{2,2}(t)\rangle + \dot{c}_{3,1}(t)|\varphi_{3,1}(t)\rangle + c_{2,2}(t)|\dot{\varphi}_{2,2}(t)\rangle + c_{3,1}(t)|\dot{\varphi}_{3,1}(t)\rangle\right] = \\ & c_{2,2}(t)\left\{|\dot{\varphi}_{2,2}(t)\rangle + \hat{H}_I(2)|\varphi_{2,2}(t)\rangle\right\} \\ & + c_{3,1}(t)\left\{|\dot{\varphi}_{3,1}(t)\rangle + \mathcal{N}_{1,3}\left[\hat{H}_I(1)|\psi_{1,3}(t)\rangle + \hat{H}_I(3)|\psi_{3,1}(t)\rangle\right]\right\} , \end{aligned} \tag{6.47}$$

with $\hat{H}_I(n)$ given in Eq. (6.28). Cancelling terms and using the orthonormality of $\varphi_{N,n-n}(t)$, we can simplify Eq. (6.47) to the two coupled differential equations

$$\begin{aligned} i\dot{c}_{2,2}(t) =& g\left\{\mathcal{N}_{1,3}(t)c_{3,1}(t)\langle\varphi_{2,2}(t)|\left[\delta(x_1-x_2)|\psi_{1,3}(t)\rangle + \delta(x_3-x_4)|\psi_{3,1}(t)\rangle\right]\right. \\ & \left. + c_{2,2}(t)\langle\varphi_{2,2}(t)|\delta(x_2-x_3)|\varphi_{2,2}(t)\rangle\right\} \end{aligned} \tag{6.48a}$$

$$\begin{aligned} i\dot{c}_{3,1}(t) =& g\left\{\mathcal{N}_{1,3}(t)c_{3,1}(t)\langle\varphi_{3,1}(t)|\left[\delta(x_1-x_2)|\psi_{1,3}(t)\rangle + \delta(x_3-x_4)|\psi_{3,1}(t)\rangle\right]\right. \\ & \left. + c_{2,2}(t)\langle\varphi_{3,1}(t)|\delta(x_2-x_3)|\varphi_{2,2}(t)\rangle\right\} . \end{aligned} \tag{6.48b}$$

We have substituted in the coordinate expression for all $\hat{H}_I(n)$ to show the proportionality to g. So far these is essentially an exact description of the two state system. As we initially have $c_{2,2} = 1$, we can consider a perturbative solution with $|c_{3,1}(t)| \ll |c_{2,2}(t)|$ as a regime of validity.

Formally, we perturb $(\hat{H}_L + \hat{H}_R)$ by $\hat{H}_I$ given in Eq. (6.24) [or $n = 2$ in Eq. (6.28)]. Within first order perturbation theory, this is equivalent to solving Eq. (6.48) after dropping all terms with a prefactor of $c_{3,1}(t)$. Hence we have

$$i\dot{c}_{2,2}(t) \simeq c_{2,2}(t)\langle\varphi_{2,2}(t)|\hat{H}_I|\varphi_{2,2}(t)\rangle, \tag{6.49}$$

$$i\dot{c}_{3,1}(t) \simeq c_{2,2}(t)\langle\varphi_{3,1}(t)|\hat{H}_I|\varphi_{2,2}(t)\rangle. \tag{6.50}$$

We note that $\langle\varphi_{2,2}(t)|\hat{H}_I|\varphi_{2,2}(t)\rangle$ is periodic with a periodicity ($T = \pi$) half that of the oscillator period. The matrix element $\langle\varphi_{3,1}(t)|\hat{H}_I|\varphi_{2,2}(t)\rangle$ is a product of a function with period $T = \pi$, and the complex exponential $\exp(-i\Delta E_{\text{int}}t)$ of the energy difference between the intra-cluster degrees of freedom in both configurations (as plotted in Fig. 6.1).

Denoting the periodic component of the interaction terms $\langle\varphi_{n,N-n}(t)|\hat{H}_I|\varphi_{2,2}(t)\rangle$

as $f_{n,N-n}(t)$, we must therefore solve

$$i\dot{c}_{2,2}(t) \simeq c_{2,2}(t) f_{2,2}(t) \ , \tag{6.51a}$$

$$i\dot{c}_{3,1}(t) \simeq c_{2,2}(t) f_{3,1}(t) \exp\left(-i\Delta E_{\text{int}} t\right) \ , \tag{6.51b}$$

with the boundary condition $c_{2,2}(0) = 1$. The interaction time between the two states is proportional to internal size of the states and inversely proportional to the relative velocity at collision which is proportional to $1/x_0$.

6.6.2 Fourier approximation

We first assume that the initial separation x_0, and the coupling magnitude $|g|$, are not large. Within this regime the interaction time is quite long and we assume that we can approximate $f_{n,N-n}(t)$ by first order Fourier series, $f(t) \approx g(1-\cos(2t))$. This implies that all $f_{n,N-n}(t)$ differ only by a constant value; hence $f_{2,2}(t) = Af(t)$ and $f_{1,3}(t) = Bf(t)$, with A and B dependent, in principle on g, and quite heavily on x_0. We can use this to solve Eq. (6.51b):

$$\begin{aligned} c_{2,2}(t) &\simeq \exp\left(i \int_0^t dt' \, Agf(t')\right) \\ &\simeq \exp(iAg[t - \sin(2t)/2 + \ldots]), \end{aligned} \tag{6.52}$$

and if we neglect ΔE_{int} under the assumption that the relative energy on both sides is similar,

$$c_{3,1}(t) \simeq \frac{B}{A}\left[\exp\left(igA \int_0^t dt' f(t')\right) - 1\right] \ . \tag{6.53}$$

For short times, we can expand $c_{31}(t) \approx B[igt + \mathcal{O}(g^2t^2, g\cos(2t))]$, i.e., proportional to gt and oscillatory terms and hence giving a linear increase when $t = n\pi$. At longer times the phase evolution of $c_{2,2}(t)$ becomes important, leading to cancellation in the terms of $c_{3,1}(t)$ and giving oscillatory behaviour with a period dependent on g. The linear increase with g after a collision is not expected to continue when $g \gtrapprox 1$ as higher-order terms become increasingly important and the perturbation theory breaks down.

We have so far neglected the difference in internal energy. This will introduce

an additional phase between $c_{3,1}(t)$ and $c_{2,2}(t)$. With this included we have

$$\begin{aligned} c_{3,1}(t) &\simeq \int_0^t dt' \left[igBc_{2,2}(t')f(t')\exp\left(-i\Delta E_{\text{int}}t'\right)\right] \\ &\simeq igB\int_0^t dt'\, f(t')\exp(i[Ag - \Delta E_{\text{int}}t' - \mathcal{T}_{\text{osc}}])\ , \end{aligned} \tag{6.54}$$

with $\mathcal{T}_{\text{osc}}$ denoting oscillatory terms such as $k\cos(2t)$, which are periodic with $t \to t+\pi$ or shorter fractions of π for the higher-order terms. Summing together terms of different phases will produce cancellation, hence if the $\exp(i[Ag - \Delta E_{\text{int}}t])$ term has the same periodicity as $f(t)$ and the "osc" terms, both π, the overall increase will be linear in time with no higher-order polynomial terms. This could therefore lead to resonant (suppressed) transfer if $Ag - \Delta E_{\text{int}} \approx n$ with n even (odd), and slightly suppressed transfer if n is a rational number not close to an even integer, e.g. $1/2, 1/3, 3/2$. As noted earlier, the $g \to \infty$ limit gives $\Delta E_{\text{int}} \sim 1$ and thus should lead to suppressed transfer if $|Ag| \lesssim 1/2$. We note that when $|g| \sim 0$ this resonance condition appears to be matched up to a factor $g[A - (2\pi)^{-2}]$, giving very long cancellation periods, however, as we see in Fig. 6.4 (and by the fact the perturbation strength scales $\propto g$) the rate of atom transfer scales proportionally to g and so cancellation can still occur before a significant population transfer is achieved.

This simple analysis neglects higher-order effects such as pseudo-periodicity,the coupling back of the $c_{13}(t)$ term, and intra-cluster excited states are not treated explicitly. However, qualitatively we expect an initially weak linear increase to c_{13}, but the population will oscillate between the states. For small $|g|$ the timescale of this population cycling would be many oscillator periods, but for $g \gtrapprox 1$ the timescale of these oscillations should drop.

6.6.3 Instantaneous interaction approximation

Predictions for N=4

Alternatively we can assume x_0 is not small and the coupling parameter g is large and negative, i.e the regime of soliton like dynamics. This actually suits this method better as now excited internal states of $|\psi_{n,N-n}(t)\rangle$ (states which

are not just an n and $N-n$ atom ground state undergoing simple harmonic oscillation) are energetically suppressed. Therefore $c_{3,1}(t)$ and $c_{2,2}(t)$ really do denote occupations of the states of Eq. (6.35), i.e. a single time-dependent wavefunction, rather than a class of states in the general case. The magnitude of interaction term, $\langle\delta(x_n - x_{n+1})\rangle$, does not increase with the collision velocity, but the time for which it is significant decreases asymptotically as $1/x_0$, along with its effect on the system. Therefore if x_0 is large we can treat the interaction as a delta function in time and thus approximate the periodic component as

$$f(t) \approx \sum_{k=0}^{\infty} \delta(t - \pi/2 - k\pi) \; . \tag{6.55}$$

We then assume $f_{2,2}(t) = A(g)f(t)$ and $f_{3,1}(t) = B(g)f(t)$ in a similar way to the Fourier case, except that we have not included a factor of g in $f(t)$ which also implies $A < 0$. This perturbation theory can also be considered valid even in the limit $|g| \gg 1$ with $g < 0$, as it does not make assumptions about the interaction strength.

We can use the results for phase shifts from soliton collisions [Eq. (4.51)] in free space, to give an expression for $A(g)$ in the strongly interacting limit

$$A(g) \approx \theta(2, 2, p_{r(2,2)}) \; . \tag{6.56}$$

Our perturbation theory does not formally include the interaction between left and right sides in the trimer-singlet configuration, which would cause a phase shift of $\theta(3, 1, p_{r(3,1)})$. However, because we are assuming $c_{3,1}$ is small, the phase of $c_{3,1}(t)$ is set purely by the unperturbed time-evolution and $c_{2,2}(t)$. This phase shift would only matter if we solved Eq. (6.48) with higher order time-dependent perturbation theory. The relative momentum per atom at collision can be approximated as $p_{r(2,2)} \approx 2x_0$ and $p_{r(3,1)} \approx 4X_1/3$ with X_n given by Eq. (6.38). This model has the considerable advantage of using only parameters known *ab initio* to determine $A(g)$, but the phase shifts may be slightly different as the solitons are modified by confinement.

Using this new function to solve Eq. (6.51b) with $c_{22}(0) = 1$ gives:

$$c_{2,2}(t) \simeq \exp\left[-iA(g)\int_0^t d\widetilde{t} f(\widetilde{t})\right] \quad = \exp\left(-iA(g)\left\lfloor \frac{t}{\pi} + \frac{1}{2}\right\rfloor\right) , \tag{6.57}$$

using $\int dt\delta(t)f(t) = \lim_{\Delta\to 0}\frac{f(t+\Delta)+f(t-\Delta)}{2}$, $\lfloor x \rfloor$ meaning round x down to the next integer, and the convention that an empty sum is zero. We can therefore calculate the time dependence of the other component to be

$$c_{3,1}(t) \simeq -i\tilde{B}(g)\sum_k^{\lfloor t/\pi - 1/2\rfloor} \exp\left[-ik\left(\Delta E_{\rm rel}\pi + Ag\right)\right] , \tag{6.58}$$

with $\tilde{B} = B\mathrm{e}^{-i\Delta E_{\rm rel}\pi/2}\left(1+\mathrm{e}^{-iAg}\right)/2$ a rescaled constant. In order to achieve resonant transfer to the c_{31} state, we require all the terms in the sum to phase match. In order to derive an accurate expression we have found it necessary to also include a correction to the pseudo period $\delta(g) = T_{\rm pseudo} - \pi \approx \alpha g$ (which is observed in our results, c.f. Sec. 6.9) and predict the kth resonance to occur when

$$2k\pi = A + \Delta E_{\rm rel}(\pi + \delta) , \tag{6.59}$$

with $\Delta E_{\rm rel} = E_{2,2} - E_{3,1}$ the energy difference at $g = g_{\rm rs}$ and k a positive integer. Analytic solutions are not available to Eq. (6.59), so in generally it will need to be solved numerically. However, we can expand A as a power series in g/x_0 to try and predict the first resonance, $A \sim 5g/2x_0 - 17g^3/96x_0^3 + \mathcal{O}(g/x_0)^5$. Using the $g \ll -1$ value of $\Delta E_{\rm rel}$ from Eq. (6.27) and approximating A to lowest order $A \sim g\tilde{A}$, we can use this expression to predict low lying resonances

$$\begin{aligned} 2k\pi &= \tilde{A}g_{\rm rs} + \frac{g_{\rm rs}^2\pi}{2} \\ g_{\rm rs} &= -\frac{\tilde{A} + \sqrt{\tilde{A}^2 + 4k\pi^2}}{\pi} \\ &\sim -2\sqrt{k} - \frac{\tilde{A}}{\pi}\left(1 + \frac{\tilde{A}}{4\sqrt{k}\pi}\right) - \mathcal{O}\left(\frac{A^4}{k}\right) . \end{aligned} \tag{6.60}$$

Additionally we can see that in the limit $g/x_0 \to -\infty$, the phase shift $\theta(2,2,p_{r(2,2)}) \to -3\pi$. Assuming also the magnitude of the pseudo period $|\delta| \approx \alpha|g| \ll 1$ to still be small, we can say the large g resonances should be

given by

$$g_{\rm rs} \approx \frac{2\sqrt{2k+1}}{\sqrt{2}-\alpha\sqrt{2k+1}} \sim 2\sqrt{k+1/2}+\alpha(k+1/2)\ , \tag{6.61}$$

In either case the proportionality to $2\sqrt{k}$ seems to be common feature, with only small corrections from the interaction phase shift. We expect the predictions of Eq. (6.59) to be only approximately correct and only valid in the regime when $c_{13}(t)$ is small; long time oscillatory behaviour in the population is not possible to predict with first order perturbation theory, we can simply say when we expect the largest early time effects.

Predictions for N>4

One can also consider the situation for $N > 4$, if we again assume our state space to be limited to that of two cluster states [formalised in Eq. (6.35)] and proceed with the same time dependent perturbation theory, assuming all $c_{N/2-n,N/2+n}$ except $c_{N/2,N/2}$ are small. The relative energy difference between two clusters of $N/2$ atoms and a state with clusters of size $N/2-n$ and $N/2+n$, is given in the limit $|g| \gg 1$, $g<0$ as

$$\Delta E_{\rm rel}(N/2-n, N/2+n) \sim \frac{g^2 N n^2}{4}\ . \tag{6.62}$$

We follow the same procedure as before to derive a condition for $c_{N/2-n,N/2+n}$ to increase resonantly, taking $A_n \approx \theta(N/2, N/2, 2x_0)$. Because we are not going to numerically determine these resonances, we just expand $A_n = g\tilde{A}_n + \mathcal{O}(g^2)$ to examine the low lying resonances, which gives

$$\begin{aligned} g_{\rm rs}(k) &= -4\left|\frac{\tilde{A}_n \pm \sqrt{\tilde{A}_n^2 + Nkn^2\pi^2}}{k^2 N\pi}\right| \\ &\sim -4\sqrt{\frac{k}{nN}} - \mathcal{O}\left(\frac{\tilde{A}_n}{n^2 N}\right)\ , \end{aligned} \tag{6.63}$$

for the kth resonance. For simplicity, we assume all A_n to be negligible in what follows. This should always be possible in the limit of $x_0 \gg 1$, as the interaction time tends to zero. Letting $n = N/2-1$, $k=1$, we obtain the

resonant condition for mixing to the singlet plus $N-1$ atom bound-state configuration, which is achieved for the weakest interaction strength of $g \sim -4/\sqrt{(N^2/2-N)}$. Full population transfer to this state would give $\Delta N_R^2 = N^2/4-N+1$, which has the same leading order term as NOON state, making it potentially interesting for interferometry. Additionally, because this state is the most energetically favoured, all the others are non resonant (in fact likely close to anti-resonant) and should only accumulate small population. The reduction in the magnitude of the rescaled interaction strengths may make this more experimentally favourable, we discuss this in Sec. 6.7.

Another interesting result comes if we consider the $k=1$, $n=1$, resonance at $g \sim -4N^{-1/2}$. In this case there is resonant mixing to *all* possible states (the $n=m$ state is at the $k=m$th resonance). This could prove an interesting result if it is visible above mixing to states with 3 or more clusters (the state with two free atoms and one $N-2$ atom bound state is for example allowed for $N>2$) and the mixing between the different cluster states does not cancel everything out.

6.6.4 Amplitude bound to oscillations

One can look at each left/right number eigenstate [Eq. (6.16)] separately, assuming that we have a probability of p for $|2,2\rangle$, and of $(1-p)/2$ for $|3,1\rangle$ (with the same for the $|1,3\rangle$ state), no occupation of $|4,0\rangle$ or $|0,4\rangle$, and that there is no overlap between the states and no mixing via the Hamiltonian. We can then state the energy $E_{1,3} = \langle 1,3|\hat{H}|1,3\rangle$ as

$$E_{1,3} = E_{\text{pot},1} + E_{\text{pot},3} + E_{\text{kin},1} + E_{\text{kin},3} + E_{\text{int},3} \,. \tag{6.64}$$

Each term in this equation refers to the kinetic, potential and interaction energy of each side, with one or three atoms, respectively (note that there is no interaction energy for the single atom side, taken without loss of generality as being left). Noting that the kinetic and potential energy terms must be positive, we can derive the inequality

$$E_{\text{pot},1} \leq E_{1,3} - (E_{\text{kin},3} + E_{\text{int},3}) \,. \tag{6.65}$$

Using the conservation of $E = \langle \hat{H} \rangle$ and $\Delta E^2 = \langle \hat{H}^2 \rangle - E^2$, it can be shown that (see Appendix D.3)

$$|E_{3,1} - E| \leq \sqrt{\frac{p}{1-p}} \Delta E \,, \tag{6.66}$$

which is equivalent to

$$E - \sqrt{\frac{p}{1-p}} \Delta E \leq E_{3,1} \leq E + \sqrt{\frac{p}{1-p}} \Delta E \,. \tag{6.67}$$

Combining the upper bound of the above equation with Eq. (6.65), we obtain

$$E_{\text{pot},1} \leq \left(E + \sqrt{\frac{p}{1-p}} \Delta E \right) - (E_{\text{kin},3} + E_{\text{int},3}) \,. \tag{6.68}$$

Finally, noting that $E_{\text{pot},1} = \langle x^2 \rangle_1 / 2 \geq \langle x \rangle_1^2 / 2$, with $\langle \hat{O} \rangle_1$ meaning the expectation value of the 1 particle side of the wavefunction, we can obtain an inequality for the 1 atom position expectation value

$$\langle x \rangle_1 \leq \sqrt{2} \sqrt{\left(E + \sqrt{\frac{p}{1-p}} \Delta E \right) - E_{\text{int},3}} \,. \tag{6.69}$$

We can see that larger, positive g will constrain this bound, up to a point of saturation at the Tonks-gas limit, whereas potentially it is unbounded as $g \to -\infty$ (energies in this regime scale proportional to $-g^2$ [162]) as the atoms gain a large amount of energy.

6.7 Possible experimental realisation of the four atom system

6.7.1 Optical lattice scheme

Our results could be tested by creating an optical super-lattice [163], of two overlapping lattices, with one double the frequency of the other, then loading this with two atoms per site (in the ground state) in a Mott insulator regime [164]. This is shown schematically in Fig. 6.2. The interactions could

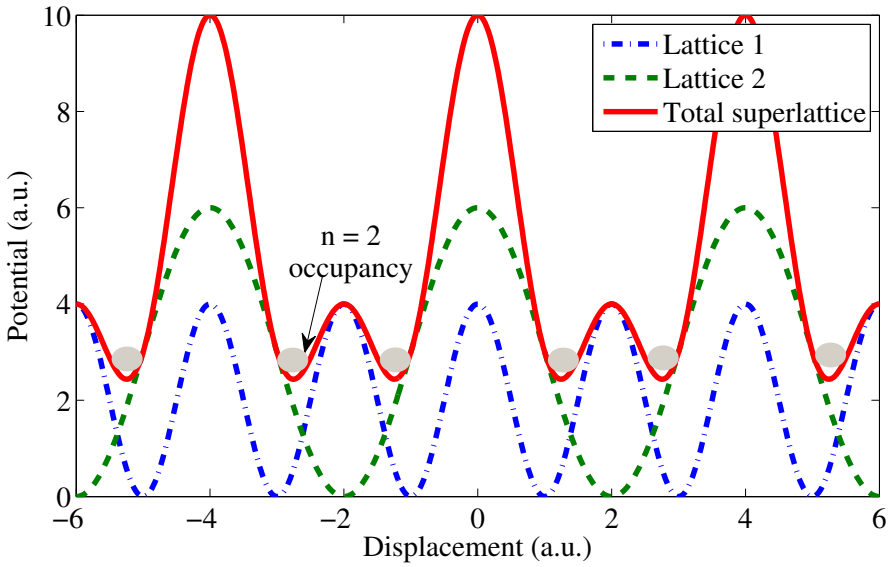

Figure 6.2: Schematic potential from an optical super-lattice created by overlapping two lattices (all units are arbitrary). Grey circles represent a loading of two atoms (or $N/2$) in the ground state of each well. Our suggested scheme tunes the interactions to the desired value and then turns off the double frequency (dotted line) lattice leaving only the broader lattice (dot-dashed line), after which the atomic dimers collide.

then be tuned to be attractive via a magnetic Feshbach resonance, at such a rate that tunnelling between sites is small, but the two atoms on each site tend to the ground state given by Eq. (6.7). The double-frequency lattice could then be ramped down, leaving only the wider lattice, thus creating the initial conditions of two equally separated dimers in an approximately harmonic potential.

Some freedom with x_0 could be achieved by modifying the relative strength of the double-frequency lattice compared with the primary lattice. Reducing it will push the minima closer together, but also make tunnelling between the sites more significant. Careful ramping-down schemes of the laser power of the double-frequency lattice could also be incorporated, which would give further freedom to move the sites closer together after creating the dimers. Slower ramping will also make things closer to adiabatic, thus reducing the excitation in each dimer created by the switch-off. The relative velocity between the two dimers in terms of the final harmonic oscillator units will

equate to an effective initial separation: approximately the separation the dimers will reach after the first collision. A faster (slower) ramping scheme would give a larger (smaller) effective x_0; however, to be most applicable to the results of this paper, a slow scheme would be ideal to minimize excitations and minimize the degree of anharmonicity in the potential that the dimers sample.

After some free-evolution time, the double frequency lattice could then be quickly restored with an extremely high lattice depth, separating the left and right components of the wavefunction, with no further tunnelling possible. This would allow for a direct measurement of $\hat{N}_R$ as defined in Eq. (6.9), by then imaging the lattice with resonant light; light-induced collisions [165] will reduce this to a parity measurement with an empty site being either a zero or two population, and a single atom being a one or three population. This is actually sufficient information, assuming we know the total atom number in the two sites was exactly 4. In terms of the states given in Eq. (6.16): no atoms on either site is a measurement of a $|2,2\rangle$ configuration (or a $|4,0\rangle$ and $|0,4\rangle$ configuration, but this is only significant during collisions), both sites occupied is a measurement of a $|3,1\rangle$ and $|1,3\rangle$ configuration. A measurement yielding a single occupied site and an empty site would imply some inelastic process has occurred (such as three-body recombination or background gas collisions) and such a result would thus be null.

If the effective x_0 were an appreciable fraction of the lattice width, this scheme could also show some more interesting physics beyond the scope of this paper, with collisions coupling energy into the centre-of-mass mode and the tunnelling of the single atom in the single-trimer states (considered in Sec. 6.6) to adjacent lattice sites. It could even have a kinetic energy greater than the maximum barrier height between sites and join an effective conduction band [166], allowing for entanglement between lattice sites. These effects may also be worthy of experimental investigation.

6.7.2 Experimental parameters

In terms of typical experimental parameters, the s-wave scattering lengths would need to be very substantial in order to give measurable effects. Strong

interactions generally require tuning scattering lengths near to Feshbach resonances, and in such strongly interacting regimes confinement effects can shift the effective 1D scattering length if $a_s/a_\perp$ is not small [46]. The chosen Feshbach resonance would ideally be broad, minimizing uncertainty in the effective interaction associated with a lack of precise control of magnetic field fluctuations.

Alternatively, some atoms such as caesium can have large background scattering lengths far from resonances [83], e.g., $a_s \sim \pm 3000 a_0$ where $a_0 \approx 5.3\times10^{-11}$ m is the Bohr radius. In terms of a rescaled g parameter in harmonic oscillator units, if we take $\omega_x \sim 2\pi \times 1$Hz and very strong radial confinement $\omega_\perp \sim 2\pi \times 0.4$kHz, we have

$$g = 2\omega_\perp a_s \sqrt{\frac{m}{\hbar\omega_x}} \sim \pm 1.2 \,, \tag{6.70}$$

which is of unitary order. This would be sufficient to access the resonances in Eq. (6.63) for $N \gtrapprox 8$ atoms, but not quite sufficient for the ones we observe numerically for $N = 4$ in Sec. 6.10.

We essentially have three experimentally tunable parameters, a_s, ω_x and $\omega_\perp$ which can be varied smoothly with small adjustments to a magnetic field or modifying laser powers, focusing, or detunings. However, dropping ω_x is undesirable as it increases experimental timescales, and increases the likelihood of loss events [c.f. Sec. 2.5.2]. Increasing the scattering length also increases the rate of unwanted three-body recombination effects, meaning one would need to determine an appropriate compromise.

6.8 Numerical method

6.8.1 Basis set expansion

To perform many-body computations we expand the field operator over the set of Hermite functions scaled by W as before

$$\varphi_k(Wx) = \sqrt{\frac{W}{k! 2^k \pi^{1/2}}} H_k(Wx) \exp\left(-W^2 x^2/2\right) \,, \tag{6.71}$$

with $H_k(x)$ the Hermite polynomials, and diagonalize the Hamiltonian in a Fock state basis $|n_0, \ldots, n_\infty\rangle$, truncated via the condition $\sum_k k n_k \leq \eta$ and projected to the zero centre-of-mass excitation subspace [c.f. Sec. 4.2.6]. For the graphs in this chapter we only use the eigenstate width $W = 1$, as the harmonic oscillator length is always a relevant scale. A compromise by taking a narrower functions ($W > 1$) proved to have other numerical issues.

6.8.2 Convergence testing

We first need to represent our initial condition in terms of this basis set, noting that due to the truncation the state cannot be represented exactly, with larger initial displacements and larger coupling magnitudes g harder to represent in this basis. We require a reasonable fidelity of our numerical initial condition to the true state, achieving fidelities of greater than 99.5% for all the numerics used in [2], but are as low as 95% for $g \sim -5$.

Measuring convergence during time evolution with such a method is more difficult. Performing the calculations with a variety of basis sizes and calculating the fidelity over time can give an indication for how long the calculations are reliable, for which we plot, in Fig. 6.3, our most extreme values of g. This is probably the strictest measure of convergence applicable, given the large number of degrees of freedom in a many body wavefunction, for example a product state with a large number of atoms would have a fidelity exponentially tending to zero for any finite difference in the product wavefunction.

6.9 Numerical results outside of the strongly attractive regime

6.9.1 Preamble

All the results graphed here are calculated for $N = 4$ and $x_0 = 3$ in order to investigate the effects of varying the strength of interaction (by varying the coupling parameter g) for small numbers. In general smaller x_0 greatly increases interaction times between clusters and thus rates of atom transfer.

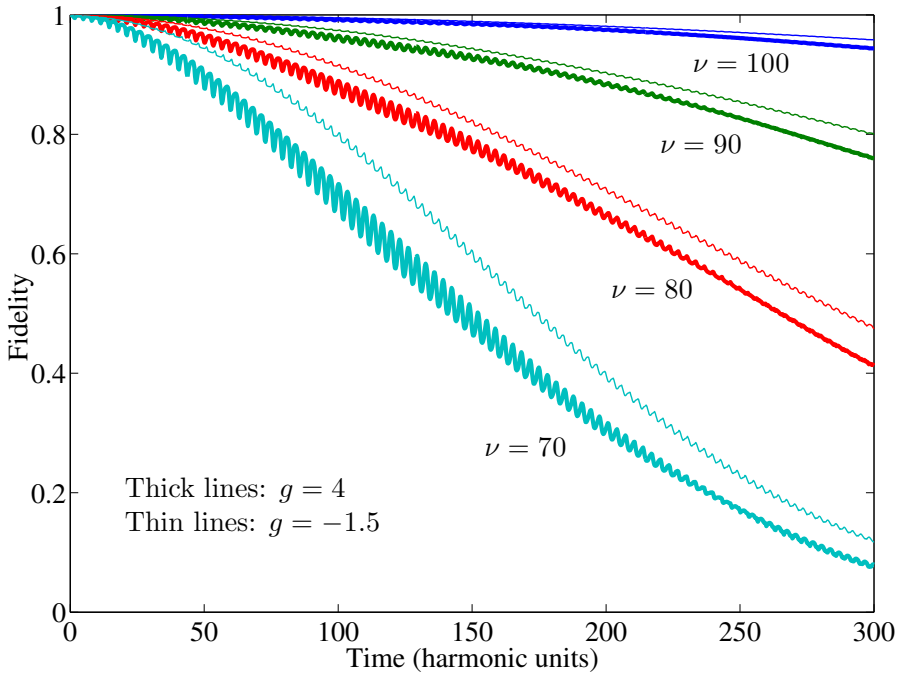

Figure 6.3: Plots of $|\langle\psi(\nu,t)|\psi(\nu_{\max},t)\rangle|^2$, the fidelity of the wavefunction computed with smaller basis (energy cut off at ν) to the wavefunction computed using a larger basis truncated at $\nu_{\max} = 113$. We have displayed results for the extreme values of g (in harmonic oscillator units) employed in the numerics that are trusted. For lower absolute values of g, the fidelity converges more rapidly with increasing ν.

It also reduces the amount of free energy in the system, however a greater amount of the wavefunction will be found towards the centre at all times and thus expectation values of $\hat{N}_R$ will be harder to interpret. The results here are broken down into three sections. The first examines the variation in left right number, the second examines the variance in position about one side and the final section examines the single body von Neumann entropy.

6.9.2 Left and right particle number dynamics

Because our initial condition has a definite number of two atoms either side of the trap, the left/right number uncertainty, ΔN_R, in our system is initially very near zero. We note that a mean-field-like state or a symmetric superposition of 3 and 1 atoms either side both give $\Delta N_R = 1$, which is also

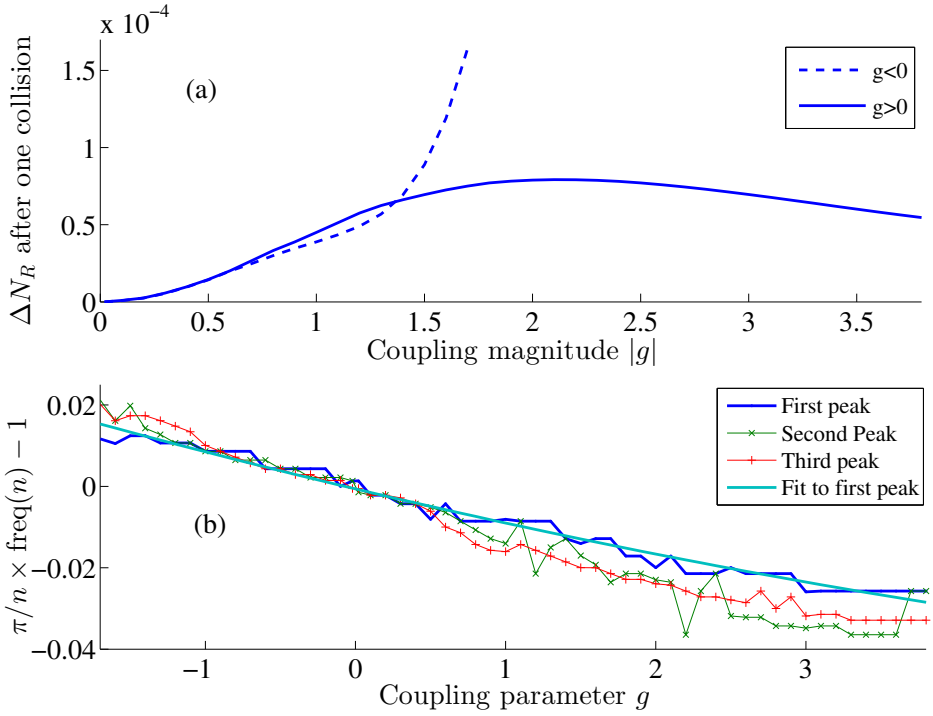

Figure 6.4: (a) Minimum value taken by ΔN_R [Eq. (D.6)], after one collision. (b) Frequency difference (in harmonic units ω) of peaks in the Fourier transform of ΔN_R from the non-interacting values ($t = n\pi$) divided by n. (a) shows that for $g > 0$, the increase to number uncertainty is greatest for $g \approx 2.3$ and decreases when interaction strength is increased further. The $g < 0$ behaviour is initially similar but deviates at around $|g| = 0.6$; rather than saturating it appears to increase even more rapidly with $|g|$. It is not clear what will happen for $g < 0$ and $|g| \gg 1$, which will be a topic for further investigation. (b) Existence of pseudo-periodicity in the system (in addition to low frequency components relating to the long time behaviour). The non-interacting system has frequency peaks at $f_n = n/\pi$, the quadratic fit (solid line) indicates these peaks shift by an amount roughly equal to $-ng/100\pi$.

the value this quantity will take in our non-interacting system when each of the clusters collide. We therefore first consider the minimum to minimum values taken by ΔN_R before and after each collision. This minimum value is taken as a non biased estimate for the maximum entanglement while left and right states are well separated. The change after the first collision is given in Fig. 6.4 and the change over the first 150 collisions is plotted in Fig. 6.5. Despite the fact that the increase after the first collision is similar for both attractive and repulsive interactions of similar magnitude, the long

time change is very different, with the timescales being much longer in the attractive case.

In either case, the left-right number does not reach an equilibrium on the timescales considered, with oscillations and revivals present. The time-dependent perturbation theory of Section 6.6 indicates that atom transfer processes are suppressed by an internal energy difference between the $|2,2\rangle$ and $|3,1\rangle$ configurations of the wavefunction, which leads to destructive mixing over a few collisions, unless a phase matching condition occurs. If intra-cluster excited states (discussed in Section 6.4.2) are present, the energy difference between each configuration, ΔE_{rel}, may be small (along with Ag) meaning cancellation occurs on longer timescales, leading to fluctuations in ΔN_R over 10s of harmonic oscillator periods.

Figures 6.6 and 6.7 (a) show the amplitude of each number component in the wavefunction as it evolves in time for $g = 3$ and $g = -1.7$; note Fig. 6.5 takes only the minimum values of these curves to avoid the spikes on collisions. The maximum amplitude of the $|3,1\rangle$ and $|4,0\rangle$ components (at least initially) occurs on collisions (corresponding to a minimum amplitude of $|2,2\rangle$). Decreasing of this peak amplitude may be interpreted as the time of collisions between clusters becoming less well defined, due to the distance between their centres of mass becoming less well-defined (i.e., its corresponding probability density becomes broader) and the forming of intra-cluster excitations.

At late times ($t > 100$) on figure 6.7, all the expectation values for $n \neq 2$ are almost the same as those for Gaussians centred on zero. This is due to only the two-dimer (attractive $n = 2$ ground states) setup being significant, as the exciting of intra-cluster excitations is suppressed by the large energy gap, and atom transfer interactions are suppressed by an energy difference, leading to a phase mismatch and hence a cancellation. However, energy is still transferred to the relative position wavefunction (described in Section 6.4.2), increasing the uncertainty in the separation of dimers, and so some component of the wavefunction is always undergoing a collision yielding a finite value for the left-right number uncertainty. As a result of our scaling in Eq. (6.13), the $n \neq 2$ values are just those of the dimer system in collision, and only a small contribution to $|3,1\rangle$ comes from states that are similar to a superposition of a cluster of 3 atoms to the left (right) and a free atom to

the right (left).

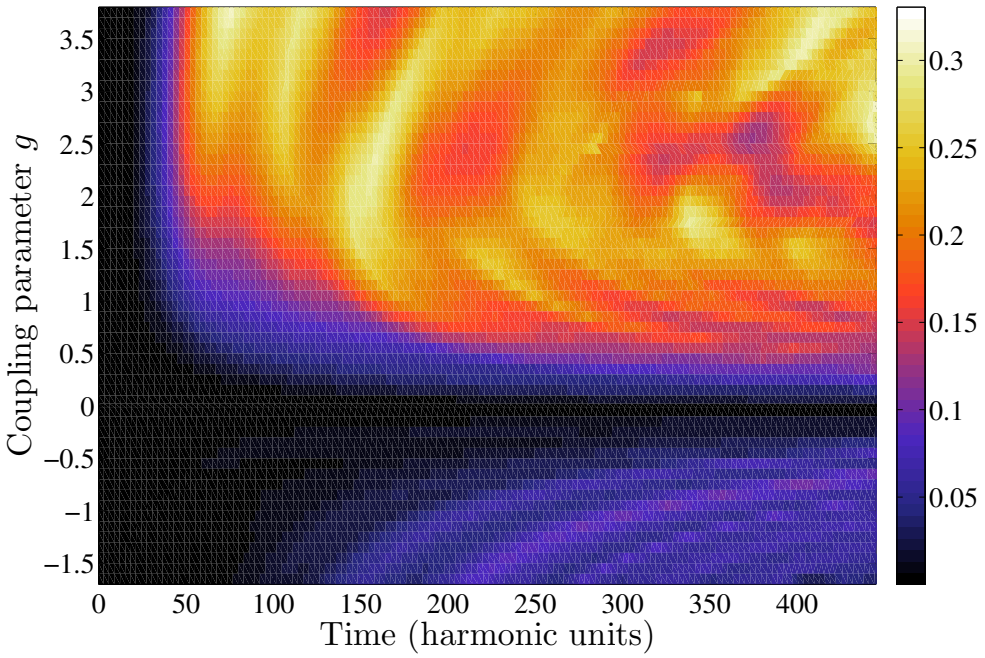

Figure 6.5: Minimum value obtained by ΔN_R, as given by Eq. (D.6), after a given collision. For weak interactions ($|g| < 0.1$) the behaviour is the same for attractive and repulsive, but for slightly larger values of g there is a clear difference in the timescales (measured in harmonic units ω^{-1}), with repulsive interactions producing larger number uncertainties more quickly, despite the fact that Fig. 6.4 shows there is little difference in ΔN_R after one collision. This difference is likely due to the increased (decreased) energy spacing between the ground and first excited state of the two atom system with attractive (repulsive) interactions, discussed in Section 6.4.2, and the energy difference between the two-two and three-one number configurations, as discussed in Section 6.6, which leads to a phase mismatch. For large repulsive values ($g > 2$), ΔN_R reaches a maximum value and then undergoes complex partial revivals on timescales of 30 time units (tens of collisions).

6.9.3 Equilibration of energy into inter/intra-cluster excited states

We wish to quantify the amount of energy transferred from the centre-of-mass energy of each cluster to excitations between the atoms, as discussed in Section 6.4.2 and Section 6.4.2. We therefore study $\sigma_{n,N-n}(t)$, the standard

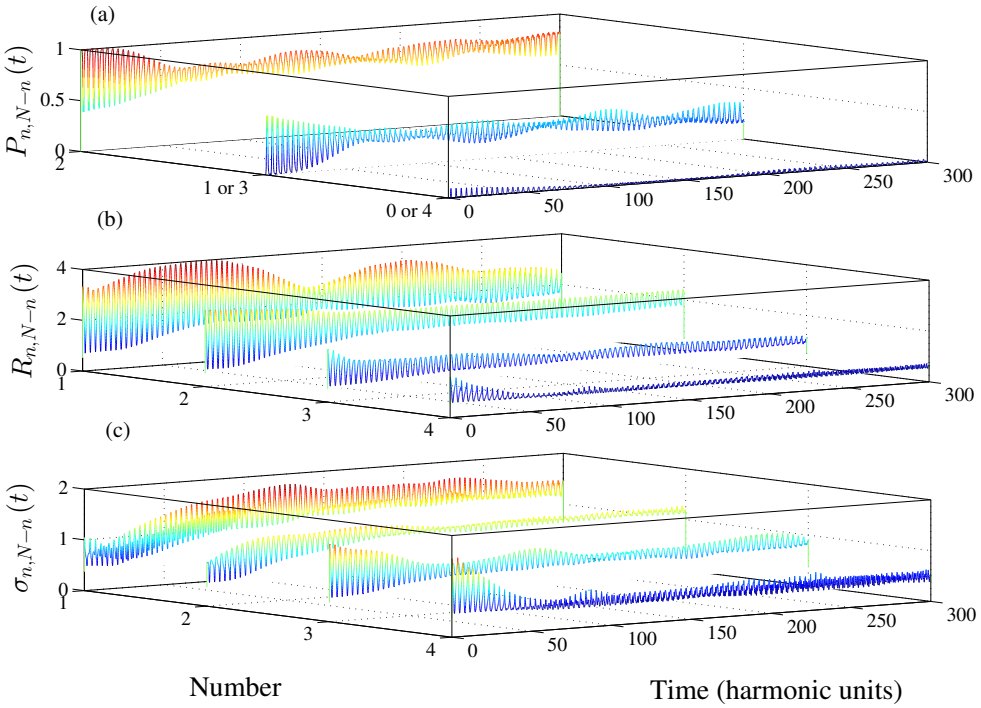

Figure 6.6: For $g = 3$, $x_0 = 3$, (a) Probability of finding n (or $N - n$) atoms to the right with the amplitudes of wavefunction components decomposed into eigenfunctions of number L/R number operator, defined in Eq. (6.14) . (b) Expectation value of position to the right on sections of wavefunction decomposed into eigenfunctions of L/R number operator, defined in Eq. (6.18)]. (c) Variance in position to the right as defined in Eq. (6.19), paralleling (b). The expectation value to the right [(b)] effectively tracks the particle-like motion, but after long times the motion appears effectively damped. (c) can quantify this effect — the peaks of $\sigma_{n,N-n}$ increase from their initial value and continue to oscillate about a maximum, except for $\sigma_{4,0}$ (which is only significantly probable during collisions) indicating a transfer of energy to the degrees of freedom described in Sections 6.4.2 and 6.4.2. This remains true even at very long times $t \sim 1000$, with progressively smaller partial revivals and so can be said to have equilibrated.

deviation in the position to the right, for a given number of atoms to the right, as defined in Eq. (6.19). This is essentially the width of the atomic density distribution on the right hand side, about the expected value for position, given that n atoms are on the right-hand side [defined in Eq. (6.18)].

These are plotted in Fig. 6.6 (c). The repulsive case shows a consistent increase in the height of the peaks (excepting the $n = 4$ peak), with only

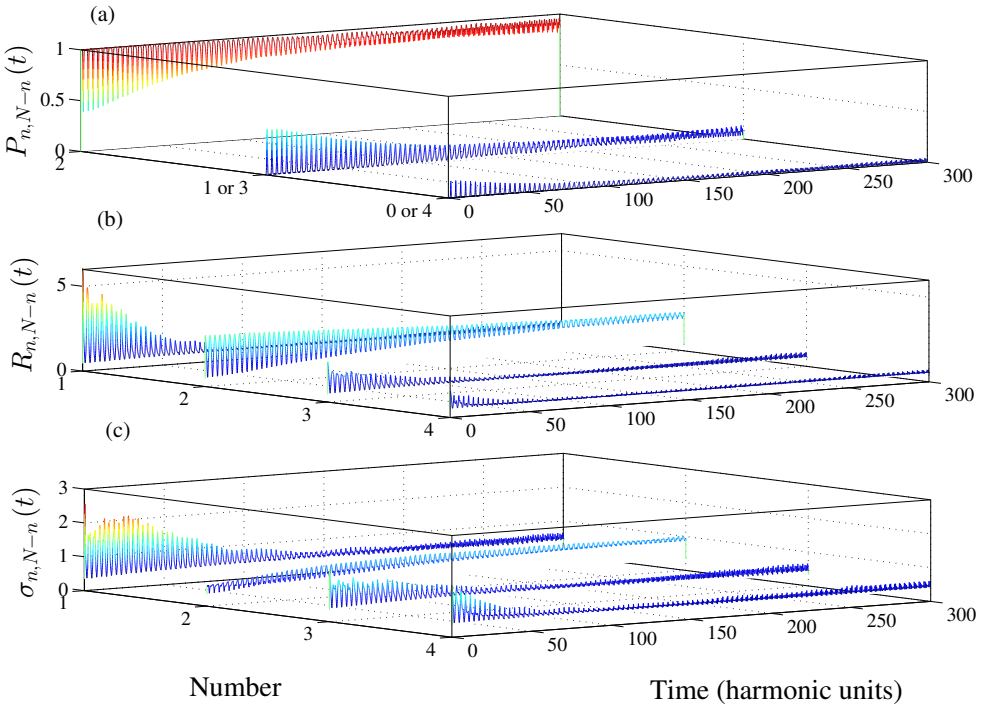

Figure 6.7: The same quantities as Fig. 6.6 but with $g = -1.7$. The short-term behaviour of the expected one-atom position (b) is similar to the repulsive case, but is increased in magnitude. At long times, the right-position expectation values drop to an approximately constant value for all but $n = 2$, this being the value of a Gaussian state in the centre of the trap, for reasons explained in section 6.9.2. This is also the case in (c) — essentially the only significant contribution to the $n \neq 2$ states comes from uncertainty in the separation of the atomic dimers, which smooths over transfer effects.

small periodic oscillations. The attractive case however shows $\sigma_{n,N-n}(t)$ to be initially similar but then dropping to a minimum value for $n \neq 2$. We note $\sigma_{n,N-n}(t)$ cuts off anything on the left side, and so is difficult to relate to the amount of excitation if the left and right states are separated by a distance smaller than the size of their internal structure, as they will contribute to all the $n \neq 2$ expectation values. Intra-cluster excitations as we have defined them are present if the wavefunction either side of the centre does not look like a displaced n-atom ground state; it is possible such excitations could reduce the position uncertainty but they are generally expected to make it broader and thus increase $\sigma_{n,N-n}(t)$. These excitations are dominant processes in the increasing of σ for the repulsive case plotted in Fig. 6.6 (c), and appear to

persist at long times.

For the $g < 0$ case, at very early times, say $t < 20$, the contribution to $\sigma_{3,1}(t)$ from states in the single particle and cluster-of-3 configuration is visible. By momentum conservation, the single atom must have considerably more energy after a collision than the 3-atom state, which explains the large $n = 1$ position expectation values away from collision. However, in the strongly attractive case this transfer process is cyclic, and it never transfers large populations to these configurations. As we noted before, contributions can come from an oscillating dimer state if the relative separation is small. Initially this only occurs during collision, but inter-cluster excitations (which can be interpreted as an increased uncertainty in how much the centres of each cluster have shifted due to interactions), lead to an increase in relative position uncertainty (although Fig. 6.5 indicates this process undergoes partial revivals). Hence, at late times there is always significant wavefunction density in the trap centre, that is to say at any time $t > t_{\text{late}}$ some non-negligible part of the wavefunction is always undergoing collision. Hence, if the contribution from the singlet-triplet state is too small to see we can conclude that the $\sigma_{2,2}(t)$ reaching a maximum corresponds to this mode reaching a steady configuration. This is the dominant effect in the attractive case shown in Fig. 6.7, but is also present for $g > 0$.

6.9.4 Relaxation to equilibrium

One questions of interest is whether the system reaches an equilibrium at long times. We attempt to quantify this by looking at the single body density matrix and its von Neumann entropy, given by Eq. (6.21); however, this quantity (like most in our system) has a time-dependence due to the repeated collisions that are a consequence of the system as a whole being held within a harmonic confining potential. In order to simplify our analysis we look at the time averaged value over a period of $T = 2\pi$ and quantify the degree of short-time change via the variance of this average. These are plotted in Fig. 6.8 (a) For both positive and negative g, S_{vN} increase towards a maximum value, with small amplitude oscillations in a similar way to ΔN but with much smaller variations. For fixed $|g|$, the $g > 0$ entropy generally

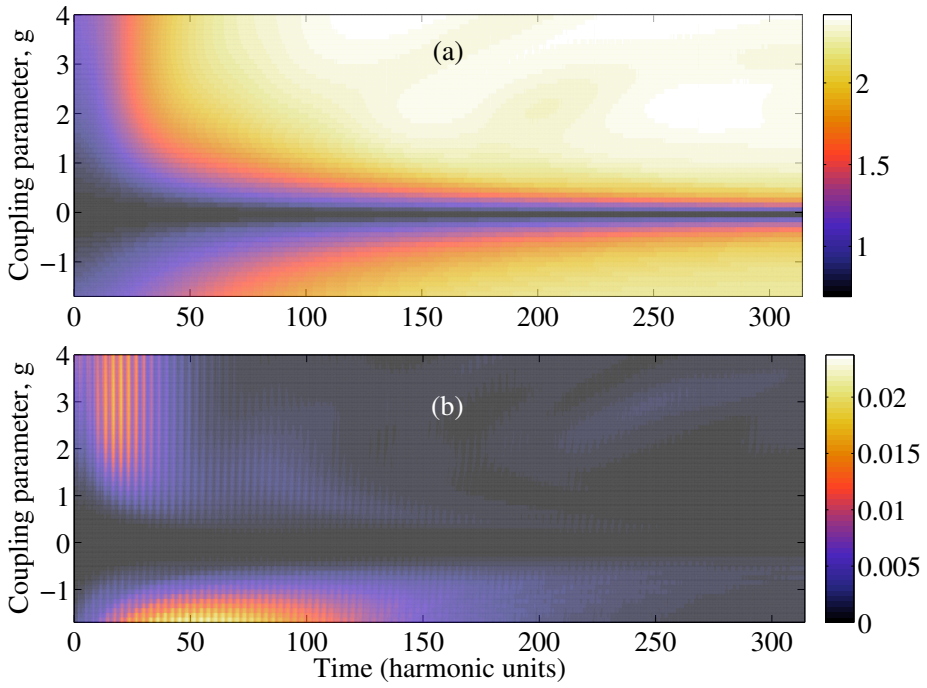

Figure 6.8: For $x_0 = 3$, (a) time evolution (measured in units of ω^{-1}) of the von Neumann entropy (averaged over a time period of 2π), as defined by Eq. (6.21) and Eq. (6.22), (b) time evolution of the standard deviation of this quantity, given by the square-root of Eq. (6.23), for a range of interaction strengths both repulsive and attractive. Entropy increases gradually at early times $t < 10\pi$, then increases at a more rapid rate before levelling off to an almost constant value with small fluctuations. This behaviour is similar for both attractive and repulsive interactions. The variance over the 2π averaging range behaves very differently for strong attractive and repulsive interactions, with the short-timescale fluctuations persisting for much longer if $g < 0$. This difference is explained by a change in the dominant processes, with the attractive system being unable to excite the relative degrees of freedom in a cluster and thus transfer of atoms between each cluster becoming more significant. Fig. 6.6 (b) shows atom transfer dynamics in the repulsive case have only small fluctuations at late times.

increases slightly faster and to higher values than the equivalent $g < 0$ case, but is otherwise quite similar. Fig. 6.8 b) shows the standard deviation over the 2π averaging period, the rapidly changing (time scales of less than 2π) effects continue for much longer in the attractive case compared to the repulsive. Transfer effects (discussed in Sec. 6.4.2) are likely the cause of this short time oscillation as they are predicted to be cyclic on the timescale of a few collisions when $g \approx 1$. The variation dying down at long times can be

explained for the $g > 0$ case by intra-cluster exited states breaking the cyclic effect, and for $g < 0$, by the broadening of the inter-cluster wavefunction to the point where the collision time is not well defined.

6.10 Preliminary numerical results for the strongly attractive regime

6.10.1 Preamble

This section focuses on numerical results obtained via the exact diagonalisation routine for $g \lesssim -1.7$. These results are inherently qualitative as they push the code to a regime in which it is unable to accurately determine energies or construct the soliton wavefunctions. This breakdown is a result of the separation of length scales between the internal structure of the bound states and the size of the harmonic confinement. Rescaling the basis improves convergence to a small extent, but is inevitably a compromise and is not sufficient with the basis size currently available.

Our numerics do confirm the presence of the transfer resonances predicted in Sec. 6.6.3, but at values of g which are not in quantitative agreement. There is also little certainty about the rates at which this occurs. The numerically calculated total energies are generally lower than analytical values (which are accurate in this regime) in this parameter range by the order of a harmonic oscillator unit (more for larger $|g|$). Adding more states improves energy convergence, but the number of states becomes infeasibly large. Convergence is very difficult to assess using the overlap method due to the fact that the behaviour changes dramatically near the resonances, which depend on internal energy differences, and thus shift in position as more states are added. Despite this we still expect qualitative agreement with the real system, at least for smaller $|g|$. We focus again on the $x_0 = 3$ case, but note the effects of varying x_0 for the initial rate of number transfer are not as predicted.

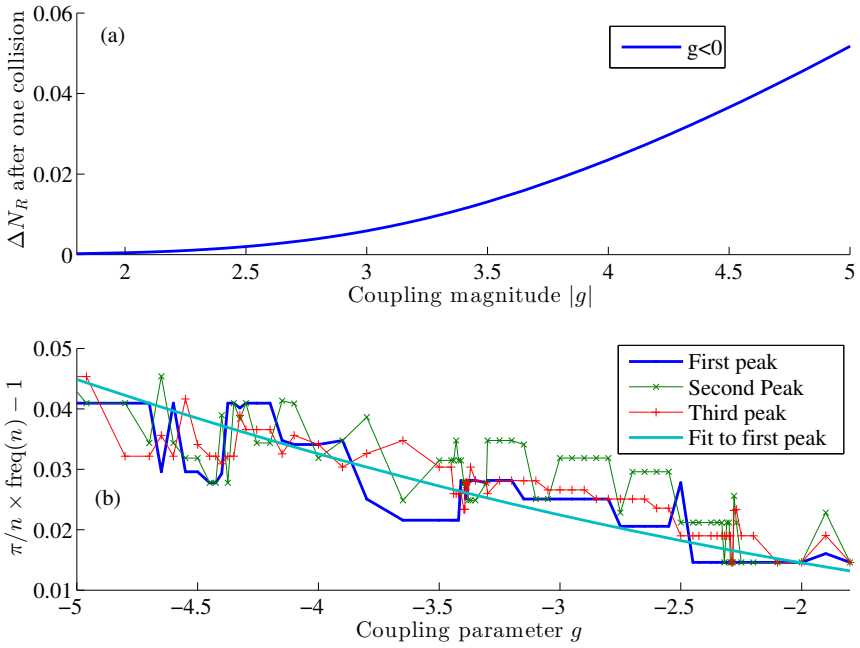

Figure 6.9: (a) Minimum value taken by ΔN_R [Eq. (D.6)], after one collision. (b) Frequency difference (in harmonic units ω) of peaks in the Fourier transform of ΔN_R from the non-interacting values ($t = n\pi$) divided by n. Figure (a) shows the continuing quadratic increase to the transfer rate with increasing coupling magnitude. Figure (b) shows considerably more "noise" than was seen in Fig. 6.4, but has a similar gradient on the linear fit to the shift in the first peak, indicating the pseudo period shift is still roughly linear with g.

6.10.2 Left and right particle number dynamics

As before ΔN_R is initially very near zero. However, strong attractive interactions significantly increase the rate of the exchange processes, which appear to scale proportional to $(g - g_0)^2$ in this regime. This can be seen on Fig. 6.9. We note this rate may be unreliable for large $|g|$ as the numerics cannot be said to have converged in this regime. However, the dependence on the transfer rate for small negative g depends heavily x_0, as we show in Fig. 6.10. If $x_0 \lesssim 2.5$ the transfer rate reaches a local maximum. The large $|g|$ behaviour is qualitatively similar for all x_0, with higher x_0 values giving a larger initial transfer over the range considered. This slightly counter intuitive behaviour appears to result from matching a rapidly increasing behaviour at small $|g|$,

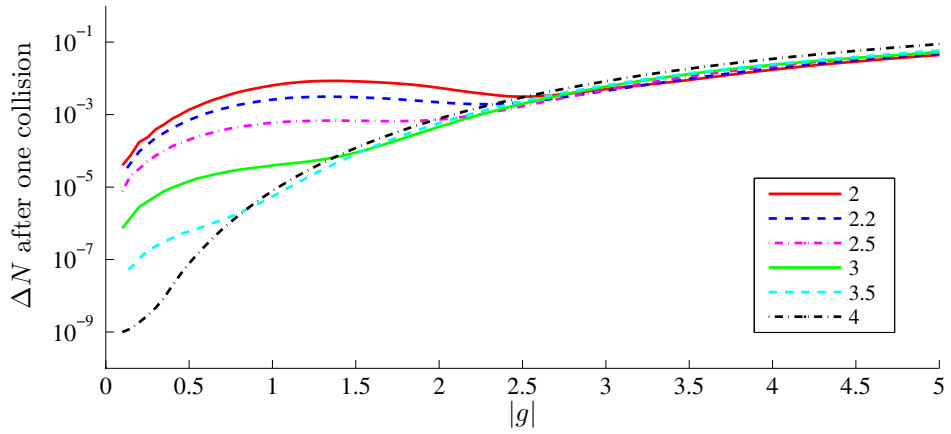

Figure 6.10: Minimum value taken by ΔN_R [Eq. (D.6)], after one collision (log scale) for a range of initial separations x_0 (given by the legend) and negative g. Smaller x_0 give much larger transfers for low $|g|$, but the behaviour is reversed at high $|g|$.

with a linear proportionality with $|g|$ and a quadratic dependence at large negative g.

By far the most significant result to note is the existence of transfer resonances for particular values of $g \sim -2.3, -3.4, -4.3, -5.2$. The minimum value of ΔN_R after each collision is shown in fig. 6.11. Again at late times it is difficult to determine when collisions occur do to a general increase in relative position uncertainty and an additional desynchronising effect (a different pseudo period for the $\{2, 2\}$ and $\{3, 1\}$ configurations). This measure is useful to see the widths of the resonances on (a), noting that the larger values of $|g|$ are less reliable. Fig. 6.11(b) shows the same measure at the centre of the resonances.

Near the resonances there is little destructive interference and the population cycles on extremely long timescales. This leads to high amplitude low frequency peaks in the Fourier transform, which are shown in Fig. 6.12 and could also be used to identify the resonances. We wish to examine the behaviour of the right side displacement and variance near to a resonance. The right-side number and displacement expectation values and position variance for the second resonance ($g = -3.39$) are plotted in Fig. 6.13. It should be noted that the initial large values with number $\neq 2$ of (b) and (c) are due to

numerical noise from dividing two small numbers as there is essentially no probability of a $\{3, 1\}$ number configuration.

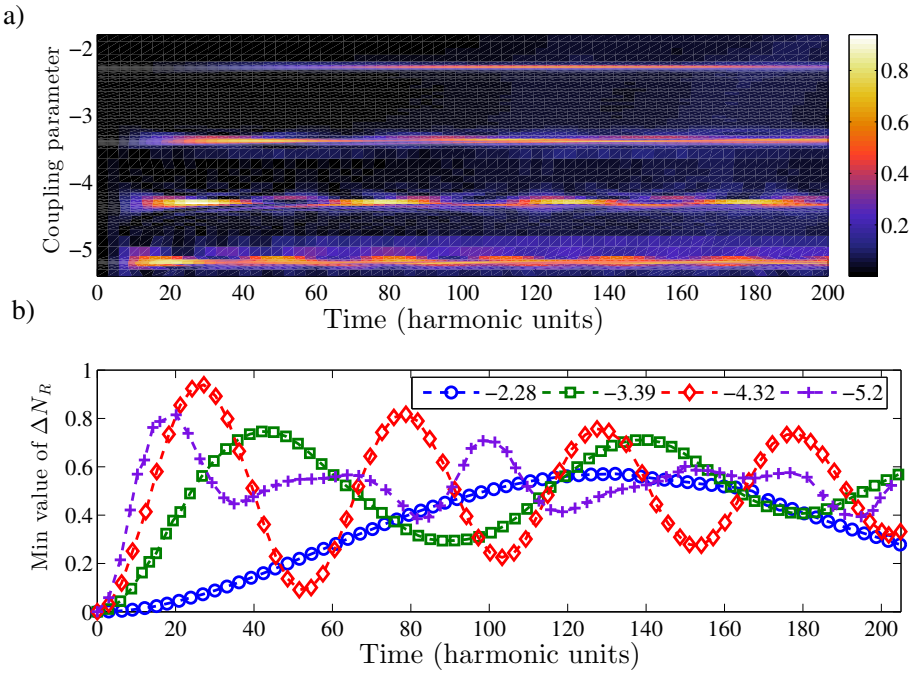

Figure 6.11: (a) Minimum value taken by ΔN_R [Eq. (D.6)] for a range of g, (b) Minimum value near the resonances. (a) Is the same quantity as Fig. 6.5, but values of g at the centre of each resonance. From (a) we can see the widths of the resonances appears to increase with $|g|$, (b) Shows ΔN_R for the first four resonances, the numerics become increasingly unreliable for large $|g|$.

Examining Fig. 6.13 (b) we see that the line corresponding to the single particle does follow a simple harmonic type path away from the origin. The maximum amplitude is 5.9 where as [Eq. (6.38)] predicts an amplitude of 5.6, in reasonable agreement given the assumptions made in the model and limited numerical convergence of the state energies.[3] Again the effect of relative displacement uncertainty "washing out" the expectation values does occur, and has partial revivals, but the effect is not strong enough to mast the effects of the $\{3, 1\}$ state. The position variances shown in (c) do all generally increase to a maximum with only small fluctuations in both the short and long term, showing a degree of equilibration, even at long times.

[3]The total energy for these parameters is around 1 harmonic energy unit great than would analytically be predicted.

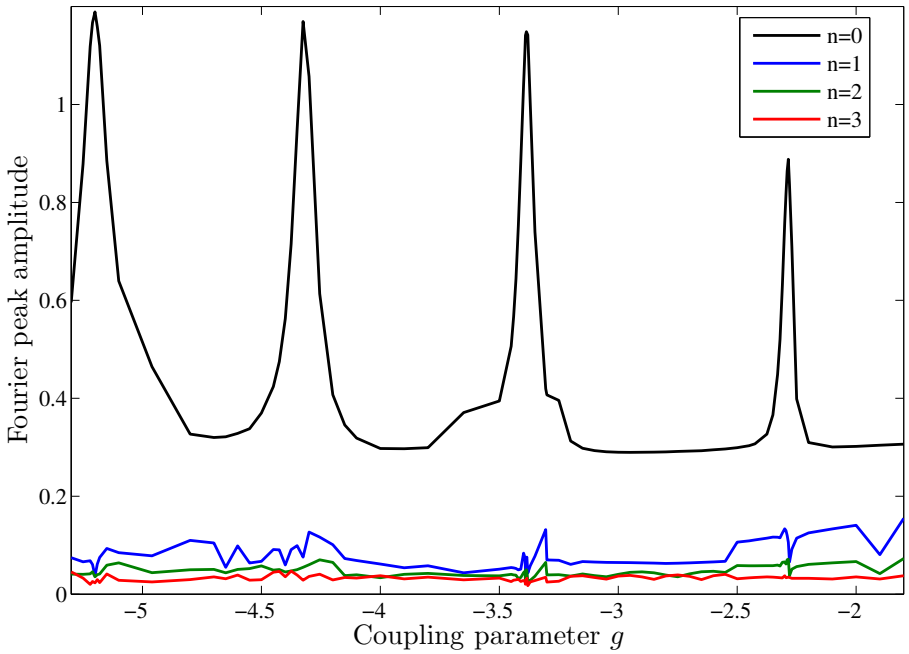

Figure 6.12: Height of the peaks in the Fourier transform of ΔN_R nearest to the integer values (peaks for the non-interacting system). Near the resonance there is a spike in the amplitude of the low frequency peak, due to the the resonant population transfer, which cycles over long timescales, beyond the scope of our time-dependent perturbation theory. A low frequency component is always present, even at $g = 0$ where it has zero frequency.

6.10.3 Position of the transfer resonances

In Sec. 6.6.3 we derived analytic estimates for the values of g at which the transfer resonances were expected to occur. We need first to calculate the correction to the period $\delta = T_{\text{pseudo}} - \pi$. Denoting the quantity plotted on Fig. 6.9 (a) by $\tilde{\delta} \approx -g/100$, these terms are related via $\delta = -\tilde{\delta}\pi/(1+\tilde{\delta})$ and can be calculated from the approximate fit. By numerically solving Eq. (6.59) for $x_0 = 3$ we estimate the first four resonances to be at

$$g_{\text{rs}} \sim -2.4,\ -3.2,\ -3.9,\ -4.4\ . \tag{6.72}$$

At first the numerics agree without our prediction, with the first resonance observed at $g = -2.28$, however the higher predicted values agree progressively less and less well with the observed positions, being found at

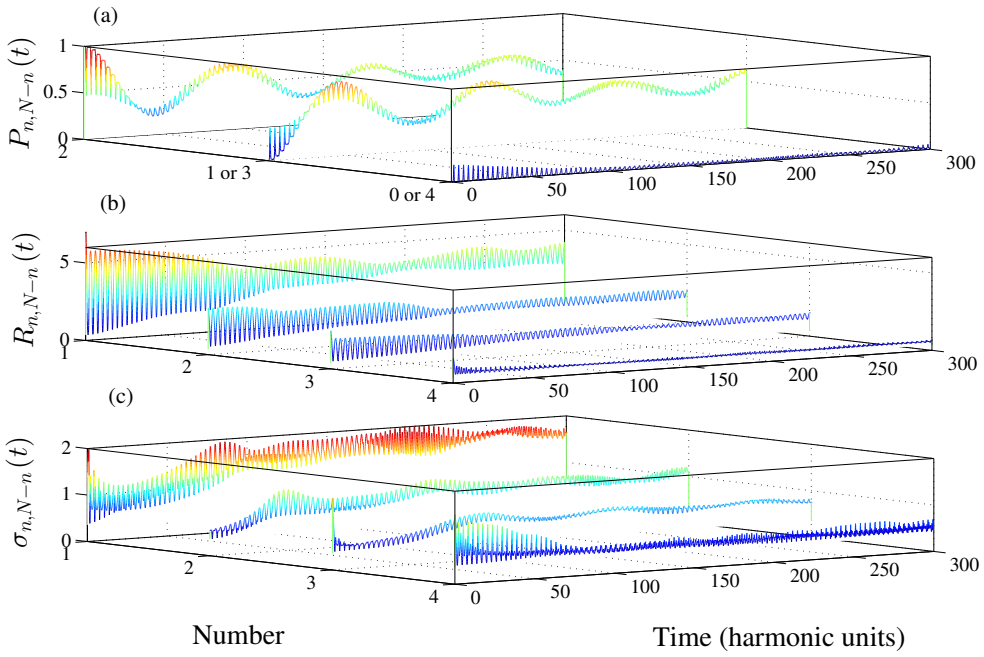

Figure 6.13: The same quantities as Fig. 6.6 but with $g = -3.39$, at the second transfer resonance. (a) Probability of finding n (or $N - n$) atoms to the right, (b) Expectation values of position to the right on left/right number eigenstates. (c) Variance in position to the right as defined in Eq. (6.19). The reduction is the height of the peaks in (a) indicates greater uncertainty in the relative displacement as before, but unlike the non-resonant attractive case in Fig. 6.7 the population of the trimer-singlet state is large enough that these expectation values are not totally lost by the normalisation, just reduced slightly. The maximum displacement of the one atom state appear to be around 5.9, the coherent state oscillation model [Eq. (6.38)] predicts a maximum amplitude of 5.6, however this lies well within the bounds set by Eq. (6.42) of $X_1 < 7.3$.

$g \sim -3.4, -4.3, -5.2$. The reason for this is almost certainly that the finite basis set used means that $(E_{2,2} - E_{3,1})$ is inaccurate. We expect the numerically calculated energy difference to be lower,[4] than the analytic estimates. This has the effect of shifting the resonances to higher values and our numerical results are qualitative rather than quantitative. We note that neither the analytic nor numerical resonance position values shift significantly as x_0 is varied.

There are also the issues of the impact of confinement, which should make

[4]While both $E_{2,2}$ and $E_{3,1}$ will be overestimated in the numerics, it is possible the difference could be larger if $E_{2,2}$ is overestimated much more than $E_{3,1}$.

the solitons narrower for a given g,[5] and therefore modify phase shift from collisions. Additionally there is a distribution of momenta which has not been accounted for, we have simply used the mean value. Finally the back-reaction of the terms proportional to $c_{3,1}$ in Eq. (6.48) could shift the resonances by an amount of the order of the width of the resonance. However, none of these effects are expected to be significant enough to account for the discrepancy at large g.

6.11 Conclusions

We have considered a system of $N = 4$ atoms with contact interactions, confined within in a harmonic potential. Our initial condition was a symmetric setup of two $N/2$ atom ground states, displaced from one another by a distance x_0 (taken to be 3 harmonic oscillator lengths for most of the numerics), which we then left to oscillate and undergo collisions. Initially there is no entanglement between the atoms on the left and on the right, however interactions lead to the generation of entanglement.

We investigated left/right number variation within the system, based on an operator which could in principle be measured directly in the experimental setup we suggest in Sec. 6.7. Initially both (left and right) states have a near-definite number of two atoms and hence a relative number uncertainty ΔN_{R}, which is initially close to zero. When the left and right states are well separated, ΔN_{R} is a measure of entanglement between the left and right sides. However when the two states are close, i.e., during collisions, $\Delta N_{\mathrm{R}} \sim N/4 = 1$; we therefore investigated the difference from minimum-to-minimum value taken over a time range of around π, i.e., the minimum value of ΔN_{R} obtained after the nth collision. There is a marked difference in the evolution of ΔN_{R} between the $g < 0$ (attractive) and $g > 0$ (repulsive) cases. When $|g| \gtrsim 0.5$, number uncertainty builds up much more slowly with attractive interactions than with repulsive, essentially resisting entanglement. This is despite a large increase to the change in number uncertainty that is generated by a single collision. This increases quadratically with $|g|$ when

[5] Using Eq. (5.40) gives a width rescaling $\lambda_0 \approx 1.09$ for $g = -2.2$ and $N = 2$.

$g \lesssim -1.3$, but in the repulsive case the increase reaches a maximum, and then drops as g increases further. Additionally for $g > 0$ we observe long-timescale high-amplitude number fluctuations, which continue even at late times (over 100 collisions).

This behaviour is explained by our time dependent perturbation theory on the atom transfer process, and the energy difference between the intra-cluster excited states. We investigated the effect of ΔE_{int}, the energy difference in intra-cluster energies between the $\{2, 2\}$ (two displaced $N = 2$ ground states) and $\{3, 1\}$ (one free atom and one $N = 3$ atom ground state) configurations. Assuming the average interaction energy between the clusters to be weak (i.e. $|Ag| \ll 1$), increases to $|\Delta E_{\text{int}}|$ lead to a phase mismatch and thus to destructive interference so that the population transfer cycles periodically, unless a resonance condition was met (only possible for $g < 0$). If intra-cluster excited states are present, this picture breaks down, since each of these excited states phase-evolves at a different rate; cancellation becomes more complicated and the states less localized, which occurs for large $g > 0$ at long times. The energy gap between the ground and excited states of each of the $N/2$ atom clusters is increased (decreased) when g gets smaller (larger, so long as $g < 2.2$), which reduces the maximum population that can be transferred to excited states. The excited states become effectively inaccessible as $g \ll 0$, resulting in an effectively two-level system of the $\{2, 2\}$ and $\{3, 1\}$ configurations. Our perturbation theory indicates that for sufficiently strong attractive interactions, with very specific values, phase matching would be possible, allowing for resonant transfer. Preliminary numerical results appear to confirm the existence of such resonances, but due to numerical limitations we were unable to use a sufficient basis size for the numerics to converge and the position and transfer rate in the resonances is not expected to be quantitatively correct.

By separating the system into components of the wavefunction with definite number (number states of the number-to-the-right operator) we have observed the evolution of the positions associated with one/two/three atom number states, and the right side position variance. For $g = 3$ the peaks in position variance increase to a maximum for all $N_R = n$ in around 100 time units ($100/2\pi$ oscillator periods or around 30 collisions) and do not fluctuate

greatly. Considering instead the case where $g = -1.7$, after 60 collisions, we find that for $N_R \neq 2$ position and position uncertainty are the same as they are for a state undergoing collision, whereas the $N_R = 2$ tends to a maximum. This indicates that the state is well described by two atomic dimers with a significant uncertainty in their relative displacement and almost no amplitude of a singlet-trimer like state is present in the wavefunction; this motion again undergoes partial revivals on very long timescales. Near a resonance value of $g = -3.39$ the single particle position is far more visible and appears to follow a path similar to that predicted by the coherent state oscillation model [Sec. 6.5], but relative displacement uncertainty still reduces the values at late times.

In addition, we have investigated the von Neumann entropy of the single-body-density matrix $S_{\mathrm{vN}}(t)$, in order to investigate to what degree the system tends to an equilibrium. We note $S_{\mathrm{vN}}(t)$ is zero for a product state (all atoms with the same wavefunction/occupying the same mode) and can be considered a measure of how mean-field-like the state is. Additionally $S_{\mathrm{vN}}(t)$ is constant for our system if $g = 0$, despite the wavefunction evolving periodically in time. At long times with repulsive interactions, S_{vN} (time averaged over a period of 2π) increases to a steady value with only small fluctuations over the averaging period. However, long-term fluctuations (over the order of twenty π time units) are still present and appear to be due to atom transfer processes which do not appear to equilibrate on the timescales considered in this paper. The time required to reach maximum entropy decreases with larger g but this appears to saturate with little change for $g \gtrsim 2$; for an initial separation of $x_0 = 3$ this takes around 30 collisions. This short-term increase appears to be due to the inter-cluster degrees of freedom discussed in the previous paragraph; the associated probability density with the separation of the two clusters becomes less peaked. With very weak attractive interactions, the system's behaviour is similar to the repulsive case, however for $|g| \gtrapprox 0.5$ higher intra-cluster excited states become less accessible, leading effectively to a reduction in the number of accessible degrees of freedom, such that the left/right states behave more like solitons. In this case, the time average of $S_{\mathrm{vN}}(t)$ does not tend to a long-term mean value as compared with the case of repulsive interactions of similar magnitude; there is also a

great deal more short-time variation, which persists for longer. The short-time variation can be attributed to the strong atom transfer effects, which are predicted to cycle population continually due to an energy difference. The effect eventually reduces as displacement uncertainty between the two bound states (which now behave like quantum solitons) increases, which is the mechanism behind the long term entropy increase.

A pseudo-periodicity effect is also present. The non-interacting system is periodic with a period π, and thus the Fourier transform of any time dependent expectation values will have frequency peaks at n/π. We have examined how these peaks shift for the left/right number uncertainty as interaction strength is varied and have found an approximately linear shift with g over the range considered. Changes to higher order components of the frequency spectrum deviate slightly from the linear dependence shown by the first order, with differences only clearly manifest for $g \gtrsim 1$).

Outlook

In this thesis we have outlined the mean-field and many-body models for describing Bose gases with both attractive and repulsive interactions in reduced dimension. We have investigated the regimes of agreement between both models for a harmonically confined ground state and also derived a variational many-body state which could be used to predict widths and energies in the case of very weak trapping. The possibility to calculate the overlap analytically between two states of different widths [Eq. (5.42)] allowed us to see what proportion of a many-body wavefunction is projected to the true ground state of the system after a rapid change to the scattering length. It would, in principle, be possible to calculate the overlap between eigenstates for different interaction strengths (assuming no harmonic trapping is present), and thus examine at a many-body level the state which this would produce. This is potentially interesting as it yields the possibility to create fragmented states [142], which could be interesting to confirm. Additionally we could consider a continuous change to the scattering length (or trapping potential) via the matrix elements $\langle\psi|\dot{\hat{H}}|\psi'\rangle$ with ψ and ψ' different many-body eigenstates.

We also investigated collisions between dimer states in harmonic confinement, which breaks the integrability present in the free case. We predicted and numerically observed resonance transfer from the dimer-dimer configuration to the singlet triplet configuration for certain interactions strengths. These resonances were observed in the numerics, but were shifted from where they were predicted due to what we suspect is badly converged numerics. Future work could be to either push our numerical method harder (more basis states etc), in order to achieve convergence, or ideally develop a new numerical method based on the Bethe ansatz, which should work even as $g \to -\infty$.

Additionally we would like to investigate systems with more than four atoms to see if this resonant transfer persists with more atoms, which we predict to be possible. With more than four atoms this system has the potential to evolve into a state with strongly squeezed relative number, with the $\{N-1,1\}$ configuration most likely. We note that this state is qualitatively similar to that considered in [167], and may therefore have uses in beyond shot-noise interferometry.

Finally it would be interesting to investigate the dynamics of initially coherent systems at a many body level. Eventually this could be related to systems with many quantum solitons (soliton trains) in harmonic confinement, to see if coherence persists for long times, and if complex entanglement builds within the system. This situation is of interest as these trains are often formed from collapsing BECs [14].

Part III

Appendices

Appendix A

Useful identities and integral results

A.1 Special functions

A.1.1 Exponential integrals and the Euler Gamma function

We have the useful result for an indefinite integral, valid for integer $n \geq 0$ and any constant k:

$$\int dx x^n e^{kx} = \frac{e^{kx}}{k^{n+1}} \sum_{j=0}^{n} k^j x^j (-1)^{n-j} \frac{n!}{j!} \,, \tag{A.1}$$

which can be proved via integration by parts. This result is used in the calculate of the first order energy correction to a soliton state in harmonic confinement in Sec. C.4. By setting $k = -1$ and taking the definite integral between 0 and ∞ we see that the component at infinity vanishes and the only component that remains at 0 is $n!$. This logic leads to the continuous extension of the factorial, known as the Euler Gamma function, defined for $\mathrm{Re}(z) > 0$ by [133]

$$\Gamma(z+1) = \int_0^\infty t^z \mathrm{e}^{-t} dt \,, \tag{A.2}$$

such that $\Gamma(n+1) = n!$ for n a positive integer. Values with $\mathrm{Re}(z) < 0$ are obtainable via the reflection formula

$$\Gamma(z+1/2)\Gamma(1/2-z) = \pi/\cos(\pi z)\ . \tag{A.3}$$

It is often referred to as the least special special-function due to the fact it is very difficult to avoid and appears in many calculations. Within this thesis it occurs in the implicit equation for the energy of two interacting particles in a harmonic oscillator [Eq. (5.20)] and [Eq. (5.48)].

A.1.2 Riemann Zeta function

The Riemann Zeta functions is defined for real $z > 1$ as [133]

$$\zeta(z) = \sum_{k=1}^{\infty} k^{-z}\ , \tag{A.4}$$

which can be analytically extended to all complex numbers via a functional equation. This is an important function as it occurs in many branches of BEC theory, appearing in functions of the critical temperature in BEC, and in the formula for the scattering amplitude of two particles in harmonic confinement [Eq.(2.43)] and the first order energy correction to classical solitons in a polynomial potential Eq. (C.28).

A.2 Identities involving Jacobi coordinates

A.2.1 First identity

We wish to show that the Jacobi coordinates defined by Eq. (5.3) satisfy

$$\sum_{k=1}^{N} x_k^2 = N x_{\mathrm{C}(N)}^2 + \sum_{k=2}^{N} \frac{k-1}{k}\xi_k^2\ , \tag{A.5}$$

and note the normalised coordinates also satisfy a similar identity. We prove (A.5) inductively. The $N = 2$ case can readily be verified, after which we

may consider the increase of number from $N-1$ to N. In particular,

$$\sum_{k=1}^{N} x_k^2 = x_N^2 + (N-1)x_{\mathrm{C}(N-1)}^2 + \sum_{k=2}^{N-1} \frac{k-1}{k}\xi_k^2. \tag{A.6}$$

Noting that $\xi_N = x_N - x_{\mathrm{C}(N-1)}$, we then deduce

$$\begin{aligned}\sum_{k=1}^{N} x_k^2 =& x_N^2 + (N-1)x_{\mathrm{C}(N-1)}^2 \\ &- \frac{N-1}{N}\left[x_N - x_{\mathrm{C}(N-1)}\right]^2 + \sum_{k=2}^{N} \frac{k-1}{k}\xi_k^2.\end{aligned} \tag{A.7}$$

Collecting terms, this reduces to

$$\begin{aligned}\sum_{k=1}^{N} x_k^2 =& \frac{1}{N}\left[x_N + (N-1)x_{\mathrm{C}(N-1)}\right]^2 + \sum_{k=2}^{N} \frac{k-1}{k}\xi_k^2 \\ =& N x_{\mathrm{C}(N)}^2 + \sum_{k=2}^{N} \frac{k-1}{k}\xi_k^2\,,\end{aligned} \tag{A.8}$$

which completes the proof. An equivalent result also holds in 3D [134].

A.2.2 Second identity

We rephrase Eq. (5.3) as $x_k = \xi_k + [1/(k-1)]\sum_{j=1}^{k-1} x_j$. Recursively substituting in equivalent expressions for $x_{k-1}, x_{k-2}, \ldots, x_{N/2+1}$ yields (for $N/2+1 < k \leq N$)

$$x_k = \xi_k + \sum_{j=N/2+1}^{k-1} \frac{\xi_j}{j} + \frac{1}{N/2}\sum_{j=1}^{N/2} x_j, \tag{A.9}$$

and for $k = N/2+1$ we have $x_{N/2+1} = \xi_{N/2+1} + (2/N)\sum_{j=1}^{N/2} x_j$. Hence, summing over all $k \in \{N/2+1, N/2+2, \ldots, N\}$,

$$\begin{aligned}\sum_{k=N/2+1}^{N} x_k &= \sum_{k=N/2+1}^{N} \xi_k + \sum_{k=N/2+2}^{N} \sum_{j=N/2+1}^{k-1} \frac{\xi_j}{j} + \sum_{k=1}^{N/2} x_k \\ &= \sum_{k=N/2+1}^{N} \xi_k + \sum_{k=N/2+1}^{N-1} \frac{N-k}{k}\xi_k + \sum_{k=1}^{N/2} x_k \\ &= \sum_{k=N/2+1}^{N} \frac{N}{k}\xi_k + \sum_{k=1}^{N/2} x_k \ ,\end{aligned} \tag{A.10}$$

from which we deduce the desired identity:

$$\sum_{k=N/2+1}^{N} x_k - \sum_{k=1}^{N/2} x_k = \sum_{k=N/2+1}^{N} \frac{N}{k}\xi_k. \tag{A.11}$$

A.3 Integral identities of Hermite and Laguerre polynomials

A.3.1 Definition

The Hermite polynomials and (generalised) Laguerre polynomials are defined by [168]

$$H_n(x) = (-1)^n e^{x^2} \frac{d^n}{dx^n} e^{-x^2} = e^{x^2/2} \left(x - \frac{d}{dx}\right)^n e^{-x^2/2} \ , \tag{A.12a}$$

$$L_n^{\alpha}(x) = \frac{x^{-\alpha} e^x}{n!} \frac{d^n}{dx^n} \left(e^{-x} x^{n+\alpha}\right) \ , \tag{A.12b}$$

the Hermite polynomials also have the generating function

$$\exp(2tx - t^2) = \sum_{n=0}^{\infty} \frac{t^n}{n!} \frac{d^n}{dt^n} \exp(2tx - t^2)|_{t=0} = \sum_{n=0}^{\infty} \frac{t^n}{n!} H_n(x) \ . \tag{A.13}$$

and orthogonality relation

$$\int_{-\infty}^{\infty} H_n(x) H_m(x) e^{-x^2} dx = \delta_{nm} n! 2^n \sqrt{\pi} \ . \tag{A.14}$$

A.3.2 Identities and recursion relations

The first notable property of the Hermite functions, is that in addition to being eigenfunctions to the Schrödinger equation, they are also Eigenfunctions to the continuous Fourier Transform, with unitary eigenvalues. This can be shown by Fourier transforming both sides of Eq. (A.13) and equating like powers of t, giving

$$\frac{1}{\sqrt{2\pi}}\int_{-\infty}^{\infty} dx \mathrm{e}^{ipx}\varphi_n(x) = (-i)^n\varphi_n(p) \; . \tag{A.15}$$

As a direct result of satisfying the Schrödinger equation with an energy $E_n = \hbar\omega(n+1/2)$, the Hermite functions satisfy the relation

$$\varphi_n''(x) + (2n+1-x^2)\varphi_n(x) = 0 \; , \tag{A.16}$$

(with a prime denoting differentiation with respect to the function argument) and from the ladder relation we have

$$\varphi_{n+1}(x) = \frac{1}{\sqrt{2(n+1)}}\left(x - \frac{d}{dx}\right)\phi_n(x) \; . \tag{A.17}$$

Combining these two equations we can derive the two useful recursion relations

$$\varphi_n'(x) = \sqrt{\frac{n}{2}}\varphi_{n-1}(x) - \sqrt{\frac{n+1}{2}}\varphi_{n+1}(x) \; , \tag{A.18}$$

as well as

$$x\varphi_n(x) = \sqrt{\frac{n}{2}}\varphi_{n-1}(x) + \sqrt{\frac{n+1}{2}}\varphi_{n+1}(x) \; , \tag{A.19}$$

which can be used to very efficiently tabulate the Hermite functions in the numerics.

A.3.3 Identities for width modifications

For some numerical calculations we will perform require the use of Hermite polynomials with a width that is not that of the eigenfunctions. For simplicity

we consider a single-body Hamiltonian in harmonic oscillator units

$$\hat{H}_{\text{single}} = -\frac{1}{2}\frac{\partial^2}{\partial x^2} + \frac{x^2}{2} \,, \tag{A.20}$$

and Hermite functions $\gamma^{1/2}\varphi_n(\gamma x)$ (the eigenstates rescaled by a factor γ) satisfy the equation via Eq. (A.16):

$$\frac{\partial^2}{\partial x^2}\gamma^{1/2}\varphi_n(\gamma x) = \gamma^2\gamma^{1/2}\varphi_n''(\gamma x) = \gamma^2(\gamma^2 x^2 - 2n - 1)\gamma^{1/2}\varphi_n(\gamma x) \,, \tag{A.21}$$

with the primes denoting differentiation with respect to the argument and therefore

$$\hat{H}_{\text{single}}\gamma^{1/2}\varphi_n(\gamma x) = \left(\frac{(\gamma x)^2}{2}(\gamma^{-2} - \gamma^2) + \gamma^2(n + 1/2)\right)\gamma^{1/2}\varphi_n(\gamma x) \,. \tag{A.22}$$

By Eq. (A.19) we have

$$\begin{aligned} x^2\varphi_n(x) &= x\sqrt{\frac{n}{2}}\varphi_{n-1}(x) + x\sqrt{\frac{n+1}{2}}\varphi_{n+1}(x) \\ &= \frac{1}{2}\left[\sqrt{n(n-1)}\varphi_{n-2}(x) + (2n+1)\varphi_n(x) + \sqrt{(n+1)(n+2)}\varphi_{n+2}(x)\right] \,, \end{aligned} \tag{A.23}$$

and so by the orthogonality properties the Hamiltonian only mixes $\varphi_n(\gamma x)$ into itself and the two states with $m = n \pm 2$. We can use this to express a many-body Hamiltonian in terms of creation and annihilation operators via $\hat{\Psi}(x) = \sum_k \gamma^{1/2}\varphi_k(\gamma x)\hat{a}_k$, leading to Eqs. (5.44) and (5.45).

A.3.4 Quadrature rules

Usually to numerically calculate any 1D integral, the process involves breaking up the integral into a sum of discrete points with different weightings, leading to an approximation (which can sometimes be exact) of the form:

$$\int_a^b f(x)dx \approx \sum_{k=1}^{n} w_k f(x_k) \,, \tag{A.24}$$

Here an n point rule is taken and w_k are the weights and x_k the points, or abiscuss. Quadrature rules are in general ways of choosing this abiscuss and related weights deterministically [168], where as Monte Carlo methods (used to obtain Fig. 5.4) choose them randomly. We consider two cases where $f(x) = p(x)W(x)$ with $p(x)$ a polynomial and either $W(x) = \exp(-x^2)$ with $[a, b] = [-\infty, \infty]$ (Gauss-Hermite Quadrature) or $W(x) = exp(-x)$ with $[a, b] = [0, \infty]$ (Gauss-Laguerre quadrature). In either case the n point quadrature rules takes x_k as the zeros of the nth Hermite (Laguerre) polynomial and

$$w_k = \begin{cases} \frac{2^{n-1}n!\sqrt{\pi}}{n^2[H_{n-1}(x_i)]^2} = \frac{e^{-x^2}}{n\phi_{n-1}(x_i)^2} & \text{Gauss-Hermite} \\ \frac{x_k}{(n+1)^2 L_{n+1}(x_k)} & \text{Gauss-Laguerre} \end{cases} \tag{A.25}$$

are the weights. This rule is exact if $p(x)$ if of order $2n - 1$ (n) or less for Gauss Hermite (Laguerre) quadrature.

Appendix B

Limiting cases of harmonically confined dimer state

B.1 Ground state energy for $H_{\mathbf{R}}(\xi_2)$ in the interaction dominated regime

Using the identity [169]

$$\frac{\Gamma(z+1/2)}{\Gamma(z)} = \sqrt{z}\left(1 - \frac{1}{8z} + \sum_{k=2}^{\infty}\frac{c_k}{z^k} + \cdots\right), \tag{B.1}$$

where the c_k are coefficients for the higher order terms in the asymptotic expansion, we see from Eq. (5.20) that

$$\sqrt{-\nu_0}\left[1 + \frac{1}{8\nu_0} + \sum_{k=2}^{\infty}\frac{c_k}{(-\nu_0)^k} + \cdots\right] = \frac{1}{2\sqrt{2\gamma}}. \tag{B.2}$$

Hence, taking the limit $\gamma \to 0$ (interaction dominated regime) implies $\nu_0 \to -\infty$, and we may truncate the asymptotic series. To lowest order $\sqrt{-\nu_0} \approx 1/2\sqrt{2\gamma}$, which we substitute into the right hand side of [rearranged from Eq. (B.2)]

$$\sqrt{-\nu_0} = \frac{1}{2\sqrt{2\gamma}} + \frac{1}{8\sqrt{-\nu_0}} + \mathcal{O}(\nu_0^{-3/2}), \tag{B.3}$$

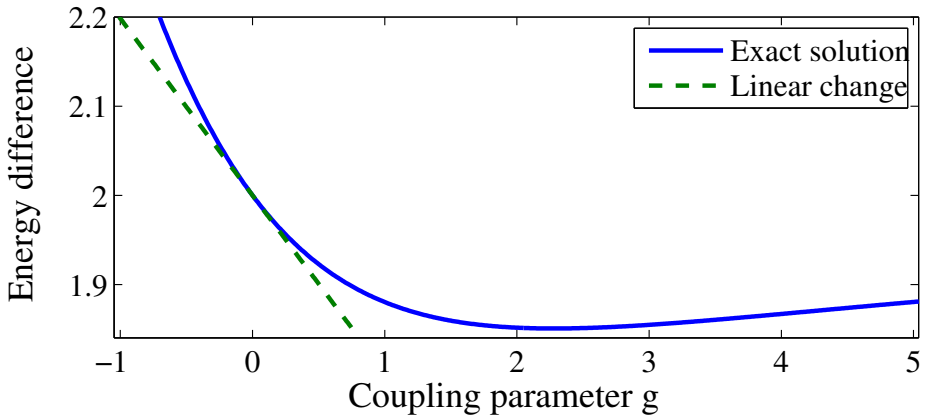

Figure B.1: The energy difference between the ground and first relative excited state, for two boson in harmonic confinement with contact interactions. Units are harmonic units, codified as $\hbar = \omega_x = m = 1$.

squaring the result to get

$$\nu_0 = -\frac{1}{\gamma}\left[\frac{1}{8} + \frac{\gamma}{4} + \mathcal{O}(\gamma^2)\right]. \tag{B.4}$$

Hence, substituting Eq. (B.4) into Eq. (5.21) for $n = 0$ yields

$$\lim_{\gamma\to 0} E_{\mathrm{R},0} = -\frac{1}{4} + \mathcal{O}(\gamma^2). \tag{B.5}$$

B.2 Energy difference between the ground and first exited state of the dimer state

In harmonic oscillator units, the eigenenergies of the dimer in harmonic confinement are set by

$$\frac{\Gamma(3/2 - E_n/2)}{1/4 - E_n/2} + \frac{g}{2\sqrt{2}} = 0\,. \tag{B.6}$$

It can be seen from the location of zeros in the gamma function, that the energy of the first excited state lies between 3/2 (as $g \to -\infty$) and 7/2 (as $g \to +\infty$). In fact the kth excited state of the $g \to -\infty$ system maps to the $k-1$th of the $g \to \infty$ with one less excitation quanta. By the bose-fermi mapping theory [116], the eigenstates are given by $\varphi_{2k-1}(|x|)$ [with $\varphi_k(x)$ a Hermite function] with $k \geq 1$ an integer and have energies $2k - 1/2$. Because

of the bosonic symmetry, the energy levels of the non-interacting system are spaced by units of 2. This must also be the case as $g \to \infty$ and hence a minimum must exist for finite positive g, which we see from Fig. B.1 is 1.85 for $g \approx 2.28$. For large negative g the difference increases proportionally to g^2 and rapidly because large.

Appendix C

Normalization, energy and overlap using the variational state

C.1 Preamble

In order to make use of our variational state given in Eq. (5.31), we must calculate the normalization constant and expectation value of energy. Calculations for the energy and normalization constants for all the eigenstates in free space ($\gamma = 0$) can readily be found in literature [118], it is also the case that the centre-of-mass component of the Hamiltonian can be considered separately and so taking a finite centre-of-mass component does not significantly alter the calculations. However, the choice of normalization condition for a non local system is somewhat arbitrary and conventions vary between papers, we choose a normalization that means both the relative and centre-of-mass parts are normalized to unity with respect to Jacobi coordinates. Also most derivations of the energy rely on the fact that the gradient discontinuity at the points $x_k = x_j$ in the wavefunction, exactly cancel the interaction terms (essentially from the condition of being an eigenstate), and thus these terms can simply be ignored. Because of our variation of λ, this will no longer be the case and thus we are forced to make a more explicit calculation of the kinetic energy. In addition to this we derive a first order energy correction to the relative degrees of freedom, for both the variational ansatz and Hartree product state.

C.2 Normalization

In order to normalize Eq. (5.16), we could insist that two states with different centre-of-mass momenta are orthonormal, i.e. $\langle p', N|p, N\rangle = \delta(p' - p)$ such as was calculated in [117] or consider wavefunction to be trapped in a box which we allow to grow infinitely large [127]. However we are interested in the normalization of the free space solution with a Gaussian centre-of-mass envelope and freedom to tune a variational parameter, denoted $\psi_{\rm var}^{(\lambda)}$ in Eq. (5.31). This result and technique will also be used in appendix C.4 and follows the method of [117]. We consider a Fourier decomposition of the wavefunction

$$\begin{aligned}\langle \vec{x}|\psi_{\rm var}^{(\lambda)}\rangle =& \mathcal{N}_\lambda \exp\left(-\sum_{k=2}^{N}\sum_{j=1}^{k-1}\frac{\sigma}{2}|x_k - x_j| - \frac{N\gamma}{2}\left[\sum_k \frac{x_k}{N}\right]^2\right)\\ =& \mathcal{N}_\lambda \int_{-\infty}^{\infty} dp\, \frac{\exp(-p^2/2\gamma)}{\sqrt{2\pi\gamma}}\\ &\times \exp\left(ip\sum_k \frac{x_k}{\sqrt{N}} - \frac{\sigma}{2}\sum_{k=2}^{N}\sum_{j=1}^{k-1}|x_k - x_j|\right)\,, \end{aligned} \tag{C.1}$$

with $\sigma = 1/(N-1)$ corresponding to Eq. (5.16), however for greater generality we allow this parameter to be free in order to use these results for variational calculations where $\sigma \to \lambda/(N-1)$, which would correspond to Eq. (5.31). Also one may wish to consider instead units in which the harmonic oscillator frequency and length are set to unity and the interaction constant rescaled to $\tilde{g}$, in which case the replacement $\sigma \to \lambda|\tilde{g}|$ would be used instead, or indeed in S.I. units $\sigma \to \lambda M|g_{1d}|/\hbar^2$. Essentially this term serves to allow easy conversion between unit systems and making variational manipulation easier.

In the form of Eq. (C.1), it is far simpler to perform the integrals of the coordinate variables. Calculating $\langle\psi_{\rm var}^{(\lambda)}|\psi_{\rm var}^{(\lambda)}\rangle$ in coordinate space will require integration over N spatial integrals and two momentum integrals, however we only need to integrate over the simplex region $x_1 \leq x_2 \ldots \leq x_N$ as by Bose symmetry any integration over any such region will be identical, hence we multiply by factor of $N!$ to include all possibilities for such a regions construction. Within this simplex region, all arguments in the absolute value

signs are positive and the wavefunction is given by

$$\langle \vec{x}|\psi_{\rm var}^{(\lambda)}\rangle = \mathcal{N}_\lambda \int_{-\infty}^{\infty} dp\, \frac{\exp(-p^2/2\gamma)}{\sqrt{2\pi\gamma}} \exp\left(\sum_k \frac{ipx_k}{\sqrt{N}} + \frac{\beta(k)x_k}{2}\right) , \qquad \text{(C.2)}$$

with $\beta(k) = (N+1-2k)\sigma$, and using the notation $\int_{-\infty\le x_1<x_2<\ldots<x_N\le\infty} \equiv \int_{-\infty}^{\infty} dx_N \ldots \int_{-\infty}^{x_3} dx_2 \int_{-\infty}^{x_2} dx_1$, we can now express the inner product as

$$\langle \psi_{\rm var}^{(\lambda)}|\psi_{\rm var}^{(\lambda)}\rangle = N!\mathcal{N}_\lambda^2 \iint_{-\infty}^{\infty} dp_1 dp_2\, \frac{\exp(-(p_1^2+p_2^2)/2\gamma)}{2\pi\gamma} \int_{-\infty\le x_1<\ldots<x_N\le\infty} \exp\left(\sum_k \frac{i(p_1-p_2)x_k}{\sqrt{N}} + \beta(k)x_k\right) , \qquad \text{(C.3)}$$

transformation of variables $p = (p_1+p_2)/2$ and $p' = p_1 - p_2$ with Jacobian unity then allows us to perform the integral over p leaving

$$\langle \psi_{\rm var}^{(\lambda)}|\psi_{\rm var}^{(\lambda)}\rangle = N!\mathcal{N}_\lambda^2 \int_{-\infty}^{\infty} dp'\, \frac{\exp(-p'^2/4\gamma)}{2\sqrt{\pi\gamma}} \int_{-\infty\le x_1<\cdots<x_N\le\infty} \exp\left(\sum_k ip'x_k/\sqrt{N} + \beta(k)x_k\right) . \qquad \text{(C.4)}$$

To perform the remaining integrals we note that $\int_{-\infty}^{y} dx \exp(ax+by) = \exp[(a+b)y]/a$, denoting

$$a(k) = \sum_{l=1}^{k} \beta(l) = \sigma k(N-k) , \qquad \text{(C.5)}$$

and noting $a(N) = 0$, we can recursively use the previous result to perform all but one of the spatial integrals and obtain

$$\langle \psi_{\rm var}^{(\lambda)}|\psi_{\rm var}^{(\lambda)}\rangle = N!\mathcal{N}_\lambda^2 \int_{-\infty}^{\infty} dp'\, \frac{\exp(-p'^2/4\gamma)A(N,p')}{2\sqrt{\pi\gamma}} \int dx_N \exp\left(ip'x_N\sqrt{N}\right) , \qquad \text{(C.6)}$$

with

$$A(\ell,p') = \prod_{k=1}^{\ell-1} \left[a(k) + \frac{ip'k}{\sqrt{N}}\right]^{-1} . \qquad \text{(C.7)}$$

Integrating the final term gives $2\pi\delta(p'\sqrt{N})$ and the momentum integral is

then trivial, noting that $A(N,0) = 1/(N-1)!^2\sigma^{(N-1)}$ gives us the final result for the normalization factor

$$\mathcal{N}_\lambda = \sqrt{\sqrt{\frac{\gamma}{N\pi}}(N-1)!\sigma^{(N-1)}}\,. \tag{C.8}$$

As was mentioned before, the normalization factor for Eq. (5.31) in our units is obtained by letting $\sigma = \lambda/(N-1)$, in the case of $\lambda = 1$ where this relates the ground state in infinitesimal trapping Eq. (5.16), we refer to this constant simply as $\mathcal{N}$. It is also worth noting that both the centre-of-mass wavefunction and the relative are both chosen to be normalized to unity with respect to Jacobi coordinates, hence the $(\gamma/N\pi)^{1/4}$ relates to the centre-of-mass part and the rest to the relative component.

C.3 Kinetic and interaction energy

We wish calculate the kinetic energy and potential energy of the variational state, i.e. the expectation of Eq. (5.10) with λ set to zero on Eq. (5.31), which we will denote $\hat{\mathrm{H}}_{\mathrm{free}}$. Due to the separability of the wavefunction and Hamiltonian, it is sufficient to consider only the relative part of the wavefunction and note that the centre-of-mass kinetic energy is given by $\gamma/4$. We first denote $\varphi(x_1,..,x_N) = \exp\left(-\sigma\sum_{k=2}^{N}\sum_{j=1}^{k-1}|x_k - x_j|/2\right)$, being the relative part of the variational wavefunction (up to a normalization factor) and calculate the second derivative with respect to some coordinate x_ℓ

$$\begin{aligned}
&-\frac{1}{2}\frac{\partial^2}{\partial x_\ell^2}\varphi(x_1,..,x_N)\\
=&\frac{\sigma}{4}\left[-\frac{\sigma}{2}\left(\sum_{k\neq\ell}\frac{\partial}{\partial x_\ell}|x_\ell - x_k|\right)^2 + \left(\sum_{k\neq\ell}\frac{\partial^2}{\partial x_\ell^2}|x_\ell - x_k|\right)\right]\\
&\times\varphi(x_1,..,x_N)\\
=&\frac{\sigma}{4}\left[-\frac{\sigma}{2}\left(\sum_{k\neq\ell}\mathrm{sgn}(x_\ell - x_k)\right)^2 + 2\left(\sum_{k\neq\ell}\delta(x_\ell - x_k)\right)\right]\\
&\times\varphi(x_1,..,x_N)\,.
\end{aligned} \tag{C.9}$$

The first term in Eq. (C.9) can be split up into terms of the form $\mathrm{sgn}^2(x_\ell - x_b) = 1$, of which there are $(N-1)$ and terms of the form $\mathrm{sgn}(x_\ell - x_a)\mathrm{sgn}(x_\ell - x_b)$ with $a \neq b$, of which there are $(N-1)(N-2)$. The former will evaluate to unity by normalization of the wavefunction, however the latter terms will equal $+1$ when $x_\ell < x_a < x_b$ or $x_\ell < x_b < x_a$ and when $x_a < x_b < x_\ell$ or $x_b < x_a < x_\ell$ and -1 when $x_a < x_\ell < x_b$ or $x_b < x_\ell < x_b$; the wavefunction must be identical in all these 6 simplicies due to Bose symmetry and so the expected value of these terms will equal $1/3$. When the sum over all ℓ is performed, these terms will total to $N(N-1)\sigma^2(1+(N-2)/3)/4$. The latter terms of the form $\delta(x_\ell - x_k)$ can then be combined with those from the interaction part of the Hamiltonian, noting that there are twice as many terms but $\delta(a-b) = \delta(b-a)$. Reinstating $\sigma = \lambda/(N-1)$ we have

$$\begin{aligned}
&\langle\psi_{\mathrm{var}}^{(\lambda)}| - \frac{1}{2}\sum_{k=1}^{N}\frac{\partial^2}{\partial x_k^2} - \frac{1}{N-1}\sum_{k=2}^{N}\sum_{j=1}^{k-1}\delta(x_k - x_j)\ |\psi_{\mathrm{var}}^{(\lambda)}\rangle \\
&= -\frac{\lambda^2 N}{8(N-1)}\left(1 + \frac{N-2}{3}\right)^2 + \frac{\gamma}{4} \\
&\quad + \frac{\lambda - 1}{N-1}\left[\langle\psi_{\mathrm{var}}^{(\lambda)}|\sum_{k=2}^{N}\sum_{j=1}^{k-1}\delta(x_k - x_j)\ |\psi_{\mathrm{var}}^{(\lambda)}\rangle\right] . \qquad \text{(C.10)}
\end{aligned}$$

all that remains now to calculate the value of the expectation value of the delta function terms. Following the method in Appendix C.2 we integrate over a simplex region $-\infty < x_1 < x_2 ... < x_N < \infty$, as a result of this we need only consider the $N-1$ terms of the form $\delta(x_k - x_{k+1})$ as the rest will be zero. Each integral will be the same as in Appendix C.2 except missing a factor of $2/a(k)$ for each term $\delta(x_k - x_{k+1})$, hence the result will equal $\sum_{k=1}^{N-1} a(k)/2$ (using the result $\int_{-\infty}^{y} dx f(x,y)\delta(x-y) = f(y,y)/2$). Hence

$$\begin{aligned}
\langle\psi_{\mathrm{var}}^{(\lambda)}|\sum_{k=2}^{N}\sum_{j=1}^{k-1}\delta(x_k - x_j)|\psi_{\mathrm{var}}^{(\lambda)}\rangle &= \frac{\sigma}{2}\sum_{k=1}^{N-1}k(N-k) \\
&= \frac{\lambda(N+1)N(N-1)}{12(N-1)} , \qquad \text{(C.11)}
\end{aligned}$$

finally, substituting in this result into Eq. (C.10) we have

$$\begin{aligned}
&\langle\psi_{\rm var}^{(\lambda)}| - \frac{1}{2}\sum_{k=1}^{N}\frac{\partial^2}{\partial x_k^2} - \frac{1}{N-1}\sum_{k=2}^{N}\sum_{j=1}^{k-1}\delta(x_k - x_j)|\psi_{\rm var}^{(\lambda)}\rangle \\
&= \frac{N(N+1)}{24(N-1)}[-\lambda^2 + 2\lambda(\lambda-1)] + \frac{\gamma}{4} \\
&= E_0(2\lambda - \lambda^2) + \frac{\gamma}{4}\,, \qquad \text{(C.12)}
\end{aligned}$$

where $E_0 = -N(N+1)/24(N-1)$. This discussion has not mentioned the harmonic envelope of the centre-of-mass function, however due to the separability of the Hamiltonian this will only add factor of the centre-of-mass kinetic energy, which will be independent of λ regardless of what the centre-of-mass wavefunction is. This energy term is combined with the potential energy calculation derived in Appendix C.4 to form the basis for a variational principle.

C.4 Derivation of the first-order perturbation energy

This section is related to the calculation of $\langle\psi_{\rm var}^{(\lambda)}|V(x)|\psi_{\rm var}^{(\lambda)}\rangle$, where $\hat{V}(x) = \gamma^2\sum_{k=1}^{N}x_k^2/2$, note that Eq. (5.27) is given by this quantity minus the centre-of-mass energy. It is again easier not to perform this integral in Jacobi co-ordinates but to Fourier transform out the centre-of-mass, we will also again replace the factor $1/(N-1)$ with σ to generalize the results for our variational principle. This calculation is similar to, although more complicated than, the calculation of the normalization factor; to that end we can start the calculation from Eq. (C.4) (as no spatial integrals are yet performed) adding

in the potential factor $V(x)$ giving

$$\langle\psi^{(\lambda)}_{\rm var}|V(x)|\psi^{(\lambda)}_{\rm var}\rangle = \frac{\sqrt{N}}{2\pi A(N,0)}\int_{-\infty}^{\infty} dp'\ \exp\left(\frac{-p'^2}{4\gamma}\right) \int_{-\infty\le x_1<x_2<\ldots<x_N\le\infty} \frac{\gamma^2}{2}\sum_k x_k^2 \times \exp\left(\sum_k ip'\frac{x_k}{\sqrt{N}} + \beta(k)x_k\right)\ . \tag{C.13}$$

The same recursive integral procedure can be applied here except we need two additional results, true for real$(k) > 0$

$$\int_{-\infty}^{y} dx\ x^n \exp(kx) = \begin{cases} \frac{1}{k}\exp(ky) & \text{if } n=0, \\ \frac{ky-1}{k^2}\exp(ky) & \text{if } n=1. \\ \frac{(ky)^2-2ky+2}{k^3}\exp(ky) & \text{if } n=2. \end{cases} \tag{C.14}$$

Let us consider only the latter part of Eq. (C.13) omitting the constant $\sqrt{N}\gamma^2/4\pi A(N,0)$, taking the integrals in order from x_1 to x_N, the integral over x_ℓ will be over a function of the form

$$I(\ell) = A(\ell,p')\left(k_0(\ell) + k_1(\ell)x_\ell + k_2(\ell)x_\ell^2 + \sum_{\ell'=\ell+1}^{N} x_{\ell'}^2\right) \times \exp\left(a(\ell)x_{\ell'} + \sum_{\ell'=\ell+1}^{N}\beta(\ell')x_{\ell'} + \frac{ip\ell x_\ell}{\sqrt{N}}\right)\ , \tag{C.15}$$

with $k_0(1) = k_1(1) = 0$ and $k_2(1) = 1$ and $A(\ell,p')$ defined in Eq. (C.7). The common prefactor of $A(\ell,p')$ is the equivalent of k from Eq. (C.14). Besides this, each integral will increase the factor in front of the x_ℓ^2 term by one each time and hence $k_2(l) = l$. Contributions to $k_1(\ell+1)$ come from $k_1(\ell)$ and $k_2(\ell)$ and as such Eq. (C.14) implies $k_1(\ell+1) = k_1(\ell) - 2k_2(\ell)(a(\ell) + ip\ell/\sqrt{N})^{-1}$, given that $k_1(1) = 0$ this implies

$$k_1(\ell+1) = -2\sum_{k=1}^{\ell}\frac{k}{a(k) + \frac{ikp'}{\sqrt{N}}} \tag{C.16}$$

$$k_1(N)|_{p'=0} = -\frac{2}{\sigma}\sum_{k=1}^{N-1}\frac{1}{k}\ . \tag{C.17}$$

Applying this same induction logic down to k_0 gives

$$\begin{aligned} k_0(\ell+1) &= k_0(\ell) - \frac{k_1(\ell)}{a(\ell)+\frac{ip'\ell}{\sqrt{N}}} + 2\frac{k_2(\ell)}{(a(\ell)+\frac{ip'\ell}{\sqrt{N}})^2} \\ &= \sum_{\ell'=1}^{\ell}\sum_{k=1}^{\ell'} \frac{2k}{(a(k)+\frac{ikp'}{\sqrt{N}})(a(\ell')+\frac{i\ell'p'}{\sqrt{N}})} \\ k_0(N)|_{p'=0} &= \frac{2}{\sigma^2}\sum_{\ell=1}^{N-1}\sum_{k=1}^{\ell}\frac{1}{\ell(N-\ell)(N-k)}\,, \end{aligned} \tag{C.18}$$

simply evaluating these at N and performing the final integration over x_N then yields

$$\begin{aligned} \int_{-\infty}^{\infty} dx_N\; I(N) =& \frac{2A(N,p')\pi}{\sqrt{N}}\left[-\frac{k_2(N)\delta''(p')}{N}\right. \\ &\left. + i\frac{k_1(N)\delta'(p')}{\sqrt{N}} + k_0(N)\delta(p')\right]\,, \end{aligned} \tag{C.19}$$

we then insert this expression back into Eq. (C.13) giving

$$\begin{aligned} \langle\psi^{(\lambda)}_{\rm var}|V(\mathbf{x})|\psi^{(\lambda)}_{\rm var}\rangle =& \frac{\gamma^2}{2A(N,0)}\int_{-\infty}^{\infty} dp' \exp\left(\frac{-p'^2}{4\gamma}\right) \\ &\times\left[-\frac{k_2(N)\delta''(p')}{N} + i\frac{k_1(N)\delta'(p')}{\sqrt{N}} + k_0(N)\delta(p')\right]\,. \end{aligned} \tag{C.20}$$

The integral over the $\delta(p')$ term can be performed immediately and gives $\gamma^2 k_0(N)/2$. Considering next the integral over $\delta'(p')$; since $\exp(-p'^2/4\gamma)$ has zero gradient at the origin it will not contribute, however the terms

$$\begin{aligned} \frac{\partial}{\partial p}k_1(N)|_{p'=0} &= \frac{2i}{\sigma^2\sqrt{N}}\sum_{k=1}^{N-1}\frac{1}{k^2} \\ \frac{\partial}{\partial p}A(N,p')|_{p'=0} &= -\frac{i}{\sigma\sqrt{N}}A(N,0)\sum_{k=1}^{N-1}\frac{1}{k}\,, \end{aligned} \tag{C.21}$$

will contribute to Eq. (C.19), giving

$$\begin{aligned}&\int_{-\infty}^{\infty} dp' i\delta'(p') \exp\left(\frac{-p'^2}{4\gamma}\right) A(\ell, p') \frac{K_1(N)}{\sqrt{N}} \\ &= -2A(N,0)\frac{1}{N\sigma^2}\left(\left[\sum_{k=1}^{N-1}\frac{1}{k}\right]^2 + \sum_{k=1}^{N-1}\frac{1}{k^2}\right) . \end{aligned} \tag{C.22}$$

Finally for the $\delta''(p')$ term we must include $A''(N,p')|_{p'=0} = -A(N,0)\sum_{k,\ell=1}^{N-1}(1+\delta_{kl})k\ell/Na(k)a(\ell)$ and the differential of a Gaussian, hence we have

$$\begin{aligned}&-\int_{-\infty}^{\infty} dp' \delta''(p') \exp\left(\frac{-p'^2}{4\gamma}\right) A(l, p') \\ &= A(N,0)\left(\frac{1}{2\gamma} + \frac{1}{N\sigma^2}\left\{\left[\sum_{k=1}^{N-1}\frac{1}{k}\right]^2 + \sum_{k=1}^{N-1}\frac{1}{k^2}\right\}\right) . \end{aligned} \tag{C.23}$$

Summing these three terms together, and substituting $k_2(N) = N$, we are left with

$$\begin{aligned}\langle\psi_{\rm var}^{(\lambda)}|V|\psi_{\rm var}^{(\lambda)}\rangle =& \frac{\gamma^2}{\sigma^2}\left[\frac{\sigma^2}{4\gamma} + \sum_{\ell=1}^{N-1}\frac{1}{\ell(N-\ell)}\sum_{k=1}^{\ell}\frac{1}{N-k}\right. \\ &\left. -\frac{1}{2N}\left(\left[\sum_{k=1}^{N-1}\frac{1}{k}\right]^2 + \sum_{k=1}^{N-1}\frac{1}{k^2}\right)\right] . \end{aligned} \tag{C.24}$$

The first term in this expression is equal to $\gamma/4$, which is simply the potential energy of the centre-of-mass component. It can be proved via induction [170] that the double sum is equal to

$$\sum_{\ell=1}^{N-1}\frac{1}{\ell(N-\ell)}\sum_{k=1}^{\ell}\frac{1}{N-k} = \frac{1}{2N}\left[\left(\sum_{k=1}^{N-1}\frac{1}{k}\right)^2 + \sum_{k=1}^{N-1}\frac{3}{k^2}\right] , \tag{C.25}$$

thus reinstating $\sigma = \lambda/(N-1)$, the remaining terms simplified down to

$$\langle\psi_{\rm var}^{(\lambda)}|V|\psi_{\rm var}^{(\lambda)}\rangle = \frac{\gamma^2(N-1)^2}{N\lambda^2}\sum_{k=1}^{N-1}\frac{1}{k^2} + \frac{\gamma}{4} , \tag{C.26}$$

which is used in Sec. 5.3. Equation Eq. (5.27) is the first order energy correction to the free soliton with Gaussian centre-of-mass envelope and is obtained

by subtracting the centre-of-mass energy and setting $\lambda = 1$

$$E^{(1)} = \frac{\gamma^2(N-1)^2}{N}\sum_{k=1}^{N-1}\frac{1}{k^2}\,. \tag{C.27}$$

C.5 Energy correction to the Hartree product state

An energy correction for general power law potentials can be derived in the mean field case. For $\mathrm{Re}(m) > -1$

$$\int_{-\infty}^{\infty} dx\,\frac{\mathrm{sech}(x/2)^2}{4}\frac{|x|^m}{2} = \begin{cases} m!\zeta(m)(1-2^{1-m}) & m \neq 1\,, \\ \log(2) & m = 1\,, \end{cases} \tag{C.28}$$

with $\zeta(m)$ the Riemann zeta function. The Hartree product state $|\Psi_{\mathrm{H}}\rangle$ is a product of N identical single-particle wavefunction $\Phi(x) = \mathrm{sech}(x/2)/2$ and hence the total energy correction is thus γNtimes the correction (C.28) ($\pi/6$ for $m = 2$). However we are interested only in the relative energy correction given by

$$\begin{aligned} E_{\mathrm{H}}^{(1)} &= \gamma^2\langle\psi_{\mathrm{H}}|\frac{1}{2}\sum_{k=1}^{N}x_k^2 - \frac{N}{2}\left(\sum_{k=1}^{N}\frac{x_k}{N}\right)^2|\psi_{\mathrm{H}}\rangle \\ &= \gamma^2\langle\psi_{\mathrm{H}}|\frac{N-1}{2N}\sum_{k=1}^{N}x_k^2 - \sum_{k<j}x_kx_j|\psi_{\mathrm{H}}\rangle\,. \end{aligned} \tag{C.29}$$

All the cross terms of the form x_kx_j will evaluate to zero as $\mathrm{sech}(x)$ is an even function, thus leaving only the x_k^2 terms. By Bose symmetry $\langle f(x_k)\rangle = \langle f(x_j)\rangle$ and thus the value of all the terms in the first sum will be identical to the single-particle correction and we have

$$E_{\mathrm{H}}^{(1)} = (N-1)\frac{\gamma^2\pi^2}{6}\,. \tag{C.30}$$

C.6 Overlap of the relative components of the variational wavefunctions

Finally we consider the overlap between the relative parts of the variational wavefunction with $\lambda > 1$ and the ground state in infinitesimal trapping $\gamma = 0,\ \lambda = 1$, given by

$$\begin{aligned}\langle\psi^{(\lambda)}_{\rm var}|\psi^{(1)}_{\rm var}\rangle =& \mathcal{N}_1\mathcal{N}_\lambda \int_{-\infty}^{\infty} dx_1 \ldots \int_{-\infty}^{\infty} dx_N |\psi_{\rm cm}|^2 \\ & \times \exp\left(-\frac{\lambda+1}{2(N-1)}\sum_{k=2}^{N}\sum_{j=1}^{k-1}|x_k - x_j|\right) . \end{aligned} \tag{C.31}$$

This calculation can be achieved by performing the calculations in Appendix C.2 with $\sigma \to (1+\lambda)/2(N-1)$, the resulting factor will not equal unity and instead will be equal to $\mathcal{N}_1\mathcal{N}_\lambda/\mathcal{N}^2_{(1+\lambda)/2}$. Therefore that the overlap is given by

$$\begin{aligned}\langle\psi^{(\lambda)}_{\rm var}|\psi^{(1)}_{\rm var}\rangle &= \frac{\lambda^{(N-1)/2}}{\prod_{k=1}^{N-1}(1+\lambda)/2} \\ &= \left(\frac{2\sqrt{\lambda}}{(1+\lambda)}\right)^{N-1} , \end{aligned} \tag{C.32}$$

which is used in Sec 5.3.3.

Appendix D

Appendix to Chapter 6

D.1 Calculations for the number-to-the-right operator

D.1.1 Analytically determined properties of $\hat{N}_R^2$

From the definition of Eq. (6.9), it follows that

$$\hat{N}_R^2 = \int_0^\infty dx dx' \, \hat{\Psi}^\dagger(x)\hat{\Psi}^\dagger(x')\hat{\Psi}(x)\hat{\Psi}(x') + \hat{N}_R \, , \tag{D.1}$$

and, given a general (symmetrized) many-body wavefunction $\psi(\vec{x})$, one may deduce the expectation values

$$\langle \hat{N}_R \rangle = N \int_0^\infty dx_1 \int_{-\infty}^\infty dx_2 \dots dx_N \, |\psi(\vec{x})|^2 \, , \tag{D.2}$$

$$\langle \hat{N}_R^2 \rangle = N(N-1) \int_0^\infty dx_1 dx_2 \int_{-\infty}^\infty dx_3 \dots dx_N \, |\psi(\vec{x})|^2 + \langle \hat{N}_R \rangle \, . \tag{D.3}$$

For a product-state wavefunction $\psi(\vec{x}) = \prod_{k=1}^N \phi(x_k)$, expectation values are simple to calculate, as all integrals are separable and most evaluate to unity.

In this case

$$\langle \hat{N}_R \rangle = N \int_0^\infty dx \, |\phi(x)|^2 \, , \tag{D.4}$$

$$\begin{aligned} \langle \hat{N}_R^2 \rangle &= N(N-1) \left[\int_0^\infty dx \, |\phi(x)|^2 \right]^2 + \langle \hat{N}_R \rangle \\ &= [(N-1)/N] \langle \hat{N}_R \rangle^2 + \langle \hat{N}_R \rangle \, , \end{aligned} \tag{D.5}$$

and so the variance of $\hat{N}_R$ for a product-state simplifies to

$$(\Delta N_R)_P = \langle \hat{N}_R \rangle (1 - \langle \hat{N}_R \rangle / N) \, . \tag{D.6}$$

We may determine analytic expressions when $g = 0$, which we limit to the $N = 4$ case. Without interactions, our many body wavefunction is given by Eq. (6.5), and we require the integrals

$$\int_0^\infty dx |\phi(x, \pm x_0, t)|^2 = \frac{1}{2} \left[1 \pm \mathrm{erf}(x_0 \cos(t)) \right] \, , \tag{D.7}$$

$$\int_{-\infty}^\infty dx \phi^*(x, \pm x_0, t) \phi(x, \mp x_0, t) = \mathrm{e}^{-x_0^2 \pm i x_0 \sin(2t)/2} \, , \tag{D.8}$$

$$\begin{aligned} \int_0^\infty dx \phi^*(x, \pm x_0, t) \phi(x, \mp x_0, t) = & \frac{1}{2} \left[1 \pm \mathrm{erf}(x_0 \sin(t)) \right] \\ & \times \mathrm{e}^{-x_0^2 \pm i x_0 \sin(2t)/2} \, , \end{aligned} \tag{D.9}$$

with erf denoting the error function. Calculating $\langle \hat{N}_R^2 \rangle$ in principle requires accounting for 36 different terms, however, assuming we can neglect terms proportional to $\exp(-2x_0^2)$, only 6 are important, and we have

$$\begin{aligned} \langle \hat{N}_R^2 \rangle \approx & \frac{N(N-1)}{24} \left\{ [1 - \mathrm{erf}(x_0 \cos(t))]^2 + 4[1 - \mathrm{erf}^2(x_0 \cos(t))] \right. \\ & \left. + [1 + \mathrm{erf}(x_0 \cos(t))]^2 \right\} + \langle \hat{N}_R \rangle \\ = & 5 - \mathrm{erf}^2[x_0 \cos(t)] \, . \end{aligned} \tag{D.10}$$

Subtracting $\langle \hat{N}_R \rangle^2 = 4$ then yields the variance as given by Eq. (6.12).

D.1.2 Numerical calculation of number variance

In order to calculate the number variance we decompose the field operator into our basis set, $\hat{\Psi}(x) = \sum_k \hat{c}_k \phi_k(x)$. In this form we can express $\hat{N}_R^2$ as

$$\hat{N}_R^2 = \sum_{i,j,k,\ell} y_{ik} y_{j\ell} \hat{c}_i^\dagger \hat{c}_j^\dagger \hat{c}_k \hat{c}_\ell + \hat{N}_R \,, \tag{D.11}$$

where $y_{j\ell} = \int_0^\infty dx\, \varphi_j(x)\varphi_\ell(x)$ is the positive space overlap between two Hermite functions, given by $\delta_{j\ell}/2$ if $j+\ell$ is even, and otherwise given by

$$\begin{aligned} y_{j\ell} = (-1)^{(j+\ell-1)/2} \;\; & {}_2F_1(-j, 1-[j-\ell]/2; 1-[j+\ell]/2, -1) \\ & \times \frac{2^{-j}(j+\ell+2)!!}{\sqrt{2\pi j!\ell!}} \,, \end{aligned} \tag{D.12}$$

where ${}_2F_1$ denotes a standard hypergeometric function. Likewise the integral from minus infinity to zero is $(-1)^{j+\ell} y_{j\ell}$. This formula is useful for small numbers and testing, but for practical purposes we calculate the integral via Gauss Laguerre quadrature, which is numerically exact for odd $j+\ell$ (all other cases are trivially zero or one half) given a rule of order $(j+\ell+1)/2$ or higher. Given our truncated basis and symmetry about $x = 0$, this can be expressed as a finite size matrix of only even-parity functions with $\langle \hat{N}_R \rangle = N/2$ just a numerical constant for our initial condition.

D.1.3 Numerical calculation of restricted region expectation values

In addition to this we wish to calculate expectation values in restricted regions via Eq. (6.13), corresponding to sections of the wavefunction with exactly n particles to the left or right, along with the associated normalization factors when the wavefunction is divided into these regions. If our many body wavefunction is $\psi(\vec{x})$ then the normalization factors are given by

$$\mathcal{N}_n = \frac{N!}{(N-n)!n!} \int_0^\infty dx_1 \dots dx_n \int_{-\infty}^0 dx_{n+1} \dots dx_N \, |\psi(\vec{x})|^2 \,, \tag{D.13}$$

and the expectation value of the distance to the right operator is equal to

$$\begin{aligned}\langle \hat{x}_{\mathrm{R}}^{(n)} \rangle =& \mathcal{N}_n^{-1} \int_{-\infty}^{\infty} dx_1 \dots dx_N \sum_{k=0}^{N} x_k \theta(x_k) \sum_{\mathcal{P}} \prod_{k=1}^{n} \Theta(x_k) \prod_{j=n+1}^{N} \Theta(-x_j) \, |\psi(\vec{x})|^2 \\ =& \mathcal{N}_n^{-1} \frac{N!}{(N-n)!n!} \int_0^{\infty} dx_1 \dots dx_n \int_{-\infty}^{0} dx_{n+1} \dots dx_N \sum_{k=n+1}^{N} x_k \, |\psi(\vec{x})|^2 \ . \end{aligned} \tag{D.14}$$

For computation, these operators are converted into matrix form by taking the matrix elements between different elements of the basis set, and then projected to our reduced (centre-of-mass ground state) basis.

D.2 Two cluster wavefunction evolution

Here we derive the time dependent wavefunction describing the centre of masses of our two cluster system, i.e. the part acted on by $\hat{H}_{L/R}^{(\mathrm{C})}$, the centre-of-mass components from Eq. (6.24); with $\hat{H}_I$ ignored. Denoting y_1, y_2 as the coordinates of the centre-of-masses of each cluster, up to a normalization factor our initial two-cluster wavefunction is given by

$$\begin{aligned}\langle y_1, y_2 | \varphi_{n,N-n}(0) \rangle \propto & \exp\left(-\frac{N-n}{2} \left[y_2 + \frac{n X_n}{N-n} \right]^2 \right) \\ & \times \exp\left(-\frac{n}{2} [y_1 - X_n]^2 \right) + \mathcal{T}_{\mathrm{perm}} \ , \end{aligned} \tag{D.15}$$

with $\mathcal{T}_{\mathrm{perm}}$ the term obtained by permuting y_1 and y_2, as required by symmetry. This gives rise to a time-dependent normalization constant which we do not discuss here. If we instead express this in terms of $y_{\mathrm{C}} = [n y_1 + (N-n) y_2]/N$ and $y_{\mathrm{R}} = y_1 - y_2$ we have

$$\begin{aligned}\langle y_{\mathrm{C}}, y_{\mathrm{R}} | \varphi_{n,N-n}(0) \rangle \propto & \exp\left(-\frac{n[(N-n) y_{\mathrm{R}} - N X_n]^2}{2N[N-n]} \right) \\ & \times \exp\left(-\frac{N y_{\mathrm{C}}^2}{2} \right) + \mathcal{T}_{\mathrm{perm}} \ , \end{aligned} \tag{D.16}$$

where in this case $\mathcal{T}_{\mathrm{perm}}$ is obtained by flipping the sign of y_{R}, and we can factor out the y_{C} dependence. If we temporarily ignore interactions between

the two clusters, it is straightforward to generalize this to the time dependent case via Eq. (6.6):

$$\begin{aligned}\langle y_{\mathrm{C}}, y_{\mathrm{R}}|\varphi_{n,N-n}(t)\rangle \propto & \exp\left(-\frac{n[(N-n)y_{\mathrm{R}} - NX_n\cos(t)]^2}{2N[N-n]}\right)\exp\left(-\frac{Ny_{\mathrm{C}}^2}{2}\right) \\ & \times \exp\left(i\left[t - ny_{\mathrm{r}}X_n\sin(t) + \frac{X_n}{4}\left(n - \frac{n}{N-n}\right)\sin(2t)\right]\right) \\ & + \mathcal{T}_{\mathrm{perm}}\ . \end{aligned} \tag{D.17}$$

Interactions between clusters can modify only the y_{R} dependent part of this wavefunction.

D.3 Energy bound for Hamiltonian variance

As the Hamiltonian is time independent, the time evolution operator commutes with all powers of the Hamiltonian. Denoting our state as $|\psi(t)\rangle$ we have for any time t

$$\langle\psi(t)|\hat{H}^n|\psi(t)\rangle = \langle\psi(0)|\hat{H}^n|\psi(0)\rangle\ , \quad n = 1, 2, \dots\ . \tag{D.18}$$

As absolute values of energy are not physically important, we consider a re-zeroed Hamiltonian

$$\hat{\mathcal{H}} = \hat{H} - \langle\psi(0)|\hat{H}|\psi(0)\rangle\ , \tag{D.19}$$

as it will make the mathematics more convenient. Introducing the notation for the variance of the re-zeroed Hamiltonian

$$\Delta E^2 = \langle\hat{\mathcal{H}}^2\rangle\ , \tag{D.20}$$

we note that this quantity must be positive and real as $\hat{H}$ is a Hermitian operator.

Let us define two wave functions $|\psi_1(t)\rangle$ and $|\psi_2(t)\rangle$ as being negligibly mixed at a certain point in time if

$$\langle\psi_1(t)|\hat{\mathcal{H}}^n|\psi_2(t)\rangle \leq \eta\ , \quad n = 1, 2 \tag{D.21}$$

with η a small parameter. Note that in lattice models η could be exactly zero up to some finite power n. If both the initial wave function and $|\psi_{1,2}(t)\rangle$ are normalized to one and the latter are negligibly mixed, the wave function at time t can be written (up to a global phase factor) as

$$|\psi(t)\rangle = \sqrt{p}|\psi_1(t)\rangle + \sqrt{1-p}e^{i\alpha}|\psi_2(t)\rangle \tag{D.22}$$

with real α and $0 \leq p \leq 1$. Introducing the notation

$$\langle\hat{\mathcal{H}}^n\rangle_j \equiv \langle\psi_j(t)|\hat{\mathcal{H}}^n|\psi_j(t)\rangle \ , \tag{D.23}$$

we can see from Eq. (D.21) and the fact that the expectation value of total Hamiltonian is zero, that these two quantities are related via

$$\langle\hat{\mathcal{H}}\rangle_1 = \frac{p-1}{p}\langle\hat{\mathcal{H}}\rangle_2 + O(\eta) \ . \tag{D.24}$$

Setting $\eta = 0$ in Eq. (D.21) we have for $n = 2$

$$\begin{aligned}\Delta E^2 &= p\langle\hat{\mathcal{H}}^2\rangle_1 + (1-p)\langle\hat{\mathcal{H}}^2\rangle_2 \\ &\geq p\langle\hat{\mathcal{H}}\rangle_1^2 + (1-p)\langle\hat{\mathcal{H}}\rangle_2^2 \ ,\end{aligned} \tag{D.25}$$

with the second step true again by the fact that $\hat{H}$ is Hermitian. Finally, substituting in for $\langle\hat{\mathcal{H}}\rangle_1$ via Eq. (D.24) we obtain

$$\Delta E^2 \geq \frac{1-p}{p}\langle\hat{\mathcal{H}}\rangle_2^2 \ , \tag{D.26}$$

$$\Delta E^2 \geq \frac{p}{1-p}\langle\hat{\mathcal{H}}\rangle_1^2 \ , \tag{D.27}$$

$$\Delta E^2 \geq \frac{\left(\langle\hat{\mathcal{H}}\rangle_1 - \langle\hat{\mathcal{H}}\rangle_2\right)^2}{p(1-p)} \ , \tag{D.28}$$

which leads to Eq. (6.66) in the main text.

D.3.1 Analytic calculations of ΔE

For our two particle initial condition, if $x_0 \gg 1$, i.e., well-separated initial clusters, we can analytically determine E and ΔE. Within this well-

separated approximation we only need to consider one cluster, displaced a distance x_0 from the centre, and multiply by 2 to get the values for the whole wavefunction. For dimers, our wavefunction is $f(x_1 - x_0, x_2 - x_0)^{(2)}$ as defined in Eq. (6.7), otherwise it is not analytic. This wavefunction is still an eigenstate of the relative Hamiltonian (for n particles), with some eigenvalue $E_{\mathrm{rel}}^{(n)}$, but not of the centre-of-mass part. Therefore we need only consider the centre-of-mass Hamiltonian

$$H_{\mathrm{C}}(x_{\mathrm{C}}) = -\frac{1}{2n}\frac{\partial^2}{\partial x_{\mathrm{C}}^2} + \frac{n x_{\mathrm{C}}^2}{2} \,, \tag{D.29}$$

acting on the displaced ground state

$$\psi_{\mathrm{C}}(x_{\mathrm{C}}) = \left(\frac{n}{\pi}\right)^{1/4} \exp(-n[x_{\mathrm{C}} - x_0]/2) \,, \tag{D.30}$$

to get all contributions to the variance. Acting the Hamiltonian on this wavefunction we obtain

$$\begin{aligned} H_{\mathrm{C}}\psi_{\mathrm{C}}(x_{\mathrm{C}}) &= \left(\frac{1}{2} + n x_0 x + \frac{n x_0^2}{2}\right)\psi_{\mathrm{C}}(x_{\mathrm{C}}) \,, \\ H_{\mathrm{C}}^2\psi_{\mathrm{C}}(x_{\mathrm{C}}) &= \left[\frac{1}{4} + \frac{n x_0}{2}(4x - 3x_0) + n^2 x_0^2 (x_0 - 2x)^2\right]\psi_{\mathrm{C}}(x_{\mathrm{C}}) \,, \end{aligned} \tag{D.31}$$

which can then be used to determine the expectation values

$$\begin{aligned} \langle \hat{H}_{\mathrm{C}} \rangle &= \frac{1}{2} + \frac{n x_0^2}{2} \,, \\ \langle \hat{H}_{\mathrm{C}}^2 \rangle &= \frac{1}{4} + n x_0^2 + \frac{n^2 x_0^4}{4} \,. \end{aligned} \tag{D.32}$$

ΔE can then be calculated as the standard deviation of two times $\hat{H}_{\mathrm{C}}$

$$\Delta E = 2\sqrt{\langle \hat{H}_{\mathrm{C}}^2 \rangle - \langle \hat{H}_{\mathrm{C}} \rangle^2} = \sqrt{2n}\, x_0 \,, \tag{D.33}$$

which is twice the square root of the difference between the initial (dimensionless) potential energy and the ground state energy. The reasons for this are similar to why a classical coherent state with an average value of N photons has a shot noise proportional to $N^{1/2}$. Note that this result relies on $\exp(-n x_0^2) \ll 1$ and so can only be considered valid to this order.

References

[1] D. I. H. Holdaway, C. Weiss, and S. A. Gardiner, *Quantum theory of bright matter-wave solitons in harmonic confinement*, Phys. Rev. A **85**, 053618 (2012).

[2] D. I. H. Holdaway, C. Weiss, and S. A. Gardiner, *Collision dynamics and entanglement generation of two initially independent and indistinguishable boson pairs in one-dimensional harmonic confinement*, Phys. Rev. A **87**, 043632 (2013).

[3] A. Einstein, *Quantum thermodynamics of ideal gases (german language)*, Berlin Academy of Sciences(1925), http://www.lorentz.leidenuniv.nl/history/Einstein_archive/.

[4] C. N. Yang, *Concept of off-diagonal long-range order and the quantum phases of Liquid He and of superconductors*, Rev. Mod. Phys. **34**, 694–704 (1962).

[5] J. F. Annett, *Superconductivity, Superfluids and Condensates* (Oxford University Press, Oxford, 1981).

[6] P. G. Drazin and R. S. Johnson, *Solitons: An Introduction* (Cambridge University Press, Cambridge, 1989).

[7] N. J. Zabusky and C. J. Galvin, *Shallow-water waves,the korteweg-devries equation and solitons*, J. Fluid Mech. **47**, 811–824 (1970).

[8] T. Heimburg and A. D. Jackson, *On soliton propagation in biomembranes and nerves*, PNAS **102**, 9790–9795 (2005).

[9] J. P. Gordon, *Interaction forces among solitons in optical fibers*, Opt. Lett. **8**, 596–598 (1983).

[10] K. E. Strecker, G. B. Partridge, A. G. Truscott, and R. G. Hulet, *Bright matter wave solitons in Bose-Einstein condensates*, New J. Phys. **5**, 73 (2003).

[11] C. A. Sackett, J. M. Gerton, M. Welling, and R. G. Hulet, *Measurements of collective collapse in a Bose-Einstein condensate with attractive interactions*, Phys. Rev. Lett. **82**, 876–879 (1999).

[12] J. M. Gerton, D. Strekalov, I. Prodan, and R. G. Hulet, *Direct observation of growth and collapse of a Bose-Einstein condensate with attractive interactions*, Nature **408**, 692–695 (2000).

[13] E. A. Donley, N. R. Claussen, S. L. Cornish, J. L. Roberts, E. A. Cornell, and C. E. Wieman, *Dynamics of collapsing and exploding Bose-Einstein condensates*, Nature **412**, 295–299 (2001).

[14] S. L. Cornish, S. T. Thompson, and C. E. Wieman, *Formation of bright matter-wave solitons during the collapse of attractive Bose-Einstein condensates*, Phys. Rev. Lett. **96**, 170401 (2006).

[15] K. E. Strecker, G. B. Partridge, A. G. Truscott, and R. G. Hulet, *Formation and propagation of matter-wave soliton trains*, Nature (London) **417**, 150–153 (2002).

[16] L. D. Carr and J. Brand, *Spontaneous Soliton Formation and Modulational Instability in Bose-Einstein Condensates*, Physical Review Letters **92**, 040401 (2004).

[17] T. P. Billam, S. L. Cornish, and S. A. Gardiner, *Realizing bright-matter-wave-soliton collisions with controlled relative phase*, Phys. Rev. A **83**, 041602 (2011).

[18] K. Sacha, C. A. Müller, D. Delande, and J. Zakrzewski, *Anderson localization of solitons*, Phys. Rev. Lett. **103**, 210402 (2009).

[19] J. M. McGuirk, D. M. Harber, J. M. Obrecht, and E. A. Cornell, *Alkali-metal adsorbate polarization on conducting and insulating surfaces probed with Bose-Einstein condensates*, Phys. Rev. A **69**, 062905 (2004).

[20] E. H. Lieb and W. Liniger, *Exact analysis of an interacting Bose gas. I. the general solution and the ground state*, Phys. Rev. **130**, 1605–1616 (1963).

[21] J. Holmer, J. Marzuola, and M. Zworski, *Fast soliton scattering by delta impurities*, Communications in Mathematical Physics **274**, 187–216 (2007), ISSN 0010-3616.

[22] J. Garnier and F. K. Abdullaev, *Transmission of matter-wave solitons through nonlinear traps and barriers*, Phys. Rev. A **74**, 013604 (2006).

[23] C. Lee and J. Brand, *Enhanced quantum reflection of matter-wave solitons*, Europhys. Lett. **73**, 321–327 (2006).

[24] X. D. Cao and B. A. Malomed, *Soliton-defect collisions in the nonlinear Schrödinger equation*, Physics Letters A **206**, 177 – 182 (1995), ISSN 0375-9601.

[25] C. Weiss and Y. Castin, *Creation and detection of a mesoscopic gas in a nonlocal quantum superposition*, Phys. Rev. Lett. **102**, 010403 (2009).

[26] A. I. Streltsov, O. E. Alon, and L. S. Cederbaum, *Scattering of an attractive Bose-Einstein condensate from a barrier: Formation of quantum superposition states*, Phys. Rev. A **80**, 043616 (2009).

[27] A. I. Streltsov, O. E. Alon, and L. S. Cederbaum, *Swift loss of coherence of soliton trains in attractive Bose-Einstein condensates*, Phys. Rev. Lett. **106**, 240401 (2011).

[28] S. Sinha, A. Y. Cherny, D. Kovrizhin, and J. Brand, *Friction and diffusion of matter-wave bright solitons*, Phys. Rev. Lett. **96**, 030406 (2006).

[29] S. Handel, *Experiments on ultracold quantum gases of 85 Rb and 87 Rb*, Ph.D. thesis, Durham University (2011).

[30] S. Komy and L. O'Raifeartaigh, *Some Properties of Ladder Operators*, Journal of Mathematical Physics **9**, 738–744 (1968).

[31] K. Hannabuss, *An introduction to quantum theory* (Oxford University Press, Oxford, 1997).

[32] G. A. Baker, *Degeneracy of the n-dimensional, isotropic, harmonic oscillator*, Phys. Rev. **103**, 1119–1120 (1956).

[33] Z. Yan, *General thermal wavelength and its applications*, Eur. Phys. J. **21**, 625 (2000).

[34] L. Pitaevskii and S. Stringari, *Bose-Einstein Condensation* (Oxford Science Publications, Oxford, 2003).

[35] F. Dalfovo, S. Giorgini, L. P. Pitaevskii, and S. Stringari, *Theory of Bose-Einstein condensation in trapped gases*, Rev. Mod. Phys. **71**, 463–512 (1999).

[36] H. A. Bethe, *Theory of the effective range in nuclear scattering*, Phys. Rev. **76**, 38–50 (1949).

[37] V. V. Flambaum, G. F. Gribakin, and C. Harabati, *Analytical calculation of cold-atom scattering*, Phys. Rev. A **59**, 1998–2005 (1999).

[38] F.S.Levin, *An Introduction to quantum theory* (Cambridge University Press, Cambridge, 2004).

[39] C. Chin, R. Grimm, P. Julienne, and E. Tiesinga, *Feshbach resonances in ultracold gases*, Rev. Mod. Phys. **82**, 1225–1286 (2010).

[40] C. Cohen-Tannoudji, B. Diu, and F. Laloe, *Quantum mechanics* (John Wiley and sons, New York, 2004).

[41] V. A. Zagrebnov and J.-B. Bru, *The Bogoliubov model of weakly imperfect Bose gas*, physrep **350**, 291–434 (2001).

[42] K. Huang and C. N. Yang, *Quantum-Mechanical many-body problem with Hard-Sphere interaction*, Phys. Rev. **105**, 767–775 (1957).

[43] S. Tan, *Energetics of a strongly correlated Fermi gas*, Annals of Physics **323**, 2952 – 2970 (2008), ISSN 0003-4916.

[44] M. Valiente, *Tan's distributions and Fermi-Huang pseudopotential in momentum space*, Phys. Rev. A **85**, 014701 (2012).

[45] S. A. Morgan, *A gapless theory of Bose-Einstein condensation in dilute gases at finite temperature*, J. Phys. B **33**, 3847 (2000).

[46] M. Olshanii, *Atomic scattering in the presence of an external confinement and a gas of impenetrable bosons*, Phys. Rev. Lett. **81**, 938–941 (1998).

[47] O. Penrose and L. Onsager, *Bose-Einstein condensation and liquid Helium*, Phys. Rev. **104**, 576–584 (1956).

[48] Y. Lai and H. A. Haus, *Quantum theory of solitons in optical fibers. I. Time-dependent Hartree approximation*, Phys. Rev. A **40**, 844–853 (1989).

[49] Y. Castin and R. Dum, *Low-temperature Bose-Einstein condensates in time-dependent traps: Beyond the $U(1)$ symmetry-breaking approach*, Phys. Rev. A **57**, 3008–3021 (1998).

[50] S. A. Gardiner and S. A. Morgan, *Number-conserving approach to a minimal self-consistent treatment of condensate and noncondensate dynamics in a degenerate Bose gas*, Phys. Rev. A **75**, 043621 (2007).

[51] O. E. Alon, A. I. Streltsov, and L. S. Cederbaum, *Multiconfigurational time-dependent Hartree method for bosons: Many-body dynamics of bosonic systems*, Phys. Rev. A **77**, 033613 (2008).

[52] J. Grond, A. I. Streltsov, L. S. Cederbaum, and O. E. Alon, *Excitation spectra of fragmented condensates by linear response: General theory and application to a condensate in a double-well potential*, Phys. Rev. A **86**, 063607 (2012).

[53] E. Gross, *Structure of a quantized vortex in boson systems*, Il Nuovo Cimento Series 10 **20**, 454–477 (1961), ISSN 0029-6341.

[54] L. P. Pitaevsk, *Vortex lines in an imperfect Bose gas*, Soviet Physics JETP-USSR **13** (1961).

[55] T. P. Billam, P. Mason, and S. A. Gardiner, *Second-order number-conserving description of nonequilibrium dynamics in finite-temperature Bose-Einstein condensates*, Phys. Rev. A **87**, 033628 (2013).

[56] T. P. Billam, S. A. Wrathmall, and S. A. Gardiner, *Variational determination of approximate bright matter-wave soliton solutions in anisotropic traps*, Phys. Rev. A **85**, 013627 (2012).

[57] H. T. C. Stoof, *Atomic Bose gas with a negative scattering length*, Phys. Rev. A **49**, 3824–3830 (1994).

[58] A. S. Desyatnikov, D. Buccoliero, M. R. Dennis, and Y. S. Kivshar, *Suppression of collapse for spiraling elliptic solitons*, Phys. Rev. Lett. **104**, 053902 (2010).

[59] J. Abdullaev, A. S. Desyatnikov, and E. A. Ostrovskaya, *Suppression of collapse for matter waves with orbital angular momentum*, Journal of Optics **13**, 064023 (2011).

[60] N. G. Parker and D. A. Smith, *p-wave stabilization of three-dimensional Bose-Fermi solitons*, Phys. Rev. A **85**, 013604 (2012).

[61] A. Gammal, T. Frederico, and L. Tomio, *Critical number of atoms for attractive Bose-Einstein condensates with cylindrically symmetrical traps*, Phys. Rev. A **64**, 055602 (2001).

[62] A. L. Marchant, T. P. Billam, T. P. Wiles, M. M. H. Yu, S. A. Gardiner, and S. L. Cornish, *Controlled formation and reflection of a bright solitary matter-wave*, Nat. Commun. **4**, 1865 (2013).

[63] D. S. Petrov, G. V. Shlyapnikov, and J. T. M. Walraven, *Regimes of quantum degeneracy in trapped 1d gases*, Phys. Rev. Lett. **85**, 3745–3749 (2000).

[64] L. Salasnich, A. Parola, and L. Reatto, *Effective wave equations for the dynamics of cigar-shaped and disk-shaped Bose condensates*, Phys. Rev. A **65**, 043614 (2002).

[65] L. Khaykovich and B. A. Malomed, *Deviation from one dimensionality in stationary properties and collisional dynamics of matter-wave solitons*, Phys. Rev. A **74**, 023607 (2006).

[66] F. London, *The λ-Phenomenon of Liquid Helium and the Bose-Einstein Degeneracy*, Nature **141**, 643–644 (1938).

[67] G. Careri, S. Cunsolo, P. Mazzoldi, and M. Santini, *Experiments on the creation of charged quantized vortex rings in liquid Helium at 1k*, Phys. Rev. Lett. **15**, 392–396 (1965).

[68] M. H. Anderson, J. R. Ensher, M. R. Matthews, C. E. Wieman, and E. A. Cornell, *Observation of Bose-Einstein condensation in a dilute atomic vapor*, Science **269**, 198–201 (1995).

[69] K. B. Davis, M. O. Mewes, M. R. Andrews, N. J. van Druten, D. S. Durfee, D. M. Kurn, and W. Ketterle, *Bose-Einstein condensation in a gas of Sodium atoms*, Phys. Rev. Lett. **75**, 3969–3973 (1995).

[70] S. L. Cornish and D. Cassettari, *Recent progress in Bose-Einstein condensation experiments*, Royal Society of London Philosophical Transactions Series A **361**, 2699–2713 (2003).

[71] S. L. C. Stephen A. Hopkins, *Ultracold Quantum Gases: Key Experimental Technique*, World Scientific Review, 41–60(2011).

[72] C. C. Bradley, C. A. Sackett, and R. G. Hulet, *Bose-Einstein condensation of Lithium: Observation of limited condensate number*, Phys. Rev. Lett. **78**, 985–989 (1997).

[73] S. Kraft, F. Vogt, O. Appel, F. Riehle, and U. Sterr, *Bose-Einstein condensation of alkaline earth atoms:* ^{40}Ca, Phys. Rev. Lett. **103**, 130401 (2009).

[74] S. Stellmer, M. K. Tey, B. Huang, R. Grimm, and F. Schreck, *Bose-Einstein condensation of Strontium*, Phys. Rev. Lett. **103**, 200401 (2009).

[75] T. Fukuhara, S. Sugawa, and Y. Takahashi, *Bose-Einstein condensation of an Ytterbium isotope*, Phys. Rev. A **76**, 051604 (2007).

[76] Q. Beaufils, R. Chicireanu, T. Zanon, B. Laburthe-Tolra, E. Maréchal, L. Vernac, J.-C. Keller, and O. Gorceix, *All-optical production of Chromium Bose-Einstein condensates*, Phys. Rev. A **77**, 061601 (2008).

[77] M. Lu, N. Q. Burdick, S. H. Youn, and B. L. Lev, *Strongly dipolar Bose-Einstein condensate of Dysprosium*, Phys. Rev. Lett. **107**, 190401 (2011).

[78] K. Aikawa, A. Frisch, M. Mark, S. Baier, A. Rietzler, R. Grimm, and F. Ferlaino, *Bose-Einstein condensation of Erbium*, Phys. Rev. Lett. **108**, 210401 (2012).

[79] F. Pereira Dos Santos, J. Léonard, J. Wang, C. J. Barrelet, F. Perales, E. Rasel, C. S. Unnikrishnan, M. Leduc, and C. Cohen-Tannoudji, *Bose-Einstein condensation of metastable Helium*, Phys. Rev. Lett. **86**, 3459–3462 (2001).

[80] D. E. Pritchard, *Cooling neutral atoms in a magnetic trap for precision spectroscopy*, Phys. Rev. Lett. **51**, 1336–1339 (1983).

[81] A. E. Leanhard, T. A. Pasquin, M. Saba, A. Schirotzek, Y. Shin, D. Kielpinski, D. E. Pritchard, and W. Ketterle, *Cooling Bose-Einstein condensates below 500 picokelvin*, Science **301**, 1513–1515 (2003).

[82] L. Khaykovich, F. Schreck, G. Ferrari, T. Bourdel, J. Cubizolles, L. D. Carr, Y. Castin, and C. Salomon, *Formation of a matter-wave bright soliton*, Science **296**, 1290–1293 (2002).

[83] C. Chin, V. Vuletić, A. J. Kerman, S. Chu, E. Tiesinga, P. J. Leo, and C. J. Williams, *Precision Feshbach spectroscopy of ultracold* Cs_2, Phys. Rev. A **70**, 032701 (2004).

[84] J. M. Vogels, C. C. Tsai, R. S. Freeland, S. J. J. M. F. Kokkelmans, B. J. Verhaar, and D. J. Heinzen, *Prediction of Feshbach resonances in collisions of ultracold Rubidium atoms*, Phys. Rev. A **56**, R1067–R1070 (1997).

[85] R. Bücker, J. Grond, S. Manz, T. Berrada, T. Betz, C. Koller, U. Hohenester, T. Schumm, A. Perrin, and J. Schmiedmayer, *Twin-atom beams*, Nature Physics **7**, 608–611 (2011), arXiv:1012.2348 [cond-mat.quant-gas].

[86] I. Bloch, *Ultracold quantum gases in optical lattices*, Nature Physics **1**, 23 (2005).

[87] V. Vuletić, C. Chin, A. J. Kerman, and S. Chu, *Degenerate Raman sideband cooling of trapped Cesium atoms at very high atomic densities*, Physical Review Letters **81**, 5768–5771 (1998).

[88] C. J. Foot, *Atomic Physics* (Oxford University Press, Oxford, 2004).

[89] D. Jacob, E. Mimoun, L. D. Sarlo, M. Weitz, J. Dalibard, and F. Gerbier, *Production of Sodium Bose-Einstein condensates in an optical dimple trap*, New J. Phys. **13**, 065022 (2011).

[90] N. Gross, Z. Shotan, S. Kokkelmans, and L. Khaykovich, *Observation of universality in ultracold* ^{7}Li *three-body recombination*, Phys. Rev. Lett. **103**, 163202 (2009).

[91] B. Sutherland, *Beautiful Models* (World Scientific Publishing Co., Oxford, 2004).

[92] M. J. Ablowitz and H. Segur, *Solitons and the Inverse Scattering Transform* (SIAM, Philadelphia, 1981).

[93] R. H. Smith and V. Szebehely, *The onset of chaotic motion in the restricted problem of three bodies*, Celestial Mechanics and Dynamical Astronomy **56**, 409–425 (1993).

[94] S. A. Gardiner, *Quantum measurement, Quantum Chaos and Bose-Einstein condensates*, Ph.D. thesis, Leopold-Franzens-Universitat Innsbruck (2000).

[95] B. Hasselblatt and A. Katok, *A First course in dynamics: with a panorama of recent developments* (Cambridge University Press, Cambridge, 2003).

[96] V. E. Zakharov and A. B. Shabat, *A scheme for integrating the nonlinear equations of mathematical physics by the method of the inverse scattering problem. I*, Sov. Phys **8**, 43–53 (1974).

[97] V. E. Zakharov and A. B. Shabat, *A scheme for integrating the nonlinear equations of mathematical physics by the method of the inverse scattering problem. II*, Sov. Phys **13**, 13–22 (1979).

[98] N. J. Zabusky and M. D. Kruskal, *Interaction of solitons in a collisionless plasma and the recurrence of initial states*, Phys. Rev. Lett. **15**, 240–243 (1965).

[99] L. D. Carr, C. W. Clark, and W. P. Reinhardt, *Stationary solutions of the one-dimensional nonlinear Schrödinger equation. II. Case of attractive nonlinearity*, Phys. Rev. A **62**, 063611 (2000).

[100] A. D. Martin, C. S. Adams, and S. A. Gardiner, *Bright solitary-matter-wave collisions in a harmonic trap: Regimes of solitonlike behavior*, Phys. Rev. A. **77**, 013620 (2008).

[101] N. N. Akhmediev and V. I. Korneev, *Modulation instability and periodic solutions of the nonlinear Schrödinger equation*, Theoretical and Mathematical Physics **69**, 1089–1093 (1986).

[102] B. Kibler, J. Fatome, C. Finot, G. Millot, G. Genty, B. Wetzel, N. Akhmediev, F. Dias, and J. M. Dudley, *Observation of Kuznetsov-Ma soliton dynamics in optical fibre*, Scientific Reports **2**, 463 (2012).

[103] B. Kibler, J. Fatome, C. Finot, G. Millot, F. Dias, G. Genty, N. Akhmediev, and J. M. Dudley, *The Peregrine soliton in nonlinear fibre optics*, Nature Physics **6**, 790–795 (2010).

[104] S. Burger, K. Bongs, S. Dettmer, W. Ertmer, K. Sengstock, A. Sanpera, G. V. Shlyapnikov, and M. Lewenstein, *Dark solitons in Bose-Einstein condensates*, Phys. Rev. Lett. **83**, 5198–5201 (1999).

[105] L. Salasnich, A. Parola, and L. Reatto, *Condensate bright solitons under transverse confinement*, Phys. Rev. A **66**, 043603 (2002).

[106] N. G. Parker, S. L. Cornish, C. S. Adams, and A. M. Martin, *Bright solitary waves and trapped solutions in Bose-Einstein condensates with attractive interactions*, J. Phys. B **40**, 3127–3142 (2007).

[107] J. L. Helm, T. P. Billam, and S. A. Gardiner, *Bright matter-wave soliton collisions at narrow barriers*, ArXiv e-prints(2012), arXiv:1203.3080 [cond-mat.quant-gas].

[108] S. M. Al-Marzoug, S. M. Al-Amoudi, U. Al Khawaja, H. Bahlouli, and B. B. Baizakov, *Scattering of a matter-wave single soliton and a two-soliton molecule by an attractive potential*, Phys. Rev. E **83**, 026603 (2011).

[109] F. Calogero, *Exactly solvable one-dimensional many-body problems*, Lettere al Nuovo Cimento **13**, 411–416 (1975), ISSN 0375-930X.

[110] W. H. Zurek, *Decoherence and the transition from quantum to classical*, Physics Today **44**, 36–44 (1991).

[111] S. Haroche and J.-M. Raimond, *Exploring the Quantum* (Oxford University Press, Oxford, 2006).

[112] C. W. Gardiner and P. Zoller, *Quantum Noise: A Handbook of Markovian and Non-Markovian Quantum Stochastic Methods with Applications to Quantum Optics* (Springer, New York, 2004).

[113] V. Jacques, E. Wu, F. Grosshans, F. Treussart, P. Grangier, A. Aspect, and J.-F. Roch, *Experimental realization of Wheelers delayed-choice gedanken experiment*, Science **315**, 966– (2007).

[114] L. Amico, R. Fazio, A. Osterloh, and V. Vedral, *Entanglement in many-body systems*, Rev. Mod. Phys. **80**, 517–576 (2008).

[115] K. Eckert, J. Schliemann, D. Bruss, and M. Lewenstein, *Quantum correlations in systems of indistinguishable particles*, Annals of Physics **299**, 88 – 127 (2002), ISSN 0003-4916.

[116] V. Yukalov and M. Girardeau, *Fermi-Bose mapping for one-dimensional Bose gases*, Laser Physics Letters **2**, 375–382 (2005), ISSN 1612-202X.

[117] Y. Lai and H. A. Haus, *Quantum theory of solitons in optical fibers. II. exact solution*, Phys. Rev. A **40**, 854–866 (1989).

[118] P. Calabrese and J.-S. Caux, *Dynamics of the attractive 1d Bose gas: analytical treatment from integrability*, J. Stat. Mech. **2007**, P08032 (2007).

[119] T. Dorlas, *Orthogonality and completeness of the Bethe ansatz eigenstates of the nonlinear Schrödinger model*, Communications in Mathematical Physics **154**, 347–376 (1993), ISSN 0010-3616.

[120] P. L. Halkyard, M. P. A. Jones, and S. A. Gardiner, *Rotational response of two-component Bose-Einstein condensates in ring traps*, Phys. Rev. A **81**, 061602 (2010).

[121] V. E. Korepin, *Norm of Bethe Wave Function as a Determinant*, ArXiv e-prints(2009), arXiv:0911.1881 [math.CO].

[122] A. G. Sykes, D. M. Gangardt, M. J. Davis, K. Viering, M. G. Raizen, and K. V. Kheruntsyan, *Spatial nonlocal pair correlations in a repulsive 1d Bose gas*, Phys. Rev. Lett. **100**, 160406 (2008).

[123] A. Minguzzi and D. M. Gangardt, *Exact coherent states of a harmonically confined Tonks-Girardeau gas*, Phys. Rev. Lett. **94**, 240404 (2005).

[124] K. K. Das, M. D. Girardeau, and E. M. Wright, *Crossover from one to three dimensions for a gas of hard-core bosons*, Phys. Rev. Lett. **89**, 110402 (2002).

[125] L. Salasnich, A. Parola, and L. Reatto, *Transition from three dimensions to one dimension in Bose gases at zero temperature*, Phys. Rev. A **70**, 013606 (2004).

[126] A. G. Sykes, P. D. Drummond, and M. J. Davis, *Excitation spectrum of bosons in a finite one-dimensional circular waveguide via the Bethe ansatz*, Phys. Rev. A **76**, 063620 (2007).

[127] Y. Castin, *Internal structure of a quantum soliton and classical excitations due to trap opening*, Eur. Phys. J. B **68**, 317–328 (2009).

[128] F. Calogero and A. Degasperis, *Comparison between the exact and Hartree solutions of a one-dimensional many-body problem*, Phys. Rev. A **11**, 265–269 (1975).

[129] L. Mandel and E. Wolf, *Optical coherence and quantum optics* (Cambridge University Press, Cambridge, 2004).

[130] D. Schumayer and D. A. W. Hutchinson, *Colloquium : Physics of the Riemann hypothesis*, Rev. Mod. Phys. **83**, 307–330 (2011).

[131] C. Weiss and M. Holthaus, *Asymptotics of the number partitioning distribution*, Europhys. Lett. **59**, 486–492 (2002).

[132] A. Kubasiak, J. K. Korbicz, J. Zakrzewski, and M. Lewenstein, *Fermi-Dirac statistics and the number theory*, Europhys. Lett. **72**, 506–512 (2005).

[133] M. Abramowitz and I. A. Stegun, *Pocketbook of mathematical functions* (Verlag Harri Deutsch, Frankfurt, 1984).

[134] T. Yamada, Y. Funaki, H. Horiuchi, G. Röpke, P. Schuck, and A. Tohsaki, *Internal one-particle density matrix for Bose-Einstein condensates with finite number of particles in a harmonic potential*, Phys. Rev. C **79**, 054314 (2009).

[135] T. Haugset and H. Haugerud, *Exact diagonalization of the Hamiltonian for trapped interacting bosons in lower dimensions*, Phys. Rev. A **57**, 3809–3817 (1998).

[136] S. Gupta, K. W. Murch, K. L. Moore, T. P. Purdy, and D. M. Stamper-Kurn, *Bose-Einstein condensation in a circular waveguide*, Phys. Rev. Lett. **95**, 143201 (2005).

[137] T. Busch, B. G. Englert, K. Rzążewski, and M. Wilkens, *Two cold atoms in a harmonic trap*, Found. Phys. **28**, 549–559 (1998).

[138] T. Sowiński, M. Brewczyk, M. Gajda, and K. Rzążewski, *Dynamics and decoherence of two cold bosons in a one-dimensional harmonic trap*, Phys. Rev. A **82**, 053631 (2010).

[139] *Wolfram MathWorld: Confluent Hypergeometric Function of the Second Kind*, http://mathworld.wolfram.com/ConfluentHypergeometricFunctionoftheSecondKind.html.

[140] Computer algebra programme mathematica.

[141] J. Satsuma and N. Yajima, *B. Initial Value Problems of One-Dimensional Self-Modulation of Nonlinear Waves in Dispersive Media*, Progress of Theoretical Physics Supplement **55**, 284–306 (1974).

[142] A. I. Streltsov, O. E. Alon, and L. S. Cederbaum, *Formation and dynamics of many-boson fragmented states in one-dimensional attractive ultracold gases*, Phys. Rev. Lett. **100**, 130401 (2008).

[143] I. W. Busbridge, *Some integrals involving Hermite polynomials*, London Math. Soc. **23**, 135–141 (1948).

[144] G. Marsaglia and W. W. Tsang, *The ziggurat method for generating random variables*, J. Stat. Softw. **5**, 1–7 (2000).

[145] I. B. Spielman, W. D. Phillips, and J. V. Porto, *Mott-insulator transition in a two-dimensional atomic Bose gas*, Phys. Rev. Lett. **98**, 080404 (2007).

[146] C. F. Wildfeuer, A. P. Lund, and J. P. Dowling, *Strong violations of Bell-type inequalities for path-entangled number states*, Phys. Rev. A **76**, 052101 (2007).

[147] B. Lucke *et al.*, *Twin matter waves for interferometry beyond the classical limit*, Science **334**, 773–776 (2011).

[148] B. Gertjerenken and C. Weiss, *Nonlocal quantum superpositions of bright matter-wave solitons and dimers*, J. Phys. B **45**, 165301 (2012).

[149] B. Gertjerenken, T. P. Billam, L. Khaykovich, and C. Weiss, *Scattering bright solitons: Quantum versus mean-field behavior*, Phys. Rev. A **86**, 033608 (2012).

[150] F. Serwane, G. Zürn, T. Lompe, T. B. Ottenstein, A. N. Wenz, and S. Jochim, *Deterministic preparation of a tunable few-fermion system*, Science **332**, 336–338 (2011).

[151] G. Zürn, F. Serwane, T. Lompe, A. N. Wenz, M. G. Ries, J. E. Bohn, and S. Jochim, *Fermionization of two distinguishable fermions*, Phys. Rev. Lett. **108**, 075303 (2012).

[152] M. Cramer, C. M. Dawson, J. Eisert, and T. J. Osborne, *Exact relaxation in a class of nonequilibrium quantum lattice systems*, Phys. Rev. Lett. **100**, 030602 (2008).

[153] C. Gogolin, M. P. Müller, and J. Eisert, *Absence of thermalization in nonintegrable systems*, Phys. Rev. Lett. **106**, 040401 (2011).

[154] M. Greiner, O. Mandel, T. W. Hansch, and I. Bloch, *Collapse and revival of the matter wave field of a Bose-Einstein condensate*, Nature **419**, 52 (2009).

[155] F. Benatti, R. Floreanini, and U. Marzolino, *Entanglement robustness and geometry in systems of identical particles*, Phys. Rev. A **85**, 042329 (2012).

[156] D. T. Pegg and S. M. Barnett, *Quantum optical phase*, J. Mod. Opt **44**, 225 (1997).

[157] C. Gerry and P. Knight, *Introductory Quantum Optics* (Cambridge University Press, Cambridge, 2004).

[158] V. V. Sokolov, B. A. Brown, and V. Zelevinsky, *Invariant correlational entropy and complexity of quantum states*, Phys. Rev. E **58**, 56–68 (1998).

[159] T. P. Billam and S. A. Gardiner, *Coherence and instability in a driven Bose-Einstein condensate: a fully dynamical number-conserving approach*, New J. Phys. **14**, 013038 (2012).

[160] M. Lewenstein and B. A. Malomed, *Entanglement generation by collisions of quantum solitons in the Born approximation*, New J. Phys. **11**, 113014 (2009).

[161] M. D. Girardeau, E. M. Wright, and J. M. Triscari, *Ground-state properties of a one-dimensional system of hard-core bosons in a harmonic trap*, Phys. Rev. A **63**, 033601 (2001).

[162] J. B. McGuire, *Study of Exactly Soluble One-Dimensional N-Body Problems*, J. Math. Phys. **5**, 622 (1964).

[163] J. Sebby-Strabley, M. Anderlini, P. S. Jessen, and J. V. Porto, *Lattice of double wells for manipulating pairs of cold atoms*, Phys. Rev. A **73**, 033605 (2006).

[164] I. Bloch, J. Dalibard, and S. Nascimbène, *Quantum simulations with ultracold quantum gases*, Nature Physics **8**, 267 (2012).

[165] J. F. Sherson, C. Weitenberg, M. Endres, M. Cheneau, I. Bloch, and S. Kuhr, *Single-atom-resolved fluorescence imaging of an atomic Mott insulator*, Nature **467**, 68 (2010).

[166] K. Sun, W. V. Liu, A. Hemmerich, and S. Das Sarma, *Topological semimetal in a fermionic optical lattice*, Nat Phys **8**, 67 (2012).

[167] J. A. Dunningham and K. Burnett, *Sub-shot-noise-limited measurements with Bose-Einstein condensates*, Phys. Rev. A **70**, 033601 (2004).

[168] G. A. Korn and T. M. Korn, *Mathematical handbook for scientists and engineers* (McGraw-Hill Book Company, London, 1961).

[169] *Wolfram MathWorld: Gamma Function*, http://mathworld.wolfram.com/GammaFunction.html.

[170] (2011), T. P. Billam, private communication.